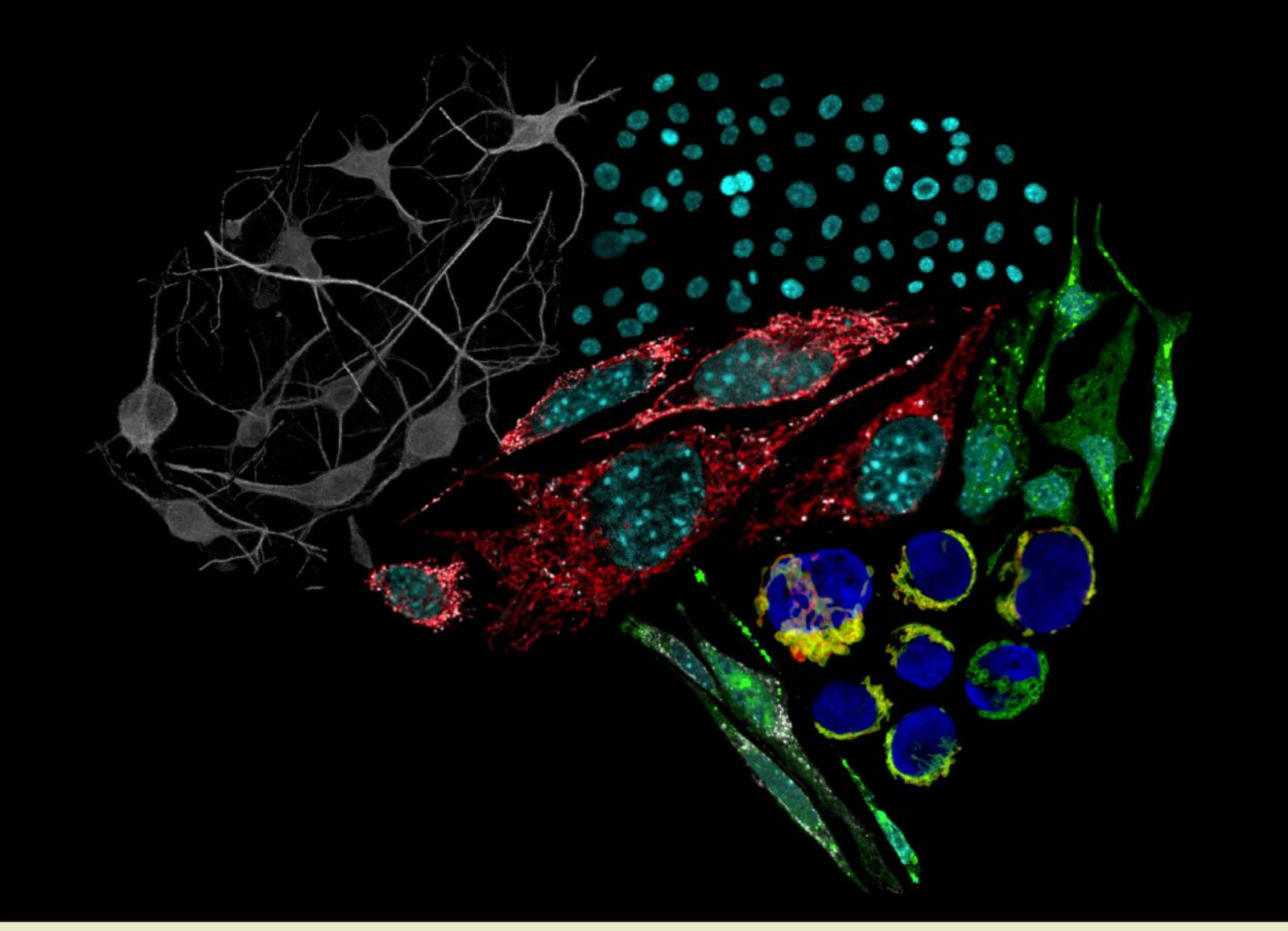

Luana Carvalho Naia

ROLE OF LYSINE DEACETYLASES ON TRANSCRIPTION REGULATION AND MITOCHONDRIAL FUNCTION IN HUNTINGTON'S DISEASE

Tese de Doutoramento do Programa de Doutoramento em Ciências da Saúde, ramo de Ciências Biomédicas,
orientada pela Professora Doutora Ana Cristina Carvalho Rego
e apresentada à Faculdade de Medicina da Universidade de Coimbra.

Setembro 2016

· U C ·

UNIVERSIDADE DE COIMBRA

Luana Carvalho Naia

Role of lysine deacetylases on transcription regulation and mitochondrial function in Huntington's disease

Setembro 2016

Tese de Doutoramento do Programa de Doutoramento em Ciências da Saúde, ramo de Ciências Biomédicas, orientada pela Professora Doutora Ana Cristina Carvalho Rego e apresentada à Faculdade de Medicina da Universidade de Coimbra

Front cover represents a brain-like assembly of fluorescence microscopy images from different cell types used in this Thesis. Rounded lymphoblasts with perinuclear yellow polarized or green swollen mitochondria are distributed in a cerebellum type structure. Neuronal-like striatal cells overexpressing either sirtuin 3, in green, or a marker for mitochondrial network, in red, are displayed in occipital and temporal lobes, respectively. Whereas nuclei labeling in blue cyan are dotted in parietal lobe. Lastly, beautiful neuronal striatal network from transgenic Huntington's disease mice, in gray, represents the complexity of the frontal lobe.

The research described in the present thesis was performed at the Center for Neurosciences and Cell Biology, University of Coimbra, Coimbra, Portugal.

Luana Naia received a PhD fellowship from '*Fundação para a Ciência e Tecnologia*' (FCT), Portugal, fellowship reference number SFRH/BD/86655/2012. The research work was funded by '*Fundo Europeu de Desenvolvimento Regional*' – FEDER funds through the '*Programa Operacional Factores de Competitividade*' – COMPETE, projects reference PEst-C/SAU/LA0001/2013-2014 and UID/NEU/04539/2013; and by national funds through FCT, projects reference PTDC/SAUFCF/108056/2008, EXPL/BIM-MEC/2220/2013, by '*Gabinete de Apoio à Investigação'* (GAI) funded by Faculty of Medicine of the University of Coimbra and Santander Totta Bank, and Mantero Belard Neuroscience prize 2013, supported by '*Santa Casa da Misericórdia de Lisboa'*, Portugal.

Aos meus pais

AGRADECIMENTOS

De todos os capítulos, este é possivelmente o mais difícil de escrever. Não há gráficos que guiem esta escrita, apenas emoções. Ao longo destes anos acompanharam-me pessoas valiosas que tornaram este percurso não mais fácil, mas certamente mais agradável. Aqui, quero deixar-lhes o meu profundo Obrigado.

Em primeiro lugar quero agradecer à minha orientadora, Professora Cristina Rego, pelo exemplo de pessoa, professora e cientista que é. Agradeço por me ter aceitado no seu laboratório e por toda a confiança que depositou em mim e no meu trabalho. Um dia a professora disse-me 'O *stress* mantém-nos ativos'. Hoje agradeço por me ter transmitido a sua energia, motivação, entusiasmo – valiosos requisitos que me ajudaram a superar os desafios constantes a que me foi proporcionando ao longo destes anos. "*To acquire knowledge, one must study; but to acquire wisdom, one must observe*." – Obrigada pelo imenso aprendizado.

No seguimento, quero agradecer à Professora Catarina Resende de Oliveira, por ter acompanhado tão cuidadosamente o meu percurso científico. Quero agradecer pelas palavras sábias e carinhosas e por estar sempre presente para esclarecer qualquer dúvida. É uma honra trabalhar tão perto de uma grande pessoa e cientista.

Agradeço à Tatiana Rosenstock, minha mestre e companheira de laboratório. Juntas partilhamos ideias, aflições, entusiasmo, alegrias, desespero. Com ela aprendi a desenhar experiências e a superar adversidades. Aprendi a orientar, espero que tão bem quanto ela me orientou a mim. Sinto saudades do '*Café?*' logo de manhã e da '*Baladinha?*' às portas do fim de semana. Obrigada por todos os bons momentos. Foi um prazer aprender e trabalhar contigo.

Agradeço ao Márcio Ribeiro, um amigo e colega extraordinário, sempre presente nos bons e maus momentos. Obrigada pelo conforto, pela preocupação, pelas conversas, pelas confissões. Tenho saudades de chegar ao laboratório de manhazinha e desejar-te '*boa noite*' e tu um '*bom dia*'. Fazes-me muita falta!

Agradeço à Carla Lopes, minha companheira nesta jornada de vários anos. Apresentou-me Coimbra. Arrancou-me de casa quando queria e quando não queria, mas quando precisava. Cresci e enriqueci culturalmente contigo.

Um profundo Obrigado à Catarina Carmo, pelo precioso contributo que deu ao laboratório e a este projeto. O último capítulo desta Tese seria certamente mais pobre sem a tua ajuda. Não sei se terei aprendido mais contigo do que ensinado. Obrigada por seres assim, boa, num mundo que hoje em dia carece de valores.

Agradeço a antigos membros do laboratório que me acompanharam nesta jornada e colaboraram neste trabalho. À Gladys, que evoluiu de caloira, para colega e finalmente amiga. Obrigada por todos os bons momentos que partilhamos, dentro e fora do CNC. Obrigada por toda a ajuda e colaboração desinteressada. Aprendi imenso contigo e agradeço por isso. À Ana Oliveira, por todo apoio e ajuda no laboratório. Ao Mário Laço, por todos os momentos descontraídos, todas as gargalhadas, e por todas as curiosidades que aprendi contigo. E acima de tudo agradeço por todo o conhecimento que sempre transmitiste ao grupo. À Sofia *Ruivinha* pela enorme boa disposição, carinho e amizade. Ao Jorge Valero que tanto contribuiu na análise e processamento de imagem do *mundo mitocôndria*. À Ana Duarte, por me ter ensinado o rigor de trabalhar num laboratório e pela colaboração na medição dos nucleótidos de adenina. À Joana Rodrigues e à Teresa Oliveira pelo contributo que ofereceram a este trabalho.

Agradeço aos restantes membros do grupo '*Mitochondrial Dysfunction and Synaling in Neurodegeneration*': à Sandra, pela amizade, pelo companheirismo, pelos desabafos (que foram muitos); à Luísa Ferreira e à Elisabete Ferreiro pela partilha de conhecimento e às meninas de mestrado Carina, Filipa e Lígia, por terem revitalizado o laboratório neste último ano letivo.

Um Obrigada à Isabel Dantas, por estar sempre disponível para ajudar naqueles dias de laboratório mais atrapalhados e por me arrancar sempre um sorriso nos dias mais cinzentos.

Agradeço à Ana, a melhor amiga de sempre e para sempre. Há vinte e três anos atrás entravamos juntas para a escola. Partilhamos segredos e confissões. Vimos o nascer do sol, viajamos, sorrimos, choramos. Nos altos e baixos desta jornada estavas sempre lá, à distância de um telefonema ou de uma viagem de carro. E foi nesta pequena distância que eu me apoiei. Obrigada por existires na minha vida.

Agradeço ao Ruben, meu companheiro, namorado, amigo, por todo o apoio incondicional. Por me levares a ouvir o mar nos dias mais insuportáveis, pelas caminhadas quando os olhos precisavam de descanso, pelas panquecas quando a energia faltava, e pelo conforto quando as experiências não davam certo. À Cacau, pelas reconfortantes boas vindas a casa no final de cada dia de trabalho.

Finalmente agradeço imensamente à minha Família pelo apoio incondicional que sempre me proporcionou. Aos meus pais, digo que palavras nenhumas poderão alguma vez expressar a profunda gratidão que vos tenho. Vocês são o meu porto de abrigo. Tudo o que sou, devo-o a vocês, à vossa educação, ao vosso carinho, ao vosso amor. Claramente, sou uma sortuda. Dedico-vos esta Tese, pois vocês acreditaram

mais nela do que eu. À minha Irmã, minha Fru-Fru, companheira de excentricidades, de viagens, de *puff* e séries à Sexta-feira à noite e de pão de queijo ao Domingo de manhã. Adoro-te. À minha querida Avó, por toda a preocupação e carinho. Ao Tio Vítor e Xana, por serem os melhores tios de sempre.

TABLE OF CONTENTS

LIST OF FIGURES

CHAPTER I

CHAPTER III

CHAPTER IV

CHAPTER V

CHAPTER VI

LIST OF TABLES

CHAPTER I

CHAPTER II

In accordance with the terms of the article 8 paragraph 2 of the Portuguese Decree-Law No. 388/70, the author certifies that this thesis includes total or partial results/revisions of the following peer-reviewed publications and book chapter. In regards to the provisions of the Decree-Law, the author of this PhD thesis declares that intervened in the design and implementation of the experimental work, analysis and interpretation of the data and in the writing of the manuscripts published under the name of **Naia L**.

Originals:

Naia L*, Cunha-Oliveira T*, Rodrigues J, Rosenstock TR, Ribeiro M, Oliveira AM, Oliveira-Sousa S, Duarte AI, Hayden MR, Rego AC. 2017. Histone deacetylase inhibitors protect against pyruvate dehydrogenase dysfunction in Huntington's disease. *J. Neurosci.* [Epub ahead of print] (*equal contribution)

Naia L, Rosenstock TR, Oliveira AM, Oliveira-Sousa SI, Caldeira GL, Carmo C, Laço MN, Hayden MR, Oliveira CR, Rego AC. 2016. Comparative mitochondrial-based protective effects of resveratrol and nicotinamide in Huntington's disease models. *Mol Neurobiol*. [Epub ahead of print]
doi: 10.1007/s12035-016-0048-3

Reviews:

Naia L, Ferreira IL, Ferreiro E, Rego AC. 2016. Mitochondrial Ca^{2+} handling in Huntington's and Alzheimer's diseases – the role of ER-mitochondria crosstalk. *Biochem Biophys Res Commun* - Thematic Issue on Emerging Mechanisms of Neurodegenerative Disorders [Epub ahead of print]
doi: 10.1016/j.bbrc.2016.07.122

Naia L, Rego AC. 2015. Sirtuins: double players in Huntington's disease. *Biochim Biophys Acta,* 1852:2183-94
doi: 10.1016/j.bbadis.2015.07.003

Book Chapter:

Carmo C, **Naia L**, Lopes C, Rego AC. Mitochondrial dysfunction in Huntington's disease. In *Polyglutamine disorders* (Pereira de Almeida L. and Nóbrega C., Eds.). Springer International Publishing. *(under revision)*

LIST OF ABBREVIATIONS

3-NP	3-Nitropropionic acid
α-KGDH	Alpha-ketoglutarate dehydrogenase
β2M	Beta-2-microglobulin
$\Delta\psi_m$	Mitochondrial transmembrane potential
ρ^0	Rho-zero
Ac	Acetyl residue
ACAT1	Acetyl-CoA acetyltransferase 1
ADP	Adenosine diphosphate
AMP	Adenosine monophosphate
AMPK	AMP-activated protein kinase
ANOVA	Analysis of variance
Apaf1	Apoptotic protease activating factor 1
ATP	Adenosine triphosphate
BAC	Bacterial artificial chromosome
BBB	Blood-brain barrier
Bcl-2	B-cell lymphoma 2
BDNF	Brain-derived neurotrophic factor
BSA	Albumin from bovine serum
Ca^{2+}	Calcium
cAMP	cyclic adenosine monophosphate
CBP	CREB-binding protein
CCCP	carbonyl cyanide 3-chlorophenylhydrazone
CMV	Cytomegalovirus
CNS	Central nervous system
CoA	Coenzyme A
COX	Cytochrome *c* oxidase
CR	Calorie restriction
CREB	Cyclic adenosine monophosphate-response element binding protein
CsA	Cyclosporin A
CTR	Control
CTX	Cortex or cortical
CypD	Cyclophilin D
Cys	Cysteine residue

cyt *c*	Cytochrome *c*
D1R	Dopamine receptors-subtype 1
D2R	Dopamine receptors-subtype 2
DA	Dopamine
DARPP-32	Dopamine- and cAMP-regulated neuronal phosphoprotein
DCA	Dichloroacetate
DCF	Dichlorofluorescein
$DCFH_2$-DA	2',7'-dichlorodihydrofluorescein diacetate
DEPC	Diethylpyrocarbonate
DIV	Days *in vitro*
DMEM	Dulbecco's Modified Eagle's Medium
DMSO	Dimethyl sulfoxide
Drp1	Dynamin-related protein 1
DRPLA	Dentatorubral pallidoluysian atrophy
DsRed	*Discosoma* sp. red fluorescent protein
DTT	1,4-dithiothreitol
ERR	Estrogen-related receptor
ETC	Electron transport chain
FAD	Flavin adenine dinucleotide
FBS	Fetal bovine serum
FCCP	Carbonyl cyanide 4-(trifluoromethoxy) phenylhydrazone
Fis1	Mitochondrial fission 1 protein
FL	Full-length
FOXO	Forkhead box class O
FVB/N	Friend leukemia virus B NIH strain
GABA	γ-aminobutyric acid
GAPDH	Glyceraldehyde-3-phosphate dehydrogenase
GFP	Green fluorescent protein
GPe	Globus pallidus external segment
GPi	Globus pallidus internal segment
GPx	Glutathione peroxidase
GST	Glutathione S-transferase
H_2O_2	Hydrogen peroxide
HAP1	Huntingtin-associated protein 1
HAT	Histone acetyltransferase
HBSS	Hank's balanced salt solution
HD	Huntington's disease

HDAC	Histone deacetylase
HDACi	Histone deacetylase inhibitor(s)
HEAT	Huntingtin, elongation factor 3, protein phosphatase 2A, and the yeast kinase TOR1
HIF-1α	Hypoxia-inducible factor-1α
HOP-β-CD	2-hydroxypropyl-β-cyclodextrin
HPLC	High-performance liquid chromatography
HSP60	Heat shock protein 60
HTT or Htt	Human or murine huntingtin protein
ICC	Immunocytochemistry
KAT	Lysine acetyltransferase
KD	Knockdown
KDAC	Lysine deacetylase
KI	Knock-in
KO	Knockout
LKB1	Liver kinase B1
Lys or K	Lysine residue
MAMs	mitochondria-associated membranes
MCU	Mitochondrial calcium uniporter
Mfn1, 2	Mitofusin 1 and 2 protein
mHTT or mHtt	Mutant human or murine huntingtin
MIM	Mitochondrial inner membrane
min	Minutes
MIS	Mitochondrial intermembrane space
MOM	Mitochondrial outer membrane
MNA	1-methylnicotinamide
mPTP	Mitochondrial permeability transition pore
MSNs	Medium-sized spiny neurons
mtDNA	Mitochondrial DNA
MTT	3-(4,5-dimethylthiazol-2-yl)-2,5-diphenyltetrazolium bromide
NAC	N-acetyl-cysteine
NAD^+	Nicotinamide adenine dinucleotide, oxidized form
NADH	Nicotinamide adenine dinucleotide, reduced form
NADt	Total nicotinamide adenine dinucleotide
NAM	Nicotinamide
nDNA	nuclear DNA
NMDA	*N*-methyl-D-aspartate

NMDAR	*N*-methyl-D-aspartate receptor
NRF-1, 2	Nuclear respiratory factor 1 or 2
Nrf2	Nuclear factor E3-related factor 2
O_2	Oxygen
$O_2^{\bullet -}$	Superoxide anion
OCR	Oxygen consumption rate
OE	Overexpression
Oligo or O	Oligomycin
Opa1	Optic atrophy 1
OXPHOS	Oxidative phosphorylation
PARP-1	Poly-ADP-ribose polymerase-1
PB	Phenyl butyrate
PBS	Phosphate-buffered saline
PCr/Pi	Phosphocreatine/inorganic phosphate
PDC	Pyruvate dehydrogenase complex
PDH	Pyruvate dehydrogenase
PDK	Pyruvate dehydrogenase kinase
PDP	Pyruvate dehydrogenase phosphatase
PGC-1α	PPARγ coactivator-1α
PI	Propidium iodide
PMSF	Phenylmethylsulfonyl fluoride
PPARα,δ,γ	Proliferator-activator receptor alpha, delta or gamma
PRD	Proline-rich domain
Prdx	Peroxiredoxins
PTM	Post-translational modifications
Q or polyQ	Glutamine or polyglutamine
qPCR	real-time polymerase chain reaction
RAR	Retinoic acid receptor
REST	RE1-silencing transcription factor
RESV	Resveratrol
Rh123	Rhodamine 123
ROS	Reactive oxygen species
rpm	Rotations per minute
RPMI	Roswell Park Memorial Institute medium
s	Seconds
SAHA	Suberoylanilide hydroxamic acid
SB	Sodium butyrate

SBMA	Spinal and bulbar muscular atrophy
SCA	Spinocerebellar ataxia
SDH	Succinate dehydrogenase
Ser	Serine residue
shRNA	short hairpin RNA
Sir2	Silent information regulator 2
SIRT	Sirtuin
SNc	*Substantia nigra pars compacta*
SNr	*Substantia nigra pars reticulata*
SOD1, 2	Superoxide dismutase 1 or 2
Sp1	Specific protein-1
STAC	SIRT-activating compound
STN	Subthalamic nuclei
STR	Striatum or striatal
TAF	TBP-associated factor
TBP	TATA-binding protein
TBS	Tris-buffered saline
TCA	Tricarboxylic acid
TFAM	Mitochondrial transcription factor A
TIM23	Translocase of the mitochondrial inner membrane 23
TMRM$^+$	Tetramethylrhodamine methyl ester
TORC1	CREB-regulated transcription coactivator 1
TRAK1, 2	Trafficking protein, kinesin-binding 1 and 2
tRNA	transfer RNA
TrkB	Tyrosine receptor kinase B
TRPC5	Short transient receptor potential channel 5
Tyr or Y	Tyrosine residue
TSA	Trichostatin A
TTP	Thiamin diphosphate
UPS	Ubiquitin-proteasome system
vs	*Versus*
WB	Western blotting
WT	Wild-type
YAC	Yeast artificial chromosome

"It is the brain, the little gray cells on which one must rely. One must seek the truth within - not without." ~ Poirot"

— *Agatha Christie*

SUMMARY

Huntington's disease (HD) is a neurodegenerative disorder that gradually affects cognitive skills and normal movements of the affected individuals and for which no disease modifying treatments exist. The disease is caused by an expanded CAG trinucleotide repeat (of variable length) in the *HTT* gene that encodes the huntingtin protein (HTT). Mutant HTT (mHTT) exhibits an abnormal elongated polyglutamine stretch that confers a toxic gain of function and predisposes the protein to fragmentation and aggregation, resulting in neuronal dysfunction and selective death in striatum and cortex. There is strong evidence that transcriptional deregulation and altered mitochondrial function occurs early and acts causally in HD pathogenesis; importantly, these events may be related to altered acetylation of proteins. Therefore, pharmacological strategies that interfere with both nuclear and mitochondrial protein acetylation may be therapeutically useful to hinder neuronal dysfunction in the course of HD pathology. In the present work, distinct lysine deacetylases (a heterogeneous group of proteins that remove acetyl groups from histones and other proteins regulating their structure and function), were pharmacologically or genetically targeted with the main purpose of counteracting mitochondrial and metabolic deficits in *in vitro* and *in vivo* models expressing human full-length mHTT.

We have previously shown that mitochondrial dysfunction in HD persists at the level of pyruvate dehydrogenase (PDH), which functionally links glycolysis to oxidative phosphorylation. In **Chapter 3** we report that decreased PDH activity in HD striatal cells expressing 111 glutamines (ST*Hdh*$^{Q111/Q111}$) occurs through enhanced PDH kinases (PDKs) and reduced PDH phosphatase 1 protein expression, which trigger inhibitory phosphorylation of catalytic PDH E1α subunit in three different serine sites (Ser293, Ser300 and Ser232). Classes I and IIa histone deacetylase inhibitors (HDACi), sodium butyrate (SB) and phenylbutyrate, increased histone H3 acetylation and enhanced metabolism and mitochondrial respiration, similar to PDH activator dichloroacetate, suggesting that HDACi may favor activation of PDH complex. Concordantly, SB significantly decreased the expression of PDK2 and PDK3 in ST*Hdh*$^{Q111/Q111}$ cells, which led to decreased PDH E1α phosphorylation in all serine sites. This effect occurs since HDACi SB stimulates HIF-1α degradation, a transcription factor that actively suppresses metabolism by directly transactivating genes encoding for PDKs. Therefore, partial depletion of PDK3 enhanced mitochondrial respiration and ATP synthesis in both wild-type and mutant ST*Hdh* cells, similarly to the effects achieved with SB treatment. YAC128 transgenic HD mice also exhibited decreased PDH E1α phosphorylation and

PDK1-3 expression after SB treatment, which positively influenced central and peripheral metabolism.

Further studies were conducted using modulators of class III lysine deacetylases, classically known as sirtuins. SIRT1, the best studied member of the sirtuins family, has been shown to exert neuroprotective roles in several models of neurodegeneration, boosting the interest in the development of SIRT1 activators. However, recent reports on SIRT1 inhibitors have also shown protective effects, casting doubt regarding previous findings. To better understand this paradox we tested resveratrol (RESV, a SIRT1 activator) and nicotinamide (NAM, a SIRT1 inhibitor) in *in vitro* models and in an animal model expressing mHTT (**Chapter 4**). We found that RESV enhanced lysine deacetylation activity and recovered abnormal mitochondrial phenotype of lymphoblasts from affected HD patients and cortical and striatal primary neurons isolated from YAC128 mice, which was associated with increased mitochondrial transcription and biogenesis. NAM had no effects on mitochondrial biogenesis, however increased NAD^+ levels following NAM treatment may explain the positive impact on mitochondrial function *in vitro*. In symptomatic YAC128 mice, RESV completely abrogated deficits in motor learning and coordination, two well-established features of this transgenic HD model, and increased transcription of mitochondrial-encoded electron transport chain genes. In turn, NAM supplementation *in vivo* proved to be deleterious.

The positive effects achieved with the SIRT-activating compound RESV led us to specifically target SIRT3 (**Chapter 5**), the major mitochondrial deacetylase that has received much attention for its role in oxidative metabolism and aging. We found increased SIRT3 levels and activity in HD lymphoblasts and in ST*Hdh*$^{Q111/Q111}$ cells. Considering its potential neuroprotective role in HD, we overexpressed (OE) SIRT3, which was shown to co-localize more in mitochondria from HD striatal cells than in wild-type counterparts. Cortical tissue from YAC128 mice also exhibited lower acetylation of superoxide dismutase 2, a recognized target of SIRT3, suggesting increased SIRT3 activity. When OE in ST*Hdh*, SIRT3 enhanced lysine deacetylation and mitochondrial transmembrane potential. SIRT3 OE also reverted the loss in mitochondrial-related transcription factors, PGC-1α and TFAM, induced by mHTT. Still, increased mitochondrial content was not observed. Ultimately, ST*Hdh*$^{Q111/Q111}$-SIRT3 OE cells showed lower susceptibility to apoptotic cell death.

Overall, this study provides novel insights into the molecular deficits underlying mitochondrial dysfunction in HD and explores promising drugs that effectively modulate acetylation landscape, further impacting on mitochondrial and mitochondrial-related

transcription proteins activity. Finally, increased mitochondrial activity and transcription partially control HD-related motor disturbances and neuronal death.

Keywords: Huntington's disease, mitochondria, pyruvate dehydrogenase, lysine deacetylases, neuroprotection.

RESUMO

A Doença de Huntington (DH) é uma doença neurodegenerativa que afeta gradualmente as capacidade cognitivas e motoras dos indivíduos afetados, e para a qual não existe tratamento neuroprotetor ou cura. A DH é causada por uma expansão de trinucleótidos CAG (de tamanho variável) no gene *HTT* que codifica para a proteína huntingtina (HTT). A HTT mutante (mHTT) possui uma expansão anormal de poliglutaminas que lhe confere uma função tóxica, predispondo-a para a fragmentação e agregação, resultando em disfunção e morte seletiva de neurónios estriatais e corticais. Fortes evidências sugerem que alterações na regulação da transcrição e na função mitocondrial ocorrem em estádios iniciais da doença e são fatores causais para a patogénese da DH; estes eventos poderão estar relacionados com alterações na acetilação de proteínas. Assim, estratégias farmacológicas que interfiram com a acetilação de proteínas nucleares e mitocondriais poderão ser profícuas no combate à disfunção neuronal no decurso da DH. Neste trabalho diferentes desacetilases de lisinas (um grupo heterogéneo de proteínas que remove grupos acetil de histonas ou outras proteínas, regulando a sua estrutura e função) foram farmacologicamente ou geneticamente moduladas com o objetivo de neutralizar os défices mitocondriais e metabólicos em modelos que expressam a mHTT.

Anteriormente o nosso grupo de investigação mostrou que a disfunção mitocondrial ocorre ao nível da piruvato desidrogenase (PDH), um complexo enzimático que faz a ligação entre a glicólise e a fosforilação oxidativa. No **Capítulo 3** desta tese mostrámos que a diminuição da atividade da PDH em células estriatais que expressam 111 glutaminas (ST*Hdh*$^{Q111/Q111}$) ocorre devido ao aumento das cinases da PDH (PDKs) e à diminuição da fosfatase 1 da PDH, desencadeando a fosforilação (inibitória) da subunidade catalítica PDH E1α em três resíduos de serina (Ser293, Ser300 e Ser232). Inibidores das classes I e IIa das desacetilases de histonas (HDACi), os compostos butirato de sódio (BS) e fenilbutirato, aumentaram a acetilação da histona H3 e melhoraram o metabolismo e a respiração mitocondrial, de forma semelhante ao observado com dicloroacetato, um reconhecido ativador da PDH, sugerindo que os HDACi poderão favorecer a atividade da PDH. Em concordância, o SB diminuiu a expressão da PDK2 e PDK3 nas células ST*Hdh*$^{Q111/Q111}$, o que levou a uma diminuição da fosforilação da PDH E1α em todos os resíduos de serina. Este efeito mediado pelo SB parece ter resultado da estimulação da degradação do HIF-1α, um fator de transcrição que inibe o metabolismo celular através da transativação de genes que codificam para as PDKs. De forma semelhante ao SB, a redução parcial da expressão

da PDK3 aumentou a respiração mitocondrial e a síntese de ATP em ambas as células ST*Hdh wild-type* e mutante. No murganho transgénico YAC128 verificou-se uma diminuição na fosforilação da PDH E1α e na expressão das PDK1-3 após tratamento com SB, influenciando positivamente o metabolismo energético.

Nos estudos que se seguiram foram utilizados moduladores de desacetilases de lisinas de classe III, conhecidas como sirtuinas. A SIRT1, o membro da família mais estudado, tem vindo a mostrar um papel neuroprotetor em vários modelos de neurodegenerescência, aumentando o interesse no desenvolvimento de ativadores da SIRT1. No entanto, em estudos mais recentes os inibidores da SIRT1 também mostraram resultados protetores, colocando em dúvida as observações anteriores. Para compreender melhor este paradoxo, testámos o efeito do resveratrol (RESV, ativador da SIRT1) e da nicotinamida (NAM, inibidor da SIRT1) em modelos *in vitro* e num animal modelo que expressa a mHTT (**Capítulo 4**). O RESV aumentou a atividade desacetilase e reverteu a disfunção mitocondrial quando testado em linfoblastos de doentes de Huntington e em neurónios corticais e estriatais isolados de embriões do murganho YAC128; estas observações foram associadas ao aumento da transcrição e biogénese mitocondrial. O tratamento com NAM não teve qualquer efeito na biogénese mitocondrial; no entanto, o aumento dos níveis de NAD^+ poderão justificar o impacto positivo observado na função mitocondrial testada *in vitro*. Quando administrado numa fase sintomática do murganho YAC128, o RESV anulou os défices de aprendizagem e coordenação motora, duas características deste animal transgénico, e aumentou a transcrição de genes da cadeia respiratória mitocondrial codificados pelo DNA mitocondrial. Por sua vez, a administração de NAM teve um efeito deletério *in vivo*.

Os efeitos positivos obtidos com o ativador da SIRT1, resveratrol, levou-nos a modular especificamente a SIRT3 (**Capítulo 5**), uma desacetilase mitocondrial que tem recebido especial atenção pelo seu papel no metabolismo oxidativo e no processo de envelhecimento. Em linfoblastos DH e em células ST*Hdh*$^{Q111/Q111}$ observámos um aumento dos níveis proteícos, de RNAm e da atividade da SIRT3. Considerando o potencial terapêutico da SIRT3 na DH, sobre-expressámos (SE) esta proteína em células estriatais e verificámos que se co-localiza preferencialmente nas mitocôndrias das células estriatais mutantes, comparativamente às células *wild-type*. O córtex do murganho YAC128 também exibiu menor acetilação da proteína superóxido dismutase 2, um alvo da SIRT3, sugerindo uma maior atividade desta sirtuína no contexto da DH. Quando SE em células ST*Hdh*, a SIRT3 aumentou a desacetilação e o potencial de membrana mitocondrial. A SE da SIRT3 também reverteu a diminuição dos fatores de transcrição associados à mitocôndria, PGC-1α e TFAM, induzida pela mHtt. Contudo, não se observou um aumento da massa mitocondrial. Por fim, as células ST*Hdh*$^{Q111/Q111}$

que com SIRT3 SE apresentaram uma menor suscetibilidade à morte celular por apoptose.

Em conclusão, este estudo fornece novas perspetivas sobre os défices moleculares subjacentes à disfunção mitocondrial na DH, e explora estratégias farmacológicas promissoras que modificam a acetilação e que têm posterior impacto na atividade da mitocôndria e nos fatores de transcrição associados a este organelo. Adicionalmente, o aumento da função e transcrição mitocondrial influenciam os distúrbios motores e a morte neuronal associada à DH.

Palavras chave: Doença de Huntington, mitocôndria, piruvato desidrogenase, desacetilases de lisinas, neuroproteção.

CHAPTER I

STATE OF THE ART

1.1. HUNTINGTON'S DISEASE: AN OVERVIEW

1.1.1. HISTORICAL BACKGROUND

Huntington's disease (HD) is also known as Huntington's chorea. The term derives from the Ancient Greek word *choreia*, which means dance. The original descriptions date from the Middle Ages when afflicted individuals with the hysterical "dancing mania" would dance wildly in circles for hours until they dropped from exhaustion. Paracelsus (1493-1541) was the first to use the term chorea to define this movement disorder, but with no detailed description of the choreaform movements we recognize nowadays [reviewed in (Vale and Cardoso, 2015)]. The disease remained largely obscure and misunderstood until the beginning of the 19th century. During this time, people with chorea were often thought to be possessed by the devil.

The first accurate description of the disease came out in the last quarter of the 19th century. In 1872, a 22 year-old American doctor named George Huntington, working in Long Island, published a brief unreferenced paper in the *Medical and Surgical Reporter of Philadelphia* entitled "On Chorea". There, one can read the following description:

> "Chorea is essentially a disease of the nervous system. The name "chorea" is given to the disease on account of the dancing propensities of those who are affected by it, and it is a very appropriate designation… Its most marked and characteristic feature is a clonic spasm affecting the voluntary muscles. (…) The tendency to insanity, and sometimes that form of insanity which leads to suicide, is marked. (…) As regards the pathology of chorea, very little satisfactory information has been gained … The most probable theory, and one which I believe is most generally accepted at the present day is, that the disease depends upon some functional derangement in the cerebellum. (…) The hereditary chorea, as I shall call it, is confined to certain and fortunately a few families … hardly ever manifesting itself until adult or middle life, and then coming on gradually but surely, increasing by degrees, and often occupying years in its development … until death relieves them of their sufferings."

The description was so comprehensive that soon gave him international recognition. Other authors named the disease Huntington's chorea, and later it was

identified as Huntington's disease because not all patients develop chorea (Young et al., 1986). The concept of inheritance was not immediately appreciated, at least until the rediscovery of Gregor Mendel's work in 1900 (Punnett, 1908), when it became accepted that HD followed a Mendelian dominant pattern of inheritance.

1.1.2. GENETICS AND PREVALENCE

Expansion of CAG (cytosine-adenine-guanine) triplet repeats has been identified as the causative mutations in, at least, nine hereditary neurodegenerative disorders. These polyglutamine (polyQ)-expansion disorders include spinocerebellar ataxias (SCA) types 1, 2, 3 (or Machado-Joseph disease), 6, 7 and 17, dentatorubral pallidoluysian atrophy (DRPLA), spinal and bulbar muscular atrophy (SBMA or Kennedy's disease) and HD.

The genetic deficit causing HD was mapped in 1983 to the short arm of chromosome 4 (4p16.3) by genetic linkage with polymorphic DNA markers (Gusella et al., 1983). A decade later, and combined with advances in DNA cloning and sequencing techniques, the *HD* gene, as has historically been called, was identified by a multicenter consortium organized by the Hereditary Disease Foundation (HD collaborative and research group, 1993). Later, the gene was renamed *HTT* by the Human Genome Organization's nomenclature committee. The unstable CAG trinucleotide expansion in *HTT* encodes a polyQ stretch at the N-terminal of the large huntingtin protein (HTT) that makes it prone to misfold and aggregate (*described in section 1.2*). The average CAG tract length in the general population is 16 to 20 repeats, but it can range from 6 to 35, whereas adult-onset HD patients have more than 39 CAG repeats (Reddy et al., 1999a). HD alleles with reduced penetrance range from 36 to 39 CAG repeats, are meiotically unstable and individuals may manifest the disease at older age, or even show no clinical and neuropathologic HD phenotype (Langbehn et al., 2004). This highly polymorphic genotype occurs, in part, due to CAG length instability through intergenerational transmission, a phenomenon known as *genetic anticipation* (Ranen et al., 1995). This phenomenon clarifies why some individuals with no symptoms, who have intermediated-sized CAG repeats ranging from 27 to 39, are at risk of transmitting the disease to offspring. Interestingly, about 10-15% of all HD cases arise from non-affected parents whose repeat lengths fall within this normal range borderline (Semaka et al., 2010). Genetic anticipation is more frequent when the disease gene is inherited from the father, since the risk of expansion due to replication slippage is more frequent in spermatogenesis than oogenesis (MacDonald et al., 1993; Pearson, 2003).

The size of CAG trinucleotide expansion is the primary and major determinant of the age of clinical onset and has been shown to explain as much as 56% of the variance in adult onset cases (Andrew et al., 1993; Duyao et al., 1993) (**Figure 1.1**). The influence of CAG repeats length on rate of disease progression is less strong but still significant (Rosenblatt et al., 2012). Nonetheless, some studies do not establish any relationship (Claes et al., 1995; Kieburtz et al., 1994). Most HD patients display onset in mid-life and rare cases of juvenile-onset HD (expressing large CAG repeats of 60 or greater) are the product of parental transmission (Ranen et al., 1995). Therefore, an inverse relationship between CAG length and age of symptomatic onset has been established (**Figure 1.1**). Importantly, a second expanded CAG allele appears to have no effect on the age of motor onset, indicating that HD pathogenesis is not *HTT* dosage-dependent, but rather reflects the dominant effect of a single mutant allele (Genetic Modifiers of Huntington's Disease (GeM-HD) Consortium, 2015). Additionally, some portion of the variance of the age at onset is not explained by the CAG repeat length. Several studies revealed that a large set of genes in the chromosomal region of *HTT* harbors variations that alter disease onset and progression (Farrer et al., 1993; Genetic Modifiers of Huntington's Disease (GeM-HD) Consortium, 2015; Lee et al., 2012). Environmental factors were also described as modulators of motor, cognitive and other symptoms found in HD [reviewed in (Mo et al., 2015)].

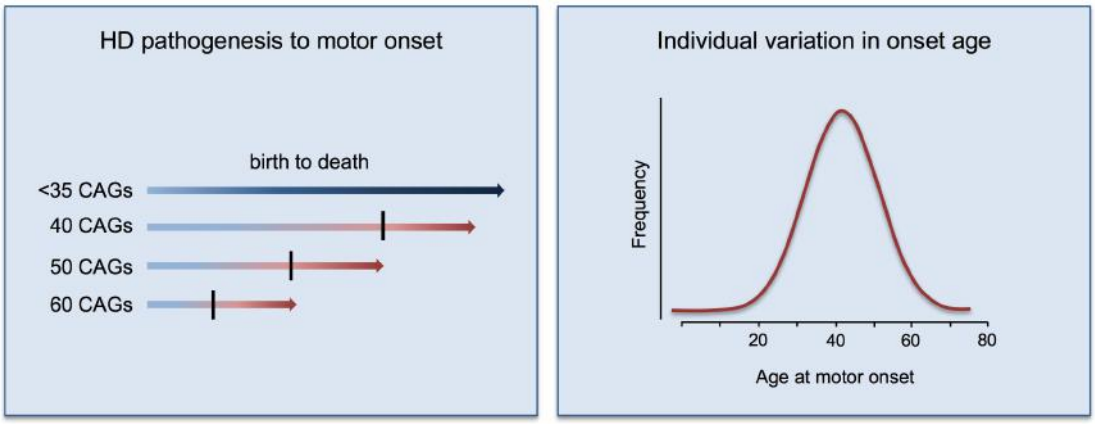

Figure 1.1 | Correlation between CAG repeats length, age at onset and its individual variation. The left square show the inverse correlation of age at neurological onset and HD CAG repeat length. The end of the arrow represents death, whereas the black bars represent the beginning of the clinical manifestations. In the right square it is possible to observe that age at onset distribution in HD is very broad and may vary from young 5 years to as old as 80 years of age, although most HD patients display clinical onset in mid-life, around 40 years of age (Myers, 2004).

The average prevalence of the HD mutation is 10.6-13.7 individuals *per* 100,000 in Western populations, with many more at risk of having inherited the mutant

gene (Fisher and Hayden, 2014). Still the global population prevalence of HD appears to show more than tenfold variation across regions (Rawlins et al., 2016). European migration explains much of the variation in HD prevalence rates around the world. North and South America, Australia and New Zealand resemble those of Europe and represent the highest frequencies of HD in the world. Nonetheless, even within Europe there is a marked heterogeneity with estimates ranging from 0.53 *per* 100,000 in Finland (Palo et al., 1987) to 10.85 or 12.3 *per* 100,000 in Italy and United Kingdom, respectively (Evans et al., 2013; Squitieri et al., 2016). Disturbingly, a very recent study concluded that HD alleles with a CAG repeat ranging from 36 to 38 occurs at high frequency in general population with approximately 1 in 400 individuals (Kay et al., 2016). Additionally, average CAG repeat length are longer in populations with high prevalence of the disease, such as European descent compared to East Asian and African populations (Morrison, 2012). Some studies also describe clusters of HD families living in small communities. HD shows a striking geographic prevalence among residents of the Western coast of Lake Maracaibo, Venezuela, where it is believed to have the highest known frequency of carriers worldwide, reaching up to 700 *per* 100,000 individuals, encompassing 10 generations (Project and Wexler, 2004).

1.1.3. NEUROPATHOLOGY: CIRCUITRY-RELATED DEGENERATION AND VONSATTEL GRADING

The major pathological hallmark of HD is the gradual and prominent cell loss and atrophy of the neostriatum (caudate nucleus and putamen). This structure is the larger component of the basal ganglia, a group of nuclei located subcortically further represented by the subthalamic nuclei (STN), *substantia nigra* (*pars reticulata* – SNr; and *pars compacta* - SNc) and globus pallidus (globus pallidus internal segment – GPi; and globus pallidus external segment – GPe). The basal ganglia are involved in motor and cognitive processes [reviewed in (Vonsattel et al., 2008)].

Striatal medium-sized spiny neurons (MSNs) are the most vulnerable (Vonsattel et al., 1985). They constitute 90-95% of all striatal neurons and use the inhibitory transmitter gamma-aminobutyric acid (GABA) and enkephalin or substance P as co-transmitters. MSNs receive glutamatergic inputs from almost all neocortical areas, while STN contains a number of modulatory components, including dopamine (DA) from projections in the SNc and cholinergic or GABAergic inputs from striatal interneurons [reviewed in (Galvan et al., 2012)]. Interestingly, not all HD MSNs appear equally vulnerable, since along the coronal axis of the neostriatum, the dorsal and rostral regions

are more affected than the ventral one, explaining why the tail of the caudate nucleus initially shows more degeneration than the body and head or the ventral putamen (Vonsattel and DiFiglia, 1998). This occurs because striatal output is primarily divided into two populations of MSNs with distinct projections with apparent opposing effect, as well as different DA receptors and neuropeptide expression (Kawaguchi et al., 1990). Under normal conditions, DA from SNc acts on dopamine receptors-subtype 1 (D1R; excitatory) at caudate/putamen GABAergic neurons expressing substance P, which release GABA and increase the inhibitory input at GPi/SNr neurons (direct pathway). On the other hand, DA also interacts with dopamine receptors-subtype 2 (D2R; inhibitory) on striatal inhibitory neurons that express enkephalin, which project to GPe controlling the release of GABA in the subthalamic nucleus that, in turn, release glutamate to the GPi/SNr (indirect pathway) [reviewed in (Rosenstock et al., 2012)].

In HD the balance between the direct and indirect pathways is affected, which leads to motor dysfunction. Striatal interneurons are generally spared (Ferrante et al., 1985), although they exhibit higher HTT immunoreactivity than the vulnerable striatal projection neurons, supporting the hypothesis that polyQ aggregation may not be a predictor of cell loss (Fusco et al., 1999; Kuemmerle et al., 1999). In both early symptomatic and presymptomatic stages, enkephalin-containing neurons projecting to the GPe (of the indirect pathway) appear to be much more affected than substance P-containing neurons projecting to the GPi (Albin et al., 1992; Deng et al., 2004; Sapp et al., 1995), resulting in decreased release of GABA from caudate/putamen to GPe. Consequently, there is a decrease in the inhibition of GPe neurons that also express GABA, leading to more GABA release to STN and GPi. In turn, glutamatergic STN neurons projecting to GPi/SNr release less glutamate, becoming hypofunctional, which reduces the inhibitory action of the GPi upon the thalamus. Ultimately, this leads to an increase in the excitatory stimulation in cortex, resulting in an exacerbation of movements [reviewed in (Rosenstock et al., 2012)] (**Figure 1.2**). This preferential involvement of the indirect pathway of basal ganglia-cortical circuitry sustain the hypothesis that chorea dominates early in the course of HD. Additionally, rigid-akinetic HD, as observed in the later stages (*described in section 1.1.4*), may be due to the additional loss of striatal neurons projecting to the GPi (of the direct pathway). A decrease in the release of GABA into GPi/SNr results in increased inhibition of thalamus and consequently decrease cortex stimulation and uncontrolled movements (Albin et al., 1990).

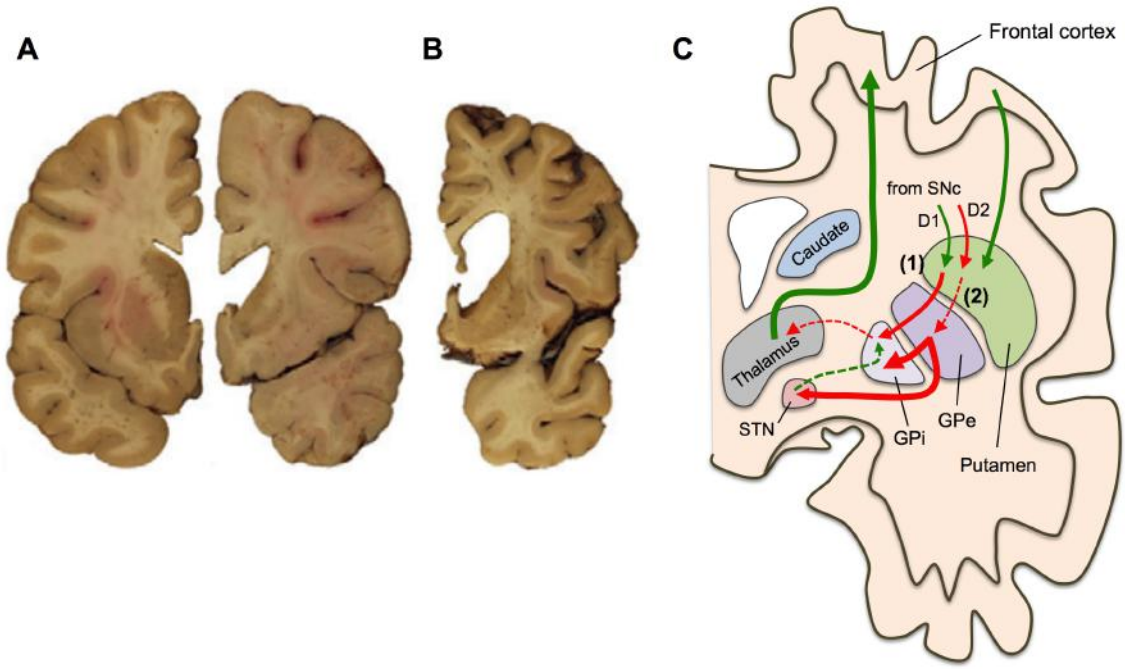

Figure 1.2 | Marked striatal degeneration in HD patient's brain and schematic representation of the respective basal ganglia circuitry. Coronal sections passing through the *nucleus accumbens* from a control 43 year-old man, for comparison (**A left**); from a 24 year-old man with 70/20 CAG and onset of symptoms at 13 years of age (**A right**); and from a 53 year-old man with 46/17 CAG and onset of symptoms at 36 years of age – Vonsattel stage 3/4 (**B**). In **C** the preferential degeneration of the inhibitory striatal neurons of the indirect pathway (2) leads to unbalanced stimulation of the direct pathway (1) and abnormal thalamocortical inputs that culminate in excessive movement generation (hyperkinetic disorder). Briefly, because of a reduction in GABA from putamen into GPe, tonic inhibition mediated from the GPi to the STN is enhanced, thus reducing the excitation from the STN to GPi. The diminished excitatory input to the GPi results in increased excitation to thalamus as well as the cortical receiving areas. The excitatory outputs are represented in green, whereas the inhibitory outputs are represented in red. The thickness of the arrow represents the strength of the output: the thicker, the higher the response. Coronal sections were obtained from (Vonsattel et al., 2011) and authorized by Elsevier (*attached*).

The most commonly used grading system to evaluate the severity of HD degeneration was developed by the neuropathologist Jean Paul Vonsattel at Columbia University in 1985 (Vonsattel et al., 1985). It is based on the pattern of striatal degeneration in a large number of *post mortem* tissues and classifies HD cases into five different severity grades (0–4). Grade 0, also termed presymptomatic, comprises less than 1% of all HD brains and appears indistinguishable from normal brains at first examination. However, 30–40% neuronal loss can be detected in the head of the caudate nucleus upon histological examination. Grade 1 comprises 4% of all HD brains. Neuronal loss involves the tail and body of the caudate nucleus, and dorsal portion of putamen. Moreover, 50% or greater loss of neurons is observed in the head of caudate

nucleus. Grade 2 comprises 16% of HD cases and, although striatal atrophy is presence, the ventricular profile of the caudate remains convex, but less so than in normal brain. The lateral half of the striatum shows relative preservation in both grades 1-2. Grade 3 displays severe striatal atrophy and the ventricular profile of the caudate is flat; it comprises 53% of HD cases (**Figure 1.2**). In grade 4, the striatum is severely atrophic, with approximately 95% caudate neurons loss, and the ventricular surface of the caudate is concave. Astrocytes are greatly increased above normal in HD grades 2-4. In at least 50% of grade 4 brains, the *nucleus accumbens* remains relatively preserved, but it cannot be considered normal (Reiner et al., 2011; Vonsattel et al., 1985, 2011).

The degree of striatal atrophy also correlates with the degeneration of other brain structures. In grades 1 and 2 nonstriatal structures are generally spared or show a slight atrophy, whereas in grades 3 and 4, the other structures that comprise basal ganglia, cerebral cortex (particularly layers III, V and VI), white matter and cerebellum can be markedly affected with superimposed morbidity [reviewed in (Vonsattel and DiFiglia, 1998)].

1.1.4. CLINICAL MANIFESTATIONS

HD patients express a triad of symptoms that include motor, behavioral and cognitive deficits, although the defining symptom has always remained that of chorea. Once the symptoms begin, they inevitable progress over the course of illness, which – with the exception of those patients with late-onset disease, who may die for other causes – is consistently fatal, with a median survival from motor onset of 18 years [reviewed in (Bates et al., 2015)]. Juvenile cases with age at onset below 20 years often progress faster, with death occurring 7 to 10 years after the onset of symptoms (Foroud et al., 1999). The cause of death is normally a consequence of cardiovascular disease or pneumonia, whereas suicide accounts for 5-6% of all deaths (Sørensen and Fenger, 1992).

Cognitive impairments emerge years before diagnosis of HD and the progression is gradual, later evolving to dementia; still, in early manifest HD significant rates of decline can be detectable over a year (Tabrizi et al., 2011). This is often characterized by executive dysfunction, especially early in the disease, but other cognitive domains are also affected, including learning and memory, motor planning and working memory. Patients with HD have problems in sustained attention and retrieval of established memory rather than formation of new memories, being generally classified as subcortical dementia syndrome [reviewed in (Ross et al., 2014a)]. Cognitive loss

often stands in the crossroads between cognitive and psychiatric domains, which include personality changes characterized by irritability, lack of awareness of deficits and disinhibition that justifies the sexual disturbances observed (Duff et al., 2010). Maniac-depressive behavior is typical and the proportion of HD patients endorsing significant depression diminish with disease progression (Paulsen et al., 2005).

The motor disorder can be divided into two prominent components – involuntary and voluntary movement disorders. Chorea and related involuntary movements such as tremors or tic-like movements, tend to be an early feature of HD. A second component of the motor disorder, termed “motor impairment” consists of voluntary movement deficits, including incoordination, orofacial dyskinesia, bradykinesia, motor sequencing difficulties and apraxia [reviewed in (Ross et al., 2014b)]. In juvenile HD, features such as bradykinesia, rigidity or dystonia may occur more frequently, while chorea may be completely absent. Patients with infantile age (earlier than 10 years of age), which occurs in 5% of all juvenile HD cases, may show particularly unusual clinical manifestations, namely autism, school performance decline and skeletal muscle spasticity, due to loss of inhibition of motor neurons causing excessive muscle contraction [reviewed in (Quarrell et al., 2013)].

A well-recognized but unexplained observation in HD patients is the relatively severe muscle wasting and progressive inability to maintain body weight, despite constant caloric intake (Hamilton et al., 2004). The reasons are not yet understood, but the high energetic demand during hyperkinetic state may lead to metabolic alterations. Results from patients’ biopsies reported myopathic changes such as angulated fibers, increased oxidative activities or increased number of enlarged mitochondria (Arenas et al., 1998). Growing evidence suggests that muscle cells are primarily damage by mutant HTT (mHTT) expression (Ciammola et al., 2006). Concordantly, myoblasts from presymptomatic HD patients showed defective differentiation and exacerbated apoptosis, which may be downstream effects of increased formation of HTT inclusions (Ciammola et al., 2006).

1.2. HUNTINGTIN PROTEIN

1.2.1. STRUCTURE, LOCATION AND FUNCTION

HTT is a soluble protein with approximately 3144 amino acids, depending on the exact number of glutamine (Q) residues, and has no similar sequence with other proteins (Faber et al., 1998). The N-terminal region of HTT has been extensively studied, as it contains the expanded polyQ domain, which is preceded by 17 amino acids and followed by a proline-rich domain (PRD). The first N-17 amino acids can form an amphipathic α-helix and functions as a nuclear export signal, whereas PRD has a rigid proline-proline helix that may be important for stabilizing the structure of the polyQ stretch. Additionally, the N-17 domain is subjected to various post-translational modifications (PTM) such as acetylation, sumoylation, ubiquitination and phosphorylation that affect the clearance of HTT and its subcellular location [reviewed in (Saudou and Humbert, 2016)]. Both polyQ stretch and the PRD are highly polymorphic in the human population. Downstream of exon 1 are a number of HEAT repeats that are 40 amino acid-long sequences that may act as a scaffold for numerous protein complexes and mediate inter- and intra-molecular interactions (Palidwor et al., 2009).

HTT expression is not confined to the brain regions that degenerate in HD. Northern blot analysis determined that HTT expression is ubiquitous; human HTT transcripts were found throughout the brain, with the highest expression levels in the neocortex, hippocampus (mainly in dentate gyrus and hippocampal pyramidal neurons), SN and cerebellum, followed by the striatum; and, in moderate amounts, in testes, liver, heart, lungs, muscle, kidney and pancreas (Li et al., 1993; Strong et al., 1993). Expression of HTT during development is vital since its knockout (KO) is lethal at embryonic day 8 (Duyao et al., 1995).

Intracellularly, HTT is detected in HD patient's and transgenic mouse brains predominantly as microscopic inclusion bodies in the nucleus or in perinuclear regions, imposing nuclear changes, including invaginations of the nuclear membrane and increased nuclear pore densities (Cooper et al., 1998b; Davies et al., 1997; DiFiglia et al., 1997). mHTT can also associate with a variety of membranous organelles, including mitochondria (Panov et al., 2002), endoplasmic reticulum (Atwal et al., 2007), endosomes (Kegel et al., 2000; Nath et al., 2015) and synaptic vesicles (Li et al., 2003; Suopanki et al., 2006).

Several studies have identified HTT protein-protein interacting network; more than 350 partners of wild-type HTT have now been identified by quantitative proteomics

(Kaltenbach et al., 2007; Ratovitski et al., 2012). Importantly, the extended polyQ domain modifies some of these interactions. The large list of HTT interactors support the idea that HTT is involved in several cellular pathways. Indeed, wild-type HTT has anti-apoptotic properties (Rigamonti et al., 2000, 2001), acts as a general facilitator of transcription (e.g. up-regulates transcription of brain-derived neurotrophic factor (BDNF), a pro-survival neurotropic factor) (Zuccato et al., 2001, 2003), coordinates cell division (Elias et al., 2014; Lopes et al., 2016), and plays an important role in endocytosis (DiFiglia et al., 1995; Velier et al., 1998), intracellular vesicle trafficking (Caviston and Holzbaur, 2009; Gauthier et al., 2004), membrane recycling (Hilditch-Maguire et al., 2000), mitochondrial bioenergetics (Ismailoglu et al., 2014) and selective macroautophagy (Rui et al., 2015). These broad range of coordinated cellular processes influenced by wild-type HTT translate in the regulation of important physiologic processes such as embryonic development and differentiation, tissue maintenance and cell morphology and, ultimately, neuronal survival.

1.2.2. LOSS-OF-FUNCTION / GAIN-OF-FUNCTION PARADING

Several studies have focused on identifying cellular cascade events promoted by mHTT expression that, ultimately, lead to neurodegeneration. mHTT is cleaved by proteases (Kim et al., 2001; Sun et al., 2002) generating N-terminal fragments containing the abnormal polyQ stretch that translocate and accumulate in the nucleus, interfering with transcription and causing neuronal cell death (Davies et al., 1997; DiFiglia et al., 1997; Steffan et al., 2000). Additionally, proteolysis may cause the loss of the wild-type HTT by inducing its cleavage (Goffredo et al., 2002). mHTT also forms aggregates, a pathological hallmark shared by all polyQ disorders, that were initially described to cause neurotoxicity. mHTT aggregates in the form of oligomeric species have been largely described to interfere with cellular functions, thereby causing cell death (Bates, 2003; Yang et al., 2002); on the other hand, mHTT inclusions were also described to be protective, as they sequester toxic soluble mHTT oligomers (Arrasate et al., 2004; Leitman et al., 2013) (**Figure 1.3**). This debate is complex as it is difficult to differentiate experimentally between the effects of large aggregates, oligomeric species and the dynamic aggregation process. It is possible that the cellular consequences of aggregates may vary according to the cell type or intracellular site of the aggregation; e.g. inclusion bodies accumulation may occur when the capacity of the ubiquitin-proteasome system (UPS) to degrade aggregation-prone HTT is exhausted (Waelter et al., 2001). Moreover, polyQ aggregates might sequester essential proteins, including transcription factors (Nucifora et al., 2001; Steffan et al., 2000), chaperones (Mitsui et al., 2002), proteasome

or other UPS components (DiFiglia et al., 1997; Donaldson et al., 2003), among others, suggesting that regulation of intranuclear neuronal inclusions is fundamental for HD pathogenesis. Interestingly, recent reports suggest that the spread of mHTT aggregates from one cell to another might be an important and underestimated contributor to the pathophysiology of HD (Cicchetti et al., 2014; Pecho-Vrieseling et al., 2014).

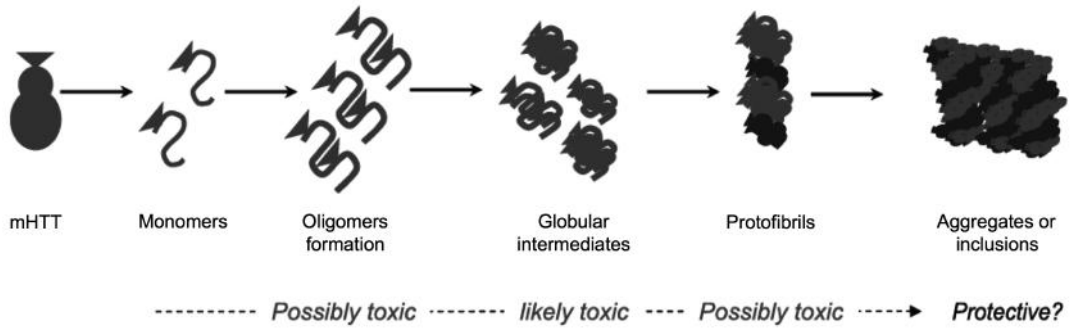

Figure 1.3 | Proposed model of polyQ aggregation in HD. The gain-of-function of mHTT is believed to occur after proteolytic cleavage to release short N-terminal fragments containing the expanded polyQ repeats. As the cleaved polyQ monomers increase, the structure compacts and oligomers or protofibrils rearrange to produce amyloid-like structures that result in aggregates or inclusions. These mHTT inclusions may not be pathogenic, but rather an attempt to sequester toxic soluble oligomers. Figure adapted from Zuccatto et al., 2010.

The current HD hypothesis suggests that the disease arises from the combined effect of a gain-of-function of mHTT along with a loss-of-function of wild-type HTT. In the preceding paragraph we describe several mechanisms that show a novel toxic gain-of-function of the mHTT; however alterations in normal endogenous HTT levels, which can occur due co-aggregation between wild-type and mutant HTT fragments (Busch et al., 2003), may also play a role in HD pathogenesis. The first evidence against a simple loss of normal HTT function in HD derived from the demonstration that deletion of a large portion of chromosome 4, which includes the *HTT* locus (in the Wolf–Hirschhorn syndrome), does not cause HD (Cattaneo et al., 2001). Nevertheless, most patients with this deletion do not survive long enough to develop HD. Also, the presence of the normal allele in pathological conditions does not improve the phenotype, since homozygous and heterozygous HD patients are indistinguishable (Squitieri et al., 2003). On the contrary, HTT KO mice has a lethal phenotype (Duyao et al., 1995) and mice with forebrain-specific HTT KO show progressive neurodegeneration that resembles HD (Dragatsis et

al., 2000). Other studies arguing that loss of HTT function could participate in the neurodegenerative process were obtained *in vitro*, in which wild-type protein overexpression (OE) reduced the polyQ toxicity induced by an exogenous mHTT construct (Ho et al., 2001). These few studies suggest that both gain-of-function and loss-of-function mechanisms co-exist and are not mutually exclusive, thereby adding some complexity to the potential molecular mechanisms underlying HD.

1.3. MODELING HUNTINGTON'S DISEASE

The British statistician George Box once said, "*All models are wrong, but some models are useful"*. The rationale behind modeling human disorders in non-human organism is the identification of central pathologic mechanisms that lead to novel therapeutic targets such as the data presented within this thesis. However, whether the current models accurately reproduce the human disease remains debatable. Several HD models have been created over time, expressing either truncated or full-length (FL) human, or mouse, mutant huntingtin, which culminates in different degrees of similarity to the human condition. Therefore, this section summarizes a few commonly used models in HD and the (dis)advantages of their use.

1.3.1. ANIMAL MODELS

1.3.1.1. Knock-in models of HD

Theoretically knock-in (KI) models should be the most faithful reproduction of human pathology since they express mutant huntingtin in an appropriate genomic and protein context. In general, these models show normal life span, develop more robust behavioral abnormalities at later stages and expression of aggregates more selectively localized in striatal neurons [reviewed in (Heng et al., 2008)]. HdhQ50 was the first KI model to be developed, carrying the most closely number of CAG repeats found in human HD. However, at six months of age no behavioral or pathological differences, compared to wild-type littermates, are observed (White et al., 1997). The HdhQ94 and HdhQ140 lines were further developed based on a gene target replacement of exon 1 of the mouse Htt homologue, *Hdh*, with a chimeric mouse/human exon 1 coding for approximately 94 or 140 CAG repeats. HdhQ94 mice present decreased locomotion at 4 to 6 months of age and nuclear Htt immunoreactive microaggregates in many striatal neurons. Only rare nuclear microaggregates are described in cortex at the same age. By contrast, nuclear inclusions are only observed when mice are older (Menalled et al., 2002). The HdhQ140 exhibit similar but more pronounced features; some Htt microaggregates are observed at 2 months, which is relatively early in the course of the disease, and footprint analysis reveal significant changes in mouse gait at 12 months of age (Menalled et al., 2003).

The HdhQ111 mice were also generated based on a chimeric human/mouse exon 1 construct expressing 111Q and it was subsequently used to create striatal lines with the same name (*described in section 1.3.2.1*). While no differences in rotarod are

present, very modest gait deficits are apparent, which occurs at 24 months of age in either heterozygous or homozygous KI mice. Heterozygous HdhQ111 mice display prominent nuclear Htt immunoreactivity at 5 months of age, whereas homozygous mutant mice exhibit nuclear Htt immunoreactivity from 1.5 months of age (Wheeler et al., 2000, 2002). Importantly, in all of these models evident neuronal loss is absent, even in older animals. As in human HD patients, this observation further suggests that neuronal dysfunction precedes cell death in HD and might be primarily responsible for early functional deficits.

In contract to the previous KI models, the $Hdh^{(CAG)150}$ mice is purely murine with approximately 150 CAG repeats inserted into the exon 1 of the murine Htt homologue (Lin et al., 2001). It exhibits an age-dependent late-onset phenotype with significant motor abnormalities at 70 and 100 weeks of age measured by rotarod, balance beam and clasping. The motor phenotype is preceded by striatal nuclear Htt inclusions that occur by 27 weeks of age. There is a significant weight loss by 70 weeks with continued weight reduction as disease progresses. Further analysis showed diminished striatal neuron number and increased gliosis (Heng et al., 2007; Lin et al., 2001), suggesting that this mouse model recapitulate key features of human HD pathogenesis.

1.3.1.2. Transgenic mouse models of HD

The first successful transgenic model of HD was generated by overexpressing exon 1 of human *HTT* gene with long CAG-repeat expansions (141-157), termed R6 mice (Mangiarini et al., 1996). Many lines were created and the most extensively studied is the R6/2. This mouse model displays an aggressive phenotype and requires clear experimental endpoints. Concisely, R6/2 mice exhibit behavioral deficits by 5 weeks, progressive brain and striatal atrophy (by about 40% reduction) and substantially reduced striatal neuron number by 12 weeks, culminating in death by 12 to 15 weeks of age (Mangiarini et al., 1996; Stack et al., 2005). Nuclear inclusions are present as early as postnatal day 1 in striatum and somatosensory cortex (Morton et al., 2000). This aggressive phenotype makes R6/2 mice, and other N-terminal fragment genetic models (e.g. N171-82Q transgenic mice (Schilling et al., 1999)), very useful for therapeutic research because the outcomes are more prevalent and definable, however it is not an exact genetic or neurophatological analogue of adult-onset HD.

From then on several mouse models have been generated using a FL human *HTT* gene as a transgene. Mice expressing the FL *HTT* cDNA clone with either 48 or 89 CAG repeats associated with a cytomegalovirus (CMV) promoter show progressive

motor phenotype and, most important, neuronal loss in the striatum, compared with control mice expressing 16 CAG repeats. Nevertheless, nuclear inclusions are extremely rare (Reddy et al., 1998, 1999b). A series of yeast artificial chromosome (YAC) transgenic models of HD expressing human FL-HTT with 18, 46, 72 and 128 CAG repeats were further created and characterized by the Hayden laboratory. These YAC models were generated after microinjection of YAC DNA construct into the friend leukemia virus B NIH strain (FVB/N) pronuclei and maintained on an inbred FVB/N background strain (Hodgson et al., 1999; Slow et al., 2003). The human *HTT* expressed from these transgenes can rescue the embryonic lethality of the mouse *Hdh* KO, indicating appropriate developmental regulation of the transgene during mouse development (Hodgson et al., 1996). Of them all, the YAC128 model is especially interesting due to its pattern of HTT expression (~75% of the levels of endogenous murine *Hdh*) and neuronal loss mainly confined to the striatum that closely resembles the human disease. YAC128 mice exhibit motor abnormalities as early as 3 months with increased open field activity (hyperkinetic state), followed by rotarod performance abnormalities at 6 months. Behavioral deficits are progressive and by 12 months, open filed activity is significantly diminished (hypokinetic state) in comparison with wild-type mice (Van Raamsdonk et al., 2005a; Slow et al., 2003) (**Figure 1.4**). Contrary to what happens in HD patients and other transgenic models (e.g. R6/2), YAC128 mice have increased body weight represented by an increase in both fat mass and fat-free (lean) mass (Van Raamsdonk et al., 2006). The increase in body weight may be a consequence of the FVB background, since backcrossing YAC128 mice from FVB/N strain onto two other distinct stains (C57BL/6 or 129) revealed no alterations in body weight (Van Raamsdonk et al., 2007a). Additionally, chimeric FL transgenic BACHD, another HD model expressing 97 CAGs with FVB background, also exhibit increased body weight, corroborating the previous hypothesis (Gray et al., 2008). Neuropathological examination of YAC128 mice shows the presence of HTT immunoreactivity at 1-2 months, HTT macroaggregates starting at 12 months, which increase in number up to 18 months, decreased striatal and cortical volume and modest reduction (approximately 15%) in striatal neurons by 12 months of age (Van Raamsdonk et al., 2005b, 2007b) (**Figure 1.4**). In accordance, striatal MSNs are highly vulnerable to activation of a subtype of the glutamate receptors, the *N*-methyl-D-aspartate receptors (NMDAR), which mediate cell death in these mice (Fernandes et al., 2007; Graham et al., 2009; Pellman et al., 2015). Unlike the R6/2 mice, other brain areas, such as cerebellum and hippocampus, exhibit normal volume in YAC128 mice (Van Raamsdonk et al., 2005a).

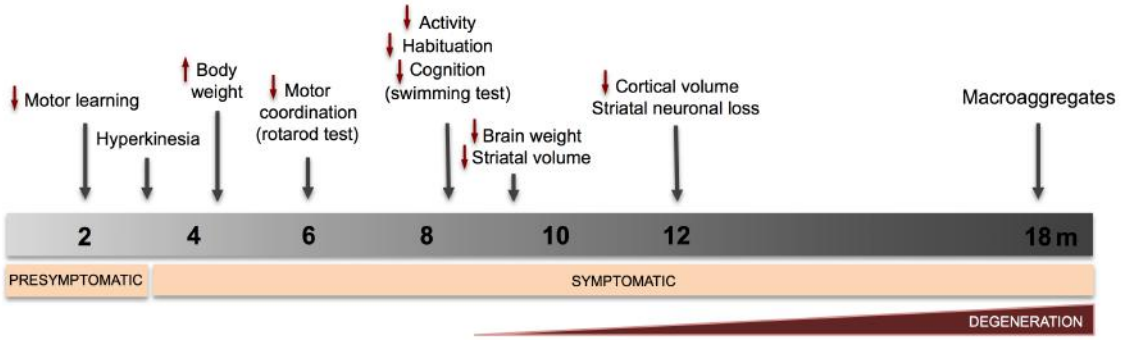

Figure 1.4 | Evolution of phenotypical abnormalities in YAC128 along aging. At 2 months (m) of age, YAC128 mice show motor learning deficits on the rotarod test. At 3 months of age, YAC128 mice exhibit increased open field activity (hyperkinetic state), followed by rotarod performance abnormalities at 6 months. Increased body weight occurs after 4 to 6 months of age. Between 8 and 9 months, YAC128 show cognitive and motor deficits in swimming tests and decreased activity and habituation in open field test. At 9 months, neuropathology becomes apparent with decreased brain weight and striatal atrophy. Cortical atrophy is only observed by 12 months of age. At 18 months macroaggregates become visible.

1.3.2. CELLULAR MODELS

1.3.2.1. Neuronal-like cell models

Cellular models have limited biological complexity for drug discovery requiring validation in more complex models, however they brought important contributions to knowledge on the molecular signaling mechanisms underlying the disease. The first model not based on transient transfections was the pheochromocytoma PC12 cell model expressing the N-terminal portion of the human HTT, containing 20Q or 150Q. PC12 cells differentiate into neuronal-like cells in the presence of nerve growth factor, and the HTT-150Q protein is predominantly present in the nucleus, suggesting an influence on gene transcription, making mutant cells more susceptible to apoptotic stimulation (Li et al., 1999). Although this model has presented relevant data, selection of PC12 subclones generated multiple phenotypes, imposing the screening of a large number of colonies to validate the results. Additionally, PC12 cells have a tumoral origin and the genetic events that lead to their continuous growth are unknown. Therefore, immortalized cell lines, which offer the possibility of being derived from different brain regions, were created. ST14A cells were obtained from embryonic day 14 rat striatal primordia by retroviral transduction of the temperature-sensitive SV40 large T antigen and, contrarily to PC12 cells, can generate subclones that maintain the properties of the original line (Cattaneo et al., 1994). ST14A cells show biochemical properties found in striatal MSNs (e.g. DARPP-32 expression, and D1- and D2-like receptor activities)

(Ehrlich et al., 2001) and expression of FL-mHTT makes them more sensitive to pro-apoptotic stimuli (Rigamonti et al., 2000). Further advance in HD modeling was based on the conditional immortalization of striatal cells obtained from murine HD models. This is the case of immortalized wild-type or homozygous mutant progenitor striatal cells that express endogenous normal/wild-type Htt (expressing 7Q) or mHtt with 111Q derived from E14 striatal primordia of wild-type or Hdh^{Q111} KI littermate embryos, respectively, using the same strategy as used to generate ST14A cells (Trettel et al., 2000). This is the only cell model in which mutant protein is expressed at physiological level, making it the most attractive cell line model in HD up-to-date. ST*Hdh*$^{Q111/Q111}$ striatal cells represent early phases of HD pathogenesis since they derived from the embryonic phase of the Hdh KI mice and present no visible Htt aggregates (Trettel et al., 2000). ST*Hdh*$^{Q111/Q111}$ striatal cells exhibit a significant decrease in Htt protein and mRNA levels (Naia et al., 2016), and although this chimeric human-mouse Htt shares properties of the normal protein, it may elicit eventual striatal cell toxicity *via* a mechanism that is distinct from its ordinary activity. Our group has been extensively studying this cell model. It is selectively vulnerable to 3-nitropropionic acid (3-NP, an irreversible inhibitor of mitochondrial complex II) and staurosporine (a generalized kinase inhibitor and apoptotic inducer), exhibiting several apoptotic features, such as increased caspase-3 activation and DNA fragmentation (Rosenstock et al., 2011). ST*Hdh*$^{Q111/Q111}$ striatal cells also show high levels of mitochondrial reactive oxygen species (ROS), and decreased general mitochondrial function that culminates in increased mitochondrial fission and fission-related proteins (Carmo, 2015; Ribeiro et al., 2012, 2013, 2014). Therefore, ST*Hdh*$^{Q111/Q111}$ striatal cells represent a reliable HD model to study mHtt-induced cytotoxicity in the striatum in early stages of the disease.

1.3.2.2. Peripheral cell models

Numerous reports had described abnormalities in the peripheral tissues of HD patients including weight loss, altered glucose homeostasis, and sub-cellular abnormalities in fibroblasts, lymphoblasts and platelets. In fact, mHTT nuclear inclusions are observed in a wide range of non-central nervous system (CNS) tissues (Moffitt et al., 2009). HD lymphoblast cell lines share several abnormalities related to mHTT expression, such as mitochondrial and metabolic dysfunction, increased apoptosis and transcriptional abnormalities (Naia et al., 2015; Sassone et al., 2009). B lymphocytes from HD patients also showed increased markers of apoptotic cell death (Almeida et al., 2008). Access to peripheral human models facilitates the comparison between molecular

mechanisms in presymptomatic and symptomatic HD patients. Interestingly, reduced mitochondrial complex I activity was observed in platelets from both presymptomatic and symptomatic HD carriers (Parker et al., 1990; Silva et al., 2013), corroborating previous evidence that mitochondrial changes occur before the onset of HD clinical symptoms.

Construction of cybrid cell lines is also an invaluable method to study fundamental aspects of mitochondrial-related disorders such as HD. There are some approaches to create cybrid lines. The most commonly used technique involves the transfer of mitochondria from non-nucleated cells (usually platelets) to ρ^0 cells (in which resident mitochondria have been made unfunctional by targeting mitochondrial DNA (mtDNA)), resulting in cybrids containing nuclear DNA from ρ^0 cells and mtDNA from patients' or donors' platelets (Chomyn et al., 1994). Following this line of research our group has shown that HD cybrids (expressing 42 to 44Q) heighten vulnerability to 3-NP, exhibiting increased oxidative stress and mitochondrial-dependent cell death by apoptosis, when compared with control cells (Ferreira et al., 2010). Previous untreated HD cybrid lines were indistinguishable from control cybrids on electron transport chain activity, oxidative stress and calcium (Ca^{2+}) homeostasis assays (Swerdlow et al., 1999), suggesting that the effects observed in these lines largely depend upon the characteristics of patients' samples and controls used for generating this model, as well as toxic stimuli to which it is subjected.

1.4. MECHANISMS OF NEURODEGENERATION: NUCLEUS - MITOCHONDRIA CROSSTALK

Given the diversity of HTT interactome, it is not surprising that a wide-scale destabilization of multiple cellular processes occurs in the presence of expanded polyQ. They encompass transcription deregulation, NMDARs-mediated excitotoxicity that further leads to Ca^{2+} dyshomeostasis, abnormal mitochondrial function, dynamics and clearance (mitophagy), oxidative stress, deficient axonal transport and neurotrophic factors supply (e.g. BDNF), UPS inhibition, and others [reviewed in (Brett et al., 2014; Gil and Rego, 2008; Labbadia and Morimoto, 2013)]. The majority of these pathogenic events are interconnected. However, the directionality and sequence in which they occur is still poorly understood. Two decades of research point to mitochondria and mitochondria-related events as central players in HD neurodegeneration. On the other hand, mitochondrial deficits may occur due to aberrant transcriptional regulation of nuclear-encoded mitochondrial proteins evoked by mHTT nuclear aggregates. Within this section the interplay amongst nuclear transcription and mitochondrial dysfunction is discussed.

1.4.1. TRANSCRIPTIONAL DEREGULATION

The first evidence indicating the disruption of transcriptional pathways in HD came from *in situ* hybridization studies on *postmortem* human HD brains showing that some mRNA species encoding for signaling neuropeptides and neurotransmitter receptors (e.g. enkephalin, substance P and D1 and D2 dopamine receptors) were specifically decreased in striatal neurons (Augood et al., 1996; Weeks et al., 1996). Later, Luthi-Carter *et al.* published the first study using DNA microarrays to measure gene expression in the striatum of R6/2 mice. Six thousands genes were analyzed but only a small number (approximately 1.7%) were found decreased, which comprised genes encoding neurotransmitters, Ca^{2+} and retinoid signaling pathway components (Luthi-Carter et al., 2000). These abnormalities in transcription were further demonstrated to be an early event in HD pathology and observed across multiple HD models (Cha et al., 1998; Luthi-Carter et al., 2000; McFarland et al., 2012; Wyttenbach et al., 2001).

In general, chromatin remodeling is altered in HD, with a pattern of hypoacetylated (particularly histone H3 at lysine (Lys, K) 9 and 14 – AcH3K9K14) and hypermethylated (particularly at MeH3K9) histones [reviewed in (Lardenoije et al.,

2015)]. The mechanism underlying histone hypoacetylation has been fairly well characterized and is thought to be triggered by deleterious interaction of mHTT with cyclic adenosine monophosphate (cAMP)-response element binding protein (CREB) binding protein (CBP) and the related co-activator p300. The polyQ stretch was found to physically interact and sequester CBP, hampering its histone acetyltransferase activity (Cong et al., 2005; Nucifora et al., 2001; Steffan et al., 2000) (**Figure 1.5, panel A**). In fact, polyQ repeats at the N-terminal region of HTT protein gives it structural similarities to known transcription factors and co-activators (Gerber et al., 1994). TATA-binding protein (TBP), TBP-associated factor TAFII130 and the pro-apoptotic transcription factor p53 are some examples of mHTT interactions [reviewed in (Sugars and Rubinsztein, 2003)]. PolyQ stretches specifically bind TAFII130, a co-activator that is involved in CREB-dependent transcription activation, impairing its association with specific protein-1 (Sp1), and directly interfering with the binding of Sp1 to DNA (Dunah et al., 2002; Shimohata et al., 2000) (**Figure 1.5, panel A**). In agreement with reduced CBP, the expression of CREB/CBP target genes related to memory were found significantly reduced in the hippocampus of heterozygous HdhQ111 mice, leading to long-term memory deficits (Giralt et al., 2012). Additionally, CREB KO mice develop HD-like phenotype with progressive neurodegeneration in the hippocampus and dorsolateral striatum (Mantamadiotis et al., 2002). In turn, the suppression of CREB-dependent transcription and cell death induced by polyQ stretches were restored by the co-expression of TAFII130 (Shimohata et al., 2000). Co-expression of Sp1 and TAFII130 in HD striatal cells also reversed the transcription inhibition of the dopamine D2 receptor gene and protected neurons from mHTT-induced cellular toxicity (Steffan et al., 2000).

Another mHTT-mediated effect on gene expression was observed by Cattaneo's group. In a paper published in *Science* the authors showed that transcriptional regulation of BDNF, a neurotropic factor expressed by cortical neurons, which project to the striatum and is critical for striatal survival, is severely altered in HD (Zuccato et al., 2001). In cytosol, wild-type HTT interacts and sequesters RE1-silencing transcription factor (REST), a potent transcriptional repressor of BDNF and other neuronal survival factors. However, mHTT fails to interact with REST, increasing its nuclear translocation and consequent BDNF downregulation in striatum, worsening the HD phenotype (Strand et al., 2007; Zuccato et al., 2001, 2003). This is one case where the loss-of-function of wild-type HTT function directly correlated with HD pathogenesis. In turn, BDNF OE in YAC128 mice normalized expression of the striatal dopamine receptor D2 and enkephalin, thereby preventing loss and atrophy of striatal neurons and motor dysfunction (Xie et al., 2010).

1.4.1.1. Mitochondrial biogenesis-related transcription

Studies with peroxisome proliferator-activator receptor γ (PPARγ) coactivator-1α (PGC-1α) were the first to support a mHTT-mediated gene repression resulting in HD-linked mitochondrial dysfunction. PGC-1α is a transcriptional co-activator that orchestrates mitochondrial function through regulation of mitochondrial respiration and biogenesis (Chaturvedi et al., 2009), oxidative stress (St-Pierre et al., 2006; Tsunemi et al., 2012) glucose and fatty acid metabolism (Gerhart-Hines et al., 2007), and adaptive thermogenesis (Uldry et al., 2006). Involvement of PGC-1α in HD was first anticipated by the finding that PGC-1α KO mice exhibit mitochondrial dysfunction, defective bioenergetics and striatal degeneration, features also observed in HD (Lin et al., 2004). But it was two years later that two distinct groups documented, almost simultaneously, that mHTT repressed PGC-1α gene transcription in HD patients and in HD N171-82Q mice striatum by associating with the promoter and interfering with the CREB/TAF4 (TBP-associated factor 4)-dependent transcriptional pathway, critical for the regulation of PGC-1α gene expression (Cui et al., 2006; Weydt et al., 2006) (**Figure 1.4, panel A**). Resultant crossbreed of PGC-1α KO mice with HD KI HdhQ140 mice showed increased neurodegeneration of striatal neurons and motor abnormalities. Moreover, expression of both PGC-1α and mitochondrial electron transport-chain genes such as cytochrome *c* (cyt *c*) and mitochondrial complex IV subunit COXIV were shown to be significantly decreased in ST*Hdh*$^{Q111/Q111}$ cells (Cui et al., 2006). Microarray expression data from *postmortem* caudate of HD patients also showed a reduction in expression of 24 out of 26 PGC-1α target genes, most of them belonging to oxidative phosphorylation (OXPHOS, in short) (Weydt et al., 2006). Decreased expression of mitochondrial genes occurs along with evidences of mitochondrial loss (Kim et al., 2010). Mitochondrial biogenesis is regulated by PGC-1α because it forms heteromeric complexes with transcription factors, including nuclear respiratory factors, NRF-1 and NRF-2, or nuclear receptors PPARα, PPARδ, PPARγ**,** that in turn regulate the expression of complexes I-V, electron carrier proteins and the mitochondrial transcription factor A (TFAM), a DNA-binding protein that activates transcription at the two major promoters of mtDNA and is diminished in HD (Chaturvedi et al., 2010; Gleyzer et al., 2005). Consistently, exogenous expression of PGC-1α rescued mitochondrial membrane depolarization evoked by 3-NP in ST*Hdh*$^{Q111/Q111}$ cells and prevented neurodegeneration in R6/2 mice (Cui et al., 2006; Weydt et al., 2006). Concomitant with the increase in PGC-1α is an increase in ROS scavenging enzymes, such as Cu/Zn-superoxide dismutase 1 (SOD1) and Mn-

superoxide dismutase 2 (SOD2), catalase and glutathione peroxidase (GPx) [reviewed in (Johri and Beal, 2012)], counterposing the harmful effects of oxidative stress.

Collectively, these data established a direct link between transcription inhibition and mitochondrial dysfunction in HD. Nevertheless, they cannot entirely explain all the mitochondrial deficits observed in HD models, such as mHTT binding to mitochondria, mtDNA deletions or Ca^{2+} dyshomeostasis in isolated mitochondria, detailed below.

1.4.2. MITOCHONDRIAL DYSFUNCTION

Mitochondria are double-membrane organelles that represent the major bioenergetic hub coordinating cell and organism homeostasis. Mitochondria control the production of energy (in the form of adenosine triphosphate, ATP) through OXPHOS, supporting the biosynthetic and degradative metabolic requirements of the cells, intracellular Ca^{2+} homeostasis, apoptotic and cell signaling pathways, among other cellular processes. The sustained integrity of mitochondria is critical for preserving cell viability; therefore, mitochondrial dysfunction is a common process connecting several age-related and neurodegenerative disorders such as HD (Chaturvedi and Beal, 2013), either due to defects in respiratory function and metabolism, modified organelle dynamics and degradation, or leading to DNA and protein damage and/or producing excessive amounts of ROS.

1.4.2.1. mHTT interaction with mitochondria

Early evidence of mitochondrial defects in HD came from a study demonstrating ultrastructural abnormalities in mitochondria isolated from *postmortem* HD cortical tissue (Goebel et al., 1978). However, the mitochondrial hypothesis only gained strength in HD when Flint Beal's group showed that systemic administration of mitochondrial complex II inhibitors (3-NP and malonate) produced preferential degeneration in the caudate–putamen that resembled many behavioral and anatomical features of HD (Beal et al., 1993). This study was subsequently confirmed by other research groups (Brouillet et al., 1995; Kodsi and Swerdlow, 1997). A few years later, mHTT was shown to directly interact with the mitochondrial outer membrane (MOM) (Choo et al., 2004; Panov et al., 2002; Song et al., 2011), triggering Ca^{2+} release and abnormal mitochondrial morphology and trafficking, as shown in *postmortem* HD patient's brain specimens, in human HD lymphoblasts or mice neurons expressing the expanded exon 1 of *HTT* (Napoli et al., 2013; Song et al., 2011; Squitieri et al., 2006). Association of HTT with mitochondria was

also observed in cells transfected with N-terminal HTT fragments containing either 23Q or 120Q. However, only mutant fragments interfere with the association of trafficking proteins with mitochondria (Orr et al., 2008). Furthermore, interaction of N-terminal fragments of mHTT with the translocase of the inner membrane TIM23 was shown recently, culminating in the inhibition of protein import machinery and neuronal death. Mitochondria from brain synaptosomes of presymptomatic HD mice also exhibited a protein import defect, but not liver mitochondria, suggesting an early and tissue-specific event of the disease (Yano et al., 2014).

1.4.2.2. Abnormal mitochondrial membrane potential and impaired respiratory chain complex activity

Electron flow along the respiratory complexes, localized at the mitochondrial inner membrane (MIM), is coupled to proton translocation into the mitochondrial intermembrane space (MIS), creating an electrochemical proton gradient (proton motive force) and thus a mitochondrial transmembrane potential ($\Delta\psi_m$) of -150 to -180 mV that drives ATP synthesis. This energy production requires $\Delta\psi_m$ to be maintained at 80-90% of its maximum value [reviewed in (Nicholls and Ward, 2000)]. However, in HD mitochondria this percentage is not preserved. Concordantly, brain mitochondria isolated from two lines of YAC72 mice expressing “low” and “high” levels of FL-mHTT displayed depolarized membrane, with mitochondria from YAC72 high expressor depolarizing faster after Ca^{2+} stimulation (Panov et al., 2002). Similar defect in $\Delta\psi_m$ was found in mitochondria from chimeric human-mouse mHTT-expressing cells in response to increasing Ca^{2+} concentrations (Milakovic et al., 2006). Remarkably, a large amount of evidence has shown that HD mitochondria from human lymphoblasts are highly susceptible to decreased $\Delta\psi_m$ (Naia et al., 2015; Panov et al., 2002), which was correlated with increased glutamine repeats (Sawa et al., 1999), suggesting that the adverse effect of mHTT is not limited to neurons. In agreement, results obtained in our laboratory in symptomatic HD cybrids *versus* control cybrids and in HD human B-lymphocytes evidenced significant changes in $\Delta\psi_m$ linked to apoptotic events (Almeida et al., 2008; Ferreira et al., 2010). Interestingly, constitutive HTT phosphorylation at serine 421 completely abrogated the deregulation in $\Delta\psi_m$ in HD lymphoblasts (Naia et al., 2015), linking the neuroprotective effects of HTT phosphorylation in this residue [e.g. (Humbert et al., 2002)] to improved mitochondrial function.

Deficiency of mitochondrial respiratory chain complexes may account for altered $\Delta\psi_m$. *Postmortem* studies in the striatum of symptomatic patients showed marked

deficiency in activities of complexes II/III and mild reduction in complex IV (Gu et al., 1996; Tabrizi et al., 1999). Accordingly, expression of two subunits of complex II, iron-sulfur 30 kDa subunit Ip and FAD containing catalytic 70 kDa subunit Fp, were found to be decreased in the striatum of HD patients, compared with control subjects, affecting its dehydrogenase activity (Benchoua et al., 2006). Decreases in state 3 respiration were associated with increased mitochondrial membrane permeability (Milakovic et al., 2006). Although complex I activity is relatively spared in HD patients brain, deficits in complex I have been described in peripheral tissues from HD patients, such as platelets (Parker et al., 1990), as described previously, and skeletal muscle (Arenas et al., 1998). Nevertheless, this subject has always produced contradictory data (Ferreira et al., 2010; Naia et al., 2015; Sawa et al., 1999; Turner et al., 2007). Conflicting results were also observed in animal models. Significant reduction was found in respiration of succinate-fueled striatal mitochondria from N171-98Q mice, compared with wild-type littermates, suggesting complex II impairment (Kim et al., 2011a). However, no significant alterations were found in measurements of complexes I-IV activities and expression in the striatum and cerebral cortex of R6/2 and YAC128 HD transgenic models (Guidetti et al., 2001; Hamilton et al., 2015, 2016). Therefore, it is not clear whether this mitochondrial defect contributes to HD pathogenesis or if it is a consequence of late stage HD neurodegeneration.

1.4.2.3. Mitochondrial calcium mishandling

The MIM possesses a Ca^{2+} uniporter (the MCU, mitochondrial calcium uniporter), providing cells with a protective high capacity for Ca^{2+} buffering. Moreover, interaction of mHTT with the MOM may induce the opening of a high conductance pathway, the mitochondrial permeability transition pore (mPTP), which is triggered by Ca^{2+}, ROS or decreased adenine nucleotide levels, causing mitochondrial swelling, depolarization and, eventually, cell death (Choo et al., 2004; Milakovic et al., 2006; Panov et al., 2002) (**Figure 1.5, panel B**). Thus, deficits in mitochondrial Ca^{2+} handling likely contribute to HD neurodegeneration. An early study by Panov *et al.* showed that when challenged repeatedly with Ca^{2+}, lymphoblast mitochondria from adult-onset cases of HD depolarized more promptly for lower Ca^{2+} loads, when compared to control mitochondria. Interestingly, the mitochondrial buffering capacity from juvenile-onset cases was largely inferior from that of adult-onset or control mitochondria (Panov et al., 2002). The authors observed similar defects in brain mitochondria from HD transgenic mice expressing FL-mHTT with 72 glutamines that preceded the onset of motor abnormalities (Panov et al., 2002). Importantly, this effect could be delayed with

cyclosporin A (CsA) and ADP, both used to inhibit the mPTP, supporting the hypothesis that mPTP opening may be important to this phenomenon (Quintanilla et al., 2013). Later, the same authors (Panov et al., 2003) hypothesized that polyQ tracts might form proton-selective ion channels in the mitochondrial membrane, as previously observed in artificial lipid bilayer membranes incubated with long-chain polyQs (Monoi et al., 2000), dissipating the electrochemical proton gradient across the MIM that would reduce ATP production. These results were subsequently corroborated by Choo *et al.* that observed that truncated HTT dramatically decreased the Ca^{2+} threshold required to induce the mPTP opening, which was accompanied by cyt *c* release (Choo et al., 2004). Years later we failed to detect Ca^{2+} handling abnormalities in isolated nonsynaptosomal mitochondria from HD *Hdh*150 KI mice (Oliveira et al., 2007). Similar results were obtained recently in nonsynaptic mitochondria isolated from R6/2 mice (Hamilton et al., 2016). Synaptosomal mitochondria have a higher content on cyclophilin D (CypD), a matrix modulatory component of mPTP, compared to nonsynaptosomal mitochondria (Naga et al., 2007). Thus, isolated nonsynaptosomal HD mitochondria could be more resistance to Ca^{2+} challenges. Assessment of *in situ* mitochondria function using intact *Hdh*Q150 striatal neurons showed a failure to reestablish Ca^{2+} homeostasis following NMDARs activation in HD neurons, when compared with wild-type neurons (Oliveira et al., 2007), corroborating the importance of assessing mitochondrial function in the appropriate cellular context.

Although quite well established, existing data implicating mitochondrial Ca^{2+} mishandling in HD pathology was not always consistent. In 2005, Brustovetsky *et al*. described that mitochondria isolated from Q92 KI young adult mice with 5 months of age showed the same pattern of striatal sensitivity to Ca^{2+} than wild-type mitochondria. Interestingly, striatal mitochondria isolated from the same mouse model with one year of age were shown to be more resistant to Ca^{2+}-induced depolarization (Brustovetsky et al., 2005). Similar results were achieved using striatal mitochondria from 8 and 12 week-old HD *Hdh*150 KI mice (Brustovetsky et al., 2005) or 2 and 12 month-old YAC128 mice (Pellman et al., 2015). In fact, we had already observed this increase in Ca^{2+} loading capacity in isolated mitochondria from symptomatic 12-13 week-old R6/2 mice and 12 month-old YAC128 mice (Oliveira et al., 2007). The latest evidence suggested that the increase in Ca^{2+} uptake capacity with age was correlated with increased mHTT associated with mitochondria (Pellman et al., 2015). Due to the large amount of glutamines it is feasible that mHTT may interact and potentially sequester free fatty acids, known to induce the mPTP (Di Paola and Lorusso, 2006), thereby increasing Ca^{2+} uptake capacity and casting doubt on the previous Panov's hypothesis. Apart from

mitochondrial mHTT accumulation, continuous exposure to low levels of excitotoxicity and changes in cytosolic Ca^{2+} concentrations may have allowed neurons to adapt to an even greater excitotoxic stimulus, as proposed by Brustovetsky and co-authors (Brustovetsky et al., 2005). Thus, increased striatal mitochondria Ca^{2+} uptake may reflect a compensatory adjustment to augmented Ca^{2+} influx through NMDARs activation or increased Ca^{2+} released from endoplasmic reticulum.

1.4.2.4. Imbalanced mitochondrial dynamics

Recent advances on neuroscience field have highlighted that neurons are particularly dependent on the dynamic properties of mitochondria. Mitochondria are highly dynamic organelles that modulate their shape and structure by two important and opposing forces – mitochondrial fission and mitochondrial fusion, which serve to intermix the contents of a population of mitochondria. In addition, mitochondria are actively recruited to subcellular sites, such as axons and dendrites to provide ATP to the synapse. Lastly, defective mitochondria is degraded by a selective form of autophagy, named mitophagy [reviewed in (Chen and Chan, 2009)] (**Figure 1.5, panel D**).

Mitochondrial fission and fusion are controlled by large GTPases belonging to the family of dynamin. Mitochondrial fission is regulated by mitochondrial fission 1 (Fis1), located in MOM, and dynamin-related protein 1 (Drp1), which is localized in the cytosol but can translocate to the MOM triggering mitochondrial fragmentation (Smirnova et al., 1998; Stojanovski et al., 2004). Mitochondrial fusion is controlled by two outer membrane proteins, mitofusin 1 and 2 (Mfn1 and Mfn2, respectively), which oligomerize through their C-terminal to adjacent mitochondria facilitating fusion, and one inner membrane protein optic atrophy 1 (Opa1) (Song et al., 2009). Increasing evidence suggests that mitochondrial dynamics is imbalanced in HD, which can occur in part by dissipation of $\Delta\psi_m$ (Legros et al., 2002) (**Figure 1.5, panel D**). Increased expression of Drp1 and Fis1 and decreased expression of Mfn1/2 and Opa1 were found in frontal cortex sections from grade III/IV HD patients, relative to the controls. These altered expression were further correlated with progressive grade-dependent mitochondrial loss in striatal MSNs (Kim et al., 2010; Shirendeb et al., 2011). Additionally, mitochondrial PCR array in HD caudate nucleus specimens showed increased transcript expression of proteins involved in mitochondrial localization, membrane translocation and transport that paralleled mitochondrial imbalance reflecting, at some degree, compensatory mechanisms (Kim et al., 2010). Mitochondrial fragmentation and cristae derangement were also observed in HD lymphoblasts and in striatal precursors expressing 111 glutamines (Costa et al., 2010). Indeed, mHTT abnormally interacts with Drp1, stimulating its enzymatic activity

and triggering mitochondrial fragmentation even before the presence of neurological deficits and the formation of HTT aggregates (Song et al., 2011). The reduction of its GTPase activity, in turn, rescued defects in anterograde and retrograde mitochondrial transport and neuronal death (Song et al., 2011). In a *Caenorhabditis elegans* model of HD, reduction of Drp1 expression rescued the motility defect associated with the expression of polyQ repeats (Wang et al., 2009).

Mitochondrial fusion and fission is directly correlated to their motility. Defective axonal transport of mitochondria is observed in few HD models both *in vivo* and *in vitro*, resulting in accumulation of the organelle in the soma (Orr et al., 2008; Trushina et al., 2004). These defects appear to occur prior to the onset of measurable neurological or mitochondrial abnormalities. Although the mechanisms remain uncertain, the interaction of soluble N-terminal polyQ fragments with mitochondria may interfere with the association of microtubule-based transport proteins with mitochondria (Orr et al., 2008). These transport proteins belong to two superfamilies of opposing motors, kinesins (mediators of mitochondrial anterograde transport) and dyneins (mediators of mitochondrial retrograde transport) (**Figure 1.5, panel D**). TRAK1 and TRAK2 (trafficking protein, kinesin-binding) and Miro (mitochondrial Rho) have been implicated as adaptors coupling mitochondria to the kinesin-dependent transport pathway [reviewed in (Birsa et al., 2013)]. Such proteins are also implicated in autophagosome dynamics along the microtubules. Normal HTT was recently shown to regulate autophagosome transport by binding to dynein and Huntingtin-Associated Protein 1 (HAP1) (Wong and Holzbaur, 2014). Indeed, HTT may serve as a scaffold protein for selective autophagy, including mitophagy (Rui et al., 2015). Therefore, HTT depletion leads to accumulation of autophagosomes with undegraded mitochondrial cargo. Similarly, mHTT prompted inefficient degradation of engulfed mitochondria and accumulation of polyQ aggregates (Wong and Holzbaur, 2014).

1.4.2.5. Energy metabolic deficit

Neurons are highly dependent on mitochondrial ATP production to maintain normal synaptic communication. Therefore, they are very sensitive to disturbed energy metabolism. A number of studies, from HD *postmortem* brains (Mochel et al., 2012a) to transgenic HD mouse brain (Lopes et al., 2014; Mochel et al., 2012b), revealed mHTT-related abnormal ATP/ADP and phosphocreatine/inorganic phosphate (PCr/Pi) ratios and energy charges. This reduction in mitochondrial ATP levels might be linked to increased Ca^{2+} influx through NMDARs, since ATP/ADP ratio could be normalized by blocking Ca^{2+} influx in mHTT-expressing striatal cells (Seong et al., 2005). Moreover, a

poor creatine kinase/phosphocreatine system in HD brain might also contribute for this reduction (Zhang et al., 2011) (**Figure 1.5, panel C**). As described before for changes in $\Delta\psi_m$, bioenergetic defects in HD were not solely confined to the brain, but were also observed in peripheral tissues, such as muscle (Lodi et al., 2000; Saft et al., 2005) or lymphoblasts (Seong et al., 2005). These findings raise the possibility that the ubiquitous expression of mHTT may place other cell types at risk, particularly those with high metabolic demand. Remarkably, recent studies conducted in our laboratory showed that glucose deprivation did not exacerbate the defects in ATP/ADP ratio in cortical primary cultures derived from YAC128 mice, contrarily to wild-type neurons, pointing to an abnormal glycolytic pathway linked to deficient ATP generation (Naia et al., 2016). Studies on mitochondrial oxidative metabolism in presymptomatic and symptomatic HD patients previously detected selective defect in glycolysis in early HD striatum (Antonini et al., 1996; Mazziotta et al., 1987; Powers et al., 2007), suggesting that metabolic deficits in HD may precede neuropathology and clinical symptoms. Glyceraldehyde-3-phosphate dehydrogenase (GAPDH) has an essential function in glycolysis, binding both normal and mHTT, but with a preferential interaction to cleaved polyQ domain, enhancing nuclear translocation of mHTT and cytotoxicity (Burke et al., 1996). Interestingly, studies using an allelic series of murine CAG KI embryonic stem cell lines have shown dominant CAG-length dependent reduction in energy metabolism (Jacobsen et al., 2011). In addition, human derived HD specific neural stem cells showed significantly decreased intracellular ATP (The HD iPSC Consortium, 2012), supporting the hypothesis that bioenergetic dysfunction is an early event in HD.

Elevated levels of lactate and increased lactate/pyruvate ratio have been also described in striatum, cortex and cerebrospinal fluid from HD patients (Jenkins et al., 1993; Koroshetz et al., 1997; Martin et al., 2007), as well as in brains from YAC128 and R6/2 transgenic mouse models (Lopes et al., 2014; Tsang et al., 2006). The irreversible oxidative decarboxylation of pyruvate to acetyl coenzyme A (CoA) is catalyzed by pyruvate dehydrogenase (PDH), which activity is declined in caudate and putamen of HD patients and in R6/2 brain (Andreassen et al., 2001; Sorbi et al., 1983), possibly explaining the increase in lactate/pyruvate ratio. Other tricarboxylic acid (TCA) cycle enzymes that provide the main pathway for generating reducing equivalents, such as aconitase, α-ketoglutarate dehydrogenase (α-KGDH) or succinate dehydrogenase (SDH, or complex II) are also compromised in central HD tissues (Klivenyi et al., 2004; Sorolla et al., 2010; Tabrizi et al., 1999) (**Figure 1.5, panel C**). Cultured striatal neurons expressing N-terminal HTT fragment showed decreased SDH activity, the only enzyme that participates in both TCA cycle and electron transport chain (ETC) (Benchoua et al.,

2006). Contrariwise, in peripheral HD cybrids α-KGDH enzymatic activity was increased (Ferreira et al., 2011), suggesting a compensatory mechanism to re-establish reduced nicotinamide adenine dinucleotide (NADH) levels.

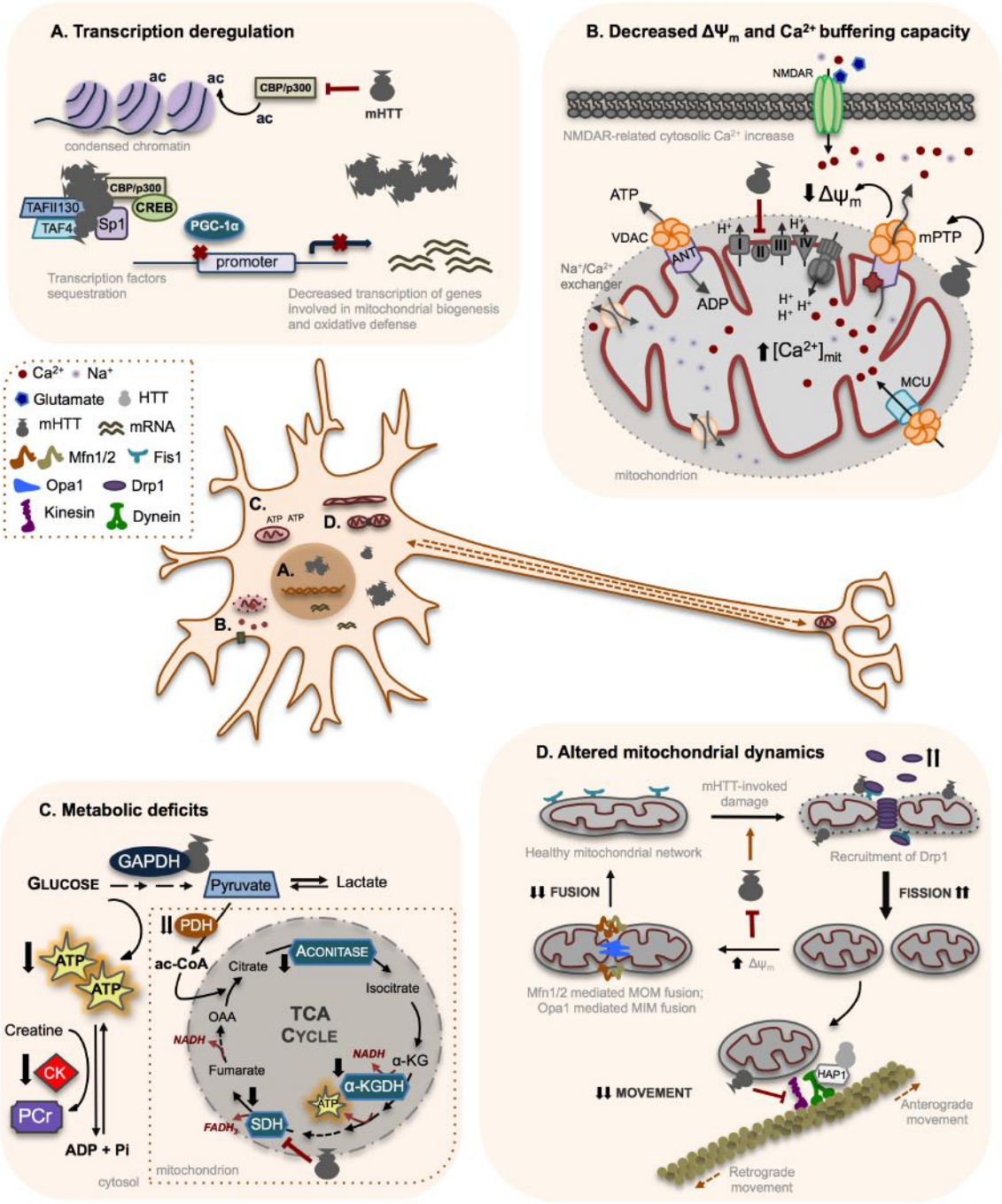

Figure 1.5 | Major nuclear-mitochondrial axis pathways disrupted in HD. Depicted neuron evidence major dysfunctional mechanisms involving mitochondria or mitochondria-related transcription caused by the presence of mHTT. (**A**) PTM of histones, such as acetylation, lead to modifications of chromatin structure from heterochromatin to euchromatin, which allows gene transcription to occur. mHTT inhibit acetyltransferase CBP/p300 complex, therefore the heterochromatin structure is favored, decreasing transcription. Additionally, soluble mHTT interferes

with specific components of transcriptional machinery to repress expression of target genes such as PGC-1α, a master regulator of mitochondrial function. (**B**) mHTT also facilitates the activation of NMDARs and exacerbates intracellular Ca^{2+} responses, leading to mitochondrial Ca^{2+} overload. Once the mitochondrial Ca^{2+} storage capacity is exceeded, the mPTP opens inducing mitochondrial depolarization and further Ca^{2+} release into the cytoplasm. Additionally, mHTT may associate with the MOM and inhibit respiratory chain complex II (SDH), boosting energy depletion and mPTP opening. (**C**) Metabolic deficits induced by mHTT include decreased ATP production along with poor PCr/Pi ratio due to decreased CK activity. Alongside, mHTT interacts with the sixth step glycolysis enzyme GAPDH. Although with compromised glycolysis, pyruvate can still accumulate due to increased inhibition of PDH, stimulating the conversion to lactate instead of entering in the TCA cycle as acetyl-CoA. Defects in TCA cycle intermediate enzymes such as α-KGDH, aconitase and SDH, as well as the susceptibility of SDH to mHTT interaction, severely compromise the generation of reduced equivalents to feed the ETC. Lastly, (**D**) mitochondrial functional network is promoted by fusion, whereas mitochondrial fragmentation into individual organelles occurs by fission. mHTT physically interacts with Drp1, a fission related protein, increasing its GTPase activity, resulting in enhanced mitochondrial fission, which disrupts normal mitochondrial cycling. In turn, adequate maintenance of $\Delta\psi_m$ is required for fusion; since mHTT decreases $\Delta\psi_m$, mitochondrial fusion is compromised in HD neurons. Furthermore, both anterograde (to synapse) and retrograde (to the soma) mitochondrial trafficking is compromised. While normal HTT regulate transport by binding to dynein and HAP1, mHTT associated to MOM may interfere with the association of microtubule-based transport proteins with mitochondria.

1.4.2.6. Mitochondrial-dependent oxidative stress and apoptosis

Free radicals are molecules containing one unpaired electron in their atomic or molecular orbitals, providing them high reactivity. Radicals derived from oxygen (O_2) represent the most important class of radicals in living systems and mitochondria are, at the same time, the major source and key targets of ROS. During energy transduction at ETC, mainly from catalytic cycles of complexes I and III, a small number of electrons leak to O_2 prematurely to generate superoxide anion ($O_2^{\bullet -}$), instead of contributing to the reduction of O_2 to water [reviewed in (Dröse and Brandt, 2012)]. In normal conditions less than 0.1% of electron slippage and $O_2^{\bullet -}$ formation is observed, however in HD models mitochondrial $O_2^{\bullet -}$ dramatically increases, which is linked to mitochondrial Ca^{2+} signaling deregulation and apoptosis (Ribeiro et al., 2013, 2014; Wang et al., 2013). Concordantly, striatum from HD patients exhibited oxidation of mitochondrial enzymes that resulted in decreased catalytic activity, in agreement with bioenergetic deficits observed in HD (Sorolla et al., 2010). $O_2^{\bullet -}$ is highly membrane impermeable but can be dismutated to less-harmful hydrogen peroxide (H_2O_2) by SODs. It can also rapidly react with nitric oxide to form peroxynitrite, which can readily cross cell membranes and damage intracellular components [reviewed in (Johri and Beal, 2012)]. In our laboratory

we observed that SOD1/2 activity and protein levels are significantly increased in striatal ST*Hdh*$^{Q111/Q111}$ cells (Ribeiro et al., 2013, 2014). Therefore, the extent of cellular oxidation was significantly increased not only in HD striatal cells, but also in R6/1 mice at different ages (Lim et al., 2008; Pérez-Severiano et al., 2004; Ribeiro et al., 2012, 2013). In contrast, synaptic mitochondria from presymptomatic 2 month-old YAC128 mice showed the same rate of H_2O_2 production as wild-type controls, which was linked with negligible levels of mHTT associated with mitochondria at this age (Pellman et al., 2015). Additionally, incubation of isolated mitochondria with pathologic length glutathione S-transferase (GST)-polyQ protein induced ROS formation and impaired mitochondrial respiration, which was prevented by the antioxidant *N*-acetyl-cysteine (NAC) and also by cyt *c*, which may act as electron scavengers (Puranam et al., 2006).

Deregulated antioxidant capacity has also been described in HD, most likely due to alterations in nuclear factor E2-related factor 2 (Nrf2)-antioxidant response element signaling pathway (Kang et al., 2005). Although a few reports describe modified Nrf2 and Nrf2 target antioxidant proteins activity in distinct HD models, the results are not consistent. Reduced Nrf2 activity was observed in N171-82Q HD mice striatum (Chaturvedi et al., 2010) and in ST*Hdh*$^{Q111/Q111}$ cells (Ribeiro et al., 2014), whereas Nrf2 protein levels were significantly increased in cortex of late-symptomatic R6/1 mice (Rué et al., 2013). In plasma and erythrocytes of HD patients a reduction in the antioxidant systems were correlated with the disease stage (Túnez et al., 2011). In HD skin fibroblasts significant lower catalase activity was documented, although no differences were found in both SOD1 and 2 or GPx activities (del Hoyo et al., 2006). Conversely, proteomic analysis from HD *postmortem* brain samples revealed that antioxidant defense proteins such as SOD2, catalase and GPx1 and 6 and peroxiredoxins (Prdx) 1, 2 and 6 were strongly induced in striatum, but also detectable in cortex (Sorolla et al., 2008). Significant increases in mRNA levels of GPx1, catalase and SOD1 were observed in ST*Hdh*$^{Q111/Q111}$ KI striatal cells (Lim et al., 2008), despite decreased Nrf-2 activation, suggesting alternative transcription regulation. As in HD patients (Túnez et al., 2011), in mouse models antioxidant defense activation may fluctuate according to disease progression. A significant increase in SOD1 activity was observed in the striatum of early-symptomatic R6/1 mice, however at the age of 35 weeks, when mice exhibited a severe phenotype, a decrease in total SODs activities was observed (Santamaría et al., 2001). These data suggest that in the early stages of the disease progression neurons are capable of compensatory responses to potentiate antioxidant defense and protect cells from free radical-induced damage.

Increased levels of oxidative stress are in close relationship with mitochondrial-associated apoptotic cell death. Recently, it was demonstrated that increased glutathione pool, indicative of an oxidized state, in the striatum of YAC128 mice leads to Ca^{2+}-permeable transient receptor potential cation (TRPC5) channel activation *via* TRPC5 S-glutathionylation at Cys176/Cys178 residues, ultimately inducing striatal neuronal cell death (Hong et al., 2015). In fact, glutathione-activated TRPC5 current results in a sustained increase in cytosolic Ca^{2+} (Hong et al., 2015), prompting the opening of the mPTP, loss of $\Delta\psi_m$, and release of pro-apoptotic proteins from the MIS into the cytosol. One of the most important factors released by mitochondria is cyt *c* which, together with deoxyATP and the adaptor protein apoptotic protease activating factor 1 (Apaf1), forms the apoptosome complex necessary for activation of caspase-9 (Hu et al., 1999). Once activated, caspase-9 further activates the apoptotic effectors caspase-3, -6 and -7, evoking the well-recognized nuclear apoptotic features, such as nuclear DNA fragmentation and chromatin condensation, observed in several HD models (Kim and Chan, 2002; Portera-Cailliau et al., 1995; Ribeiro et al., 2013). A direct correlation between the number of CAG repeats in *HTT* gene and the degree of DNA fragmentation was also described in HD patients' striatum (Butterworth et al., 1998). Importantly, activated caspase-6 and -3 were found in the brain of presymptomatic and degenerating HD brain, respectively (Graham et al., 2010; Wellington et al., 2002), suggesting that caspase-6 activation may occur early in the disease progression, which in turn influences caspase-3 activity. In fact, cleavage at the 586 amino acid caspase-6 site in mHTT is required for the formation of the toxic N-terminal fragments and development of behavioral and neuropathological features of HD; in turn, YAC128 mice expressing of caspase-6-resistant mHTT maintain normal neuronal function and do not develop striatal neurodegeneration (Graham et al., 2006). Lately, this event has been questioned since BACHD caspase-6 KO mice striatum exhibited a significant reduction of FL-mHTT and the presence of toxic fragments of mHTT (Gafni et al., 2012). mHTT can also be selectively cleaved by caspase-2, and expression of catalytically inactive forms of caspase-2 and -7 (but not caspase-3, -8 and -9) reduced cell death of YAC72 primary striatal cells (Hermel et al., 2004). Reduction of ROS levels by antioxidants also contributes to prevent caspase activation and increased neuronal density both in cells expressing 111Q (Ribeiro et al., 2013) and in R6/2 mice (Ju et al., 2014).

The control and regulation of apoptotic mitochondrial events also occurs through the members of the B-cell lymphoma 2 (Bcl-2) family, enclosing both apoptosis inducers (e.g. Bax, Bak, Bim) and inhibitors (e.g. Bcl-2, Bcl-X_L). In grades 2 and 3 HD brains, expression of the pro-apoptotic protein Bax was found to be increased compared

to controls. Conversely, in severely affected grade 4 brains anti-apoptotic Bcl-2 immunoreactivity was markedly enhanced (Vis et al., 2005). Studies in HD mouse brains, in turn, reported unchanged or downregulated levels of Bcl-2 (Ju et al., 2014; Zhang et al., 2003). However, both chronic treatment with NAC or Bcl-2 OE significantly enhanced Bcl-2 levels in R6/2 mice, which resulted in slight prolonged survival (Ju et al., 2014; Zhang et al., 2003). Peripheral HD models also exhibited deregulation of apoptotic inducers. HD human cybrid lines showed increased mitochondrial Bim and Bak levels and cyt *c* release (Ferreira et al., 2010), whereas particular peripheral blood cells from HD patients (B and T lymphocytes and monocytes) showed increased Bax levels associated with increased cellular oxidation (Almeida et al., 2008).

Five decades of research have been made in HD mitochondrial-related pathogenesis (**Figure 1.6**). Compelling evidence indicates that oxidative damage is most likely an execution step for cell death mechanisms induced by mHTT in HD brain. The prime candidates for defective pathways may include bioenergetic and mitochondrial defects. Alternatively, mHTT primarily deleterious action may occur at the level of gene transcription. In this regard, strategies targeting these pathogenic pathways may be beneficial to HD patients.

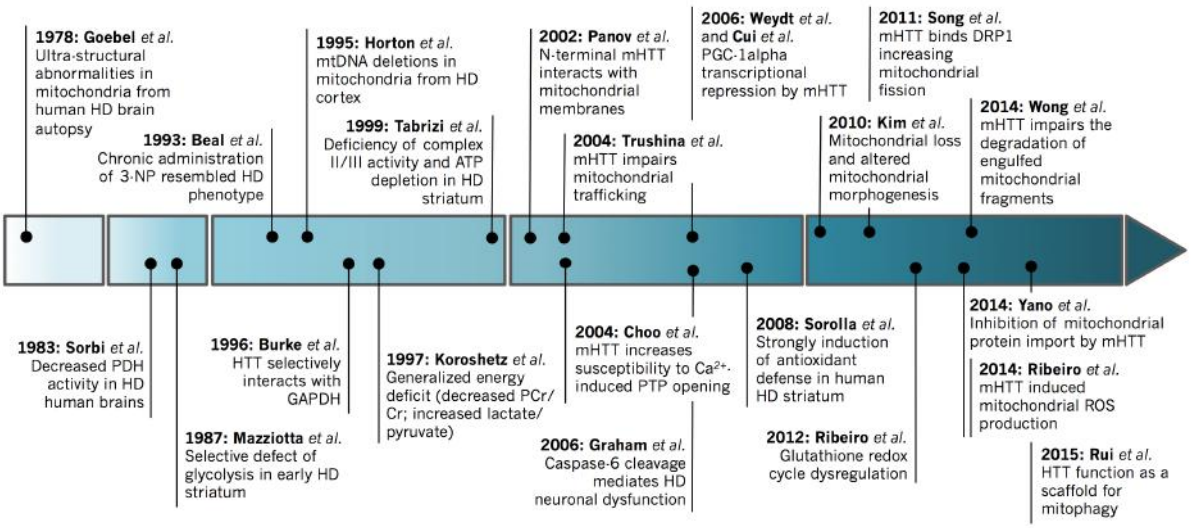

Figure 1.6 | Key discoveries involving mitochondria in HD pathogenesis. This timeline resumes some of the major discoveries involving mitochondrial dysfunction in HD and related oxidative stress changes, from dysfunctional glycolysis described in the late 80s, to deficiency of respiratory chain complexes in the late 90s, which was later explained by the interaction of mHTT with mitochondria and by transcriptional deregulation. More recently, research has focused on the role of both wild-type and mHTT on mitochondrial dynamics and turnover. All studies are indicated in the reference list (Carmo et al., *unpublished*).

1.5. NEUROPROTECTIVE TARGETS IN HUNTINGTON'S DISEASE

HD causes increasing disability over the years and current treatments may alleviate symptoms, but are not curative. Modulation of mitochondrial function by targeting mitochondrial enzymes or mitochondrial-related nuclear transcription have provided interesting insights into some of the pathological mechanisms in HD, opening new avenues for therapy. Along this section some targets for neuroprotection in HD are described.

1.5.1. PYRUVATE DEHYDROGENASE COMPLEX

Pyruvate dehydrogenase complex (PDC) is heterogeneously distributed within mitochondrial matrix and, as explained before in this work, plays a key role in glucose metabolism by catalyzing oxidative decarboxylation of pyruvate and providing acetyl-CoA and NADH for the TCA cycle and other biosynthetic processes. In 1992 the atomic structure of the cubic core of the PDC was determined (Mattevi et al., 1992). This is a large multienzyme complex composed by several copies of three core catalytic components working sequentially: 20-30 heterotetramers ($\alpha_2\beta_2$) of pyruvate dehydrogenase (E1), 60 subunits of dihydrolipoamide acetyltransacetylase (E2) and 6-12 homodimers of dihydrolipoamide dehydrogenase (E3) [reviewed in (Patel et al., 2014)]. The E1 is a thiamine diphosphate (TTP)-dependent enzyme and catalyzes two consecutive steps, the decarboxylation of pyruvate to CO_2 and the reductive acetylation of the lipoyl groups covalently attached to the E2. The E2 catalyzes the transfer of an acetyl moiety to CoA to form acetyl-CoA. The transfer of electrons from the dihydrolipoyl moieties of E2 to flavin adenine dinucleotide (FAD) and then NAD^+ is carried out by E3. In higher eukaryotes PDC have two additional regulatory enzymes, 1-2 homo (or hetero) dimers of PDH kinase (PDK, four human isoforms) and 2-3 heterodimers of PDH phosphatase (PDP, two human isoforms), which catalyze the phosphorylation and dephosphorylation of the E1α component, respectively. A structural component was also described to play a critical role in the organization and function of the complex, a second lipoyl-bearing component, the protein X (Mattevi et al., 1992; Patel and Roche, 1990), totaling 11 proteins in PDC.

1.5.1.1. Regulation of PDC activity: complexity of multiple post-translational modification

Like other rate-limiting enzymes, the PDC is tightly regulated in a large part by interconversion of the E1α component between an active/dephosphorylated form and inactive/phosphorylated form. This interconversion is catalyzed by PDKs and PDPs in three different serine residues designated site 1 (Ser293), site 2 (Ser300) and site 3 (Ser232), that undergo alterations depending on the specie (Dahl et al., 1987; Linn et al., 1969). PDK is stimulated by the end products of the PDC reaction, acetyl-CoA and NADH, leading to phosphorylation and inactivation of the PDC; whereas pyruvate, TPP and, to some extent, NAD^+ and CoA, inhibits the phosphorylation reaction (**Figure 1.7**). In contrast, NADH inhibits phosphatase activity. An additional level of complexity in the PDC regulation has emerged after the discovery of several isozymes of PDK (PDK1, PDK2, PDK3 and PDK4) and PDP (PDP1 and PDP2) that differ in their kinetic, regulation and expression patterns (Gudi et al., 1995; Huang et al., 1998). All four PDKs phosphorylate site 1 and 2 in PDC, although with different rates, and only PDK1 phosphorylates site 3 (**Figure 1.7**). Phosphorylation rates are 4.6-fold higher for site 1 than for site 2 and 16-fold higher for site 1 than for site 3 (Korotchkina and Patel, 1995); regardless of which site is phosphorylated complete inactivation of the E1α component is detected. For site 1 PDK2 has the maximal level of activity, and PDK3 has the higher activity towards site 2, however slight changes in microenvironment (e.g. concentration of potassium salts) may modify PDKs sensitivity (Korotchkina and Patel, 2001; Patel and Korotchkina, 2001). Besides, kinetics of phosphorylation of PDC show that PDK3 can incorporate approximately 1.8-fold more phosphate than PDK2, with a stoichiometry of 2.8 mol of phosphate *per* mol of E1α for PDK3, in contrast with 1.6 mol of phosphate *per* mol of E1α for PDK2 (Kolobova et al., 2001). The rates of dephosphorylation and reactivation are similar for sites 1, 2 and 3, suggesting a random dephosphorylation mechanism (Korotchkina and Patel, 1995). E2 facilitates the enhanced function of both PDKs and PDPs. This enhancement of the catalytic efficiency by E2 may be explained by the co-localization of PDK/PDP with E1 bound to the subunit-binding domain of E2 (Kato et al., 2005; Yang et al., 1998). PDKs and PDPs can also regulate themselves by phosphorylation. Tyrosine phosphorylation of PDK1 (Try243/244) enhances its activity by promoting ATP binding to PDK1, which consequently facilitates PDC scaffold to access substrate PDH E1α; phosphorylation at Tyr94 inhibits PDP1 by reducing the binding ability of PDP1 to lipoic acid, which is covalently attached to E2 component to recruit PDP1 to PDC (Hitosugi et al., 2011; Shan et al., 2014).

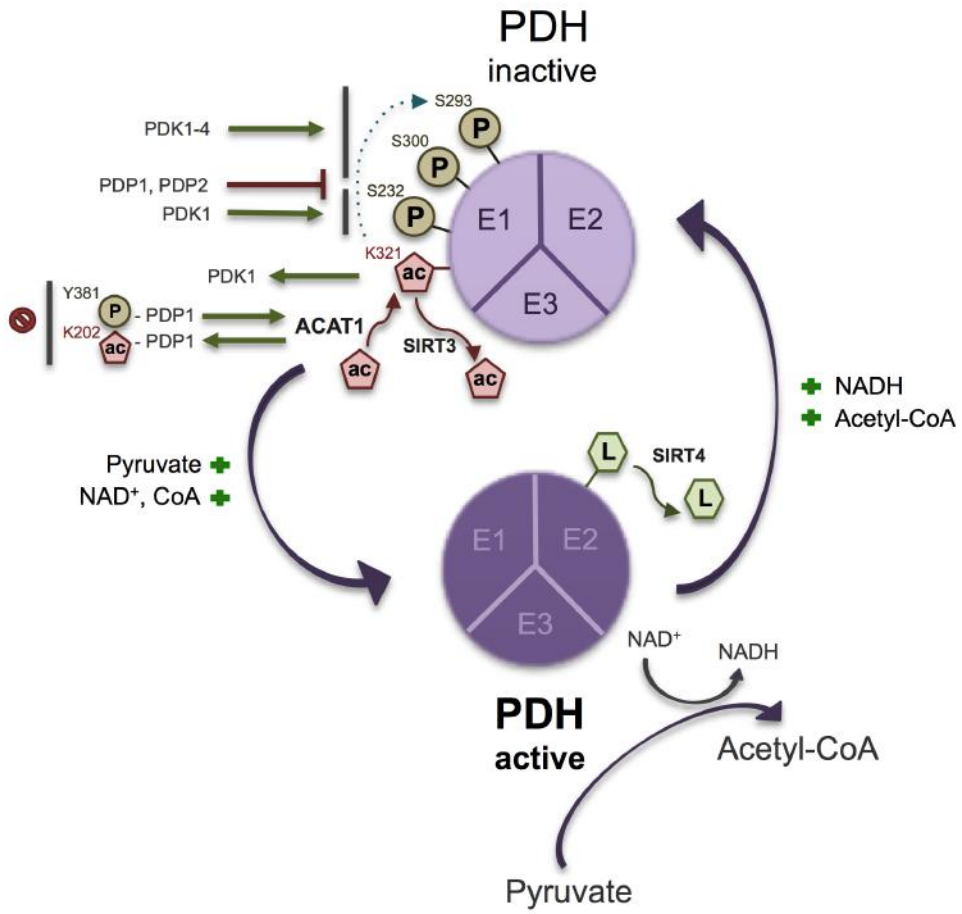

Figure 1.7 | Regulation of the pyruvate dehydrogenase multienzyme complex. PDC is regulated by a variety of PTM and by its products and substrates. When activated, PDC converts pyruvate into acetyl-CoA, generating NADH. The phosphorylation/ dephosphorylation of PDH E1α subunit at three different Ser residues (S293, S300, S232) is the most described modification that controls PDC activity. Phosphorylation is conducted by PDK1-4, inhibiting PDC activity, whereas dephosphorylation is carried out by PDP1-2, activating PDC. In addition, PDP1 can also be phosphorylated at a tyrosine residue (Y381) that induces the dissociation of SIRT3 (with deacetylase activity) and enhances ACAT1 binding to PDP1. Acetyl groups added by ACAT1 inhibit PDC activity: Lys321 acetylation inhibits PDH E1α by recruiting PDK1 and facilitating Ser293 phosphorylation, and Lys202 acetylation inhibits PDP1. PDH E2 subunit can also be lipoylated; SIRT4 efficiently catalyzes the removal of lipoyl groups, inhibiting PDC.

Mammalian PDK isozymes are expressed in a tissue-specific manner. PDK1 is present mostly in the heart, whereas PDK2 and PDK4 are particularly enriched in the heart, skeletal muscle and liver, and exhibit increasing activities in other tissues (e.g. kidney and lactating mammary gland) in response to starvation and diabetes. However, PDK2 has a more balanced expression between tissues. PDK3 is highly enriched in testis and lung [reviewed in (Harris et al., 2001; Patel et al., 2014)]. There is no available data about PDKs expression in human brain, however, in rat brain, PDK activity

corresponds primarily to isozymes PDK2 and PDK3 (Bowker-Kinley et al., 1998). This tissue-specific distribution is substantially controlled by transcription pathways that obviously change depending on the cellular type. Insulin and ROS levels and its downstream transcriptional targets, such as forkhead box class O (FOXO) and hypoxia-inducible factor-1α (HIF-1α), respectively, are major regulators of PDKs expression [reviewed in (Jeong et al., 2012b)].

Besides phosphorylation, other PTM have been described lately. With the development of precise mass spectrometry techniques, acetylation and lipoylation were described as important regulators of the PDC activity. First proteomic survey using deacetylase sirtuin 3 (SIRT3) KO mice revealed increased acetylation of enzymes involved in mitochondrial metabolism, including 2- and 1.5-fold increase in E1α and E3 subunits of PDC. Acetylation of the structural component PDHX was also increased in SIRT3 deficient cells (Sol et al., 2012). However, no functionality was attributed to this acetylated status. Recently, a rather complex study on the PDC regulation showed that K321 acetylation inhibits PDH E1α by recruiting PDK1, and K202 acetylation inhibits PDP1 by dissociating its substrate PDH E1α, consequently inhibiting PDC. Mitochondrial SIRT3 and ACAT1 (acetyl-CoA acetyltransferase 1) were described as being the upstream deacetylase and acetyltransferase, respectively, of PDH E1α and PDP1 components (Fan et al., 2014). Additionally, tyrosine phosphorylation (Tyr381) of PDP1 recruits ACAT1 and dissociates SIRT3 to promote Lys acetylation of PDP1 and PDH E1α. On the other hand, PDH E1α acetylation (K321) functions as an upstream event that facilitates Ser293 phosphorylation of PDH E1α (Fan et al., 2014) (**Figure 1.7**). Together, this remarkable study suggests that Lys acetylation of PDH E1α and PDP1 primarily regulates phosphorylation and molecular composition of PDC, leading to inhibition of PDH E1α and, subsequently, PDC. Months later, another study reported that some PDC subunits may be regulated by lipoyl-Lys modifications (Mathias et al., 2014). The authors showed that physical and functional interaction between mitochondrial sirtuin 4 (SIRT4) and PDC results in decreased lipoylation of the catalytic E2 component and structural PDHX component, diminishing PDC activity (Mathias et al., 2014) (**Figure 1.7**).

1.5.1.2. PDC activation as a therapeutic strategy in HD

It has long been known that diminished brain glucose metabolism in neurodegenerative brains precedes the appearance of overt clinical manifestations (Caselli et al., 2008; Mazziotta et al., 1987), suggesting that PDC may have a role in neurodegeneration. However, this matter was never extensively addressed and few studies exist involving PDC in HD. Pioneer studies showing PDC deficiency in HD human brain date from 1983, when Sorbi and colleagues demonstrated that PDC activity was decreased in caudate, putamen and hippocampus, but not in HD fibroblasts (Sorbi et al., 1983), which was in accordance with increased brain lactate levels (Jenkins et al., 1993). Moreover, decreased PDC activity directly correlates with increasing duration of illness, possible due to a progressive loss of MSNs in HD caudate nucleus (Butterworth et al., 1985). Similar reduced PDH activity was observed in *Escherichia coli* carrying GST-polyQ construct expressing 62Q, in comparison with 10Q-expressing control (Cooper et al., 1998a). Studies conducted in our laboratory also suggested that bioenergetic dysfunction in HD human cybrids and in YAC128 mouse striatal neurons was associated with decreased PDC activity, protein levels and increased phosphorylation/inactivation of PDH E1α subunit (Ferreira et al., 2011; Naia et al., 2016).

Such results raise the possibility that regulation of PDC activity might have therapeutic benefits in HD patients. Dichloroacetate (DCA) has effects on bioenergetics by stimulating PDC activity by two distinct mechanisms – it inhibits PDKs and decreases the degradation of the PDH E1α subunit (Morten et al., 1998; Whitehouse et al., 1974). Andreassen *et al.* showed that increasing PDC activity by DCA administration significantly improved survival and motor function, delayed weight loss and prevented diabetes in both R6/2 and N171-82Q transgenic models of HD. In R6/2 mice at 12 weeks of age the amount of active form of PDH was reduced by 42%, which was completely reversed after DCA treatment. Furthermore, atrophic striatal neurons were rescued in DCA-supplemented R6/2 mice. In contrast, mHTT aggregates remained unchanged in striatum and cortex after treatment (Andreassen et al., 2001). Increased striatal vulnerability to PDC deficiency was confirmed since deficient mice for E3 component of PDC exhibited pronounced striatal lesion volumes induced by malonate and 3-NP, in comparison with wild-type mice (Klivenyi et al., 2004).

1.5.2. LYSINE DEACETYLASES

Epigenetic is a quickly growing field encompassing the study of heritable changes in genome function that occur independently of alterations in DNA sequence. It covers multiple levels of genome function, from direct modifications of the DNA and histone tails, regulating the level of transcription (e.g. DNA acetylation and methylation), to interactions with messenger RNAs, regulating the level of translation (RNA interference, e.g. non-coding microRNA) [reviewed in (Probst et al., 2009)]. Histone Lys acetylation has probably been the most studied of these pathways. Acetylation neutralizes the positive change of histone tails and reduces their affinity for DNA that results in more relaxed chromatin structure, making it more accessible to transcription factors [reviewed in (Shahbazian and Grunstein, 2007)]. In addition to histones, many other proteins are subjected to Lys acetylation, making this speedily reversible and controlled PTM an extensively regulator involved not only in gene transcription, but also in signal transduction, cellular transport and metabolism. Cumulating evidences indicate that acetylation rivals phosphorylation as a regulatory modification (Chen et al., 2012; Henriksen et al., 2012). Histones were the first substrates identified for eukaryotic Lys acetyltransferases (KATs) and Lys deacetylases (KDACs), explaining their common designation as histone acetyltransferases (HATs) and deacetylases (HDACs), respectively.

Based on homology with yeast KDACs, mammalian KDACs were divided in classical zinc-dependent HDACs and NAD^+-dependent sirtuins (SIRTs). Classes I, II (IIa and IIb) and IV comprise classical HDACs, while class III comprises SIRTs [reviewed in (Guedes-Dias and Oliveira, 2013)].

1.5.2.1. Class I/II lysine deacetylases in HD

Class I HDACs (HDAC1, 2, 3 and 8) are predominantly nuclear and widely expressed in most tissues, except for HADC8 that is confined to smooth muscle where it interacts with cytoskeleton α-actin, mediating contraction (Waltregny et al., 2005). Class IIa (HDAC4, 5, 7 and 9) and class IIb (HDAC6 and 10) HDAC enzymes generally shuttle between the nucleus and the cytoplasm and are expressed in a cell and tissue-specific manner, mainly in the brain, heart and muscle [reviewed in (Guedes-Dias and Oliveira, 2013)]. Binding-induced phosphorylation by regulatory 14-3-3 proteins promotes class IIa HDACs nuclei-cytoplasmic shuttling towards the cytoplasm, inhibiting nuclear import (Nishino et al., 2008). In turn, class IIb HDACs are primarily cytosolic.

HDAC1 is the most widely studied of all classical HDAC enzymes. It is highly homologous to HDAC2, acting together as catalytic core of the two major repressor complexes NuRD/Mi2/NRD and Sin/HDAC (Knoepfler and Eisenman, 1999). Similarly, both HDAC4 and HDAC5 do not possess intrinsic enzymatic activity as isolated polypeptides; they interact with HDAC3 *via* the transcriptional corepressor N-CoR/SMRT complex (Fischle et al., 2002). Remarkably, HDAC1-HDAC3 interaction is greatly induced in the presence of expanded polyQ fragments. The neurotoxic effect of HDAC1 requires interaction with HDAC3, which has been shown to selectively induce neuronal death (Bardai and D'Mello, 2011). HDAC3 KO suppresses HDAC1-induced neurotoxicity and *vice-versa* (Bardai et al., 2012). Several studies have measured HDACs mRNA and protein expression levels in different HD mouse models. Quinti and colleagues showed increased levels of HDAC1 protein, but not HDAC3, in cortical samples from R6/2 mice between 4 and 12 weeks of age and in striatum of 9 week-old R6/2 mice, compared with wild-type littermates (Quinti et al., 2010). Conversely, they observed no changes in HDAC1 levels in HdhQ140 KI mice (Quinti et al., 2010). Another study demonstrated increased nuclear expression of HDAC1 in cortex of 18 week-old N171-82Q transgenic mice, but no changes in HDAC2 or 4 (Jia et al., 2012). Unchanged HDAC(1-10) transcripts were found in cortex and brainstem of R6/2 mice (Mielcarek et al., 2011). In 4 month-old YAC128 mice striatum HDAC1 and 2 transcripts were also unchanged (Moreno et al., 2016). Highly variable HDAC1 protein expression levels were reported in HD human brain samples, possibly due to the patients' heterogeneity (e.g. disease grade or age) (Quinti et al., 2010). Conversely, elevated HDAC4 and 5 immunoreactivity were described in *postmortem* HD caudate nucleus, accompanied by significant losses of histones H2, H3 and H4 acetylation (Yeh et al., 2013), which contribute to the repressive chromatin environment in HD.

Previously we have pointed some protective functions of wild-type HTT (*section 1.2.1.*). This neuroprotection also involves HTT sequestration of HDAC3. In contrast, mHTT interacts poorly with HDAC3 and further promotes the dissociation of the HTT-HDAC3 complex in neurons exposed to apoptotic stimuli and in striatum of R6/2 mice (Bardai et al., 2013), providing a good example for the loss-of-function and gain-of-toxic-function mechanisms proposed for HD. In agreement, neuronal knockdown (KD) of HDAC3 suppressed toxicity in *Caenorhabditis elegans* neurons expressing the human HTT fragment with 150Q (Bates et al., 2006). However, not all studies support these data. Besides no described alteration in HDAC3 protein and mRNA levels in HD models, partial depletion of HDAC3 in R6/2 mice did not ameliorate the severe physiological and behavioral phenotype characteristic of these HD transgenic mice and did not affect

dysregulated transcripts such as *BDNF* either. Nonetheless, heterozygous KD was not effective in reducing HDAC3 expression levels in the cytoplasm and the reduction in the nucleus was approximately 40% (Moumné et al., 2012). HDAC4 also interacts with mHTT in a polyQ length-dependent manner through its glutamine-rich domain in cytoplasmic brain inclusions of HD models. HDAC4 KD delayed cytoplasmic aggregate formation in both R6/2 and HdhQ150 mice and rescued cortico-striatal synaptic function and motor coordination, and increased lifespan (Mielcarek et al., 2013).

HDAC6 is particularly interesting since it contains a C-terminal ubiquitin binding domain and two functional deacetylase domains (Seigneurin-Berny et al., 2001). In cytoplasm, it deacetylates α-tubulin, cortactin and heat shock protein 90, regulating axonal trafficking, cell motility and degradation of misfolded proteins [reviewed in (Simões-Pires et al., 2013)], all processes involved in HD pathogenesis. Various disease stages of R6/2 mice displayed significant increase in HDAC6 levels (Quinti et al., 2010). However, HDAC6 KO in R6/2 mice did not slow down the progression of behavioral, physiological and molecular HD-related phenotypes, despite the marked increase in α-tubulin acetylation. HDAC6 genetic depletion had no effect in efficiency of BDNF transport from the cortex to the striatum or in HTT aggregates (Bobrowska et al., 2011), suggesting that, at list in this HD mouse model, HDAC6 is not important for mHTT aggregate clearance. Recently, another study weaken the validity of HDAC6 depletion as a possible therapeutic strategy for HD. R6/1 mice KO for HDAC6 showed no improvement in cognitive abilities and even worsened their social impairments and hypolocomotion in Y-maze spontaneous alternation behavioral test (Ragot et al., 2015).

Although the results for genetic deletion of HDCA6 do not seem promising, new data involving pharmacological inactivation of non-specific or class-specific HDACs are encouraging and are discussed in the next section.

1.5.2.1.1. HDAC inhibitors in HD neuroprotection

Treatment with HDAC inhibitors (HDACi) result in increased acetylated levels of histones, promoting the expression of silenced regulatory genes, becoming attractive therapeutic agents for neurodegeneration (**Figure 1.8**). In the past decade more than 400 clinical trials have been initiated with different HDACi; currently more than a dozen different inhibitors are being tested in clinical trials, many of them involving patients with neurodegenerative diseases, including HD [reviewed in (Brett et al., 2014)]. Most of classical HDACi act by chelating zinc atom surrounded by two histidine-aspartic acid dyads (His131-Asp166 and His132-Asp173) and one tyrosine (Tyr297) in the catalytic

domain, contributing to non-selective inhibition of HDAC isoforms [reviewed in (Bertrand, 2010)]. This structure is common to all zinc-dependent HDACs, and some residue changes at the HDAC active site determine isoform-selective inhibitors. Therefore, *in vitro* deacetylation assays with recombinant deacetylases or chemical proteomic-based approaches have been developed lately in order to determine HDAC specificities at the level of the enzyme that they target, which will allow the development of more selective inhibitors. Recently, a quantitative mass spectrometry assay evaluated the specificities of 19 structural divergent KDACs at the level of acetylation sites affected in human cells (Scholz et al., 2015). Trichostatin A (TSA) and suberoylanilide hydroxamic acid (SAHA) are unselective pan-Lys HDACi; however they are closely related to the group of HDACi targeting only class I KDACs, including MS-275, apicidin and valproic acid. Butyrates, such as sodium butyrate (SB) and phenylbutyrate (PB), showed different patterns of acetylation in the pair-wise Pearson correlation coefficient in relation to other class I KDACi. Nevertheless, all of these class I and IIa HDACi have similar regulatory profiles for histones and strongly increase acetylation of N-terminal Lys. Tenovin-6, bufexamac and tubacin are among the most efficient HDACi, each upregulating acetylation at more than 10 percent of all quantified sites (Scholz et al., 2015) (**Figure 1.8**).

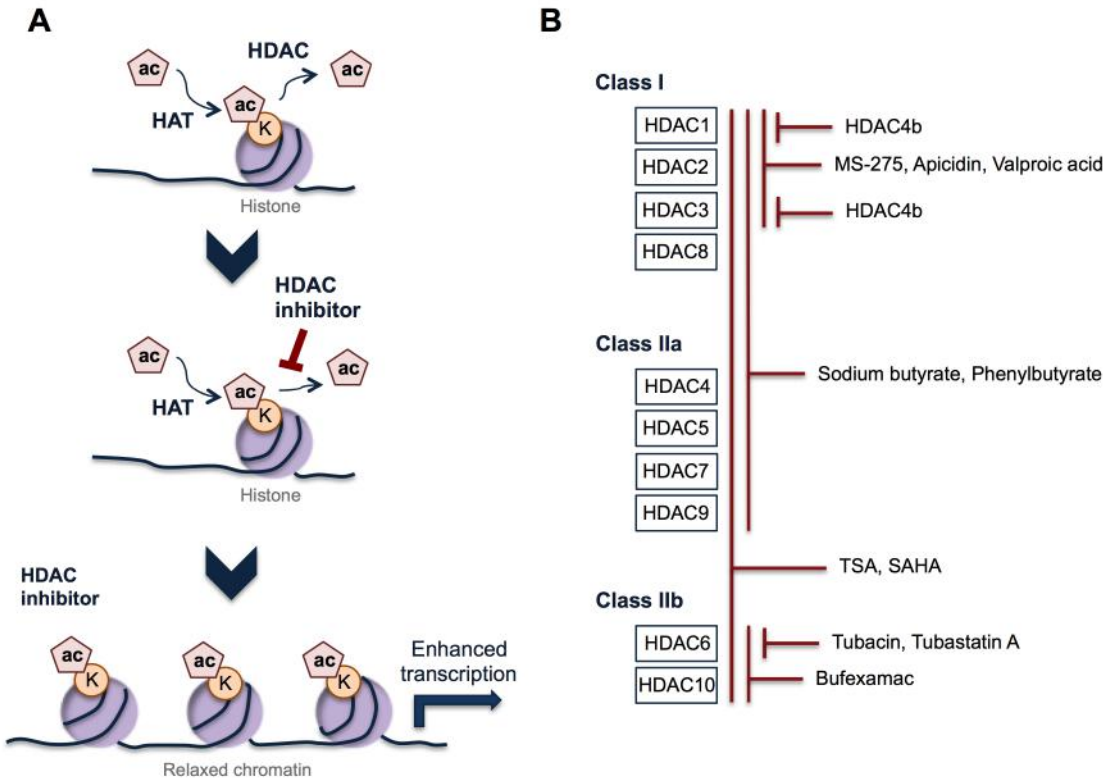

Figure 1.8 | Schematic representation of histone acetylation and transcription activation induced by HDACi. In panel **A**, acetylation in Lys residues of histones is catalyzed by the action of HATs and is reversed by the action of HDACs. Treatment with HDAC inhibitors leads to a more

relaxed chromatin state, resulting in enhanced transcription activation. In panel **B** are schematized the different classes and isoforms of HDACs, as well as the most common inhibitors.

TSA was the first hydroxamic acid to be characterized as a potent broad-range HDACi (Yoshida et al., 1990). Its core chemical structure was further used to design new synthetic compounds of this class – such as SAHA, the first HDACi approved by the U.S. Food and Drug Administration for the treatment of cutaneous T-cell lymphoma (Marks and Breslow, 2007). In *vivo* SAHA crosses the blood-brain barrier (BBB) and increases histone H2 and H4 acetylation in brain. When administered to 4 to 12 week-old R6/2 mice, SAHA improved motor coordination and cellular brain morphology, more closely resembling wild-type mice, although no treatment-related differences in HTT aggregates were detected (Hockly et al., 2003). SAHA treatment also increased survival rates of two *Drosophila* models of polyQ disease (Steffan et al., 2001). More recently, it was shown that prolonged SAHA treatment promotes HDAC2 and HDAC4 protein degradation, and diminishes *HDAC7* transcript levels in both R6/2 and wild-type mice cortex. Additionally, treatment with SAHA reduced HTT insoluble aggregates and restored *BDNF* cortical transcript levels (Mielcarek et al., 2011). Previously it was reported that both TSA and SAHA treatments increased α-tubulin acetylation and BDNF intracellular transport in 109Q-expressing cells, but through an HDAC6-dependent mechanism, since MS-275, a specific HDAC1 inhibitor, had no effect on the movement of BDNF vesicles (Dompierre et al., 2007). HDAC4b is structurally related to SAHA, but is not a hydroxamic acid, being selective for HDAC1 and 3. It can also cross the BBB, increasing nearly 2-fold histone H4 acetylation in the CNS. Chronic oral administration of HDAC4b significantly improved motor performance and body weight, and attenuated gross brain-decline and striatal atrophy of symptomatic R6/2 mice (Thomas et al., 2008).

The butyrates are fatty acid derivatives that inhibit most class I and IIa HDACs. They have been the best clinically studied compounds and are known to readily reach the brain (Egorin et al., 1999). Concordantly, SB treatment extended survival in a dose-dependent manner, improved body weight and motor performance in R6/2 mice. Additionally, SB treatment for 2 weeks with simultaneous administration of 3-NP during the second week resulted in marked neuroprotection from 3-NP striatal damage in R6/2 mice, compared with 3-NP or PBS-treated R6/2 mice. In this study SB failed to attenuate HTT aggregation (Ferrante et al., 2003). Microarray analysis also revealed specific mRNA changes, but not global mRNA expression, in SB-treated R6/2 mice (Ferrante et al., 2003).

Some HDACi also have an effect on mitochondrial function. Both treatment with TSA and SB decreased the proportion of homozygous ST*Hdh*^{Q111} striatal cells losing Ca^{2+} homeostasis after Ca^{2+} stimuli and accelerated the recovered of intracellular Ca^{2+} concentrations in primary YAC128 striatal neurons challenged with NMDA (Oliveira et al., 2006). Very recently, pharmacological inhibition of the HDAC6 with tubastatin A was shown to increase acetylated α-tubulin levels, stimulating mitochondrial motility and fusion in striatal neurons (Guedes-Dias et al., 2015), which was observed to be compromised in HD models [e.g. (Wang et al., 2009)]. Moreover, tubastatin A promoted clearance of diffuse mHTT in striatal neurons expressing 74Q (Guedes-Dias et al., 2015).

1.5.2.2. Class III lysine deacetylases in HD

Mammalian SIRTs comprise seven enzymes, SIRT1-7, which are functionally nonredundant and linked to a wide range of cellular processes, including DNA repair (Madabushi et al., 2013), apoptosis (Luo et al., 2001), circadian rhythm (Chang and Guarente, 2013) and metabolic regulation (Price et al., 2012). The unique deacetylation reaction of sirtuins requires NAD^+ cleavage, generating nicotinamide (NAM), -O-acetyl-ADP ribose and the deacetylated substrate (Tanner et al., 2000). All sirtuins remove acyl groups, predominantly acetyl, but also succinyl, malonyl, palmitoyl and lipoyl; of relevance, the presence or absence of acyl groups on specific Lys residues in proteins can change their function and subcellular localization [reviewed in (Verdin, 2014)]. Interestingly, the generation of NAM at high concentrations can bind and thereby feedback-inhibit sirtuin's activity (Bitterman et al., 2002). Although these enzymes are rather conserved, their N- and C-terminus vary (Frye, 2000), allowing the interaction with different substrates and distinct subcellular localizations. SIRTs 1, 6, 7 are primarily nuclear proteins, SIRTs 3, 4, 5 are imported into mitochondria, while SIRT2 is cytosolic (Guarente, 2011) (**Table 1.1**). SIRTs 1, 2 and 3 have strong deacetylase activity, whereas SIRTs 4, 5, 6 and 7 display weak deacetylase activity [reviewed in (Choudhary et al., 2014)].

Table 1.1 | Diversity of human SIRTs, location and proposed role in HD.

	MW	LOCATION	ACTIVITY	EFFECTS IN HD	REFERENCES
SIRT1 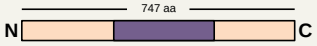	120	Nucleus Cytosol	Deacetylase	Mainly neuroprotective	*Jeong et al., 2011 Jiang et al., 2012 Smith et al., 2014 Jiang et al., 2014*
SIRT2 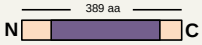	43	Cytosol	Deacetylase	Toxic	*Luthi-Carter et al., 2010*
SIRT3 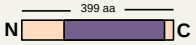	28 44	Mitochondria Nucleus	Deacetylase	Neuroprotective	*Lombard et al., 2007 Fu et al., 2012 Cheng et al., 2016*
SIRT4 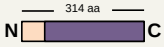	35	Mitochondria	ADP-ribosyl transferase Lipoamidase Deacetylase	*Unknown*	*Laurent et al., 2013 Mathias et al., 2014*
SIRT5 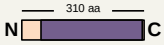	34	Mitochondria	Desuccinylase Deacetylase	*Unknown*	*Nakagawa et al., 2009 Park et al., 2013*
SIRT6 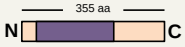	37	Nucleus	ADP-ribosyl transferase Deacetylase	*Unknown*	*Liszt et al., 2005 Zhong et al., 2010*
SIRT7 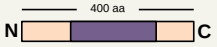	45	Nucleus	Deacetylase	*Unknown*	*Barber et al., 2012*

The SIRT family consists of seven proteins that have a highly conserved catalytic core domain. Nevertheless, these enzymes have varied enzymatic activities, subcellular locations and, consequently, function. Although all SIRTs have been described as having deacetylase activity, SIRT4-6 have limited and specific deacetylase activity (Barber et al., 2012; Laurent et al., 2013; Nakagawa et al., 2009; Zhong et al., 2010). To counteract this deficit, certain SIRTs exhibit other enzymatic activities such as ADP-ribosylation (Liszt et al., 2005), lipoylation (Mathias et al., 2014) or desuccinylation (Park et al., 2013). This diagram illustrates the catalytic core domain (in violet), molecular weight (in kDa), cellular location, predominant enzymatic activity(ies) and the putative role of each SIRT in HD. Figure adapted from Naia and Rego (2015).

There is growing evidence, although still controversial, that these proteins may extend lifespan in numerous lower eukaryotes (Burnett et al., 2011; Rogina and Helfand, 2004; Satoh et al., 2013; Tissenbaum and Guarente, 2001). Calorie restriction (CR), which entails reduced calorie consumption without malnutrition, increases yeast replicative lifespan and was proposed to work through a Sir2 (SIRT1 orthologue)-dependent mechanism (Lin et al., 2002). However, whole body OE of SIRT1 does not affect lifespan in mice (Herranz et al., 2010). Additionally, Burnett and co-authors cast doubt on the robustness of previous findings. The authors re-examined the reported effects of Sir2 OE on survival and found that the use of appropriate controls abolished the apparent effects in both *Caenorhabditis elegans* and *Drosophila* (Burnett et al., 2011), concluding that the studies of gene effects on aging are vulnerable to confounding effects of genetic background. Despite this, Sir2/SIRT1 was shown to promote healthy aging by preventing age-associated neurodegeneration (Gräff et al., 2013; Guedes-Dias and Oliveira, 2013). In particular, class III KDAC modulators attenuate degeneration in eukaryotic cells, namely yeast, *Caenorhabditis elegans* and

Drosophila models of polyQ toxicity (Jiang et al., 2012, 2014; Luthi-Carter et al., 2010; Parker et al., 2005).

SIRTs have provided interesting insights into some of the fundamental mechanisms implicated in disease progression, since their targets are linked to metabolic and survival signaling pathways, which led researchers to investigate their role in HD pathogenesis. Although pioneer results were encouraging, some recent evidences are inconsistent. In this section we debate the recent advances in SIRTs cellular activities and their implications for HD neuroprotection.

1.5.2.2.1. SIRT1: function and targets in HD

SIRT1 is the best-characterized sirtuin and probably the most important sirtuin involved in epigenetic regulation (Konsoula and Barile, 2012). Deletion of SIRT1 affects nearly 10% of all deacetylation sites, most of which occur on nuclear proteins, further affecting their enzymatic activities (Chen et al., 2012). SIRT1 is predominantly nuclear, however it has both nuclear import and export sequences and was found in cytosolic fractions of the mouse brain (Tanno et al., 2007). SIRT1 mediates heterochromatin formation through deacetylation of K26 on histone H1 (Vaquero et al., 2004), K9 on histone H3 and K16 on histone H4 (Pruitt et al., 2006). In addition to histones, SIRT1 also deacetylates non-histone substrates, such as transcription factors (p53, p65, FOXO1 and FOXO3a, retinoic acid receptor beta (RARβ), PGC-1α, and others), DNA repair proteins (thymine DNA glycosylase, Ku70) and signaling factors such as AMP-activated protein kinase (AMPK) (Donmez and Outeiro, 2013; Madabushi et al., 2013). SIRT1 is ubiquitously expressed, but is greatly enriched in brain since embryogenesis until adult age, having a crucial role as an energy metabolic regulator in neurons (Ramadori et al., 2011). However, during aging its expression is decreased (Sommer et al., 2006) and this decline appears to be important along the progression of many neurodegenerative disorders, including amyotrophic lateral sclerosis (Kim et al., 2007a), Alzheimer's disease (Donmez et al., 2010), Parkinson's disease (Donmez et al., 2012) and HD (Hathorn et al., 2011; Jeong et al., 2012a).

The first evidence about the putative beneficial effects of SIRT1 modulation in HD came out in 2005 when Parker and collaborators reported that both increased gene expression of Sir2 or treatment with resveratrol (RESV), a potent activator of Sir2/SIRT1 *in vitro*, prevented early neuronal dysfunction in a transgenic *Caenorhabditis elegans* model expressing an exon 1-like N-terminal fragment with 128Q (Parker et al., 2005). Moreover, the authors showed that RESV (in a lower μM range) protected striatal

neuronal cultures isolated from the HdhQ111 KI mice against polyQ-mediated cell death, probably through a SIRT1-related mechanism (Parker et al., 2005). In accordance, yeast expressing the first 17 N-terminal amino acids of *HTT* exon 1 containing 47Q, which harbors a mid-size polyQ tract, showed aggravated aggregation upon deletion of Sir2 (Cohen et al., 2012). Similarly, ΔSir2 yeast cells expressing expanded 103Q showed higher levels of oxidative stress. Also, in 97Q mHTT-transfected mammalian cells, expression of SIRT1 prevented cell death through deacetylation of Ku70 at K539 and K542, two critical deacetylation sites that influence Ku70-Bax binding, hindering the translocation of Bax to mitochondria, which prompts apoptotic cell death (Li et al., 2007). With regard to lifespan regulation in HD mice or invertebrates, and similarly to non-pathogenic models (discussed above), the results are not always consistent. In a HD fly model, Sir2 OE did not decrease the lethality caused by mHtt (Pallos et al., 2008), however, the complete loss of Sir2 was deleterious in both fly and worm models (Parker et al., 2005; Smith et al., 2014). Interestingly, Sir2 activation increased neuronal survival, but did not rescue the early death phenotype of mHtt-challenged flies, suggesting that longevity promoting strategies may operate through mechanisms that are independent from those that protect against neurodegeneration (Pallos et al., 2008). In contrast with the previous results, Jeong and collaborators observed that SIRT1 OE significantly extended the survival of R6/2 mice in nearly 30 days (Jeong et al., 2012a).

Although there is not a consensus regarding the role of SIRT1 in slowing HD lethal phenotype, the majority of the published studies systemically describe beneficial effects of SIRT1 activation in multiple cellular pathways, which culminates in neuronal survival and motor improvement. One of them is the enhancement of transcriptional activity, since SIRT1 is primarily nuclear and deacetylates several transcription factors and co-activators (Okazawa, 2003; Zhai et al., 2005). As described before in this chapter, transcriptional activity is severely impaired in HD models (Luthi-Carter et al., 2002; Nucifora et al., 2001; Wyttenbach et al., 2001). mHTT interacts with SIRT1 and inhibits SIRT1 deacetylase activity, resulting in hyperacetylation of SIRT1 substrates, such as FOXO3a transcription factor, inhibiting its pro-survival function (**Figure 1.9**). Concordantly, acetylated FOXO3a levels were significantly increased in BACHD mice and in striatal cells expressing mHTT (Jiang et al., 2012). Furthermore, mHTT also impacts on SIRT1 phosphorylation (on Ser/Thr residues) in striatal nucleus from R6/2 mice and HdhQ150 homozygotes. Decreased SIRT1 phosphorylation aggravated with the progression of the disease and was related to the abnormal expression and cellular localization of AMPKα1 in these models. This kinase was proposed to stimulate SIRT1 activation, however this mechanism appears to be compromised in R6/2 mice since

AMPKα1 does not reach the nucleus until 14 weeks of age, close to the end stage of these animals (Tulino et al., 2016). Conversely, SIRT1 OE counteracted mHTT-induced deacetylase deficits, restoring ATP levels in HD striatal-like cells (Jiang et al., 2012). Additionally, SIRT1 OE in HD mouse models expressing truncated or FL human mHTT significantly slowed the progression of motor deficits observed in the rotarod test (Jiang et al., 2012).

SIRT1 also prevents mHTT-induced BDNF transcription decline and the intracellular signaling pathways mediated by its receptor, TrkB, as described in two recent studies (Jeong et al., 2012a; Jiang et al., 2012). Jeong and co-authors showed that brain-specific KO of SIRT1 resulted in exacerbation of brain pathology, whereas OE of SIRT1 improved survival and expression of BDNF in R6/2 mice (Jeong et al., 2012a). Previous studies suggested that TORC1 (CREB-regulated transcription coactivator 1) activated CREB-regulated transcription by promoting the recruitment of transcriptional co-activators to BDNF promoter (Iourgenko et al., 2003). Researchers showed that mHTT may affect TORC1-CREB interaction, repressing BDNF transcription; contrariwise, SIRT1 deacetylates and activates TORC1 by promoting its interaction with CREB (Jeong et al., 2012a) (**Figure 1.9**).

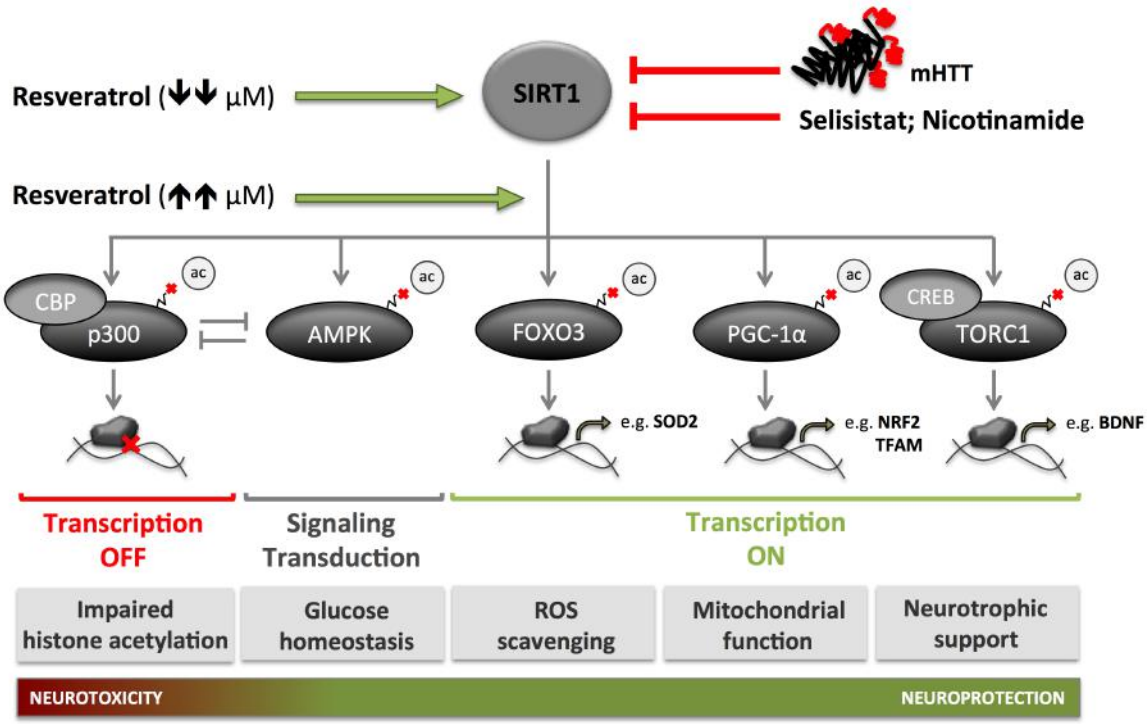

Figure 1.9 | Potential protective role of SIRT1 activation in HD. mHTT aggregates in the nucleus and directly interacts and inhibits SIRT1 activity, affecting multiple downstream targets such as PGC-1α, FOXO3a and TORC-CREB complex, decreasing transcription of genes that modulate mitochondrial biogenesis (e.g. NRF2 and TFAM), antioxidant defense (e.g. SOD2) and neurotrophic

support (e.g. BDNF), respectively. Moreover, SIRT1 inhibition also blocks AMPK-dependent survival pathways. In the presence of lower (↓↓) μM doses of resveratrol, SIRT1 is activated counteracting dysfunctional transcription and increasing neuronal survival. Importantly, similar neuroprotective effects may also occur in a SIRT1-independent way, using higher (↑↑) μM doses of resveratrol. On the epigenetic level, SIRT1 represses p300-CBP complex, which is already affected by mHTT, leading to further transcription repression, as depicted by the red crosses at the promoter. Adapted from Naia and Rego (2015).

If we consider SIRT1 as a factor involved in chromatin regulation, constitutive SIRT1 OE may not always be beneficial. Besides histone deacetylation, SIRT1 can modulate chromatin function through methylation of histones and DNA, forming repressive heterochromatin (Vaquero et al., 2004). Moreover, SIRT1 antagonizes p300-mediated activation of FOXO3a (Cantó et al., 2009). SIRT1 physically associate with and repressed p300 (through deacetylation of K1020/K1024 residues), which transcriptional activity was already compromised by mHTT (Bouras et al., 2005; Zuccato et al., 2001) (**Figure 1.9**). Indeed, this dual role of Sir2/SIRT1 on transcriptional activation may explain why 50% reduction of Sir2 activity was shown to be neuroprotective in HD invertebrates typically containing fewer neurons, arranged in less complex networks than vertebrate systems (Pallos et al., 2008; Smith et al., 2014). Importantly, most of the studies that achieved neuroprotection through SIRT1 inhibition in more complex neuronal systems used drug-like and non-selective inhibitors of SIRT1, calling into question the direct effect of SIRT1 inhibition in HD models.

Clearly the role of SIRT1 in cellular protection is complex; however the understanding of all pathways behind SIRT1 activation may answer why the activation and partial reduction (but not complete deletion) of Sir2/SIRT1 leads to the same phenotype in different HD models.

1.5.2.2.1.1. SIRT1-activating compounds

Either SIRT1 activation or inhibition has been found to exert neuroprotective properties through modulation of diverse cascade pathways. In light of this knowledge, both SIRT1 activators and inhibitors are being actively explored. RESV, a naturally occurring polyphenolic SIRT-activating compound (STAC) isolated from the skin of red grapes, was reported to be a potent activator of SIRT1 *in vitro*, protecting against detrimental effects of high-fat diet exposure such as glucose intolerance, insulin resistance or lifespan reduction [reviewed in (Nogueiras et al., 2012)]. A screen for

molecule activators for SIRT1 identified 21 different SIRT1-activating molecules, and the most potent of which was RESV (Howitz et al., 2003). Although the legitimacy of STACs as direct SIRT1 activators has been widely debated (Pacholec et al., 2010), in 2013 Sinclair's laboratory showed a mechanism of direct activation mediated by an N-terminal activation domain in SIRT1 that is responsible for some of the physiological effects of STACs (Hubbard et al., 2013). Importantly, RESV has the ability to activate important enzymes for energy and glucose homeostasis such as AMPK and PGC-1α, increasing mitochondrial function (Lagouge et al., 2006; Price et al., 2012) and so, it cannot be excluded that RESV might induce SIRT1 activation *via* other pathways that still remain to be identified. In fact, RESV was identified as a phytoestrogen that binds and activates estrogen receptors and estrogen-related receptors (ERRs) (Gehm et al., 1997). Accordingly, high doses of RESV can positively modulate the levels of ETC complexes and O_2 consumption through ERRα activation, a master regulator of mitochondrial ETC and biogenesis (Lopes Costa et al., 2014). Moreover, RESV, *per se*, is a powerful oxidant that in a moderate to high μM range (>50 μM) was shown to activate AMPK in a SIRT1-independent manner, improving mitochondrial function and, consequently, neuronal survival (Price et al., 2012) (**Figure 1.9**). Likewise, RESV failed to improve metabolic parameters and mitochondrial biogenesis in AMPKα1 subunit KO mice (Um et al., 2010), revealing an important role of this kinase regulated under conditions favoring ATP metabolism. In the same way, high doses of RESV improved neuronal survival in Sir2 homozygous null flies expressing mHtt exon 1 with 93Q (Pallos et al., 2008).

Energy deficits have been largely associated with impaired PGC-1α expression and/or function, which is regulated by SIRT1 (Nemoto et al., 2005; Price et al., 2012; Weydt et al., 2006). In this respect, an oral dosing by gavage of RESV of 25 mg/mouse/day, 5 days per week, for 45 days, was able to rescue PGC-1α and NRF-1 mRNA expression in peripheral tissues of N171-82Q HD transgenic mice as a consequence of its deacetylation by SIRT1 (Ho et al., 2010) (**Figure 1.9**). Indeed, it was previously shown that muscle fibers of RESV-treated mice presented increased mitochondrial size and density, mitochondrial DNA content and higher maximum O_2 consumption and citrate synthase activity, suggesting an increased oxidative capacity (Lagouge et al., 2006); however, the treatment failed to improve motor deficits, survival or striatal atrophy associated with the HD phenotype (Ho et al., 2010). The authors explained these negative results with the inefficacy of RESV in the CNS, since the treatment did not improve transcriptional response in the striatum, when compared with peripheral tissues (Ho et al., 2010). However, previous studies showed that orally

administered RESV could cross the BBB and accumulate in the cerebral cortex, but not in the striatum or hippocampus (Vingtdeux et al., 2010).

More recently, several synthetic molecules with the same enzymatic mechanism as RESV, but structurally unrelated, were reported, such as SRT1720, SRT2183 and SRT2104. These molecules were described to be 1000 times more potent than RESV (Milne et al., 2007), recapitulating the beneficial effects in mice fed high-fat diet and other diabetic model systems (Mercken et al., 2014; Smith et al., 2009), with improved selectivity for SIRT1 and well tolerated in healthy volunteers (Hoffmann et al., 2013). Indeed, diet-administered 0.5% SRT2104 was able to pass through the BBB of N171-82Q HD transgenic mice, improving motor function, attenuating neocortical atrophy and extending median lifespan by about 16%, compared to HD mice subjected to control diet (Jiang et al., 2014). Similarly as RESV, SRT2104 improved whole-body metabolism, increasing mitochondrial content and mouse survival (Mercken et al., 2014). These studies revealed that interventions aimed towards a more selective pharmacological modulation of SIRT1 activity could represent an attractive approach for delaying HD onset.

1.5.2.2.1.2. SIRT1-inhibiting compounds

The existent SIRT1 inhibitors so far exhibit low potency and unattractive pharmacological and biopharmaceutical properties. Moreover, their inhibitory activity may be questionable. All SIRTs require NAD^+ as an essential cofactor and, as described before, NAM is predominantly used for NAD^+ biosynthesis in mammals and has been identified as an end-product inhibitor of SIRT1 (Peled et al., 2012). Recently, a quantitative mass spectrometry assay showed that NAM effects are indeed primarily mediated by SIRT1 inhibition, since the acetylome changes of $SIRT2^{-/-}$ and $SIRT6^{-/-}$ cells correlated weakly with NAM-induced changes, compared to $SIRT1^{-/-}$ cells (Scholz et al., 2015). However, there are uncertain observations regarding the metabolic effects of NAM, since it modulates the sirtuin system in a complex way. NAM inhibits SIRT1 activity through non-competitive binding, which promotes a base-exchange reaction at the expense of deacetylation (Jackson et al., 2003), and/or competitively binds at the SIRT1 conserved pocket that participates in NAD^+ binding and catalysis (Avalos et al., 2005). Conversely, NAM offers multiple protective mechanisms as a positive NAD^+ donor, preventing NAD^+ depletion and protecting neurons against excitotoxicity (Liu et al., 2009). Indeed, prolonged administration of high doses of NAM can increase SIRT1 mRNA expression and its enzymatic activity (Yang et al., 2014). Concordantly, treatment

with 250 mg/kg/day NAM for 12 weeks in B6.HD6/1 mice increased both mRNA and protein levels of BDNF and PGC-1α, concomitantly with reduction of PGC-1α acetylated levels, improving motor deficits tested by open field, rotarod and balance beam activities. Still, the improvement in motor function was not accompanied by a reduction in mHTT aggregation (Hathorn et al., 2011). Although retaining SIRT1 protein levels, in this study NAM seems to serve as a SIRT1 activator by increasing NAD^+ levels, since it increased deacetylation of PGC-1α and, probably, TORC1, which in turn activates BDNF transcription (Hathorn et al., 2011).

During the last years, a large number of SIRT1 inhibitors have been identified by *in silico* screenings and, although they have low affinity for SIRT3 and SIRT5, most of them also modulate SIRT2 activity (Chen, 2011). Sirtinol is a well-known SIRT inhibitor which inhibits human SIRT1 with an inhibitory constant $(IC)_{50}$ of 131 mM, 3.25-fold higher than for SIRT2 (IC_{50}=40 mM) (Grozinger et al., 2001). However, a recent acetylation-screening assay showed that the fraction of downregulated acetylation sites in sirtinol-treated cells was greater than the fraction of upregulated sites. Moreover, NAM enhanced 12% of acetylation sites, whereas sirtinol affected less than 2% of sites, indicating that the scope of these inhibitors is vastly different (Scholz et al., 2015). Despite this, studies with sirtinol argue against the protective role of SIRT1 inhibition in HD. Sirtinol treatment for 12 h abolished pro-autophagic activity in human cells expressing exon 1 of HTT with 97Q, increasing mHTT aggregation (Shin et al., 2013). More recently, a pharmacological compound described as being a highly selective inhibitor of Drosophila Sir2 and mammalian SIRT1 named selisistat was described. Notably, Htt-challenged flies treated with selisistat displayed a concentration-dependent (in μM range) rescue of photoreceptor neurons and extended lifespan with the greatest percentage of survival achieved in 10-20 days (Smith et al., 2014). Furthermore, selisistat, which has proven to be safe in healthy human volunteers, is currently being tested in HD phase I clinical trials [(Grozinger et al., 2001); http://clinicaltrials.gov, NCT01485965 and NCT01485952]. Importantly, no obvious effects of short-term daily doses of 10 or 100 mg selisistat were observed in terms of soluble HTT levels in HD patients (Süssmuth et al., 2015). Besides, the role of selisistat as selective Sir2/SIRT1 inhibitor is debatable. Smith and co-authors (Smith et al., 2014) assessed the specificity of selisistat for Sir2/SIRT1 by observing increased levels of acetylated p65 (at K310; a described SIRT1 substrate) in SIRT1 and Sir2 transfected cells (Smith et al., 2014; Yeung et al., 2004). However, there are evidences that p65 is also deacetylated by SIRT2 in the cytoplasm in the same Lys residue (Rothgiesser et al., 2010). Therefore,

the question that remains open is: Can selisistat also inhibit SIRT2 deacetylase activity, which in turn appears to be deleterious in HD models (Luthi-Carter et al., 2010)?

Many questions remain unanswered regarding the role of SIRT1 inhibitors in HD. So far, the lack of structural information has hindered the use of modern drug design methods in the search for highly selective SIRT1 inhibitors that have no influence on other family members, especially SIRT2. Additionally, the effort in finding pharmacological modulators has always been more prominent for activators, since there is more convincing data supporting their beneficial effects. However, more effective and selective SIRT1 inhibitors need to be generated, as well as their specificity improved at the level of individual acetylation sites, which is critical for understanding the distinct modes of action and to demystify the exact role of SIRT1 in neuronal survival and lifespan in health and disease.

1.5.2.2.2. SIRT3 and HD: current data and further connections

SIRT3 research in HD boils down to two publications so far, by Fu *et al*. (2013) and Cheng *et al.* (2016), using ST*Hdh*$^{Q111/Q111}$ striatal cells and mice subjected to 3-NP to elicit mitochondrial dysfunction, respectively, as described below. As has often been pointed out, mitochondrial dysfunction is a hallmark of HD (Kim et al., 2010) and, therefore, a relevant role for SIRT3 in HD must be hypothesized. SIRT3 provides a unique tool to understand mitochondrial metabolism since it is the greatest regulator of the global acetylation landscape of mitochondrial proteins and, like SIRT1, it is highly expressed in kidney, brain and heart (Jin et al., 2009). Remarkably, although nuclear protein acetylation patterns are dramatically altered in HD cells (McFarland et al., 2012), there is no study showing that this pattern also occurs in HD mitochondria. A quantitative mass spectrometry method in wild-type mice *versus* SIRT3$^{-/-}$ mice or in wild-type murine embryonic fibroblasts *versus* SIRT3 KO cells revealed multiple proteins regulated by acetylation, often at multiple sites, across several pathways, including fatty acid oxidation, ketogenesis, amino acid catabolism and urea and TCA cycles (Hebert et al., 2013; Lombard et al., 2007; Qiu et al., 2010; Rardin et al., 2013). The hyperacetylation results in altered activity of these proteins, eventually leading to mitochondrial dysfunction. Indeed, the most acetylated protein is the highly abundant urea cycle enzyme carbamoyl phosphate synthase 1 with 70 of 97 Lys acetylated. Moreover, SIRT3-dependent deacetylation was also observed in isocitrate dehydrogenase at K360 and in glutamate dehydrogenase at K527; SOD2 was also found to be acetylated in three different Lys sites (K53, K68 and K89) (Chen et al., 2011; Lombard et al., 2007;

Qiu et al., 2010; Rardin et al., 2013; Sol et al., 2012). Importantly, acetylation of SOD2 at K68 was reported to decrease its activity (Chen et al., 2011). In ST*Hdh*$^{Q111/Q111}$ striatal cells, ε-viniferin treatment, a resveratrol dimer, but not resveratrol itself, was able to significantly increase SIRT3 expression and decrease ROS levels through SOD2 deacetylation/activation (Fu et al., 2012) (**Figure 1.10**). Interestingly, cells expressing mHTT and subjected to cellular stress following serum deprivation displayed reduced SIRT3 levels that were reset after ε-viniferin treatment (Fu et al., 2012). ε-viniferin activates AMPK in a SIRT3-dependent manner, through deacetylation of the primary upstream AMPK kinase, liver kinase B1 (LKB1, also known as Ser/Thr kinase 11), enhancing PGC-1α levels and, consequently, mitochondrial biogenesis and preventing the loss of $\Delta\psi_m$ and NAD^+/NADH ratio in HD cells (Fu et al., 2012) (**Figure 1.10**). In a very recent and well-designed study, Cheng *et al*. also aimed to determine whether SIRT3 influences striatal vulnerability induced by 3-NP administration in SIRT3 KO mice (Cheng et al., 2016). The authors observed that after only one week of 3-NP administration the motor performances of both SIRT3 KO and wild-type mice were impaired, however the magnitude of motor impairment was significantly higher in 3-NP-treated SIRT3 KO mice, when compared to 3-NP-treated wild-type animals. Further histological analysis revealed that the same dosage of 3-NP caused a much larger lesion area in the striatum, with complete neuronal loss, in SIRT3 KO mice than in wild-type mice (Cheng et al., 2016), supporting the protective role of SIRT3 in a model that resembles HD neuropathology. Additionally, they showed that SIRT3 is essential for sustained bioenergetics even without any cytotoxic stimuli, since SIRT3 KO destabilized mitochondrial membranes (increasing Ca^{2+}-induced swelling) and compromised neuronal Ca^{2+} handling (Cheng et al., 2016); however this was not tested in pharmacological or genetic-based HD models.

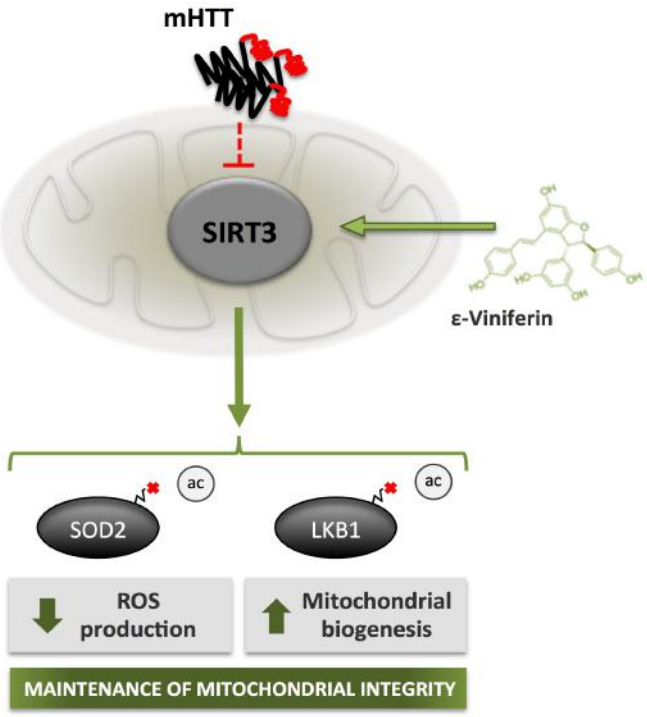

Figure 1.10 | SIRT3 controls mitochondrial dysfunction induced by mHTT. Upon activation with ε-viniferin, SIRT3 deacetylates and activates SOD2, causing resistance to oxidative stress, and LKB1, increasing mitochondrial biogenesis in an AMPK-dependent manner, thus counteracting mitochondrial impairment induced by mHTT.

In light of these recent data we can anticipate that some strategies involving SIRT3 can actually influence HD mitochondria. As discussed above, SIRT3 was discovered as an upstream deacetylase of PDHA1 and PDP1 (Fan et al., 2014; Jing et al., 2013). SIRT3 also deacetylates components of complexes I, II and V (Ahn et al., 2008; Finley et al., 2011; Rahman et al., 2014), indicating a role in regulation of OXPHOS machinery and ATP production that were found to be impaired in several HD models and in *postmortem* brain tissues from HD cases with substantial neuronal loss (Gu et al., 1996; Napoli et al., 2013). In mice (as in humans), complex I is composed by more than 40 distinct proteins that together function as NADH dehydrogenase; SIRT3 can physically interact and deacetylate at least five of this complex subunits, NDUFA3, 5, 9 and NDUFV1, 6 (Rardin et al., 2013). Interestingly, complex I inhibition with either rotenone or H_2O_2 can lead to the dissociation of the SIRT3-complex I interaction, reducing more than 50% of basal ATP levels in the heart, kidney and liver (Ahn et al., 2008). Moreover, the flavoprotein subunit of SDH was previously identified as having a total of 13 acetylated Lys, six of which (K182, K250, K480, K550, K624 and K633) increased in SIRT3 KO mice (Ahn et al., 2008).

Recently reports have questioned the distribution of SIRT3 limited to mitochondria. This uncertainty arises from the two different isoforms (a ~28 kDa processed/short and a ~44 kDa FL) of SIRT3, which are expressed in both humans and mice and appear to be differentially distributed (Hallows et al., 2008). Indeed, it was

shown that FL-SIRT3 localizes and functions in the nucleus (Iwahara et al., 2012; Scher et al., 2007); however, its role in this organelle remains controversial. In the nucleus, FL-SIRT3 was shown to deacetylate histone H3K9 and H4K16 *in vivo*, repressing transcription in a gene-specific manner when recruited to its promoter (Scher et al., 2007); also the non-global hyperacetylation of SIRT3 KD suggests that this action occurs in specific regions of the genome. It has been shown that FL-SIRT3 is able to deacetylate particular targets in the nucleus of cardiomyocytes such as FOXO1 (Zhang et al., 2013), elevating the expression of FOXO1 target genes, catalase and SOD2, while decreasing senescence phenotypes; SIRT3 also deacetylates Ku70 increasing its activity and hindering apoptotic signals (Sundaresan et al., 2008). FL-SIRT3 can also be translocated from the nucleus to the mitochondria upon cellular stress, such as DNA damage induced by etoposide and UV-irradiation (Scher et al., 2007). Although there are no previous studies of nuclear SIRT3 in neurons, Fu and collaborators (2012) showed that ε-viniferin treatment attenuates mHTT-mediated decline of PGC-1α. Inversely, PGC-1α strongly stimulates SIRT3 gene expression on SIRT3 promoter through ERRα co-activation, and the deacetylase is essential for PGC-1α-dependent induction of ROS-detoxifying enzymes and several components of the respiratory chain (Kong et al., 2010).

The beneficial effect of SIRT3 in regulating bioenergetics and activating antioxidant defense system seems unequivocal; however its role in HD neuroprotection remains vague. Although the first evidence point to a protective role of SIRT3 activation on energy metabolism homeostasis, thereby protecting cells from mHTT toxicity, further studies using genetic modulation and animal models needed to be performed. Additionally, novel agents that could selectively modulate SIRT3 activity might be of great therapeutic value, providing means for enhancing neuroprotection.

1.6. HYPOTHESIS AND SPECIFIC AIMS OF THE PRESENT WORK

As described along this chapter, defective mechanisms across mitochondria and nucleus can largely explain selective striatal and cortical neurodegeneration observed in mHTT-expressing neurons. HD is a fatal neurodegenerative disorder and the symptomatic treatments applied so far may alleviate symptoms, but are not curative. Rather than treating specific symptoms, therapy should target abnormal pathways underlying HD pathology with the ultimate goal of preserving neuronal structures, function and viability. Therefore, the present work aimed to evaluate the protective/therapeutic role of KDACs, which target either chromatin remodeling or protein activity through post-translational modifications, on mitochondrial function, and the impact on neuronal viability and motor performance in HD models. For this purpose, and to achieve the most possible robust results, we took advantage of several models expressing FL-mutant huntingtin: i) striatal cells derived from HD KI mice expressing mHtt with 111Q (ST*Hdh*$^{Q111/Q111}$; mutant cells) *versus* wild-type striatal cells (ST*Hdh*$^{Q7/Q7}$); ii) lymphoblastoid cell lines obtained from HD patients and age-matched unaffected (control) siblings; iii) primary cortical and striatal neurons isolated from YAC128 *versus* wild-type embryos at E16-E17; and iv) 9 month-old symptomatic hemizygous YAC128 mice *versus* wild-type controls.

To pursue the described aim this study was divided into three parts.

I) Previous data obtained by us and other research groups have shown that PDC has a central role in metabolic dysfunction in HD. PDC is a highly controlled complex, and modified transcription may be involved in the regulation of its subunits. In this first part of the work we aimed to thoroughly study the regulation of PDC system in HD models. Furthermore, we analyze the influence of HDACi SB and PB, which mainly target classes I and IIa HDACs, on mitochondrial-related PDC function; *in vitro* data were further validated in YAC128 mouse brain.

II) SIRTs and STACs were initially described as rejuvenation molecules due to their effects on lifespan. During the last decade some studies reported neuroprotective effects of SIRT1 and its activators, in several HD modes, ranging from invertebrates to mice. However, recent data cast doubt on these results. Thus, in the second part of this work we aimed to understand the molecular mechanisms that determine whether SIRT1 activation (with RESV) and inhibition (with NAM) improve mitochondrial function in HD models and alleviate motor dysfunction, characteristic of the disease.

III) Mitochondrial SIRT3 is the most recent pivotal player in mitochondrial function, oxidative stress and aging. However, little is known about its role in neurodegeneration. In this last section we propose to evaluate the role of SIRT3 in HD, from its protein levels and activity, to how its expression influences mitochondrial function, mitochondrial-related transcription and biogenesis and cell death.

We hypothesized that the use of HDACi, and pharmacological or genetic activation of SIRT1 and SIRT3 could prevent unbalance cellular acetylation status, helping to restore PDH-related metabolism and general mitochondrial function. Moreover, RESV-dependent SIRT1 activation was hypothesized to improve HD motor phenotype. We consider that the present study reveals potential therapeutic strategies that effectively target gene transcription as well as the activity of core proteins related to mitochondria, opening new avenues to minimize or delay HD pathology.

CHAPTER II

MATERIAL AND METHODS

2.1. MATERIALS

Fetal Bovine Serum (FBS), Opti-MEM medium (ref. 22600), B27 supplement and penicillin/streptomycin, geneticin (G418; ref. 11811-031) were from Gibco (Paisley, Scotland, UK). Trypsin type IX-S from porcine pancreas, soybean (trypsin inhibitor type II-S), diethylpyrocarbonate (DEPC), dimethyl sulfoxide (DMSO); 2-hydroxypropyl-β-cyclodextrin (HOP-β-CD), Mowiol 40-88, 3-(4,5-dimethylthiazol-2-yl)-2,5-diphenyltetrazolium bromide (MTT), nicotinamide, resveratrol, trichostatin A (TSA), sodium butyrate (SB), phenyl butyrate (PB), fatty-acid free albumin from bovine serum (BSA), oligomycin, carbonyl cyanide 3-chlorophenylhydrazone (CCCP), carbonyl cyanide 4-(trifluoromethoxy) phenylhydrazone (FCCP), protease cocktail inhibitors, RPMI 1640 medium, Dulbecco's Modified Eagle's Medium (DMEM) medium (ref. D5648) and other analytical grade reagents were purchased from Sigma Aldrich (St. Louis, MO, USA). Enhanced ChemiFluorescence reagent (ECF), anti-rabbit IgG (from goat), anti-mouse IgG+IgM (from goat) were from GE Healthcare (Little Chalfort, UK). Anti-goat IgG-AP (from donkey) was from Santa Cruz Biotechnology (Santa Cruz, CA, USA). PureLink Genomic DNA mini kit, Rhodamine 123, Tetramethylrhodamine methyl ester ($TMRM^+$), 2',7'-dichlorodihydrofluorescein diacetate (H_2DCF-DA), MitoTracker Deep Red FM (ref. M22426), Hoechst 33342 nucleic acid stain, Propidium Iodide (PI), Lipofectamine® 3000 and Alexa Fluor-647 donkey anti-rabbit (ref. A31573) were obtained from Invitrogen/Molecular Probes (Life Technologies Corporation, Carlsbad, CA, USA). PureZOL RNA isolation reagent, iScript cDNA Synthesis kit, SsoFast EvaGree Supermix, Bio-Rad Protein Assay and Polyvinylidene fluoride (PVDF) membrane were from Bio-Rad (Hemel Hempstead, UK). Nuclear/Cytosol Extraction Kit was from BioVision (Milpitas, CA, USA). NAD/NADH assay kit (ref. ab65348) and SIRT3 activity assay kit (ref. ab156067) were from Abcam (Cambridge, UK). XF Cell Mito Stress Test Kit and XF24 cell culture microplates were from Seahorse Bioscience (Billerica, MA, USA). Mini osmotic pumps were from Alzet (Cupertino, CA, USA). Isoflurane was from Esteve (Barcelona, Spain). All other reagents were of analytical grade. The primary antibodies used for western blotting (WB) and immunocytochemistry (ICC) are listed in **Table 2.1**. The primers used for real-time PCR (qPCR) are listed in **Table 2.2**.

Table 2.1 | List of the primary antibodies used in this work.

Antibody	Molecular Weight	Reference/Brand	Dilution	Host
α-Tubulin	50 kDa	T-6199, Sigma-Aldrich	1:5,000	mouse
β-Actin	42 kDa	A5316, Sigma-Aldrich	1:5,000	mouse
Acetylated lysine	-	#9441S, Cell signaling	1:500	rabbit
CREB, phospho S133	46 kDa	ab32096, Abcam	1:500	rabbit
HIF-1α	~130 kDa	ab1, Abcam	1:500	mouse
Histone H3, acetyl K9	17 kDa	ABE18, Millipore	1:750	rabbit
Histone 3	17 kDa	#9715, Cell Signaling	1:2,000	rabbit
HSP60	60 kDa	MAB3844, Chemicon	1:1,000	mouse
HTT (D7F7)	~350 kDa	#5656, Cell Signaling	1:300	rabbit
PDH-E1α, phospho S232	44 kDa	AP1063, Calbiochem	1:750	rabbit
PDH-E1α	43 kDa	#2784, Cell Signaling	1:1,000	mouse
PDH kinase 1 (PDK1)	47 kDa	#3820, Cell Signaling	1:1,000	rabbit
PDK kinase 3 (PDK3)	47 kDa	ab182574, Abcam	1:1,000	rabbit
PGC-1α	90 kDa	sc-5816, Santa Cruz Biotech	1:500	goat
SIRT3 (D22A3)	28/44 kDa	#5490, Cell Signaling	1:500	rabbit
SDHA	70 kDa	A11142, Molecular Probes	1:5,000	mouse
SOD2, acetyl K68	24 kDa	ab137037, Abcam	1:500	rabbit
SOD2	24 kDa	Ab13533, Abcam	1:2,500	rabbit
TBP	37 kDa	ab51841, Abcam	1:1,000	mouse
TFAM (for ICC)	27 kDa	ab49134, Abcam	1:300	rabbit
TFAM (for WB)	27 kDa	sc-28200, Santa Cruz Biotech	1:200	rabbit

Table 2.2 | Sequence (5'→3') of primers used for qPCR experiments.

Specie	Gene	Forward primer	Reverse primer
human	*MT-COXI*	GGCCACCTACGGTGAAAAGA	TTAGCTGACTCGCCACACTC
	MT-ND5	GAGTCAGGGGTGGAGACCTA	ACGCTAATCCAAGCCTCACC
	CYCS	CTTTGGGCGGAAGACAGGTC	TTATTGGCGGCTGTGTAAGAG
	tRNA^{Leu}	CACCCAAGAACAGGGTTTGT	TGGCCATGGGTATGTTGTTA
	B2M	TGCTGTCTCCATGTTTGATGTATCT	TCTCTGCTCCCCACCTCTAAGT
	SIRT3	CGGCTCTACACGCAGAACATC	CAGCGGCTCCCCAAAGAACAC
	GAPDH	ATTCCACCCATGGCAAATTC	GGGATTTCCATTGATGACAAGC
mouse	*Actin*	GTGACGTTGACATCCGTAAAGA	GCCGGACTCATCGTACTCC
	MT-CO1	TGGGTGCCCAAAGAATCAGA	ACAGACCGCAACCTAAACACA
	MT-ND5	AGGACTGGAATGCTGGTTGG	ACCCAATCAAACGCCTAGCA
	CYCS	CCAAATCTCCACGGTCTGTTC	ATCAGGGTATCCTCTCCCCAG
	GAPDH	CGGCCTTCCGTGTTCCATC	GAGTTGCTGTTGAAGTCGCA
	PDHA1	TCATCACTGCCTATCGAGCAC	GTTGCCTCCATAGAAGTTCTTGG
	PDK1	GGACTTCGGGTCAGTGAATGC	CGCAGAAACATAAACGAGGTCT
	PDK2	CGGACTCTAAGCCAGTTCACA	GTGGGCACCACGTCATTGT
	PDK3	CCGTCGCCACTGTCTATCAA	TGCGCAGAAACATATAGGAAGTTT
	PDK4	CCGCTTAGTGAACACTCCTTC	TCTACAAACTCTGACAGGGCTTT
	PDP1	CGGGCACTGCTACCTATCCTT	ACAATTTGGACGCCTCCTTACT
	PDP2	GGCTGAGCATTGAAGAAGCATT	GCCTGGATTTCTAGCGAGATGT
	SIRT3	GCCTGCAAGGTTCCTACTCC	TCGAGGACTCAGAACGAACG
	TBP	ACCGTGAATCTTGGCTGTAAAC	TCAGCATTTCTTGCACGAAGT
	tRNA$^{Tyr/CO1}$	CAGTCTAATGCTTACTCAGC	GGGCAGTTACGATAACATTG

2.2. EXPERIMENTAL ANIMALS

YAC128 mice, previously described by Slow *et al.* (2003b), express human FL-mHTT with ~128 CAG repeats from a yeast artificial chromosome (YAC) transgene. Colonies of homozygous [line HD55] and hemizygous [line HD53] YAC128 (king gift from Dr. Michael Hayden, University of British Columbia, Vancouver, Canada), and wild-type (WT) mice, with FVB/N background, were housed in the Housing Facility of the Center for Neuroscience and Cell Biology (CNC) and Faculty of Medicine, at University of Coimbra, Coimbra, Portugal, under conditions of controlled temperature (22–23ºC) and

under a 12 h light/12 h dark cycle. Food and water were available *ad libitum*. Animals' maintenance and procedures were performed in accordance with the guidelines of the Institutional Animal Care and Use of Committee and the European Community directive (2010/63/EU). All efforts were made to minimize animal suffering and to reduce the number of animals used. L. Naia is certified by the Portuguese Veterinary Authority to handle animals.

2.2.1. GENOTYPING

Twenty two day-old mice were genotyped using a tail-tip DNA polymerase chain reaction (PCR) standard procedure. Primers used were LyA1 (CCT GCT CGC TTC GCT ACT TGG AGC), LyA2 (GTC TTG CGC CTT AAA CCA ACT TGG), RyA1 (CTT GAG ATC GGG CGT TCG ACT 213 CGC), RyA2 (CCG CAC CTG TGG CGC CGG TGA TGC), actin forward (GGA GAC GGG GTC ACC CAC AC), and actin reverse (AGC CTC AGG GCA TCG GAA CC). PCR protocol consisted in 35 cycles, with the following temperatures and times for each step: denaturation—94 °C for 30 s; annealing—63 °C for 30 s; and elongation—72 °C for 30 s. At the end of the cycles, DNA was left at 70 °C for 10 min. PCR products were analyzed on 1.7 % agarose gels followed by staining with ethidium bromide and visualized under a UV trans-illuminator, Gel Doc XR system (BioRad, Hercules, USA). A 100-bp ladder (Invitrogen) was used as a size marker.

2.2.2. MINI-OSMOTIC PUMPS IMPLANTATION

For the present experiment, we used nine month-old hemizygous male YAC128 mice and age- and gender-matched wild-type mice, as controls. Briefly, mice were divided into ten experimental groups (7-9 animals per group) and then subcutaneously implanted with a micro-osmotic pump (Alzet 2004), after a small incision in the skin between the scapulae. Micro-osmotic pumps were filled to continuously infusing resveratrol (RESV, 1 mg/kg/day) or HOP-β-CD, which was used to solubilize RESV; or nicotinamide (NAM, 250 mg/kg/day) or sodium butyrate (SB, 1 mg/kg/day) or saline solution (SAL, 0.9% NaCl), the latter used as a control for NAM and SB, for 28 days. RESV is relatively insoluble in aqueous solution and DMSO is not well tolerated for continuous infusion. Thus, RESV is capable of forming a complex with HOP-β-CD with greatly enhanced aqueous solubility and efficacy (Berta et al., 2010; Tiwari et al., 2010). All the surgery procedures were performed under isoflurane anesthesia through isoflurane vaporizer apparatus (EZ Anesthesia, Palmer, PA, USA). Accuracy of micro-

osmotic pumps was verified according to manufacturer's instructions. Behavior analysis was performed one day before and three days after (recovery period) the surgery. The animals were sacrificed the day after the application of behavioral test by isoflurane anesthesia and decapitation, in accordance to EU guideline 86/609/EEC and Annex II of Portuguese decree-law No. 113/2013. The brains were collected and cortex (CTX) and striatum (STR) were dissected.

2.2.3. BEHAVIOR ANALYSIS: ROTAROD MOTOR EVALUATION

Mice were allowed to adapt to the behavior test room for 2 h before the behavior studies. Procedures were consistent for all subjects and tests made at minimum noise levels. Motor coordination and motor learning were assessed on an accelerating rotarod apparatus (Letica Scientific Instruments, Panlab, Barcelona, Spain). Behavior equipment was cleaned thoroughly with 70% ethanol before each animal trial. In this test, mice must learn to run when placed on a constant rotating rod to prevent them from falling. Once the task is learned, the accelerating rotarod can be used to assess motor coordination and balance. Separate cohorts of mice were trained at a fixed-speed of 4 rpm to a maximum time of 40 s. The training time corresponds to the time it took the mice to stand on the rod without falling for 40 consecutive seconds. For the accelerating task (motor coordination), the rotarod was accelerated from 5 to 40 rpm over 5 min and the latency to fall was recorded for each of the four trials and averaged to generate the overall time for each mouse. Resting time between each experiment was set for 30 minutes.

2.2.4. CORTICAL AND STRIATAL PRIMARY CULTURES

Primary cortical and striatal cultures were generated from the offspring of crosses between wild-type mice (used as controls) or between homozygous YAC128 mice males and wild-type females from the same genetic FVB/N background. Brains from E16-17 embryos were rapidly removed into ice-cold Hank's balanced salt solution (HBSS containing (in mM): 5.4 KCl, 0.4 KH_2PO_4, 137 NaCl, 4.2 $NaHCO_3$, 0.3 $NaH_2PO_4.H_2O$, 5 glucose, 5.4 sodium pyruvate, 5.4 HEPES, 0.001% phenol red) supplemented with 0.3% BSA. Cortex and striatum were dissected under the microscope at a magnification of 25x. Tissues were firstly chemically digested with HBSS supplemented with 0.003% trypsin and subsequently mechanically digested. Soybean was used to block the trypsin. Neurons were cultured in Neurobasal medium

supplemented with 2% B-27, 1 mM glutamine, 100 U/ml penicillin, and 100 mg/ml streptomycin and plated at a density of 9×10^4 cells/cm^2 in poly-L-lysine (0.1 mg/ml) coated 48 or 6-well plates. Cultures were maintained at 37ºC in a 95/5% air/CO_2 incubator and used for experiments after 11 days *in vitro* (DIV). Expression of wild-type and mutant forms of HTT were confirmed by western blotting. Cultures were treated with 0.5 to 5 μM RESV and 0.1 to 1 mM NAM for 96 hours before experiments.

2.3. CELL LINES CULTURE

2.3.1. HUMAN LYMPHOBLASTS

Human lymphoblastoid cell lines were obtained from Coriell Institute for Medical Research (USA), derived from HD affected patients containing heterozygous expansion mutation, four males (43/15, 45/15, 42/18, 49/17) and one female (47/18), or from unaffected voluntary control siblings, three males and one female, defined in this work as control (CTR) lymphoblasts. Cells were maintained at a density of 400,000–600,000 cells/mL and cultured in RPMI-1640 medium supplemented with 15% (v/v) non-inactivated FBS, 2 mM L-glutamine and 50 μg/mL streptomycin plus 100 IU/mL penicillin in T25 or T75 flasks, in upright position, using an incubator chamber containing 95/5% air/CO_2, and 100% humidity, at 37ºC. In these conditions, lymphoblastoid cell lines grow in suspension with cells clumped in loose aggregates. When used, these aggregates were dissociated by gently homogenization with a pipette. After 3–4 DIV, the cultures were either re-fed with fresh medium or split according to the rate of cell growth or the required number of cells needed for the experiments. For each experiment, HD or CTR lymphoblasts were plated at 500,000 cells/mL in fresh RPMI medium and incubated for 24 h, in the absence (basal) or presence of 1 μM or 5 μM RESV and 0.5 mM or 1 mM NAM.

2.3.2. STH*dh*$^{Q7/Q7}$ AND STH*dh*$^{Q111/Q111}$ STRIATAL CELLS

Immortalized striatal neurons derived from KI mice expressing FL normal (ST*Hdh*$^{Q7/Q7}$, clone 2aA5, referred as wild-type cells) or FL-mHtt with 111Q (ST*Hdh*$^{Q111/Q111}$, clone 109-1A, referred as mutant cells) were obtained from Coriell Institute for Medical Research (USA), and treated according to slight modifications of established procedures (Trettel et al., 2000). Briefly, cells were grown adherent, at 33ºC, in DMEM medium supplemented with 10% FBS, 4 mM glutamine, 100 U/ml penicillin,

0.1 mg/ml streptomycin, and 400 g/ml geneticin, in an atmosphere of 95% air/5% CO_2. Twenty-four hours before the experiment (and one day after cell plating), the cells were incubated with SB (100 µM, 250 µM and 500 µM) or PB (100 µM, 250 µM and 500 µM) or DCA (3 mM). For hypoxia-inducible factor 1 alpha (HIF-1α) stabilization/accumulation, striatal cells were maintained for 1 h before the experiment in a controlled hypoxic atmosphere (0.1%-0.5% O_2) (Forma Anaerobic System, Thermo Fisher Scientific), at 33ºC. The HIF-1α subunit is continuously synthesized and degraded under normoxic conditions, while it accumulates rapidly following exposure to low oxygen tensions (Salceda and Caro, 1997).

2.3.3. CONSTRUCTS AND TRANSFECTION

Immortalized striatal cells were cultured in DMEM medium supplemented with 10% FBS and transient transfected on the following day (80% confluence) with: a) the pLKO.1/shRNA-PDK3 vector (clone ID: TRCN0000023835, Dharmacon), designed by The RNAi Consortium, or the pLKO.1-scrambled negative control (TRC-RHS6848; Open Biosystems), for knock-down experiments in Chapter III; b) the green fluorescent protein (GFP)-tagged human SIRT3 (SIRT3-GFP; ref. number RG217770) or pCMV-AC-GFP (GFP; ref. number PS100010), obtained from Origene (MD, USA), for overexpression experiments in Chapter V; and c) the pDsRed2-Mito plasmid (MitoDsRed; ref. number 632421), obtained from Clontech (CA, USA), to specifically label mitochondria. ST*Hdh* cells were transfected with 0.5-0.75 µg DNA/cm^2 of growth area in opti-MEM medium without FBS or antibiotics and supplemented with 28.5 mM $NaHCO_3$, following the Lipofectamine 3000 (ThermoFisher Scientific) manufacturer instructions. Medium was changed 4 hours after transfection and cells were cultured for 48 h. Percentage of transfection for SIRT3-GFP or GFP plasmids was 10.94±1.15% (mean±SEM) for wild-type cells and 6.43±1.07% for mutant cells.

2.4. TISSUE AND CELL EXTRACTIONS

2.4.1. TOTAL, MITOCHONDRIAL AND NUCLEAR-ENRICHED SUBCELLULAR PROTEIN FRACTIONS

Striatal cells and lymphoblasts were washed with phosphate-buffered saline (PBS) solution containing (in mM): 137 NaCl, 2.7 KCl, 1.4 K_2HPO_4, and 4.3 KH_2PO_4, at pH 7.4. Since lymphoblasts growth in suspension, they were previously centrifuged at 145 *g*, for 5 min at 4ºC.

Total fractions: Extracts were prepared in ice-cold lysis buffer (in mM: 20 Tris, 100 NaCl, 2 EDTA, 2 EGTA, 50 NaF, 1 Na_3VO_4, 1% Triton; pH 7.4) supplemented with 1 mM 1,4- dithiothreitol (DTT), 100 µM phenylmethylsulfonyl fluoride (PMSF), 100 nM okadaic acid, 1 µg/mL protease inhibitor cocktail (chymostatin, pepstatin A, leupeptin, and antipain), 1 µM TSA (HDAC inhibitor) and 10 mM nicotinamide (SIRT inhibitor). In particular, for dot blotting assay, 0.05% Triton was used since higher concentrations can inhibit protein binding to the membrane. The homogenates (total fractions) were then frozen/thawed three times in liquid nitrogen and centrifuged at 20,800 x*g* for 10 min, at 4ºC, in order to remove cell debris; the resulting supernatant was collected and stored at -80ºC for later use.

Mitochondrial-enriched fractions: Cells were scraped or re-suspended in ice-cold sucrose buffer (in mM: 250 sucrose, 20 HEPES/KOH (pH 7.5), 100 KCl, 1.5 $MgCl_2$, 1 EGTA, and 1 EDTA), supplemented with 1 mM DTT, 100 µM PMSF, 100 nM okadaic acid, 1 µg/mL protease inhibitor cocktail, 1 µM TSA and 10 mM nicotinamide. Lysates, obtained after homogenization, were centrifuged at 1,088 x*g* for 12 min (4ºC) to pellet the nuclei and cell debris. The supernatant was further centrifuged at 12,000 x*g* for 20 min (4ºC) and the resulting pellet (mitochondrial-enriched fraction) resuspended in supplemented sucrose buffer and stored at -80ºC for later use.

Nuclear-enriched fractions: Nuclear fractions were obtained using the Nuclear/Cytosol Extraction Kit from BioVision (Milpitas, CA, USA), following the manufacturer instructions. Briefly, cells were scraped or resuspended in cytosol extraction buffer A containing DTT and protease inhibitors and vigorously vortex for 15 seconds to fully resuspend the cellular suspension. Extracts were then incubated on ice for 10 minutes. To isolate the cytoplasmic fraction, ice-cold cytosol extraction buffer-B was added to the extract and, after a 5 seconds vortex, centrifuged at 16,000 x*g* for 5 minutes. The remaining pellet (containing nuclei) was resuspended in ice-cold nuclear extraction supplemented buffer and vortex for 15 seconds for every 10 minutes, totaling 40 minutes. The final extracts were then centrifuged at 16,000 x*g* for 10 minutes, at 4ºC and stored at -80ºC for later use.

2.4.2. PROTEIN FRACTIONS OF YAC128 MICE CORTEX AND STRIATUM

Total fractions from cerebral cortex and striatum were obtained from treated nine month-old YAC128 or wild-type mice. Cortex and striatum from one brain hemisphere was dissected on ice and homogenized with a Potter-Elvejhem 377 homogenizer with a Teflon pestle in supplemented ice-cold lysis buffer described in the

previous section. The homogenates were then sonicated for 15 s and centrifuged at 20,800 *xg* for 10 min, at 4°C, to remove cell debris.

Mitochondrial- and cytosolic-enriched fractions were obtained from cortex of twelve month-old YAC128 or wild-type mice and homogenized in supplemented ice-cold sucrose buffer described previously. Resulting lysates were centrifuged at 1,088 x*g* for 12 min (4ºC) to pellet the nuclei and cell debris. The supernatant was further centrifuged at 12,000 x*g* for 20 min (4ºC) and the resulting pellet (mitochondrial-enriched fraction) resuspended in supplemented sucrose buffer. Trichloroacetic acid (15%) was added to the supernatant, and precipitated proteins were centrifuged at 16,300 x*g* for 10 min (4ºC). The resulting pellet (cytosolic-enriched fraction) was resuspended in supplemented sucrose buffer and brought to pH 7 with KOH.

All samples were kept at −80°C until use.

2.4.3. TOTAL RNA EXTRACTION

RNA from different samples was extracted with PureZOL RNA isolation reagent according to the manufacturer's protocol. Briefly, mice cortex was lysed after potter homogenization, whereas striatal cells and lymphoblasts were scraped or homogenized with a pipette. RNA was precipitated with isopropyl alcohol and the final pellet was resuspended with DEPC (diethylpyrocarbonate) 0.1% (v/v) water. The concentration of RNA was measured using a Nanodrop 2000 (ThermoScientific, Walthem, MA, USA) and the RNA integrity was confirmed by A260/280>1.9. Samples were maintained at -80ºC until complementary DNA (cDNA) conversion.

2.5. PROTEIN EXPRESSION QUANTIFICATION

2.5.1. WESTERN BLOTTING

Total, mitochondrial and nuclear extracts, obtained as described previously, were denatured with denaturing buffer (50 mM Tris-HCl pH 6.8, 2% SDS, 5% glycerol, 600 mM DTT, 0.01% bromophenol blue) at 95ºC, for 5 min. Equivalent amounts of protein were separated on a 10-15% SDS-PAGE gel electrophoresis and electroblotted onto polyvinylidene fluoride (PVDF) membranes. The membranes were blocked for 1 h in Tris-buffered saline (TBS) solution containing 0.1% Tween (TBS-Tween) and 5% fat-free milk or 5% BSA, followed by an overnight incubation with primary antibodies listed in **table 2.1**, at 4ºC, with gentle agitation. Membranes were then washed 3 times, for 15 min, with TBS-Tween, and incubated with secondary antibodies conjugated with alkaline

phosphatase (1:20,000), for 1 h, at room temperature, with gentle agitation. Immunoreactive bands were visualized by alkaline phosphatase activity after incubation with ECF substrate, in a Bio-Rad Versa Doc 3000 Imaging System or ChemiDoc Touch Imaging System (Bio-Rad). Bands were quantified using the Quantity One or Image Lab software (Bio-Rad).

2.5.2. DOT BLOTTING

Equivalent amount of total striatal extracts (5 μg) were directly applied onto a previous methanol-activated and equilibrated PVDF membrane. After sample is absorbed, membrane was blocked for 1 h in TBS-Tween with 5% fatty-free BSA, followed by an overnight incubation with primary anti-acetyl lysine antibody, at 4ºC, with gentle agitation. Membranes were then washed 3 times, for 15 min, with TBS-Tween, and incubated with secondary antibody conjugated with alkaline phosphatase (1:20,000), for 1 h, at room temperature, with gentle agitation. Immunoreactive dots were visualized and quantified using the same equipment and software as used for western blotting analysis.

2.5.3. IMMUNOCYTOCHEMISTRY

Striatal cells plated in 18 mm coverslips were washed twice with warm PBS, fixed with 4% paraformaldehyde (pre-warmed at 37ºC) for 20 minutes, permeabilized in 0.1% Triton X-100 in PBS for 2 minutes and blocked for 1 hour, at room temperature in 3% (w/v) BSA in PBS. Incubation with primary antibody (listed in **table 2.1**) occurred overnight, at 4ºC. In the following day, cells were incubated for 1 hour, at room temperature, with secondary antibody alexa fluor-647. All antibodies were prepared in 3% (w/v) BSA in PBS. Finally, cells were incubated with Hoechst 33342 (4 μg/mL) for 20 minutes and mounted using Mowiol 40-88. Confocal images were obtained using a Plan-Apochromat/1.4NA 63x lens on an Axio Observer.Z1 confocal microscope (Zeiss Microscopy, Germany) with Zeiss LSM 710 software. Protein quantification and co-localization analysis was achieved using Macros designed by Dr. Jorge Valero (Center for Neuroscience and Cell Biology – University of Coimbra, presently at Achucarro – Basque Center for Neuroscience, Spain) in Fiji software (ImageJ, National Institute of Health, USA).

2.6. ANALYSIS OF GENE EXPRESSION BY QUANTITATIVE qPCR

RNA was transcribed into cDNA in a template–primer mix using the iScript cDNA Synthesis Kit (Bio-Rad). The reaction was done in a CFX96 qPCR system (Bio-Rad, Hemel Hempstead, UK) as follow: 5 minutes at +25°C, 30 minutes at +42°C and 5 minutes at +85°C. The concentration of the resulting single-stranded cDNA was determined by NanoDrop 2000 spectrophotometer. qPCR was performed using the SsoFast Eva Green Supermix, in the same CFX96 qPCR system (Bio-Rad, Hercules, CA, USA), with the primers defined in **table 2.2**, at 500 nM (for cell extracts) or 300 nM (for tissue extracts). Amplification of 10 ng (50 ng for *SIRT3* mouse gene) template was performed with an initial cycle of 30 sec at 95.0ºC, followed by 40 cycles of 5 sec at 95ºC plus 5 sec at 63ºC (for cell extracts) or 61ºC (for tissue extracts). At the end of each cycle, Eva Green fluorescence was recorded to enable determination of Cq. After amplification, melting temperature of the PCR products were determined by performing melting curves, with 0.5ºC increments every 5 sec, from 65ºC to 95ºC, with fluorescence recording after each temperature increment. For each set of primers, amplification efficiency was assessed, and no template and no transcriptase controls were run. For cell extracts, relative normalized expression was determined by the CFX96 Manager software (v. 3.0; Bio-Rad), using TBP or GAPDH as a reference genes. Normalization was also performed for the reference gene hypoxanthine guanine phosphoribosyl transferase (Hprt; accession number NM_013556.2), with similar results. For tissue extracts, beta-actin (NM_007393.3), POLR2F (NM_027231.1), GAPDH (NM_008084.2) and Hprt (NM_013556.2) were tested as reference genes, but none of these genes were stable in YAC128 mice treated with SB or RESV. Thus, normalizations were carried out in relation to vehicle-treated wild-type mice.

2.7. KDACS ACTIVITY QUANTIFICATION

2.7.1. HDAC ACTIVITY COLORIMETRIC ASSAY

HDAC activity was measured using a commercially available kit (#K331-100; BioVision, Milpitas, CA, USA), following the manufacturer instructions. Lymphoblasts were centrifuged at 145 *g*, for 5 min, and washed with PBS solution. Extracts were prepared in ice-cold lysis buffer (in mM: 20 Tris, 100 NaCl, 2 EDTA, 2 EGTA, 1% Triton; pH 7.4) without supplementation to avoid interference with enzymatic activities. HDAC activity was measured immediately after protein extraction to avoid loss of activity. Briefly, the HDAC colorimetric substrate, which comprises an acetylated K side chain,

was incubated with the extracted sample for 1 h, at 37°C. Deacetylation of the substrate sensitizes the substrate, so that, in the second step, treatment with the lysine developer produces a chromophore. The reaction occurred at 37°C for 30 min. Absorbance was monitored using a microplate reader Spectra Max Plus 384 (Molecular Devices, USA) at 450 nm. HDAC activity was calculated as the relative O.D. value per μg protein sample and the results expressed as the % of control lymphoblasts.

2.7.2. SIRT3 ACTIVITY FLUORIMETRIC ASSAY

SIRT3 activity was measured using a commercially available kit from Abcam (ab156067) following the manufactured instructions. Cell extracts were prepared in a SIRT3 assay buffer without supplementation. SIRT3 activity was measured immediately after protein extraction to avoid loss of activity. Briefly, the protein extract were added to a solution containing a fluorophore and a quencher linked to amino terminal and carboxyl terminal, respectively, of an acetylated substrate peptide. In the presence of SIRT3, the substrate was deacetylated and become cut by the action of a peptidase, added simultaneous to the solution. This reaction detached the quencher from fluorophore, and the fluorescence emitted was proportional of SIRT3 activity. The fluorescence was monitored for 40 minutes at 1 minute intervals using a microtiter plate reader fluorometer with excitation at 350 nm and emission at 450 nm. The rate of reaction was expressed as slope per minute.

2.8. CELL VIABILITY AND APOPTOSIS MEASUREMENT

2.8.1. MTT REDUCTION ASSAY

Neuronal viability was measured by determining the cellular reducing capacity, through the extent of MTT reduction to the insoluble intracellular formazan. MTT assay was performed as previously described (Duarte et al., 2005). Cortical and striatal neurons treated for 96 h with RESV or NAM were incubated with MTT (0.5 mg/ml, prepared in the dark in Krebs medium containing (in mM): 132 NaCl, 4 KCl, 1 $CaCl_2$, 1.2 NaH_2PO_4, 1.4 mM $MgCl_2$, 6 glucose, 10 HEPES) for 2 h, at 37ºC, and the insoluble formazan crystals were dissolved in an equal volume of acid-isopropanol (0.04 M HCl in isopropanol). Then the mixture was collected and the extent of MTT reduction was measured spectrophotometrically at 570 nm.

2.8.2. HOECHST 33342/PI DOUBLE STAIN

The nuclear morphology of the transfected striatal wild-type and mutant cells was analyzed by live fluorescence microscopy, using a double staining procedure with Hoechst 33342 and PI. Following a washing step with Krebs medium, the cells were incubated with 2 µg/ml Hoechst 33342 and 2 µg/ml PI for 10 min, at 37ºC. Cells were then washed 5 times in saline medium, in order to remove extracellular dyes, and further examined in a Axioskop 2 plus upright epi-fluorescence microscope (Zeiss, Jena, Germany) with PlanNeofluar/0.75NA 40x lens. Viable and apoptotic cells were counted in Fiji software (ImageJ, National Institute of Health, USA) using the Cell Counter plugin.

2.9. MITOCHONDRIAL FUNCTION ANALYSIS

2.9.1. MITOCHONDRIAL MEMBRANE POTENTIAL

2.9.1.1. Rhodamine 123 fluorescence

$\Delta\psi_m$ was assessed using the fluorescent probe Rhodamine 123 (Rh123), which predominantly accumulates in polarized mitochondria. Thus the variation of Rh123 retention was studied in order to estimate changes in $\Delta\psi_m$. Following a washing step, neurons were incubated in Krebs medium containing 1.5 µM Rh123 for 45 h at 37°C. Basal fluorescence (505 nm excitation and 525 emission) was measured using a microplate reader Spectrofluorometer Gemini EM (Molecular Devices, USA), for 4 min, followed by the addition of 2.5 µM carbonyl cyanide 4-(trifluoromethoxy) phenylhydrazone (FCCP, mitochondrial uncoupler) + 2 µg/mL oligomycin (ATP synthase inhibitor), which produced maximal mitochondrial depolarization.

2.9.1.2. Single-cell $TMRM^+$ confocal fluorescence

Striatal cells cultured on 18 mm coverslips were loaded with 2 µg/ml Hoechst 33342 and 10 nM $TMRM^+$, a concentration sufficient low to avoid quenching of the fluorescent signal in the matrix (Nicholls and Ward, 2000), for 30 minutes at 33°C. Coverslips were mounted in a pre-warmed insert and images were collected using LCI PlanNeofluar/1.3NA 63x lens on a Carl Zeiss Axio Observed Z1 inverted confocal microscope using the CSU-X1M spinning disc technology with Zen Black 2012 software (Zeiss, Jena, Germany). $TMRM^+$ fluorescence was monitored in a controlled temperature in basal medium containing 10 nM $TMRM^+$, by excitation at 543 nm and emission at 458

nm, as described previously (Rego et al., 2001). Four single positions were captured for each coverslip using the multi-position tiles tool. Images were collected each 10 seconds with definite focus between each 6 cycles for a total of 54 cycles. Cells were exposed to 2.5 µg/mL oligomycin (cycle 18) and 2.5 µM FCCP (cycle 36) to induce $TMRM^+$ release from mitochondria. Fluorescence intensity at each time point was analyzed in Fiji software (ImageJ, National Institute of Health, USA) using the time series analyzer plugin (v 3.0) developed by Balaji J. (2007) at Department of Neurobiology from University of California, Los Angeles (UCLA).

2.9.2. OXYGEN CONSUMPTION RATE (OCR)

2.9.2.1. Oxygraph oxygen electrode

Striatal cells were detached by trypsinization and trypsin was inactivated by adding culture medium containing FBS. $5x10^6$ lymphoblasts, in turn, were centrifuged at 145 *g*, for 5 min at 4ºC. Then, both cells were washed in pre-warmed respiration buffer (containing, in mM: 132 NaCl, 4 KCl, 1 $CaCl_2$, 1.2 NaH_2PO_4, 1.4 mM $MgCl_2$, 6 glucose, 10 HEPES, pH 7.4) and resuspended in 300 µL respiration buffer. The rate of O_2 consumption was recorded under constant magnetic stirring in an Oxygraph DW1 O_2 electrode chamber (Hansatech Instruments, Norfolk, UK), previously calibrated for the O_2 dissolved in oxygenated water (maximum) and in N_2-saturated water (minimum). The experiments were performed at 33ºC in the case of striatal cells and 37ºC for human lymphoblasts. After recording the basal rate of O_2 consumption, cells were sequentially exposed to oligomycin (10 µg/mL), to avoid the reversal of ATP synthase, and FCCP (2.5 µM), to assess maximal respiration rates. Potassium cyanide (700 µM) was then added to confirm mitochondrial O_2 consumption, manifested as a decrease in O_2 consumption due to inhibition of mitochondrial complex IV. At the end of the experiment the striatal cells were pelleted, resuspended in 1 M NaOH, and protein was quantified by the Bio-Rad protein assay. Results were expressed in nmol O_2/min/mg protein.

2.9.2.2. Seahorse oxygen respirometry

OCR of transfected striatal cells was measured using Seahorse XF24 flux analyzer (Seahorse Bioscience, Billerica, MA, USA) following the manufacturer's instructions. Striatal cells were grown on the 24-well custom plates at 30,000 cells per well, and transfected 48 h before the experiment (as described in *2.3.3. section*) or incubated with 500 µM SB 24 h before the experiment. Prior running the experiment, cell

culture medium was removed, and cells were washed once with 1 ml DMEM 5030 medium (pH 7.4) supplemented with 4.5 g/L glucose, 4 mM glutamine, and then incubated in 450 µL of supplemented DMEM medium, at 33ºC, in a CO_2-free incubator for 1 h. Four baseline measurements of OCR were sampled prior to sequential injection of mitochondrial inhibitors, and four metabolic determinations were sampled following addition of each mitochondrial inhibitor prior to injection of the subsequent inhibitors. The mitochondrial inhibitors used were oligomycin A (1 µM), FCCP (0.9 µM) and antimycin A (1 µM) plus rotenone (1 µM). OCR was automatically calculated and recorded by the Seahorse software. After the assays, protein level was determined for each well to confirm equal cell density per well. Results were expressed in pmol O_2/min/µg protein.

2.10. MITOCHONDRIAL DNA COPY NUMBER

Genomic DNA (gDNA) was obtained with Purelink genomic DNA kit according to the manufacturer's protocol. Briefly, genomic DNA was extracted from $5x10^6$ lymphoblasts or from two wells in a 6 multiwell plate cultured with ST*Hdh* cells with genomic lysis/binding buffer supplemented with proteinase K, after incubation at 55ºC for 10 minutes to promote protein digestion. DNA was precipitated with 96-100% ethanol. After serial washing steps purified gDNA was eluted using a genomic elution buffer. The concentration of gDNA was measured and 10 ng was used for each reaction. The mtDNA of each sample was amplified using sequence-specific primers to $tRNA^{Leu\ (UUR)}$ (for lymphoblasts) or $tRNA^{Try/CO1}$ (for ST*Hdh* cells), gene regions that are rarely deleted and contain only a few rare single nucleotide polymorphisms; whereas nuclear DNA (nDNA) was amplified using sequence-specific primers to beta-2-microglobulin (β2M) or β-actin, listed in **Table 2** and described previously by (Venegas and Halberg, 2012). The reaction was performed using SsoFast Eva Green Supermix and thermal cycling conditions described in *section 2.6.* mtDNA levels were expressed in relation to nDNA levels.

2.11. MITOCHONDRIAL METABOLISM ANALYSIS

2.11.1. NAD^+/NADH QUANTIFICATION

The total levels of NAD (NADt) and NAD^+ were measured using a commercially available kit (Abcam, Cambridge, UK), following the manufacturer instructions. Briefly, cells were plated in T25 flasks and cell extracts were obtained with NADH/NAD

extraction buffer. The samples were frozen 3 times in liquid nitrogen and centrifuged at 20,800 *xg* for 10 min (Eppendorf Centrifuge 5417R) to remove cell debris. The extracted samples were divided in two: one remained in ice (NADt) and the other was heated to 60ºC for 30 minutes to decompose NAD^+ (NADH). Both samples were transferred to a 96-well plate followed by addition of a NAD^+ cycling mix enzyme and incubated at room temperature for 5 minutes to convert NAD^+ to NADH. Finally, NADH developer was added into each well and the reaction occurred at room temperature for 90 min. Absorbance was monitored using a microplate reader Spectra Max Plus 384 (Molecular Devices, USA) at 450 nm. NAD^+ was calculated by the difference between NADt and NADH, and normalized for protein content.

2.11.2. MEASUREMENT OF INTRACELLULAR LEVELS OF ADENINE NUCLEOTIDES

Striatal cells were washed and then scraped with ice-cold PBS, whereas mice cortex from one brain hemisfere was homogenaized with ice-cold PBS. The same volume of 0.6 M perchloric acid supplemented with 25 mM EDTA-Na^+ was added. Extracts were then centrifuged at 20,800 x*g* for 2 min at 4°C to remove cell debris. The resulting pellet was solubilized with 1 M NaOH and further analysed for total protein content by the Bio-Rad Protein assay. After neutralization with 10 M KOH/1.5 M Tris, samples were centrifuged at 20,800 x*g* for 5 min, at 4°C. The resulting supernatants were assayed for ATP, ADP and AMP determination by separation in a reverse-phase high-performance liquid chromatography (HPLC), with detection at 254 nm. The chromatographic apparatus used was a Beckman-System Gold controlled by a computer. The detection wavelength was 254 nm, and the column used was a Lichrospher 100 RP-18 (5 µm). An isocratic elution with 100 mM phosphate buffer (KH_2PO_4), pH 6.5 and 1% methanol was performed with a flow rate of 1 ml/min. Peak identity was determined by following the retention time of standards. Energy charge was used as a measurement of general energy status of mice cortex, taking into account both ATP, ADP and AMP concentrations, and was calculated according to the following formula: (ATP+1/2*ADP)/(ATP+ADP+AMP).

2.11.3. PDH ACTIVITY ASSAY

PDH activity was assayed at 30°C by measuring the reduction of NAD^+ at 340 nm, in a Spectra Max Plus 384 microplate reader (Molecular Devices, USA), upon mixing 9 µg protein with 0.5 mM NAD^+, in the presence of 200 µM TPP^+, 40 µM CoA,

and 4.0 mM pyruvate. The assay was carried out in the presence of 2.5 µM rotenone to prevent NADH consumption by complex I (Zhou et al., 2009). PDH activity was calculated as absorbance units *per* minute per mg protein and converted in percentage of wild-type cells.

2.11.4. PDH E1α PROTEIN LEVELS AND PHOSPHORYLATION BY ELISA ASSAY

PDH expression and phosphorylation were assessed using the Phospho-PDH In-Cell ELISA kit from MitoSciences, Abcam (Cambridge, UK), following the manufacturer instructions. Briefly, cells were plated in 96-well plates, transfected with shRNA-PDK3 or scramble shRNA control or incubated with the HDACi compounds, and fixed with 3.7% formaldehyde in PBS. Cells were permeabilized, blocked and incubated overnight with an antibody against total PDH E1alpha, combined with another antibody against one of the phosphorylated forms of PDH E1α at Ser293 (site 1), Ser300 (site 2) or Ser232 (site 3). Separate secondary antibodies were used against PDH E1α or the phosphorylated serines, and developed by dual colorimetric detection. Cell density was normalized after Janus Green staining. Absorbance was monitored using a microplate reader Spectra Max Plus 384 (Molecular Devices, USA).

2.12. STATISTICAL ANALYSIS

Results are expressed as mean ± SEM (standard error of the mean) of the number of independent experiments or animals indicated in figure legends. Comparisons between multiple groups were performed by two-way or one-way analysis of variance (ANOVA), followed by Bonferroni post-hoc test, for comparison between experimental groups. Comparison between two groups was performed by the Student´s t-test (GraphPad Prism Version 6.0). The F-test was performed to analyze the interaction term. Significance was accepted at $p<0.05$.

CHAPTER III

HISTONE DEACETYLASE INHIBITORS PROTECT AGAINST PYRUVATE DEHYDROGENASE DYSFUNCTION IN HD*

* Based on the following published manuscript: Naia L.*, Cunha-Oliveira T.* *et al.* 2017. *J neurosci.* [Epub ahead of print]

3.1. SUMMARY

Transcriptional deregulation and changes in mitochondrial bioenergetics, including PDC dysfunction, have been described in HD. DCA, an indirect activator of PDH, was shown to significantly attenuate the development of striatal neuron atrophy and improve motor function in transgenic HD mice models, emphasizing PDH as an interesting therapeutic target in HD. In previous studies, we showed that HDACi, TSA and SB, ameliorated mitochondrial function in cells expressing mHTT. In this work we investigated the effect of HDACi on regulation of PDH activity in striatal cells derived from HD KI mice and in YAC128 mouse brain. Mutant cells exhibited decreased PDH activity and increased PDH E1α phosphorylation/inactivation, accompanied by enhanced protein levels of PDK1 and PDK3. Treatment with SB and PB (another HDACi) increased histone H3 acetylation, mitochondrial respiration and energy levels in mutant cells. Exposure to SB also suppressed HIF-1α stabilization, decreasing the transcription of the two most abundant PDK isoforms, PDK2 and PDK3, culminating in increased PDH activation in mutant cells. In accordance, PDK3 knockdown improved mitochondrial function, highlighting the role of PDK3 inactivation on the positive effects achieved by SB treatment. YAC128 mouse brain cortex presented higher mRNA levels of PDK1-3 and PDH phosphorylation, as well as decreased energy levels, which were significantly ameliorated following SB treatment. These results suggest that HDACi, particularly SB, may promote the expression and activity of PDH in HD brain, helping to counteract HD-related deficits in mitochondrial bioenergetics.

3.2. INTRODUCTION

HD is a devastating neurodegenerative disease with autosomal inheritance, progressive course and a combination of motor, cognitive and behavioral features that culminate in death approximately 20 years after the onset of the first symptoms. It is caused by an expanded glutamine stretch at the N-terminal of HTT protein, leading to specific neuronal dysfunction and death in striatum and cortex [reviewed in (Gil and Rego, 2008)]. Among several targets, mHTT interferes with mitochondrial homeostasis [reviewed in (Rosenstock et al., 2010)] and disturbs gene expression by interfering with nuclear transcription cofactors (Benn et al., 2008; Zhai et al., 2005), some linked to mitochondrial biogenesis and function (Cui et al., 2006; Cunha-Oliveira et al., 2012). mHTT also affects $\Delta\psi_m$ (Naia et al., 2015; Panov et al., 2002), Ca^{2+} buffering capacity (Damiano et al., 2010), OXPHOS (Milakovic and Johnson, 2005; Schatz, 1995) and production of ROS that are originated in mitochondria (Ribeiro et al., 2014).

Symptomatic and presymptomatic HD patients present evidences of altered brain glucose metabolism in the caudate, putamen, cortex and cerebrospinal fluid (Jenkins et al., 1993; Koroshetz et al., 1997; Kuhl et al., 1982; Kuwert et al., 1989). The onset of energy and mitochondrial modifications at presymptomatic stages suggest that energy deficits may constitute early phenomena in HD pathogenesis (Mochel and Haller, 2011). Previously, we observed reduced activity of complex I in mitochondria from platelets of presymptomatic and symptomatic HD carriers (Silva et al., 2013). Moreover, bioenergetic dysfunction in HD human cybrids was associated with PDH activity and protein levels, and increased phosphorylation/inactivation of E1α subunit (Ferreira et al., 2011). PDH was shown to be impaired in HD human brains (Butterworth et al., 1985; Sorbi et al., 1983), and the PDH indirect activator DCA showed protective effects in HD mouse models (Andreassen et al., 2001), revealing PDH as a central player in HD-associated mitochondrial dysfunction. This is in agreement with the observation of elevated lactate levels in the striatum of presymptomatic HD patients (Jenkins et al., 1998), which suggests the occurrence of PDH defects *in vivo*. PDC is a large complex of three functional enzymes: E1, E2 and E3; and the current understanding of PDC regulation involves inhibitory serine phosphorylation of PDH E1α by specific PDKs, whereas dephosphorylation of PDH E1α by PDPs activates the PDC (Harris et al., 2002; Patel and Korotchkina, 2006). Importantly, the activity of PDKs may be regulated at the transcriptional level (Kim et al., 2006; Patel and Korotchkina, 2006), suggesting that PDH dysfunction may be related to transcriptional deregulation in HD.

Gene transcription is generally favored by HATs, whereas HDACs mainly repress gene expression (Struhl, 1998), similarly to mHTT. Previous studies indicated that HDACi ameliorate the transcriptional changes in HD (Zuccato et al., 2010). A phase I clinical trial with the HDACi PB showed recovery of expression of 12 transcripts that were up-regulated in untreated HD patients (Borovecki et al., 2005; Hogarth et al., 2007). Also in R6/2 mice, a microarrays analysis showed that SB induces a non-homogenous upregulation of transcripts that are normally decreased by the disease progress, significantly extending survival, improving body weight and motor performance (Ferrante et al., 2003). SAHA, a synthetic and potent HDACi, has also revealed beneficial effects, crossing the BBB and increasing histone acetylation in the brain of R6/2 mice, leading to dramatically improved motor coordination (Hockly et al., 2003).

We previously showed that mHTT induced deficits in mitochondrial Ca^{2+} handling, which was ameliorated by treatment with HDACi TSA, a pan-Lys HDACi, and SB, which acts preferentially on class I and IIa HDACs (Oliveira et al., 2006), similarly to PB. Therefore, in this work we analyzed the influence of SB and PB in improving PDH function in striatal cells expressing FL-mHtt, ST*Hdh*$^{Q111/Q111}$, and confirmed the effect of SB in YAC128 mouse brain. Our results suggest that the HDACi SB promotes PDH activity in both *in vitro* and *ex vivo* models by regulating the expression of PDKs, helping to counteract HD-related deficits in mitochondrial function.

3.3. RESULTS

3.3.1. STHdh$^{Q111/Q111}$ striatal cells show dysfunctional PDC activity

Mitochondrial bioenergetics has been described to be altered in HD [reviewed in (Cunha-Oliveira et al., 2012)]. PDC is a central mitochondrial enzymatic complex in cellular bioenergetics, linking glycolysis to the TCA cycle and OXPHOS (Harris et al., 2002; Patel and Korotchkina, 2006). Moreover, PDC activity can be modulated by phosphorylation (Kolobova et al., 2001), and deregulation of PDH E1α activity and phosphorylation levels was previously shown by us in HD cybrids, together with a decrease in NADH/NADt ratio (Ferreira et al., 2011).

Using HD mutant striatal cells, we observed an increase in mitochondrial NAD^+/NADH levels by 2.3 fold (p<0.001) (**Figure 3.1A**), suggesting a dysfunction in cellular dehydrogenases. We also assessed PDH activity by following the production of NADH that accompanies pyruvate conversion into acetyl-CoA; a decrease in PDC

activity by about 30% (p<0.0001) was observed in ST*Hdh*$^{Q111/Q111}$ cells, when compared to wild-type striatal cells (**Figure 3.1B**), which may explain the substantial increase in pyruvate levels detected in mutant cells (Naia et al., 2016). The protein levels of the E1α subunit of PDH, along with its phosphorylation at three regulatory sites (site1- Ser293, site 2- Ser300 and site 3- Ser232) were assessed using a kit based on an immunocytochemistry protocol (**Figure 3.1C,D**). The total protein levels of the PDH E1α subunit decreased by about 33% (p<0.0001) in mutant cells, when compared to wild-type cells (**Figure 3.1C**). In mutant striatal cells, all the three regulatory serines exhibited pronouncedly high phosphorylation levels (**Figure 3.1D**). In Ser232 the increase reached 2.4 fold (p<0.001), compared to wild-type cells. This serine corresponds to the regulatory site 3 of PDH and is phosphorylated by PDK1 (Patel and Korotchkina, 2006). In accordance with increased Ser232 phosphorylation, PDK1 protein levels were found increased by 54% (p<0.05) in mutant cells (**Figure 3.1E**). Additionally, we analyzed the protein levels of PDK3 and the catalytic subunit of the PDH phosphatase PDP1, PDP1c (**Figure 3.1F,G**), described to be the most abundant forms of PDK and PDP, respectively, in the brain (Kolobova et al., 2001; Patel and Korotchkina, 2006). In accordance with the phosphorylation levels of PDH E1α subunit, we detected an increase by about 39% in PDK3 protein levels (p<0.05) (**Figure 3.1F**), while PDP1 protein levels decreased by about 30% (p<0.05) (**Figure 3.1G**) in ST*Hdh*$^{Q111/Q111}$ cells.

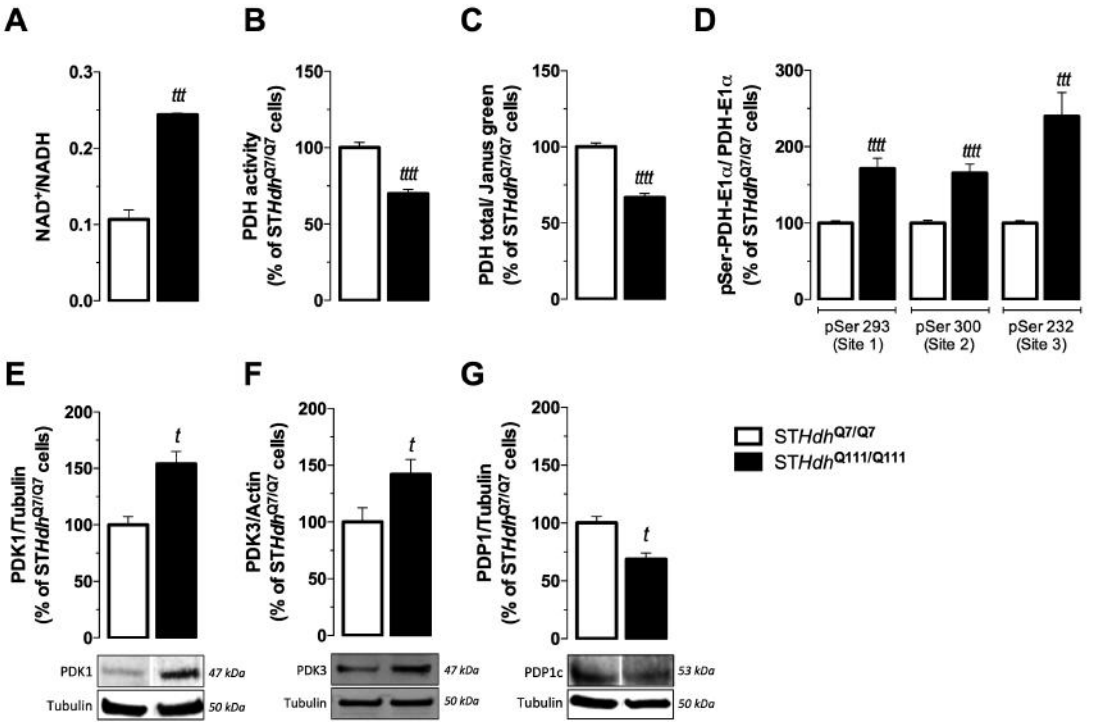

Figure 3.1 | Altered NAD$^+$/NADH ratio and PDC activity and regulation in ST*Hdh*$^{Q111/Q111}$ cells. NAD$^+$/NADH ratio (**A**) and PDC activity (**B**) were measured in total extracts of wild-type and mutant cells. Total PDH E1α protein levels (**C**) and phosphorylation at regulatory Ser293 (site 1), Ser300 (site 2) or Ser232 (site 3) were assessed using a phospho-PDH in cell ELISA kit (**D**). Protein levels of PDK1 (**E**), PDK3 (**F**) and PDP1c (**G**), in wild-type and mutant cells were determined by western blotting. Data are the mean ± SEM of total NAD$^+$/NADH ratio (in pmol/mg protein), total PDH activity (slope/mg protein), PDH E1α/Janus Green, phosphorylated form/total PDH E1α. Where mentioned the average value obtained for wild-type was considered 100%. Statistical analysis: $^{t}p<0.05$, $^{ttt}p<0.001$ and $^{tttt}p<0.0001$ compared with the respective wild-type cells.

3.3.2. HDACi enhance histone acetylation and rescue PDH-related mitochondrial dysfunction in STHdh$^{Q111/Q111}$ cells

HDACi were previously shown to prevent cell death (Beal and Ferrante, 2004) and ameliorate mitochondrial Ca^{2+} handling and dynamics (Guedes-Dias et al., 2015; Oliveira et al., 2006) in HD models. A recent mass spectrometry assay described that SB acts preferentially on HDACs classes I and IIa, favoring Lys acetylation sites in the nucleus, with higher preference for Lys residues in histones H3 and H4 (Scholz et al., 2015). Therefore, we started to evaluate the influence of HDACi on the acetylation of nuclear histone H3. Both wild-type and mutant cells were incubated for 24 h with 100, 250 and 500 μM PB or SB. ST*Hdh*$^{Q111/Q111}$ cells showed a tendency for a slight decrease in H3 acetylation (data not shown), as previously described (Oliveira et al., 2006). For

both PB (**Figure 3.2A, C**) and SB (**Figure 3.2B, D**), the most significant effect was observed at the higher concentration tested, 500 μM, increasing H3 acetylation by about 1.6 (p<0.001) and 2.1 (p<0.01) fold (respectively) in wild-type cells, and by 1.4 (p<0.01) and 1.3 (p<0.01) fold (respectively) in mutant cells. PB and SB at 250 μM also showed a non-significant tendency for increased H3 acetylation in mutant cells by about 1.4- and 1.3-fold, respectively, concomitantly with significant increase in cell viability (data not shown).

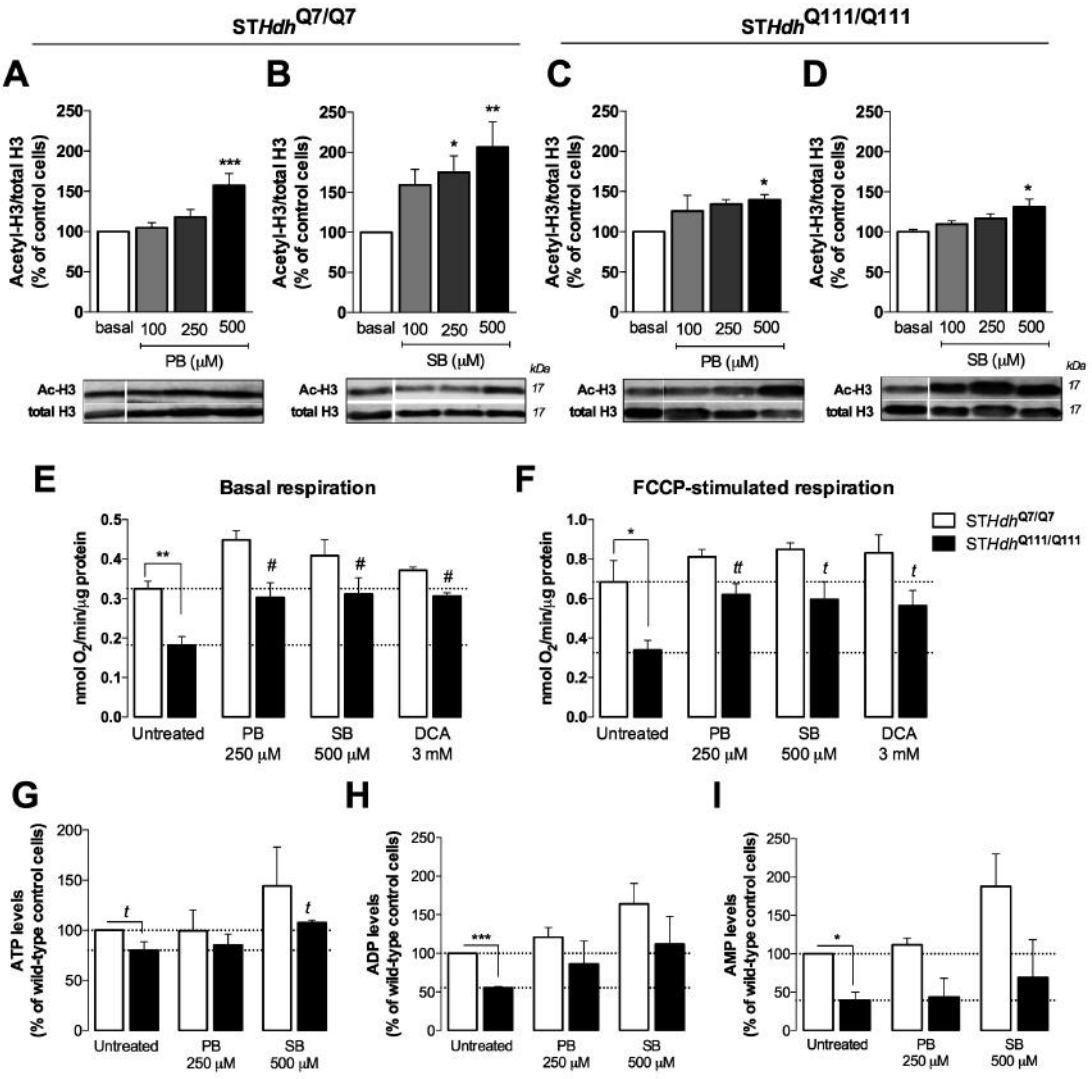

Figure 3.2 | Increased histone H3 acetylation and mitochondrial function followed HDACi treatment. ST*Hdh*$^{Q7/Q7}$ and ST*Hdh*$^{Q111/Q111}$ cells were incubated for 24 h with different concentrations of the HDACi PB (100-500 μM; **A,C**) and SB (100-500 μM; **B,D**) and histone H3 acetylation were quantified by western blotting using specific antibodies for ac-H3 and total H3 (used as loading control). Oxygen consumption was measured in an O_2 Clark electrode, after incubation with PB (250 μM), SB (500 μM) and DCA (3 mM), before (**E**) and after (**F**) sequential addition of oligomycin (2.5 μg/mL) and FCCP (2.5 μM), and compared with untreated controls. Energy metabolism was

evaluated by measurement of ATP (**G**), ADP (**H**) and AMP (**I**) levels by HPLC. Dotted lines represent average control basal values for wild-type and mutant cells. Results were expressed as mean ± SEM of 4-5 independent experiments. Statistical analysis: There is no interaction between treatment and genotype, however a significant effect of the treatment was found in **E** [$F(3,28)=9.102$, $p=0.0002$] and **F** [$F(3,28)=4.291$, $p=0.0134$], with $^{\#}p<0.05$, $^{*}p<0.05$, $^{**}p<0.01$, $^{***}p<0.001$ when compared to the respective control. $^{t}p<0.05$, $^{tt}p<0.01$, when compared to the respective control, by the Student's t-test.

To assess whether enhanced H3 acetylation induced by HDACi was accompanied by an improvement in mitochondrial function, we evaluated mitochondrial respiration and adenine nucleotide levels in ST*Hdh* cells. Mutant cells exhibited a decrease in mitochondrial respiration under basal conditions (by about 44%, $p<0.01$) (**Figure 3.2E**) and the difference was still observed in the presence of the uncoupler FCCP (by about 50%, $p<0.05$), although FCCP enhanced O_2 consumption by about 2-fold (**Figure 3.2F**). Mutant cells also presented lower ATP (by about 20%, $p<0.05$), ADP (by about 45%, $p<0.001$) and AMP (by about 60%, $p<0.05$) levels, compared with wild-type cells (**Figure 3.2G-I**). In the presence of PB (250 µM) and SB (500 µM), the respiratory activity of mutant cells was recovered nearly to the levels observed in untreated ST*Hdh*$^{Q7/Q7}$ cells (**Figure 3.2E**, **F**). Treatment with SB (500 µM) also restored intracellular ATP levels in mutant cells (**Figure 3.2G**). Remarkably DCA (3 mM), a PDK inhibitor previously shown to increase PDH activity and decrease E1α subunit turnover (Fouque et al., 2003), enhanced mitochondrial respiration in ST*Hdh*$^{Q111/Q111}$ cells (**Figure 3.2E**, **F**), suggesting that the improvement in PDH activity may counteract HD-associated mitochondrial deficits.

To understand if the protective effects achieved by HDACi on mitochondrial function could reflect a recovery of PDH function, next we evaluated the effect of the HDACi on protein and phosphorylation levels of PDH E1α subunit. In ST*Hdh*$^{Q7/Q7}$ cells, only 500 µM PB increased the protein levels of E1α subunit by about 1.5-fold ($p<0.05$) (**Figure 3.3A**). Furthermore, 500 µM PB significantly decreased PDH E1α phosphorylation at all serines, by about 31% ($p<0.05$) for Ser293, 22.5% ($p<0.01$) for Ser300 and 44.5% ($p<0.001$) for Ser232. SB (at 500 µM) also significantly decreased PDH E1α phosphorylation at Ser293 and Ser232 ($p<0.05$) (**Figure 3.3C**), which are mainly regulated by PDK2 and PDK3 (Korotchkina and Patel, 2001). In ST*Hdh*$^{Q111/Q111}$ cells, both 250 µM PB and 500 µM SB increased E1α PDH subunit levels by 1.3- and 1.4-fold ($p<0.001$), respectively (**Figure 3.3B**). Phosphorylation at Ser293 decreased by about 33.6% ($p<0.01$) in the presence of 250 µM PB (**Figure 3.3D**). Importantly, 500 µM SB was the most efficient condition in mutant cells by decreasing the phosphorylation at

all the three serines, reducing the phosphorylation of Ser293 by about 41.6% (p<0.01), Ser300 by 46.5% (p<0.05) and Ser232 by 29.4% (p<0.05) (**Figure 3.3D**). Therefore, we can speculate that SB (at 500 μM) may activate PDC through modified transcriptional activity, more specifically by increasing acetylation, which culminates in enhanced mitochondrial function and metabolism.

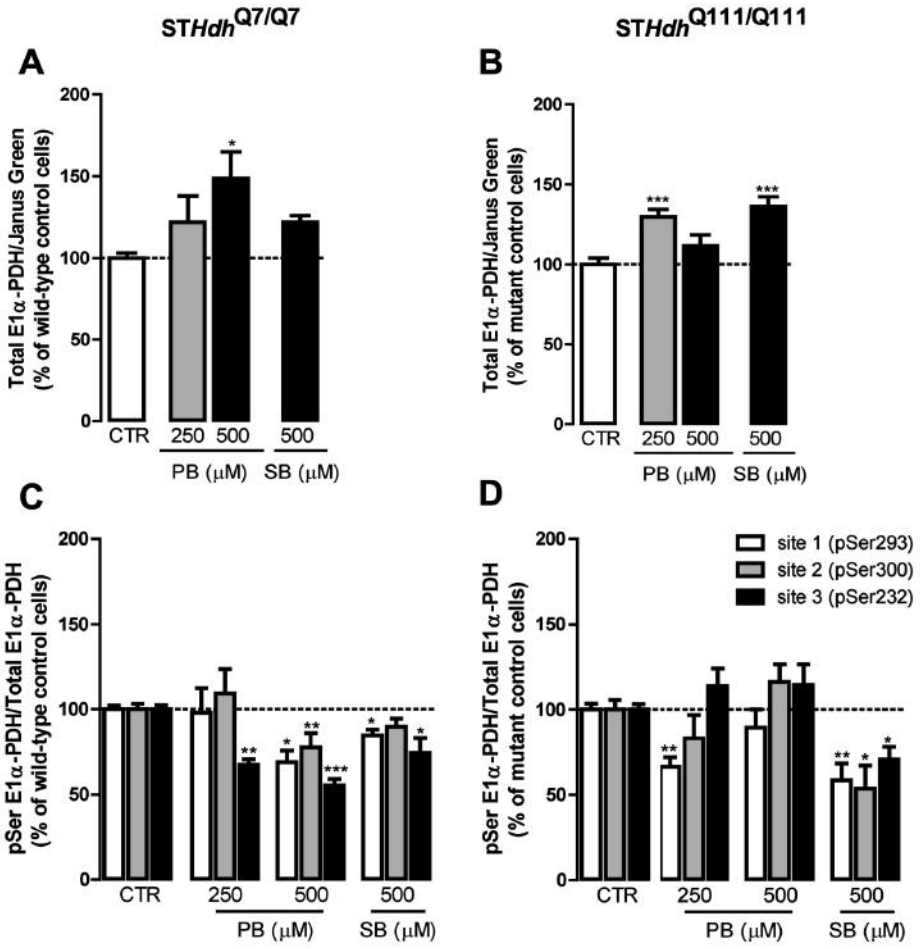

Figure 3.3 | HDACi regulate both protein levels and phosphorylation/inactivation of PDH E1α subunit of PDC. ST*Hdh*$^{Q7/Q7}$ (**A, C**) and ST*Hdh*$^{Q111/Q111}$ (**B, D**) cells were incubated with HDACi PB (250 and 500 μM) and SB (500 μM), and the total protein levels (**A, B**) and phosphorylation (**C, D**) of PDH subunit E1α were assessed using phospho-PDH in cell ELISA kit. Results were expressed as mean±SEM of 3-5 independent experiments (performed in duplicates or triplicates). Statistical analysis: *p<0.05, **p<0.01 and ***p<0.001 when compared to respective control, by one-way ANOVA, followed by Bonferroni post-hoc test.

3.3.3. HDACi SB rescues PDH-related mitochondrial dysfunction through transcriptional repression of specific PDKs

As described previously, PDC activity is primarily controlled by phosphorylation, a PTM strictly regulated by the action of four PDK and two PDP isoforms present in mammalian cells (Karpova et al., 2003; Rardin et al., 2009). Since 500 μM SB decreased PDH phosphorylation in mutant cells in all serine residues tested, we assessed the effect of this compound on mRNA expression of each of its regulatory kinases and phosphatases, namely PDKs1-4 and PDPs1-2, respectively, and the expression of PDHA1, the gene that encodes the PDH E1α subunit, in ST*Hdh* striatal cells (**Figure 3.4**). Concordantly with what was previously described for the brain (Bowker-Kinley et al., 1998; Patel and Korotchkina, 2006), PDK2 and PDK3 are the most abundant PDK isoforms, while PDK1 exhibits low expression and PDK4 mRNA is almost negligible; as for the phosphatases, PDP1 is about 8-fold more abundant than PDP2 in both striatal cell lines (**Figure 3.4A**).

ST*Hdh*$^{Q111/Q111}$ cells presented no significant changes in the mRNA levels of PDHA1 or in each of the regulatory kinases or phosphatases. Consistently with mRNA data (**Figure 3.4C,E**), 500 μM SB did not affect PDK1 or PDP1 protein levels (data not shown). However, exposure to SB induced a decrease in the expression of PDK2 by about 39% (p<0.01) and 24.5% (p<0.05), in wild-type and mutant cells, respectively (**Figure 3.4F**); this was accompanied by a decrease in the expression of PDK3, by about 26.5% (p<0.05) and 19.6% (p<0.05), in wild-type and mutant cells, respectively (**Figure 3.4G**), suggesting that the decrease in PDH E1α phosphorylation observed in the presence of SB may be associated with decreased transcription of PDKs 2 and 3.

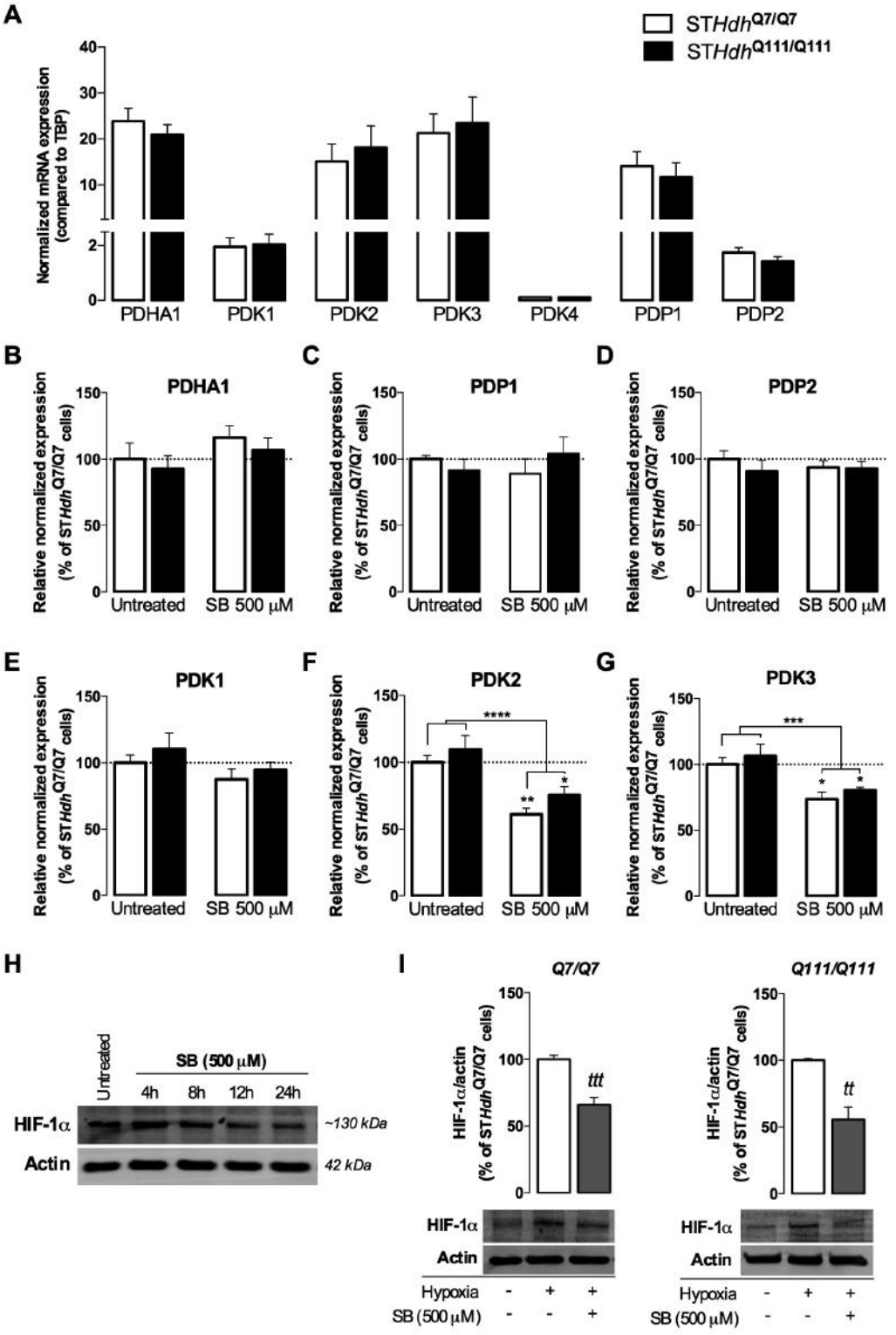

Figure 3.4 | SB modifies mRNA expression of PDH-related genes and associated HIF-1α transcription factor in HD knock-in striatal cells. Cells were incubated in the absence (untreated) or presence of 500 µM SB, for 24 h, and PDH-related mRNA transcripts were quantified by qPCR (**A-G**). In **A,** Comparison of mRNA expression levels of PDHA1, PDKs and PDPs in wild-type and mutant cells. **B-G,** Effect of SB on PDHA1 **(B)**, PDP1 **(C)**, and PDP2 **(D)**, PDK1 **(E)**, PDK2 **(F)** and PDK3 **(G)**. In **H-I**, striatal cells were submitted to hypoxia for 1 h following SB treatment at different time-points (**H**) or for 24 h (**I**). Protein levels of HIF-1α in wild-type and mutant cells were determined

by western blotting. Results are the mean ± SEM of 4-5 independent experiments, performed in duplicate for qPCR experiments. Statistical analysis: two-way ANOVA revealed a strong significant effect of SB treatment in **F** [F(1,25)=27.31, p<0.0001] and **G** [F(1,22)=19.68, p=0.0002], as indicated in brackets; *p<0.05, **p<0.01 compared to the respective control. In **I**, ^{tt}p<0.01, ^{ttt}p<0.001 by the Student's t-test.

To confirm this hypothesis we also looked at transcription factors that control the up-regulation of PDKs. Elevated mitochondrial-derived ROS, as observed in ST*Hdh*$^{Q111/Q111}$ cells (Ribeiro et al., 2013), have been implicated in the activation and stabilization of HIF-1α, an important component of the O_2 sensing pathway that has been largely described as a suppressor of metabolism and mitochondrial O_2 consumption (Papandreou et al., 2006) by directly trans-activating the genes encoding for PDK1 (Kim et al., 2006), as well as PDK2 and 3 (Lu et al., 2008; Prigione et al., 2014). In striatal cells pre-incubated at different time-points with SB (500 μM), we induced hypoxia for 1 h to allow HIF-1α stabilization/accumulation, since in normal O_2/ROS levels this transcription factor is rapidly degraded by the proteasome (Chandel et al., 1998; Movafagh et al., 2015). At basal conditions or in cells treated with SB for only 4 to 8 h, hypoxia caused HIF-1α accumulation (**Figure 3.4H**). However, after 24 h of SB incubation a significant decrease in HIF-1α levels was observed in both wild-type (p<0.001) and mutant cells (p<0.01) (**Figure 3.4I**). Similar results were obtained with other potent HDACi TSA (100 nM) (data not shown), suggesting an effect primarily mediated by HDACi activity. In fact, HIF-1α acetylation enhances its ubiquitination (Jeong et al., 2002; Kong et al., 2006), corroborating the hypothesis that HDACi may be critical for HIF-1α proteasomal degradation and, consequent PDK2-3 transcriptional inhibition. FOXO1 also regulates PDKs genes expression (Jeong et al., 2012b) and its acetylation attenuates its transcriptional activity (Daitoku et al., 2011); however, no changes in acetyl-FOXO1 (Lys259/262/271) levels were observed in both ST*Hdh* cells treated with SB (data not shown). Thus, we showed that SB treatment could reduce PDH E1α phosphorylation/inactivation through decreased HIF-1α and related PDKs 2 and 3 expression.

To further link PDKs inhibition with improved mitochondrial function (observed previously in **Figure 3.2**), we knocked down PDK3, since this enzyme can incorporate almost 50% more phosphate than PDK2 (Kolobova et al., 2001). The KD was confirmed by the 50% and 79% reduction of PDK3 protein levels in wild-type and HD striatal cells, respectively (**Figure 3.5A**). PDK3 KD significantly reduced PDH E1α phosphorylation at Ser293 (by about 47.4% and 47.7%, in wild-type and mutant cells, respectively) and Ser300 (by about 43.7% and 49.6%, in wild-type and mutant cells, respectively) (**Figure**

3.5B). PDH E1α phosphorylation at Ser232 (site 3) remained unchanged, since this residue is phosphorylated by PDK1 (Kolobova et al., 2001) (**Figure 3.5B**). Mitochondrial function was evaluated by the OCR using Seahorse XF24 flux analyzer. We measured basal respiratory capacity, oligomycin-sensitive respiration coupled to ATP synthesis and maximal respiration in the presence of FCCP (**Figure 3.5C**). At the end of the experiment, striatal cells were treated with a combination of rotenone and antimycin A to assess non-mitochondrial respiration. Although the decrease in basal respiration in ST*Hdh*$^{Q111/Q111}$ cells did not reach statistical significance, maximal respiratory capacity was significantly reduced by about 43.7% (p<0.001) in the same cells. Exposure to SB increased basal respiration by about 2.2 fold (p<0.05) and ATP production by about 1.5 fold (**Figure 3.5C*i, iii***), and nearly recovered maximal respiration in HD cells (**Figure 3.5C*ii***), corroborating the previous results (**Figure 3.2E,F**). Remarkably, PDK3 KD increased by 1.5 (p<0.05) and 3.0 (p<0.001)-fold basal respiration in wild-type and mutant cells, respectively (**Figure 3.5C*i***). Likewise, maximal respiration and ATP production were enhanced after PDK3 KD in both wild-type (by about 1.5 and 1.6 fold, respectively) and mutant cells (2.3 and 2.0 fold, respectively) (p<0.05).

These results confirmed that defective PDK3 expression counteracts mitochondrial dysfunction observed in HD mutant cells and that SB treatment may exert its effect through partial suppression of PDK3 expression, as shown in **Figure 3.4**.

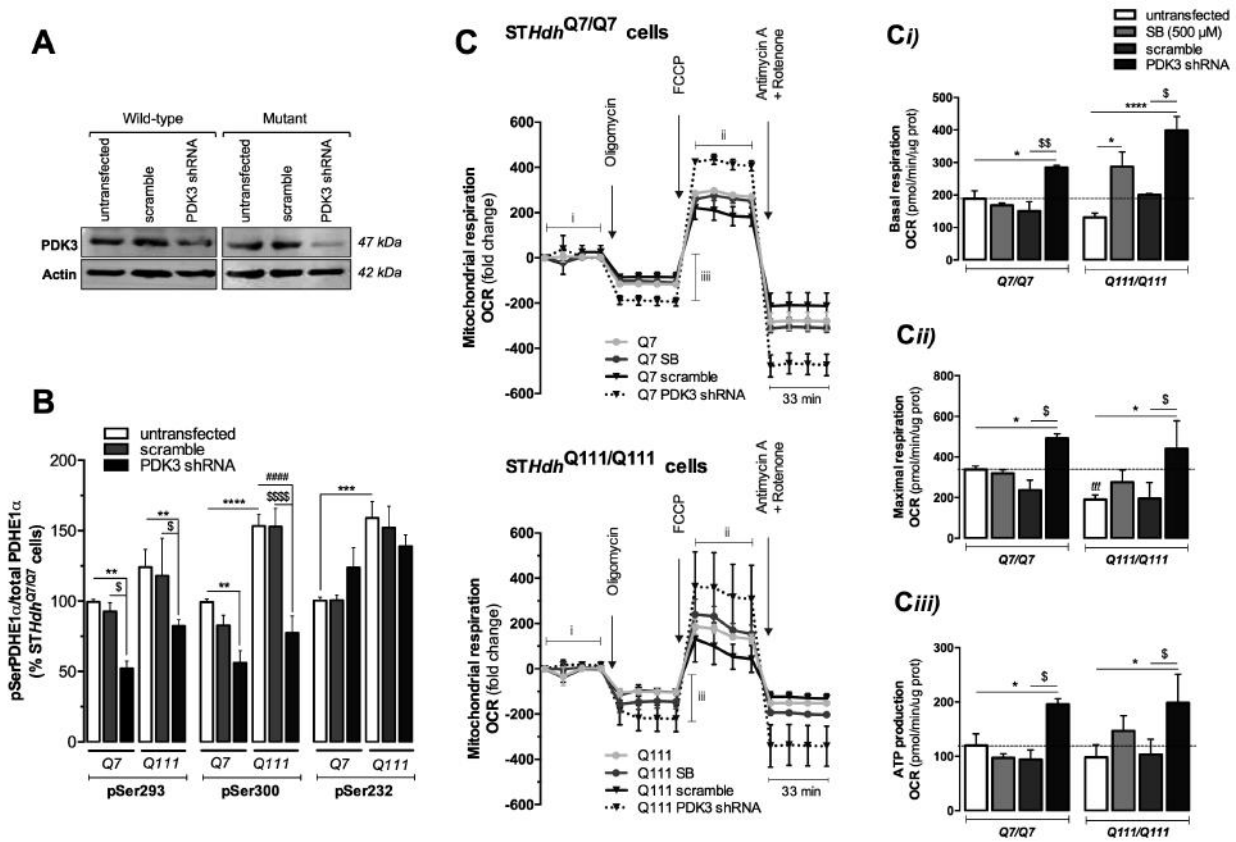

Figure 3.5 | PDK3 KD decreases PDH phosphorylation and improves mitochondrial respiration. Striatal cells were transfected with plko.1-shRNA against PDK3 or plko.1-scramble vector 48 h before the experiments, or incubated for 24 h with 500 μM SB. The efficacy of the KD was confirmed by western blotting probed for PDK3 (**A**), and by decreased PDH E1α subunit phosphorylation (at Ser293 and Ser300) (**B**). Statistical analysis was performed by two-way ANOVA and a significant interaction between genotype and PDK3 KD was found [$F(2,40)=3.675$, $p=0.0343$]. Additionally, PDK3 KD had a significant effect on Ser293 [$F(2,40)=7.693$, $p=0.0015$] and Ser300 [$F(2,40)=27.62$, $p<0.0001$] phosphorylation. OCR was measured with Seahorse XF24 flux analyzer (**C**). Basal mitochondrial respiration is represented in **C*i***, and exhibits a significant interaction between genotype and treatment [$F(3,25)=3.248$, $p=0.0387$]. A strong significant effect of treatment on basal respiration was also observed $F(3,25)=12.57$, $p<0.0001$]. For the indicated length time, striatal cells were treated with 1 μM oligomycin A, 0.9 μM FCCP and 1 μM antimycin A plus 1 μM rotenone, to determine the proportion of O_2 consumption due to ATP turnover (**C*iii***) and maximal rate of respiration (**C*ii***). PDK3 KD or SB treatment had a significant effect on both **C*ii*** [$F(3,26)=4.817$, $p=0.0085$] and **C*iii*** [$F(3,26)=4.436$, $p=0.0120$]. Results were expressed as mean±SEM of 3-4 independent experiments. Statistical significance: *$p<0.05$, **$p<0.01$, ***$p<0.001$ and ****$p<0.0001$, compared to Q7 untransfected cells; $^{\#\#\#\#}p<0.0001$, compared to Q111 untransfected cells; $^{\$}p<0.05$, $^{\$\$}p<0.01$ and $^{\$\$\$\$}p<0.0001$, compared to plko.1-transfected cells, by two-way ANOVA followed by Bonferroni post-test; $^{ttt}p<0.001$ when compared to the untransfected Q7 (in **C*ii***), by the Student's t-test.

3.3.4. SB rescues PDH metabolism in HD mice

In other to confirm the relevance of these results in an HD animal model, we also analyzed the levels of PDH phosphorylation, PDKs (1-3) mRNA transcripts and adenine nucleotides in the cortex of 9 month-old YAC128 and wild-type mice treated with 1 mg/kg/day SB or saline solution, for 28 days, using osmotic mini-pumps. YAC128 mice at 9 months of age were previously described to exhibit motor abnormalities with dysfunctional open field activity, and rotarod performance abnormalities, followed by brain weight loss and evident striatal atrophy (Van Raamsdonk, 2005; Slow et al., 2003). Additionally, cortical metabolic defects related with decreased sterol levels were previously described at this age (Valenza et al., 2007), suggesting that metabolic alterations in this brain region precede cortical atrophy, which is significant at 12 months of age (Van Raamsdonk, 2005). In the present study, YAC128 mouse cortex presented lower levels of acetylated H3, by about 58% ($p<0.05$), when compared to wild-type mice. Importantly, SB treatment increased H3 acetylation in both wild-type ($p<0.01$) and YAC128 ($p<0.01$) mice, the latter presenting acetylation levels comparable to those observed in saline-treated wild-type mice (**Figure 3.6A**). Moreover, YAC128 mice presented an increase by about 50% ($p<0.05$) in PDH E1α subunit phosphorylated at Ser232 (**Figure 3.6B**) and an increase by about 1.88 ($p<0.0001$), 1.80 ($p<0.0001$) and 3.44 ($p<0.001$) fold, respectively, in cortical PDK 1, 2 and 3 mRNA levels, when compared to wild-type mice (**Figure 3.6C**). These mice also showed a tendency for decreased cortical ATP/ADP levels (by about 45%, $p=0.07$) and reduced energy charge (by about 68%, $p<0.01$) (**Figure 3.6E,F**). SB-treated YAC128 and wild-type animals showed a large reduction in PDK1, PDK2 and PDK3 mRNA levels in the cortex. In wild-type mice cortex, SB treatment induced a reduction in PDK1, PDK2 and PDK3 mRNA levels, respectively, by about 87.7% ($p<0.001$), 85.2% ($p<0.001$) and 96.7% ($p<0.05$), in comparison with saline-treated wild-type mice (**Figure 3.6C**). Importantly, in the brain cortex of YAC128 mice, SB treatment also decreased phosphorylated PDH levels (at Ser232) by about 62% ($p<0.001$) (**Figure 3.6B**) and mRNA levels of PDK1, PDK2 and PDK3, respectively, by about 91.7% ($p<0.0001$), 90.2% ($p<0.0001$) and 98.4% ($p<0.0001$) (**Figure 3.6C**), and normalized ATP/ADP levels and energy charge (**Figure 3.6E,F**). This improvement in energy metabolism in SB-treated YAC128 mice led to a recovery in body weight, comparable to those observed in saline-treated wild-type mice (**Figure 3.6D**).

Taking together, these findings indicate that HDACi SB acts at the transcription level enhancing YAC128 central and peripheral metabolism, corroborating the changes observed *in vitro*.

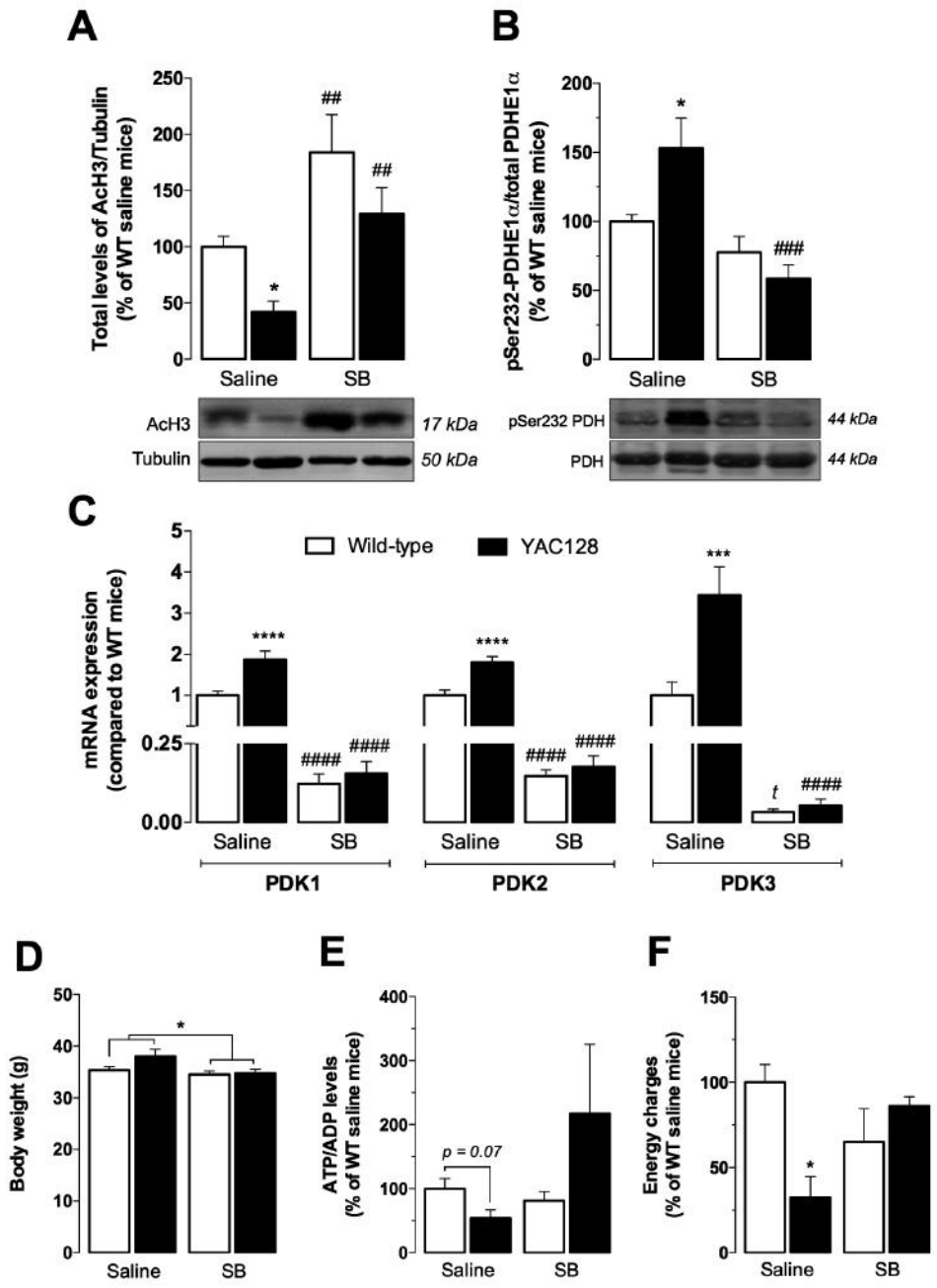

Figure 3.6 | SB ameliorates PDH dysfunction and metabolic abnormalities in symptomatic YAC128 mice brain. Histone 3 acetylation (Ac-H3) (n=6/7) (**A**), PDH E1 α subunit phosphorylation at Ser232 (n=5) (**B**), relative mRNA expression of PDKs 1-3 (n=6/8) (**C**), ATP/ADP ratio (n=4/5) (**E**) and energy charge (n=4/5) (**F**) were analyzed in cortical brain fractions from YAC128 (HD53 line) and wild-type mice, after treatment with saline (control group) or SB (1 mg/kg/day), for 28 days. Body weight was measured after the removal of the pump (n=7-9) (**D**). Data are the mean±SEM of the indicated animals from each treatment run in duplicates. Statistical analysis was performed by two-way ANOVA and revealed a significant interaction between genotype and SB treatment in **B** [$F(1,31)=6.113$, $p=0.0191$], **E** [$F(1,14)=5.627$, $p=0.0326$] and **F** [$F(1,14)=9.536$, $p=0.0086$]. A strong significant effect of SB treatment on **A** [$F(1,31)=25.22$, $p<0.0001$], **B** [$F(1,31)=16.08$, $p=0.0004$] and **D**

[F(1,27)=4.275, p=0.0484] was also observed. *p<0.05, ***p<0.001 and ****p<0.0001 compared to wild-type saline-treated group; $^{\#\#}p$<0.01, $^{\#\#\#}p$<0.001 $^{\#\#\#\#}p$<0.0001, compared to the respective saline-treated group by two-way ANOVA followed by Bonferroni post-test; and by Student's t-test: ^{t}p<0.05 (in **C**).

3.4. DISCUSSION

The present work shows that FL-mHtt inhibits PDH activity by decreasing the levels of PDH E1α subunit and increasing its phosphorylation at 3 serine regulatory sites. Ser232 (site 3) may be phosphorylated due to enhanced PDK1 and reduced PDP1c protein levels, whereas PDK3 ensures Ser293 (site 1) and Ser300 (site 2) phosphorylation. Remarkably, the observed regulation of PDH dysfunction in cells expressing FL-mHtt by HDACi and DCA was linked to increased mitochondrial function and metabolism. HDACi SB efficiently decreased PDH phosphorylation, which was accounted for by a decrease in mRNA expression of PDKs, specifically PDK3 (the most active and abundant PDK isoform in the brain), in HD striatal cell line and in YAC128 mouse brain cortex, two HD models expressing full-length mutant huntingtin.

Mitochondrial deficits in HD linked to bioenergetic dysfunction were previously associated with decreased NADH/NAD^+ ratio and PDC activity (Ferreira et al., 2011; Perluigi et al., 2005; Sorbi et al., 1983). As shown by us, the use of pyruvate as an energetic substrate, instead of glucose, accentuated the bioenergetic evidences of mitochondrial dysfunction in HD striatal neurons (Oliveira et al., 2006); moreover, metabolically supplementing mitochondria with pyruvate under glycolysis inhibition did not recover ATP levels in HD cybrids, which, together with decreased mitochondrial NADH/NADt ratio and unaltered activity of mitochondrial complexes I-IV, signalized to alterations in mitochondrial function upstream OXPHOS (Ferreira et al., 2010, 2011). In the present work, we showed a decrease in PDC activity in striatal ST*Hdh*$^{Q111/Q111}$ cells, which may be explained by decreased PDH E1α protein levels and higher phosphorylation at the three regulatory serines (293, 300 and 232) of E1α subunit. Moreover, YAC128 mice cortex exhibited increased PDH E1α phosphorylation at Ser232. Similar findings were previously described by us in HD cybrids (Ferreira et al., 2011) and in primary YAC128 cortical neurons (Naia et al., 2016), exhibiting a tendency for enhanced phosphorylation of PDH E1α at Ser232 and Ser293. This suggested a dysfunction in the mechanisms responsible for phosphorylation/dephosphorylation of these regulatory sites (Rardin et al., 2009). Indeed, mutant cells showed increased PDK1 and PDK3 protein levels, accompanied by a decrease in the levels of the catalytic

subunit of the most abundant PDH phosphatase, PDP1. Decreased E1α protein levels could be accounted for by alterations in protein expression (Perluigi et al., 2005), in response to alterations of transcription factors known to regulate PDH, such as PGC-1α (Kiilerich et al., 2010), which was described to be altered in HD models, including ST*Hdh*$^{Q111/Q111}$ cells (Cui et al., 2006). Nevertheless, expression of PDHA gene, which encodes for PDH E1α subunit, was not significantly affected in mutant cells. Similarly, no changes in mRNA levels of PDKs or PDPs were observed in HD cells. Thus, modified protein levels of PDH E1α, PDK1, PDK3 and PDP1c may be due to altered protein turnover and degradation. Conversely, saline-treated YAC128 showed increased mRNA expression of PDKs1-3. An increase in ROS levels in mutant cells may also contribute to inhibit PDH activity, since this enzyme was described to suffer oxidative modifications (Samikkannu et al., 2003; Tabatabaie et al., 1996; Vlessis et al., 1991). Moreover, H_2O_2-induced oxidative stress was also described to activate PDK1 (Prasad et al., 2000).

Transcriptional deregulation is a recognized mechanism of HD pathogenesis [reviewed in (Cunha-Oliveira et al., 2012; Gil and Rego, 2008; Naia and Rego, 2015)]. Thus, increasing gene transcription with HDACi is an interesting therapeutic strategy to recover mitochondrial function and energy metabolism in HD. HDACi were reported to increase acetylation of a small, specific subset of acetylome, including sites on histones and other chromatin-associated proteins, affecting the expression of 2% of mammalian genes (Van Lint et al., 1996; Scholz et al., 2015). HDACi were found to have beneficial effects in HD by reducing cell death (Beal and Ferrante, 2004), ameliorating mitochondrial Ca^{2+} handling (Oliveira et al., 2006), dynamics (Guedes-Dias et al., 2015) and metabolism (Jia et al., 2012). In addition, HDACi were previously shown to ameliorate neurodegenerative phenotype in HD mice (Ferrante et al., 2003; Thomas et al., 2008), which can occur transgenerationally, via crosstalk between different epigenetic mechanisms (Jia et al., 2015). Here, we show that exposure to HDACi induced histone H3 acetylation and rescue mitochondrial and metabolic dysfunction in *in vitro* and *in vivo* HD models, suggesting that altered gene expression is linked to energy defects in HD. The HDACi-induced mitochondrial recovery was similar as those observed with DCA, previously described to have beneficial effects in R6/2 and N171-82Q HD mouse models by restoring the active form of PDH (Andreassen et al., 2001). Concordantly, HDACi could reverse PDH dysfunction in mutant cells. Both PB (250 μM) and SB (500 μM) increased PDH E1α subunit protein levels in mutant cells, suggesting that HDACi could be protective in HD cells by rescuing PDH protein levels; this could occur through direct PTM and/or decreased protein degradation (as described below), since no changes in PDHA1 mRNA expression were observed in the presence of SB. In

ST*Hdh*$^{Q111/Q111}$ cells, SB also decreased the phosphorylation of E1α subunit at all regulatory sites, whereas PB decreased Ser293 phosphorylation. This alteration in PDH phosphorylation suggested that HDACi modulate the activity of enzymes that regulate PDH phosphorylation, PDKs and PDPs, or its associated transcription factors (Rardin et al., 2009).

In addition to histones, HDACi have been reported to stimulate the transactivation potential of various transcription factors, another way to modulate transcription. A large body of evidence proposes that mitochondrial ROS is sufficient for the stabilization of HIF-1α under normoxia (Brunelle et al., 2005; Kaelin, 2005). In this condition HIF-1α escapes degradation and translocates into the nucleus, where it initiates a gene expression program that includes transcription of several metabolism-related genes such as PDK1-3 (Kim et al., 2006; Prigione et al., 2014), culminating in decreased PDH activity. Here, we observed the HDACi SB produced a marked inhibition of HIF-1α accumulation, which suggests increased degradation. In fact, earlier studies demonstrated that therapeutic concentrations of HDACis are sufficient to repress the activation of HIF-1α (Fath et al., 2006; Kim et al., 2007b; Kong et al., 2006). Acetylation of HIF-1α enhances its ubiquitination, targeting HIF-1α for proteasomal degradation (Jeong et al., 2002; Kim et al., 2007b). Therefore, SB-mediated protection in mutant cells may be explained by a decrease in mRNA expression of PDK2 and PDK3 (the most abundant PDKs in ST*Hdh* cells), decreasing PDH E1α phosphorylation. The isoenzyme PDK3 was found to have fairly high specific activity and approximately 2-fold higher ability to incorporate phosphate than PDK2 (Bowker-Kinley et al., 1998; Kolobova et al., 2001). In agreement, genetic suppression of PDK3 reduced PDH E1α site 1 and site 2 phosphorylation, greatly increasing mitochondrial respiration in mutant cells, corroborating the previous hypothesis. Analysis of PDKs 1-3 mRNA levels and PDH phosphorylation in the cortex of 9 month-old YAC128 *versus* wild-type mice treated with SB confirmed the relevance of data obtained in striatal cells. We found increased PDH E1α phosphorylation (at Ser232) and mRNA expression of PDKs 1-3 in the cortex of YAC128 mice, which were largely reduced in animals treated with SB. Moreover, SB-treated YAC128 mice showed improved cortical energy levels, along with increased H3 acetylation, reinforcing the protective role of this HDACi. These data corroborate SB-mediated mitochondrial function and energy metabolism in HD striatal cells.

The activity of PDKs and PDPs have been described to be regulated mainly by changes in gene expression (Harris et al., 2002; Sugden and Holness, 2006), however it was recently described that the activity of PDK1-2 and PDP1 may be modulated by phosphorylation (Churchill et al., 2005; Hitosugi et al., 2011; Shan et al., 2014). Tyr

phosphorylation (Tyr136, Tyr243, and Tyr244) enhances PDK1 activity by promoting PDC binding, whereas phosphorylation of PDP1 (Tyr94) recruits acetyltransferase ACAT1 to PDC, resulting in inhibition of PDH (Hitosugi et al., 2011; Shan et al., 2014). Thus, in addition to changes in HIF-1α-mediated expression of PDKs induced by SB, modulation of PDKs phosphorylation, due to possible expression or modified activity of other kinases (e.g. Tyr kinases) following treatment with HDACis, may also account for the effects of these inhibitors. Recently, it was also shown that phosphorylation of PDP1 (Try381) recruits ACAT1 and dissociates the mitochondrial deacetylase SIRT3 to promote lysine acetylation of PDH E1α (Lys321) and PDP1 (Lys202), which facilitates Ser293 phosphorylation of PDH E1α, leading to PDH E1α inhibition and, consequently, reduced activity of PDC (Fan et al., 2014; Jing et al., 2013; Schwer et al., 2009), in contrast to the effect of HDACi found in the present study. Conversely, acetylation of PDH E2 subunit is known to increase PDH activity (Behal et al., 1993). Lysine acetylation may prevent lysine ubiquitination, when occurring in the same residues, thereby preventing protein degradation by proteasomal or lysosomal machineries, and resulting in increased protein half-life (Sadoul et al., 2008; Zhao et al., 2010); on the other hand (as in the case of HIF-1α at Lys532), lysine acetylation can promote ubiquitination, leading to protein degradation. Thus, besides the indirect effect of HDACis on PDH activity *via* PDK gene transcription through regulation of HIF-1α stabilization, these compounds may also directly interfere with the turnover of the protein by increasing its acetylation, and possibly modulating its ubiquitination and degradation.

Overall this work provides a better understanding of mitochondrial dysfunction in cells expressing full-length mutant huntingtin by providing evidence for a central role of PDH dysfunction in HD. Data also give support for PDH as a promising therapeutic target in HD. In particular, the HDACi SB was shown to be a promising neuroprotective agent for the treatment of mitochondrial bioenergetic dysfunction in HD KI striatal cells and YAC128 mice by decreasing the expression of the most abundant PDK isoforms.

CHAPTER IV

COMPARATIVE MITOCHONDRIAL-BASED PROTECTIVE EFFECTS OF RESVERATROL AND NICOTINAMIDE IN HD MODELS*

* Based on the following published manuscript: Naia L., *et al*. 2016. *Mol Neurobiol*. [Epub ahead of print]

4.1. SUMMARY

SIRT1 is a nicotinamide adenine dinucleotide NAD^+-dependent KDAC that regulates longevity and enhances mitochondrial metabolism. Both activation and inhibition of SIRT1 were previously shown to ameliorate neuropathological mechanisms in HD, a neurodegenerative disease that selectively affects the striatum and cortex, and is commonly linked to mitochondrial dysfunction. Thus, in this study, we tested the influence of RESV (a SIRT1 activator) *versus* NAM (a SIRT1 inhibitor) in counteracting mitochondrial dysfunction in HD models, namely striatal and cortical neurons isolated from YAC128 transgenic mice embryos, HD human lymphoblasts and an *in vivo* HD model. HD cell models displayed a deregulation in $\Delta\psi_m$ and respiration, implicating a decline in mitochondrial function. Further studies revealed decreased PGC-1α and TFAM protein levels, linked to mitochondrial DNA loss in HD lymphoblasts. Remarkably, RESV completely restored these parameters, while NAM increased NAD^+ levels, providing a positive add on mitochondrial function in *in vitro* HD models. In general, RESV decreased while NAM increased H3 acetylation at Lys9. In agreement with *in vitro* data, continuous RESV treatment for 28 days significantly improved motor coordination and learning and enhanced expression of mitochondrial-encoded ETC genes in YAC128 mice. In contrast, high concentrations of NAM blocked mitochondrial-related transcription, worsening motor phenotype. Overall, data indicate that activation of deacetylase activity by RESV improved gene transcription associated to mitochondrial function in HD, which may partially control HD-related motor disturbances.

4.2. INTRODUCTION

Epigenetic modifications play an important role in the regulation of metabolism, gene expression and lifespan. In particular, (de)acetylation of Lys residues is a high dynamic PTM that regulates a wide range of cellular functions. One group of Lys deacetylases, the SIRTs, has garnered much attention in the last decade. SIRTs are a highly conserved family of primarily NAD^+-dependent deacetylases that generate acetyl-ADP-ribose plus NAM, which is subsequently used to generate nicotinamide adenine mononucleotide and then NAD^+ (Tanner et al., 2000). Interestingly, a great fraction of mitochondrial proteins, as well as most metabolic enzymes in the cytosolic/nuclear pool, are regulated by deacetylation [reviewed in (Choudhary et al., 2014)].

Alterations of cellular metabolism have a crucial role in HD pathogenesis, a progressive and still incurable neurodegenerative disorder commonly characterized by psychiatric disturbances, abnormal chorea-like movements and cognitive decline [reviewed in (Gil and Rego, 2008)], raising the possibility of developing epigenetic-based therapeutic interventions that enhance mitochondrial and metabolic defenses. HD is caused by a polyQ repeat expansion in the ubiquitous expressed HTT protein, leading to selective striatal degeneration of MSNs and, later, of cerebral cortex (Naia et al., 2011). Although most HD symptoms reflect preferential neuronal death, numerous reports described additional abnormalities in peripheral tissues, including weight loss, altered glucose homeostasis and subcellular abnormalities in fibroblasts, lymphoblasts and platelets [e.g. (Ferreira et al., 2011; Naia et al., 2015; Silva et al., 2013)].

Initial evidence that SIRTs modulation might provide a therapeutic option in HD arose from a genetic study in *Caenorhabditis elegans,* where overexpression of the SIRT1-orthologue rescued polyQ toxicity (Parker et al., 2005). However, these observations were not always consistent in mammals (Naia and Rego, 2015; Pallos et al., 2008). mHTT can interact with SIRT1 and inhibit its activity (Jiang et al., 2012; Tulino et al., 2016); resulting in hyperacetylation and, consequently, inactivation of SIRT1 substrates, such as FOXO3a, and thereby inhibiting its pro-survival function. Moreover, overexpression of SIRT1 protected neurons against mHTT toxicity (Jiang et al., 2012) and alleviated peripheral deficits in a HD N171-82Q transgenic mouse model (Ho et al., 2010). The beneficial effects of SIRT1 may be enhanced by RESV, a natural polyphenolic antioxidant compound found predominantly in the skin of red grapes (Hubbard et al., 2013; Price et al., 2012). This polyphenol has been suggested to modulate cellular processes by activating SIRT1 (Borra et al., 2005; Howitz et al., 2003), which in turn activates key metabolic proteins, including AMPK and PGC-1α (Lagouge et

al., 2006; Pearson et al., 2008; Price et al., 2012). Although studies on how RESV enhances mitochondrial function have led to different and often conflicting mechanisms, apparently this compound increases NAD^+ levels and mitochondrial biogenesis in a SIRT1-dependent manner (Price et al., 2012). Nevertheless, NAM, a well-characterized water-soluble vitamin B3 and a selective SIRT1 inhibitor at high concentrations (Jackson et al., 2003; Scholz et al., 2015), was also shown to be protective in HD (Hathorn et al., 2011; Pallos et al., 2008). NAM increased mRNA levels of BDNF and PGC-1α in a mouse model of HD (Hathorn et al., 2011) and suppressed polyQ toxicity in an *in vivo* model of spinocerebellar ataxia (Ghosh and Feany, 2004). Furthermore, NAM rescued motor impairment in both HD *Drosophila* model and in B6.HDR6/1 transgenic mice (Hathorn et al., 2011; Pallos et al., 2008). More recently, it was shown that NAM and its metabolite 1-methylnicotinamide (MNA) extended lifespan in *C. elegans*, even in the absence of *Sir2* (Schmeisser et al., 2013).

These studies raise a number of questions about the effects of SIRT modulators in HD pathogenesis and the most intriguing of them is how compounds that exert opposed actions on SIRT1 activation can trigger similar survival pathways. To clarify this paradox in the context of HD we took advantage of central and peripheral models expressing human FL-mHTT. Our data reveal that RESV strongly induces mitochondrial activity by augmenting PGC-1α and TFAM levels, which culminates in increased transcription of mitochondrial-encoded genes. Enhanced mitochondrial function triggered by RESV may justify the improvement in motor function in HD YAC128 transgenic mice, as evidenced by the decrease in latency to fall off on the rotarod test. Remarkably, NAM also enhanced mitochondrial function in *in vitro* models, however prolonged *in vivo* treatment was not effective.

4.3. RESULTS

4.3.1. RESV and NAM modify histone H3 acetylation and improve mitochondrial function in vitro

HD has been associated with abnormal mitochondrial function, such as impaired mitochondrial ATP synthesis, intracellular calcium rise and decreased $\Delta\psi_m$, as described by many investigators including our group [e.g. (Ferreira et al., 2011; Naia et al., 2015, 2016)]. It has been well established that stimulation of SIRT1 can have

beneficial effects on mitochondrial function and biogenesis (Lagouge et al., 2006; Price et al., 2012), however the consequences of SIRT1 inhibition are still controversial. Several mitochondrial proteins are multiple acetylated and this process is dynamic and regulates many processes inside the cell. Therefore, we took advantage of two promising compounds, the SIRT1-activator RESV, a bioactive compound extracted from red grapes, and a SIRT1-inhibitor NAM, a water-soluble vitamin B3, previously described to contribute for restoration of abnormal metabolic pathways in motor-related disorders (Hathorn et al., 2011; Parker et al., 2005; Pearson et al., 2008), to demystify the paradox SIRT1 activation/inhibition in the context of HD.

As described in the literature for other HD models, we found decreased $\Delta\psi_m$ in both YAC128 cortical (by about 50%, $p<0.01$) and striatal (by about 32%, $p<0.05$) primary neurons, when compared to WT neurons (**Figure 4.1D, E**). In addition of two murine Htt copies, this model expresses FL human HTT with 128Q (**Figure 1.4A**), which may interact with mitochondria, deregulating their membrane potential. Remarkably, the $\Delta\psi_m$ in both mutant neurons was completely recovered in the presence of 5 μM RESV ($p<0.05$); this concentration increased cell viability by 25% in YAC128 striatal neurons ($p<0.05$) (**Figure 4.1B**). RESV at 1 μM also enhanced the $\Delta\psi_m$ in striatal neurons ($p<0.05$) (**Figure 4.1E**), without affecting cell viability. Of note, low doses of RESV were used in this *in vitro* study to prevent the activation of pathways in a SIRT1-independent manner (Price et al., 2012). NAM, at both concentrations, was also efficient at increasing the $\Delta\psi_m$ in YAC128 striatal neurons (by about 4.4- and 6-fold, for 0.5 mM and 1 mM, respectively; $p<0.0001$) (**Figure 4.1E**). Although no significant effects on $\Delta\psi_m$ were observed in cortical neurons, 1 mM NAM significantly increased the viability of WT neurons (by about 23.2%, $p<0.01$) (**Figure 4.1C**). Importantly, these effects on mitochondrial function were accompanied by modifications in histone H3 acetylation on Lys 9 (K9H3), which reduction mediates heterochromatin formation dependent on SIRT1 activity (Pruitt et al., 2006; Vaquero et al., 2004). The SIRT1-activator RESV (1 and 5 μM) showed a large tendency (not significant) for decreased K9H3 acetylation in cortical and striatal primary neurons, whereas NAM (0.5 and 1 mM) had the opposite effect (**Figure 4.1F-I**). The high variability, evidenced by data deviation, reflects the transient nature of this transcriptional modification [e.g. (Masri et al., 2013; Nakahata et al., 2008)].

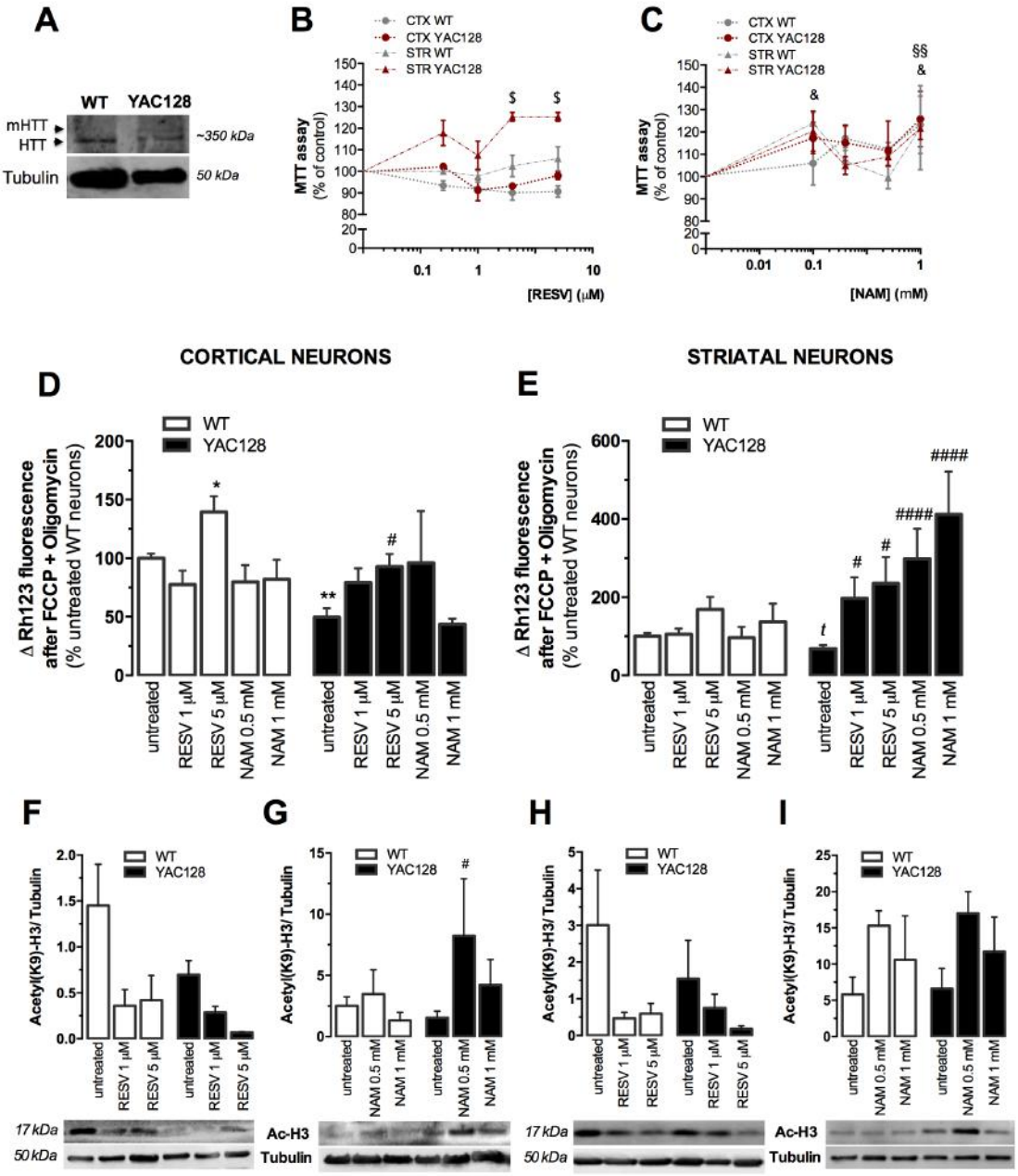

Figure 4.1 | RESV and NAM regularize $\Delta\psi_m$, modulate viability and histone H3 acetylation in YAC128 mouse cortical and striatal primary neurons. Wild-type and YAC128 mouse cortical (CTX; **B-D, F, G**) and striatal (STR; **B, C, E, H, I**) primary neurons were untreated or incubated in Neurobasal medium with RESV or NAM for 96 h, at 37°C. (**A**) Protein levels of wild-type and mHTT were detected by western blotting using a specific antibody against HTT. Dose-response effect of RESV (0.5 μM; 1 μM, 2 μM; 5 μM) (**B**) and NAM (0.1 mM; 0.2 mM; 0.5 mM; 1 mM) (**C**) on cell viability in primary neurons was assessed by the MTT assay. Rh123 fluorescence was recorded after complete mitochondrial membrane depolarization with oligomycin (2 μg/mL) plus FCCP (2.5 μM) (**D**, **E**). Two-way ANOVA analyses revealed a significant effect of treatment on $\Delta\psi_m$ of cortical [$F(4,74)=4.134$; $p=0.0045$] and striatal [$F(4,88)=4.624$; $p=0.002$] primary neurons; and a significant interaction between genotype and treatment in striatal neurons [$F(4,88)=3.363$; $p=0.013$] (**E**). Histone K9H3 acetylation, normalized for tubulin, was analyzed by western blotting; the blots are representative of the graphs (**F-I**). Two-way ANOVA analyses revealed a significant effect of NAM

treatment (in **G**) on histone H3 acetylation [F(2,43)=3.439; p=0.0412]. Data in graphs are the mean ± SEM of three-to-four independent experiments, run in duplicates. $^{\$}p$<0.05 RESV treated vs. untreated STR YAC128 neurons, $^{\&}p$<0.05 NAM treated vs. untreated STR WT neurons, $^{\S\S}p$<0.01 NAM treated vs. untreated CTX WT neurons, by one way ANOVA followed by Bonferroni post-hoc test; $^{*}p$<0.05, $^{**}p$<0.01 *versus* WT untreated neurons, $^{\#}p$<0.05, $^{\#\#\#\#}p$<0.0001 *versus* YAC128 untreated neurons by two-way ANOVA, followed by Bonferroni post-hoc test; unpaired Student's t-test revealed a ^{t}p<0.05 significance between WT and YAC128 striatal neurons.

Although most HD symptoms reflect preferential neuronal death in specific brain regions, mHTT is ubiquitously expressed and peripheral tissues display similar mitochondrial phenotype as the affected neurons (Sassone et al., 2009). In fact, we observed that HD lymphoblasts display a significant decrease (by about 36%, p<0.01) in basal O_2 consumption, in comparison with CTR lymphoblasts; notably, 5 μM RESV completely restored cellular respiration (p<0.05) (**Figure 4.2A**). Additionally, complete mitochondrial uncoupling and inhibition of mitochondrial ATP hydrolysis with CCCP plus oligomycin, to stimulate the maximal respiration rate of the organelle, was shown to be decreased in HD lymphoblasts (by about 33%); this effect was largely prevented by RESV (p<0.01) (**Figure 4.2A**). Similarly, 1 mM NAM enhanced by 2-fold the maximal mitochondrial respiration (p<0.01) (**Figure 4.2B**). Surprisingly, in human lymphoblasts, 1 μM RESV increased histone H3 acetylation (p<0.05), whereas 5 μM RESV showed a tendency for decreased acetylation (**Figure 4.3A**). Nevertheless, treatment of CTR and HD lymphoblasts with 5 μM RESV significantly increased HDAC activity (p<0.05) (**Figure 4.3C**) and completely restored CREB phosphorylation at Ser133 (reflecting its activation) in HD lymphoblasts (**Figure 4.3D**), a positive regulator of SIRT1 transcription (Noriega et al., 2011).

These data imply that, although with opposite effects on histone acetylation, both compounds have beneficial effects on mitochondrial function in cell models expressing full-length mHTT.

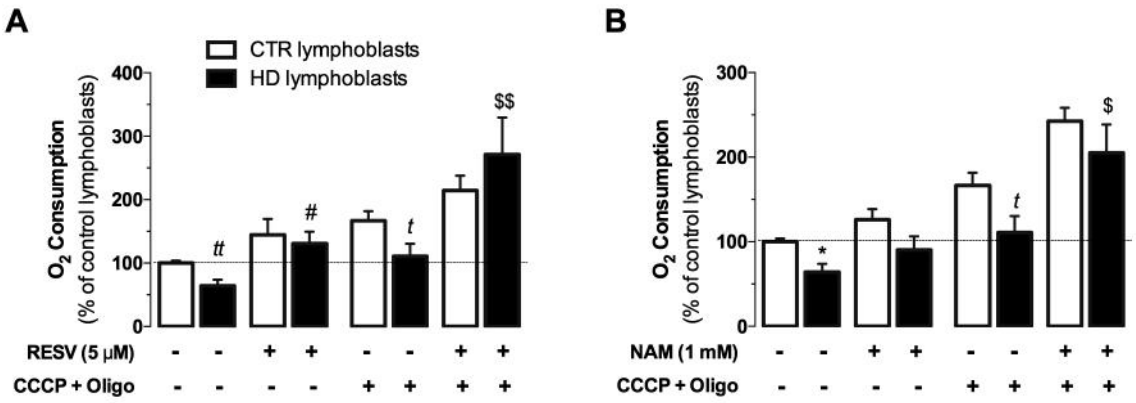

Figure 4.2 | RESV and NAM recover the rate of O_2 consumption in HD lymphoblasts. CTR and HD lymphoblasts were incubated in RPMI medium in the absence (-) or presence (+) of RESV (5 µM) (**A**) or NAM (1 mM) (**B**) for 24 h, at 37°C. Basal recording rate of O_2 consumption is represented in the first four bars; maximum respiration was achieved following addition of oligomycin (Oligo, 2 µg/mL) plus CCCP (2.5 µM) (last four bars). Two-way ANOVA analyses revealed a significant effect of RESV treatment (in **A**) on O_2 consumption [$F(1,31)=16.35$; $p=0.0003$] and a significant interaction between genotype and treatment [$F(1,31)=4.210$; $p=0.0487$]. In turn, NAM treatment revealed a significant effect on both basal [$F(1,29)=7.112$; $p=0.0124$] and maximal respiration [$F(1,28)=15.12$; $p=0.0006$] (in **B**). Unpaired Student's t-test revealed a $^{t}p<0.05$, $^{tt}p<0.01$ significance between CTR and HD lymphoblasts; $^{*}p<0.05$ *versus* CTR untreated lymphoblasts, $^{\#}p<0.05$ *versus* HD untreated lymphoblasts, $^{\$}p<0.05$, $^{\$\$}p<0.01$ *versus* HD CCCP-treated lymphoblasts by two-way ANOVA, followed by Bonferroni post-hoc test.

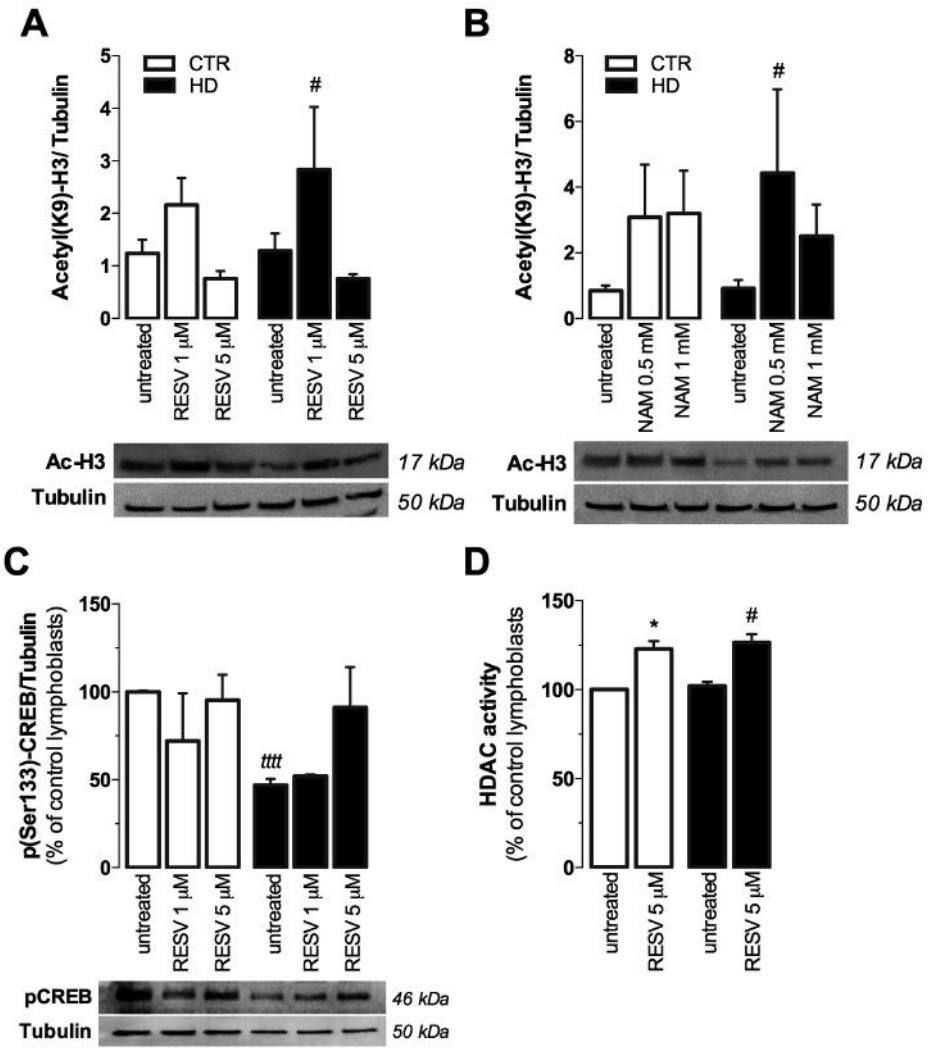

Figure 4.3 | NAM increases acetylation and RESV enhances HDAC activity. CTR and HD lymphoblasts were incubated in RPMI medium in the absence (untreated) or presence of RESV (1 µM and 5 µM) or NAM (0.5 mM and 1 mM) for 24 h, at 37°C. Histone K9H3 acetylation (**A, B**) and CREB phosphorylation (at Ser133) (**C**), normalized for tubulin, were analyzed by western blotting; the blots are representative of the graphs. Two-way ANOVA analyses revealed a significant effect of NAM treatment (in **B**) on Ac-H3 levels [$F(1,49)=11.46$; $p=0.0014$]. Colorimetric HDAC activity assay revealed a significant effect of RESV treatment [$F(1,12)=25.39$; $p=0.0003$] (**D**). Data are the mean ± SEM of four-to-six independent experiments. Unpaired Student's t-test revealed a $^{tttt}p<0.0001$ significance between CTR and HD lymphoblasts; $^{*}p<0.05$ *versus* CTR untreated lymphoblasts, $^{\#}p<0.05$ *versus* HD untreated lymphoblasts by two-way ANOVA, followed by Bonferroni post-hoc test.

4.3.2. RESV increases mtDNA copies and mitochondrial-related transcription factors in HD human lymphoblasts

A major question concerns how RESV and NAM trigger mitochondrial function. Mitochondrial proteins are encoded by both nuclear and mitochondrial genomes. Consequently, the process of mitochondrial biogenesis requires coordination between the two genomes. This coordination is primarily regulated by PGC-1α, which works by activating transcription factors such as the NRF-1 and TFAM [e.g. (Cui et al., 2006; Taherzadeh-Fard et al., 2011)]. Accordingly, we observed a significant decrease in PGC-1α nuclear levels (by about 37%, $p<0.01$) and TFAM mitochondrial levels (by about 40%, $p<0.05$) in HD human lymphoblasts, as previously described in other HD models (Cui et al., 2006; Weydt et al., 2006). Both RESV (5 μM) and NAM (1 mM) recovered PGC-1α nuclear levels in HD lymphoblasts, comparable to those observed in CTR lymphoblasts (**Figure 4.4A**). Nonetheless, only RESV was able to rescue TFAM levels ($p<0.01$) in HD mitochondria (**Figure 4.4B**). Concordantly, RESV treatment significantly increased mtDNA copy number by 2.5-fold ($p<0.001$) in HD lymphoblasts (**Figure 4.4C**), since mtDNA is primarily transcribed, coated and packed by TFAM (Ngo et al., 2014).

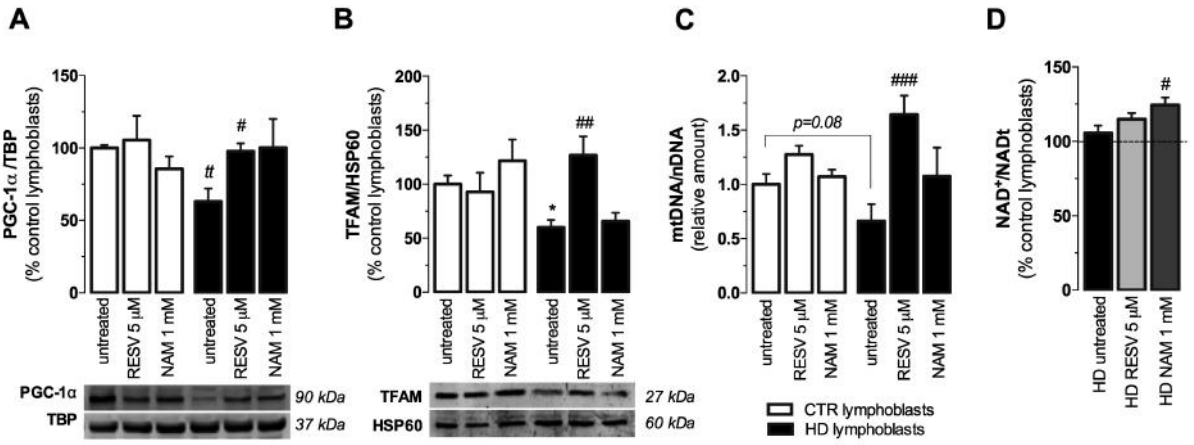

Figure 4.4 | RESV modulates mitochondrial biogenesis in HD lymphoblasts. CTR and HD lymphoblasts were incubated in RPMI medium in the absence (untreated) or presence of RESV (5 μM) or NAM (1 mM) for 24 h, at 37°C. Nuclear levels of PGC-1α (**A**), normalized for TBP, and mitochondrial levels of TFAM (**B**), normalized for HSP60, were analyzed by western blotting. Two-way ANOVA analyses revealed a significant effect of RESV treatment in **A** [$F(1,15)=5.203$; $p=0.0376$] and **B** [$F(1,21)=6.9$; $p=0.0158$]; TFAM analysis also revealed a significant interaction between treatment and genotype [$F(1,21)=10.55$; $p=0.0038$]. mtDNA copy number, normalized for nDNA (total genomic DNA), were analyzed by quantitative PCR (**C**). NAD^+/NADt ratio (**D**) was calculated considering CTR lymphoblasts as 100% (dashed line). One-way ANOVA analyses revealed a significant effect of NAM treatment [$p<0.05$] (**D**). Data in graphs are the mean ± SEM of three-to-six independent experiments. Unpaired Student's t-test revealed a significance ($^{tt}p<0.01$) between CTR

and HD lymphoblasts; $^{*}p<0.05$ *versus* CTR untreated lymphoblasts; $^{\#}p<0.05$, $^{\#\#}p<0.01$, $^{\#\#\#}p<0.001$ *versus* HD untreated lymphoblasts by two-way ANOVA, followed by Bonferroni post-hoc test.

As described previously, SIRTs require NAD^+ as an essential cofactor, and NAM, being an end-product inhibitor of SIRT1, is predominantly used for NAD^+ biosynthesis in mammals, preventing NAD^+ depletion and excitotoxicity (Naia and Rego, 2015). HD human lymphoblasts showed unchanged NAD^+/NADt ratio when compared to control cells (data not shown), however NAM treatment (at 1 mM) significantly increased NAD^+ levels ($p<0.05$) (**Figure 4.4D**). The increase in NAD^+ levels may justify enhanced mitochondrial function in HD lymphoblasts regardless of changes in mitochondrial transcription.

These data indicate that RESV is able to restore mitochondrial function in HD cells through a mtDNA-dependent manner, whereas NAM may feed the sirtuin pathway by increasing NAD^+ levels.

4.3.3. RESV alleviates motor dysfunction in YAC128 mouse model

We further confirmed the relevance of SIRT1 modulators in an HD animal model, the YAC128 transgenic mice, using the rotarod test to evaluate motor performance. YAC128 mice have a well-characterized phenotype exhibiting motor learning deficits at 2 months of age that progress up to 12 months of age, when both striatal and cortical atrophy is observed (Van Raamsdonk et al., 2005a; Slow et al., 2003). Along this age YAC128 mice show significantly increased body weight that is dose-dependent of HTT expression (Van Raamsdonk et al., 2006). Moreover, motor deficits on the rotarod begin at 6 months of age (Van Raamsdonk et al., 2005a). In agreement, a pre-treatment analysis confirmed a significant decrease in motor coordination and motor learning ($p<0.05$) along with increased body weight ($p<0.0001$) in nine month-old YAC128 mice, compared to WT mice (**Figure 4.5**). This pattern of cognitive and motor dysfunction in YAC128 mice is similar to the chronic progression of motor symptoms and cognitive deficits observed in HD patients (Brandt et al., 1984), providing a good opportunity to explore potential therapies for HD.

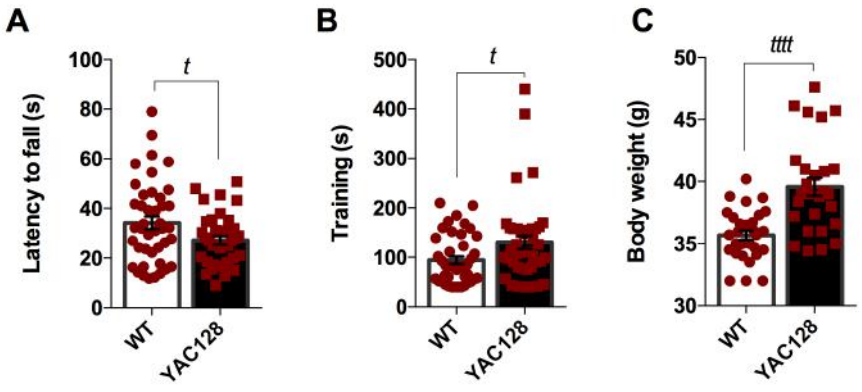

Figure 4.5 | Nine-month old YAC128 mice show deficits in motor function and learning. Before treatment, nine month-old wild-type and heterozygous YAC128 mice were subjected to rotarod motor evaluation. Accelerating rotarod test (from 5 to 40 rpm, over 5 min) was used as motor coordination test (**A**). The training time (constant 5 rpm, over 5 min) was used to assess motor learning (**B**). Body weight was measured before motor evaluation, showing that YAC128 mice weight significantly more than wild-type littermate controls (**C**). Results are the mean ± SEM of 42 WT and 40 YAC128 animals. Statistical analysis: unpaired Student's t-test revealed a $^{t}p<0.05$ and $^{tttt}p<0.0001$ significance between WT and YAC128 mice.

We administered 1 mg/kg/day RESV and 250 mg/kg/day NAM, for 28 days, in nine month-old YAC128 transgenic mice and age-matched WT controls using subcutaneous mini-osmotic pumps for continuous delivery (**Figure 4.6A**). HOP- or SAL-treated YAC128 mice exhibited 45% or 31% decrease ($p<0.05$) in the latency to fall off the rotarod, respectively (Figure **4.6B, C**). Treatment with RESV was able to completely restore YAC128 motor deficits (1.9-fold increase in the latency to fall ($p<0.05$)) (**Figure 4.6B**); conversely, NAM treatment did not have any effect on YAC128 mice and further aggravated the WT mice phenotype (**Figure 4.6C**). Motor learning was also assessed using the rotarod test for analysis of motor coordination. Hayden's group has previous described cumulative motor learning deficits along aging in YAC128 mice (Van Raamsdonk et al., 2005a). In this test, the maximal score was 40 s at a fixed speed of 5 rpm, and WT mice were able to stay on the rotarod for the full duration of the test on most trials, in a total of four trials (HOP, 58.1 ± 6.9 s; SAL, 48.7 ± 4.8 s). Although both WT and YAC128 mice learned the rotarod task, vehicle-treated WT mice required almost half the time to learn the task when compared to YAC128 mice ($p<0.05$) (**Figure 4.6D, E**). However, when treated with RESV, YAC128 mice took precisely the same time to learn the task as HOP-treated WT mice (58.3 ± 6.9 s; $p=0.0128$ for the effect of the treatment); moreover, RESV-treated WT mice improved by 23% the training time (**Figure 4.6D**). Conversely, NAM-treated WT mice worsened the training score by 52%, compared to SAL WT mice. In YAC128 mice, NAM treatment did not affect motor

learning (**Figure 4.6E**).

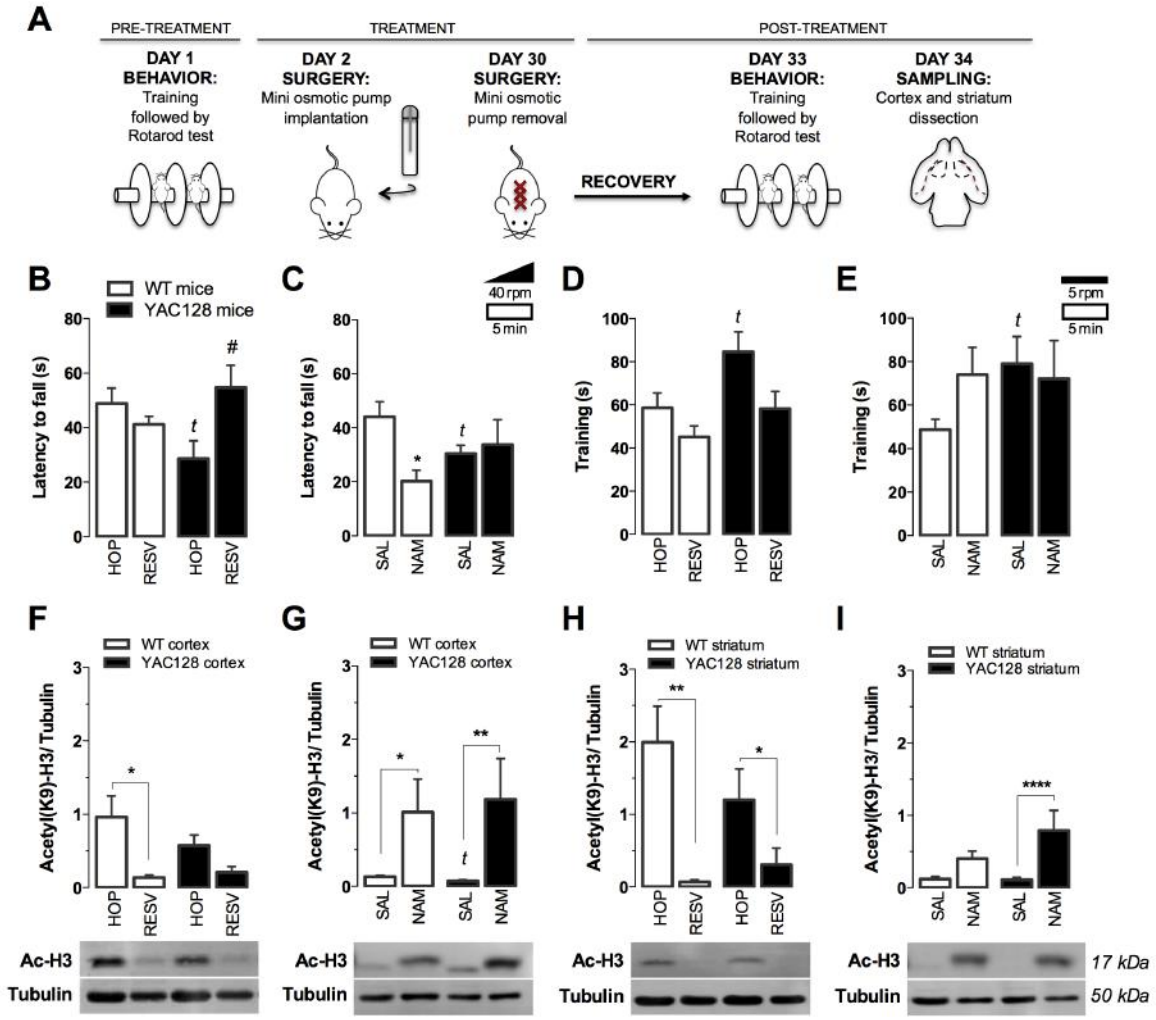

Figure 4.6 | RESV modulates acetylation and improves motor learning and coordination in YAC128 mice. Nine month-old male WT and heterozygous YAC128 mice were divided into eight experimental groups. In four groups, mice were implanted subcutaneously with an osmotic mini-pump and continuously infused with RESV (1 mg/kg/day) (n=8) (**B, D**) or NAM (250 mg/kg/day) (n=7) (**C, E**), for 28 days. The remaining four groups received the vehicles HOP (n=9) or SAL (n=9) infusion. Representative scheme of the *in vivo* experiment is depicted in **A**. Accelerating rotarod test (from 5 to 40 rpm, over 5 min) was used as motor coordination test (**B**, **C**). The training time (constant 5 rpm, over 5 min) was used to assess motor learning (**D**, **E**). Two-way ANOVA analyses revealed a significant interaction on rotarod test between genotype and RESV [F(1,27)=7.901; p=0.0091] or NAM treatment [F(1,24)=5.751; p=0.0246]. Histone H3 acetylation (at Lys9), normalized for tubulin, was analyzed in cortex (**F-G**) and striatum (**H-I**) samples by western blotting, using five-to-six animals/group. Representative blots are depicted. Two-way ANOVA analyses revealed a significant effect of RESV treatment on Ac-H3 levels of mice striatum [F(1,21)=14.80; p=0.0009] and cortex [F(1,20)=10.08; p=0.0048]; NAM treatment also shows a significant effect on ac-H3 levels in both cortex [F(1,36)=19,25; p<0.0001] and striatum [F(1,38)=25.04; p<0.0001]. In **i**, a significant interaction was found between genotype and treatment [F(1,38)=4.324; p<0.0444]. Unpaired Student's t-test revealed a ^{t}p<0.05 significance between WT and YAC128 mice; $^{*}p$<0.05, $^{**}p$<0.01,

$^{****}p<0.0001$ *versus* respective control; $^{\#}p<0.05$ *versus* HOP-treated YAC128 mice by two-way ANOVA, followed by Bonferroni post-hoc test.

The next experiments sought to determine whether RESV and NAM regulated protein acetylation in YAC128 and WT mice brain samples. K9H3 acetylation levels were measured in cortex and striatum dissected from the eight groups of mice. We observed a significant decrease in K9H3 acetylation in cortex (by about 86%; $p<0.05$) and striatum (by about 96.5%; $p<0.01$) in RESV-treated WT mice (**Figure 4.6F, H**); in YAC128 mice, a significant decrease was only observed in striatum (by about 74.3%; $p<0.05$) (**Figure 4.6H**). Regarding NAM treatment, we observed a significant increase in K9H3 acetylation in both WT (by about 7.6-fold, $p<0.05$) and YAC128 cortex (by about 16.1-fold, $p<0.01$) (**Figure 4.6G**). In striatum, NAM treatment significantly increased acetylation by 7.1-fold in YAC128 mice ($p<0.0001$) (**Figure 4.6I**).

These data confirm the feasibility of systemic administration of both compounds, influencing brain histone acetylation and motor function, and further support the hypothesis that RESV rescues motor deficits in symptomatic YAC128 HD mice.

4.3.4. RESV restores the expression of mitochondrial-encoded electron transport chain genes in YAC128 mouse model

To extend our findings about the role of RESV in improving mitochondrial function in a mtDNA-dependent manner (as defined in **Figure 4.4**), we next determined the mRNA expression levels of ETC candidate genes downstream of PGC-1α and NRF1, namely the mitochondrial-encoded complex I subunit NADH dehydrogenase 5 (MT-ND5) and complex IV subunit cytochrome *c* oxidase I (MT-CO1), and the nuclear-encoded cyt *c* (CYCS) in the cortex and striatum of YAC128 mice. No differences were observed in the cortex of HOP vehicle-treated YAC128 and WT mice groups; however, SAL vehicle-treated YAC128 mice cortex showed a significant increase in MT-ND5 and CYCS expression, compared to WT cortex (about 1.3- and 1.7-fold, respectively; $p<0.05$) (**Figure 4.7**). Interestingly, similar results were previously reported in the same mitochondrial-encoded genes in the cortical brain specimens from grade III and IV HD patients (Shirendeb et al., 2011), suggesting that this upregulation may be a compensatory response for the loss of mitochondrial function caused by mHTT. Treatment with RESV increased by 2-fold the mRNA levels of MT-ND5 ($p<0.05$), and by 1.5-fold the mRNA expression of MT-CO1 ($p<0.05$) in YAC128 mouse cortex, whereas

the expression levels of nuclear encoded CYCS gene declined in both WT and YAC128 cortex (**Figure 4.7A**). In striatum, HOP-treated YAC128 mice showed increased mRNA levels of mitochondrial-encoded genes, which were re-established to the levels of WT mice following RESV treatment (data not shown). In turn, treatment with 250 mg/kg NAM, for 28 days, completely abolished mRNA expression of mitochondrial- and nuclear-encoded ETC genes in both WT and YAC128 mouse cortex (p<0.001) (**Figure 4.7B**).

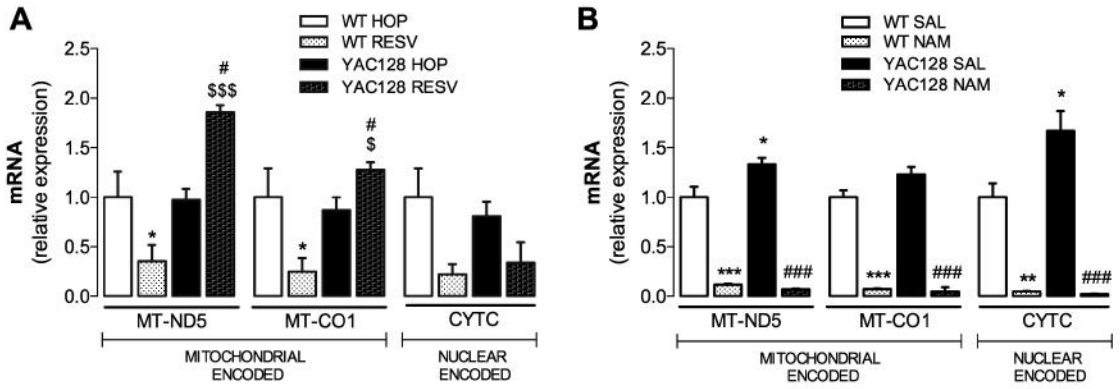

Figure 4.7 | RESV and NAM modify mRNA expression of candidate mitochondrial-encoded genes of complexes I and IV in YAC128 mice cortex. Relative mRNA expression of MT-CO1, MT-ND5 and CYCS were analyzed in cortical brain fractions from 9 month-old YAC128 and wild-type mice, after treatment with RESV (1 mg/kg/day) (**A**) or NAM (250 mg/kg/day) (**B**). Results are expressed as the mean ± SEM of four different animals from each treatment, run in duplicates. Statistics: $^{*}p$<0.05, $^{**}p$<0.01, $^{***}p$<0.001 *versus* SAL/HOP-treated WT mice; $^{\#}p$<0.05, $^{\#\#\#}p$<0.001 *versus* SAL/HOP-treated YAC128 mice; $^{\$}p$<0.05, $^{\$\$\$}p$<0.01 *versus* RESV-treated WT mice by two-way ANOVA, followed by Bonferroni post-hoc test.

Overall, data support the protective role of RESV on mitochondrial function in HD brain, as previously observed *in vitro*. The decline in ETC genes expression caused by NAM treatment appears to be in accordance with the aggravated phenotype observed on the rotarod test.

4.4. DISCUSSION

Differential modulation of SIRT1 pathways using RESV and NAM has shown to exert protective effects. First studies using nematode models of polyQ cytotoxicity showed that RESV treatment and genetic overexpression of SIRT1 were neuroprotective (Parker et al., 2005). New highly selective small molecules activators of SIRT1 (e.g. SRT2104) exhibited great ability to attenuate brain atrophy and motor dysfunction in HD mouse models (Jiang et al., 2014), and a clinical trial phase III on the effect of RESV on caudate volume in early affected HD patients by analyzing volumetric MRI has begun in 2015 (ClinicalTrials.gov Identifier: NCT02336633). In contrast, a phase I clinical trial is underway to treat HD with the highly specific SIRT1/*Sir2* inhibitor, selisistat (EX-527) (ClinicalTrials.gov Identifier: NCT01485952). In fact, the cytoprotective role of SIRT1 is complex; therefore the understanding of all pathways behind SIRT1 function may answer why the activation and partial reduction of SIRT1 pathways lead to a similar phenotype in different HD models. In the present study we showed that RESV were able to increase deacetylase activity and the levels of important enzymes for energy homeostasis, such as PGC-1α and TFAM, enhancing mitochondrial ETC biogenesis and, consequently, mitochondrial function. Additionally, 1 mg/kg/day of RESV (a significant lower dose compared with previous published data [e.g. (Ho et al., 2010)], for 28 days, significantly decreased K9H3 acetylation in both cortex and striatum of 9 month-old YAC128 mice, with significant improvement of motor coordination. In turn, lower mM doses of NAM may function as a NAD^+ donor, enhancing mitochondrial metabolism without affecting *in vitro* mitochondrial biogenesis. Notwithstanding, continuous *in vivo* treatment with 250 mg/kg/day of NAM completely blocked ETC biogenesis and, although it did not affect YAC128 mice motor balance, aggravated the phenotype of WT mice.

In 2003, a screen for STACs identified RESV, a natural phytophenol present in high concentrations in red grapes and wine, as the most potent SIRT1-deacetylation mediator (Howitz et al., 2003). Although the effectiveness of STACs as selective SIRT1 activators has been widely debated (Pacholec et al., 2010), in 2013 Sinclair's laboratory showed that RESV significantly increases SIRT1 activity through an allosteric interaction, resulting in increased SIRT1 affinity for both NAD^+ and the acetylated substrate (Hubbard et al., 2013). In the present study we showed that RESV increased CREB phosphorylation/activation in HD lymphoblasts, a transcription factor that binds SIRT1 promoter and robustly induces its transcription (Noriega et al., 2011). Moreover, RESV also induced K9H3 deacetylation in primary neurons and in both cortex and striatum of WT and YAC128 mice. Indeed in an *ex vitro* trial, a series of STACs, including RESV, activated SIRT1 with an aminomethylcoumarin-tagged peptide serving as a substrate,

which is only activated when it is directly adjacent to the acetylated K9H3 (Hubbard et al., 2013). Additionally, RNA interference-mediated decreased expression of SIRT1 caused hyperacetylation of K9H3 *in vivo* (Vaquero et al., 2004), supporting the role of RESV as a STAC in this work.

Although several reports have shown that RESV can prevent or slow the progression of a variety of illnesses, including neurodegenerative and cardiovascular diseases, cancer, as well as enhance stress resistance and extend lifespan, most *in vivo* studies showing its protective effect against mHTT were performed in lower eukaryotes such as *C. elegans* and *Drosophila melanogaster* (Pallos et al., 2008; Parker et al., 2005). So far, only one study has shown that SIRT1 overexpression significantly slowed the progression of motor deficits in mice models expressing both truncated and FL mHTT (Jiang et al., 2012). An oral dose (by gavage) of 25 mg/mouse/day RESV, for intermittent 45 days, failed to improve motor deficits associated with the HD phenotype in N171-82Q transgenic mouse model (Ho et al., 2010). The authors justified the negative results with the inefficacy of RESV in the CNS, since the treatment did not improve PGC-1α or NRF-1 mRNA expression in the striatum, contrasting with results in peripheral tissues (Ho et al., 2010). Conversely, herein we treated 9 month-old YAC128 mice with 1 mg/kg/day RESV for consecutive 28 days and observed a complete rescue on the latency to fall off on the rotarod test, up to the levels of vehicle-treated WT mice. Moreover, RESV-treated mice learned the rotarod task faster. Acetylated K9H3 also decreased, suggesting that RESV could have crossed the BBB and accumulated in the cerebral cortex and striatum (Baur and Sinclair, 2006). Importantly, this is the first study showing a recovery of motor coordination with RESV in a HD mammalian model at a stage exhibiting striatal atrophy (Slow et al., 2003). The efficacy of low doses was observed despite RESV low bioavailability, as a consequence of its poor aqueous solubility (although improved by HOP) and rapid metabolism, suggesting that concentrations of RESV near those obtained from Mediterranean dietary sources might be therapeutic. Nevertheless, treatment with NAM, a B3 vitamin that can rapidly penetrate the BBB (Hankes et al., 1991), provided no significant improvement in motor learning and coordination in YAC128 mice, contradicting previous results using the same NAM dosage in B6.HDR6/1 transgenic mice (Hathorn et al., 2011).

One of the most robust effects of RESV is the increase in mitochondrial mass (Baur et al., 2006; Lagouge et al., 2006). Remarkably, the role of mitochondria in HD pathogenesis is under close scrutiny since abnormalities in mitochondrial function and bioenergetics were described as important contributors for cell death in HD-affected individuals, in both central and peripheral tissues (Ferreira et al., 2011; Naia et al., 2015; Panov et al., 2002; Silva et al., 2013). Mitochondrial dysfunction may occur as a

consequence of a direct interaction of mHTT with the MOM and MIM (Panov et al., 2002; Yano et al., 2014) or by disruption of transcription of nuclear-encoded mitochondrial proteins, leading to abnormal mitochondrial biogenesis, reduced trafficking to synapses, decreased ATP production and/or ETC impairment (Cunha-Oliveira et al., 2012). In this respect, rodents treated with RESV or overexpressing SIRT1 showed enhanced mitochondrial biogenesis linked to deacetylation and activation of PGC-1α, which co-activates NRF-1 and NRF-2, enhancing the transcription of genes involved in mitochondrial biogenesis (Baur et al., 2006; Pearson et al., 2008; Scarpulla, 2011). More recently, it was demonstrated that the increase in NAD^+ levels, mitochondrial biogenesis and function by a moderate concentration of RESV (25 μM) are entirely dependent on SIRT1 activation (Price et al., 2012). In agreement, we administered a low μmolar concentration of RESV in primary cortical and striatal neurons obtained from mouse brain and in human lymphoblasts expressing FL-mHTT and observed a significant increase in mitochondrial function and biogenesis, which was prompted by PGC-1α and TFAM, a DNA-binding protein that activates transcription of mtDNA (Ngo et al., 2014; Taherzadeh-Fard et al., 2011). Consistent with these findings, RESV treatment increased mRNA expression of few PGC-1α downstream genes, which are components of the mitochondrial ETC, namely MT-CO1 and MT-ND5, in the cortex of YAC128 RESV-treated mice, suggesting that increased mitochondrial biogenesis may underline the ability of RESV to improve mitochondrial function in the presence of mHTT. Interestingly, RESV effects on ETC may also involve estrogen and estrogen-related receptors activation, master regulators of mitochondrial ETC (Lopes Costa et al., 2014).

Notably, NAM improved mitochondrial function in both central and peripheral HD *in vitro* models, as observed by the increase in $\Delta\psi_m$ and oxygen consumption. Nevertheless, this boosted effect seems to be independent of mitochondrial biogenesis. NAM is an end-product of the SIRT1 deacetylation reaction with a strong feedback inhibitory effect *in vivo* and *in vitro* (Bitterman et al., 2002). Recently, a quantitative mass spectrometry assay showed that NAM effects are primarily mediated by SIRT1 inhibition, and not by SIRT2 or SIRT6 (Scholz et al., 2015). However, it may enhance energy production since it is a positive NAD^+ donor, a versatile acceptor of hydride equivalents to form the reduced dinucleotide, NADH, that fuels OXPHOS (Sauve, 2008). In agreement, NAM treatment increased NAD^+ in HD lymphoblasts, suggesting that its protective role may be induced by changes in cellular redox status. Additionally, NAM may preserve NAD^+ levels by inhibiting NAD^+ hydrolysis mediated by the activities of SIRT1 and poly-ADP-ribose polymerase-1 (PARP-1), an enzyme that depletes NAD^+ supply by transferring poly-ADP-ribose subunits from NAD^+ to various DNA repair

enzymes (Chong et al., 2005; Klaidman et al., 2003; Liu et al., 2009). *In vitro* results have been encouraging; however, treatment with NAM completely abolished the expression of mitochondrial ETC genes downstream to PGC-1α, in both WT and YAC128 mice cortex. Although decreased CYCS mRNA was documented before in NAM-treated primary hippocampal neurons (Chong et al., 2005), previous studies in HD B6.HDR6/1 transgenic mice showed an increase in PGC-1α expression after NAM treatment for 12 weeks (Hathorn et al., 2011). Nevertheless, increased PGC-1α deacetylation suggests that NAM may act as a SIRT1 activator (Hathorn et al., 2011).

Years ago a systematic review reported that people were consuming resveratrol beyond the dose that can be obtained from dietary sources (Vang et al., 2011). This knowledge underscores the importance of understanding the biochemical mechanisms and safety of RESV and its derivatives. Our data clearly show that treatment with moderate doses of RESV results in increased motor balance linked to enhanced mitochondrial function and biogenesis in a manner that is dependent on protein deacetylation. The increase in NAD^+ levels induced by NAM likely contributes to a positive feedback cycle, however continued treatment was shown to be deleterious. Therefore, our data support that pharmacological activation of SIRT1 deacetylase activity provides a therapeutic opportunity to slow down the progression of HD-related symptoms.

CHAPTER V

SIRT3 ACTS AS A NEUROPROTECTIVE DEACETYLASE IN MITOCHONDRIAL HD PATHOLOGY

5.1. SUMMARY

HD is a genetic neurodegenerative disorder linked to expanded polyQ tract in the HTT protein. Striatal MSNs are the most affected population. Although a direct causative pathway from protein mutation to the selective neostriatal neurodegeneration remains unclear, several lines of evidence suggest that mitochondrial dysfunction plays a prominent role in HD pathogenesis. SIRT3 is a member of the sirtuin family of protein deacetylases that is located in mitochondria and serves as a primary regulator of mitochondrial protein acetylation, controlling mitochondrial metabolism, redox status and cell death. Given the versatile nature of SIRT3 metabolic functions, we speculated that its targeting might influence HD neurodegeneration. In the present work we show that ST*Hdh*$^{Q111/Q111}$ striatal cells and HD patients-derived human lymphoblasts exhibited an increase in SIRT3 protein and mRNA levels, along with increased SIRT3 enzymatic activity, in comparison with control cells. Symptomatic YAC128 HD transgenic mice also presented increased SIRT3 mRNA levels and deacetylation of SOD2, a pre-recognized mitochondrial SIRT3 target. SIRT3 efficiently decreased Lys acetylation in both mutant and control genotypes, and enhanced viability in cells successfully transfected with SIRT3. Failure to maintain $\Delta\psi_m$ and a decrease in mitochondrial mass are features of ST*Hdh*$^{Q111/Q111}$ striatal cells. Data from single-cell functional imaging revealed that SIRT3 OE improves $\Delta\psi_m$ in both wild-type and mutant striatal cells, without changing mitochondrial or mtDNA content. Nevertheless, analysis of PGC-1α and mitochondrial transcription factor TFAM showed that SIRT3 was able to reestablish reduced levels of these transcription factors triggered by mHtt. Overall, we report that increased SIRT3 modulates Lys acetylation in ST*Hdh* striatal cells, selectively enhancing mitochondrial function in cells expressing mHtt.

5.2. INTRODUCTION

SIRT3 belongs to a larger family of NAD^+-dependent KDACs named sirtuins, which have important roles in controlling metabolism in a variety of organisms. It was first described in 2002 as a mitochondrial deacetylase highly expressed in metabolically active tissues, including the brain (Onyango et al., 2002). Indeed, SIRT3 is the major deacetylase in mitochondria, controlling more than 1,500 acetylated sites in mitochondrial enzymes involved in fatty acid oxidation, ATP production, pyruvate metabolism and antioxidant defenses (Hebert et al., 2013; Lombard et al., 2007; Rardin et al., 2013). More specifically, five subunits of complex I and two subunits of complex II/SDH are direct targets of SIRT3 deacetylase activity (Finley et al., 2011; Rardin et al., 2013). Additionally, SIRT3 may stimulate O_2 consumption indirectly by deacetylating (at Lys166) and inhibiting CyD activity. SIRT3-induced inactivation of CyD causes a detachment of hexokinase II from the mitochondrion that is necessary for stimulation of OXPHOS (Shulga et al., 2010). Moreover, SIRT3 activity can diminish ROS levels by directly deacetylating (at Lys68) and activating the antioxidant protein SOD2. Although the processed (short form) of SIRT3 has well-established mitochondrial functions, FL-SIRT3 was previously described in the nucleus, although its functional relevance is not clear. Nuclear FL-SIRT3 was suggested to act as a transcriptional repressive histone deacetylase, revealing a strong specificity for deacetylation of histones K9H3 and K16H4 (Scher et al., 2007). Moreover, FL-SIRT3 can be rapidly degraded under conditions of cellular stress, such as oxidative stress, whereas the mitochondrial processed form is unaffected (Iwahara et al., 2012).

More recently, it was observed that SIRT3 is suppressed with aging, whereas SIRT3 upregulation reverses aging-associated degeneration (Brown et al., 2013). SIRT3 overexpression also protects cultured motor neurons against mitochondrial fragmentation and cell-death induced by SOD1 mutant that causes familial Amyotrophic Lateral Sclerosis (Song et al., 2013), suggesting neuroprotective roles for SIRT3.

HD is a genetic neurodegenerative disorder caused by an expansion of CAG repeats within the coding region of the *HTT* gene, that in turn leads to the expression of mHTT throughout the human body, causing prominent cell death in the striatum [reviewed in (Gil and Rego, 2008)]. Among several mechanisms of neurodegeneration, oxidative stress and deregulated mitochondrial function and dynamics are of particular interest. Early changes in HD mitochondrial function were previously reported to be due to a direct interaction of mHTT with the MOM, causing depletion of $\Delta\psi_m$ (Panov et al., 2002). Similarly, mitochondrial complex II irreversible inhibition evoked by 3-NP, which recapitulates HD-like motor symptoms, causes mitochondrial fragmentation and

neuronal cell death via ROS-dependent pathways (Liot et al., 2009). In this context, it was recently reported that SIRT3 deficiency aggravated motor function and striatal degeneration caused by 3-NP administration (Cheng et al., 2016). SIRT3 is capable of deacetylating OPA1 (at K926/931), a mitochondrial fusion protein that is hyperacetylated under pathological stress, elevating its GTPase activity, preserving mitochondrial network and protecting from oxidative damage-mediated cell death (Samant et al., 2014). In HD striatal cells, ε-viniferin-induced SIRT3 activation preserved $\Delta\psi_m$, replenished NAD^+ and reduced ROS levels induced by mHtt expression (Fu et al., 2012). Although this resveratrol dimer seems to have a protective role in HD, it cannot be excluded that this effect may be in part due to SIRT1 activation, which indirectly influences SIRT3 transcription through transactivation of ERRα (Bell and Guarente, 2011). Considering that very few studies reported a possible role for SIRT3 in the context of HD, in this study we aimed to verify the role of overexpressing SIRT3 on mitochondrial-related functions in HD KI striatal cells. Here we show that mitochondrial deacetylase SIRT3 is extensively expressed and activated in several HD human and mouse models. Moreover, SIRT3 OE in ST*Hdh*$^{Q111/Q111}$ striatal cells decreased overall Lys acetylation and rescued $\Delta\psi_m$ and mitochondrial TFAM expression, suggesting a role in mitochondrial homeostasis in HD pathology.

5.3. RESULTS

5.3.1. Mouse central and human peripheral HD models show increased SIRT3 expression and activity

SIRT3 levels appear to be regulated by aging, neurodegenerative processes or by additional stimulatory mechanism such as calorie restriction, exercise and ROS [reviewed in (Kincaid and Bossy-Wetzel, 2013)]. We characterized the mitochondrial levels of SIRT3 protein, mRNA and activity in different models of HD, namely human lymphoblasts derived from HD affected patients containing heterozygous expansion mutation *versus* unaffected voluntary control siblings, mice striatal ST*Hdh*$^{Q111/Q111}$ cells *versus* ST*Hdh*$^{Q7/Q7}$ cells and 12 month-old YAC128 transgenic mice cortex *versus* wild-type cortex. Interestingly, we observed that both HD lymphoblasts and STHdh$^{Q111/Q111}$ cells displayed, respectively, a 1.6- and 1.4-fold increase in ~28 kDa processed mitochondrial SIRT3 form, when compared to control cells (p<0.05) (**Figure 5.1A, D**), which was accompanied by increased mRNA levels (p<0.05) (**Figure 5.1B, E**).

Increased SIRT3 activity was also observed in both HD models and, although the fold-increase for protein and mRNA levels were similar between them, in comparison with respective controls, ST*Hdh*$^{Q111/Q111}$ cells showed the most exacerbated SIRT3 activity ($p<0.001$) (**Figure 5.1C, F**). Moreover, ST*Hdh*$^{Q111/Q111}$ showed a significant decrease in ~44-kDa cytosolic FL-SIRT3 form. Although modified SIRT3 protein levels was not detected in YAC128 mouse cortex (**Figure 5.1G**), increased mRNA and deacetylation of SOD2, a pre-recognized mitochondrial SIRT3 target, were observed in this transgenic model ($p<0.05$) (**Figure 5.1H, I**). This increase in SIRT3 activity may represent a compensatory mitochondrial stress response.

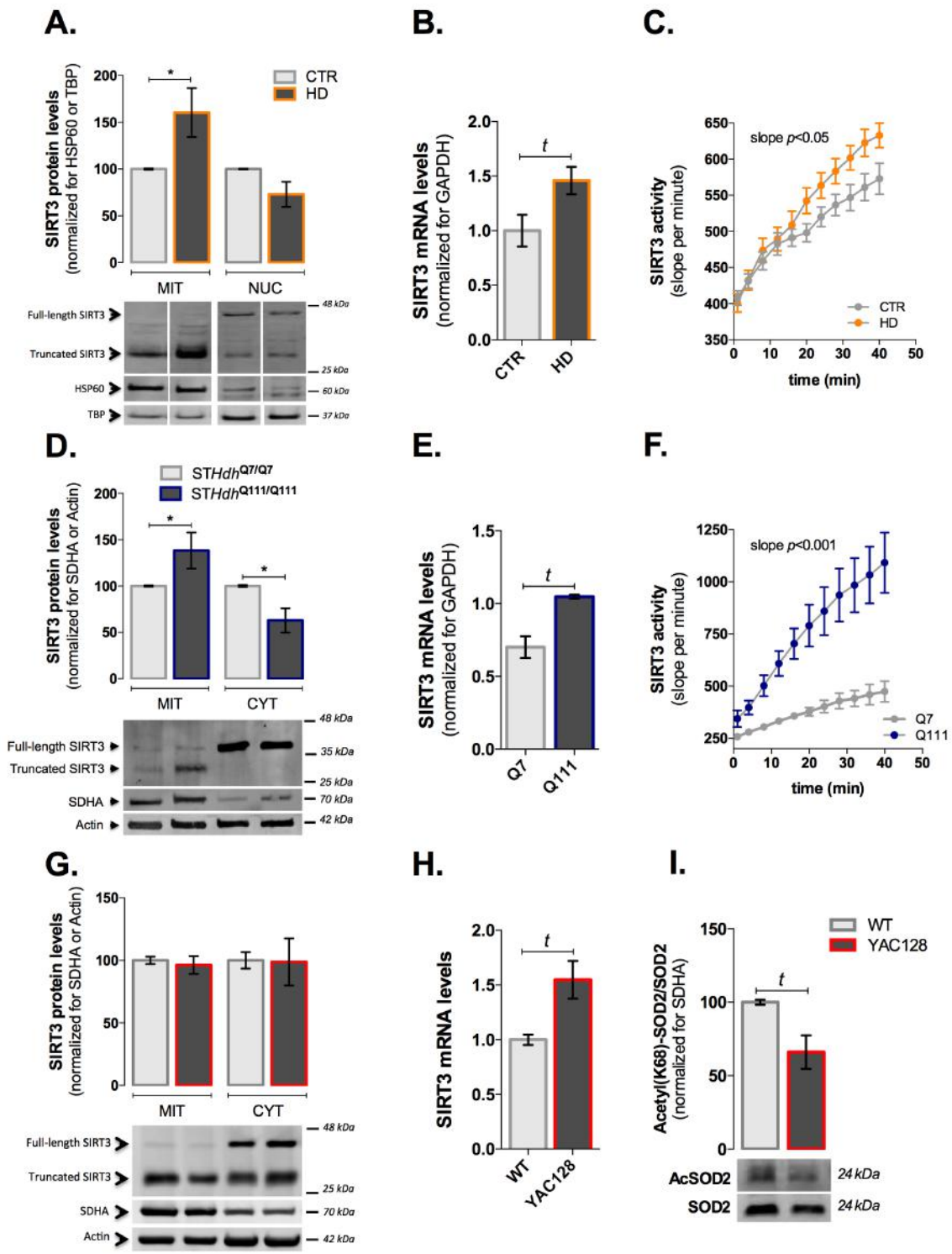

Figure 5.1 | Increased mitochondrial SIRT3 levels and activity in different HD cell models. SIRT3 protein levels were quantified by western blotting in mitochondrial (MIT), nuclear (NUC) and cytosolic (CYT) enriched-fractions from human lymphoblasts (**A**), KI mice striatal cells (**D**) and 12 month-old mice brain cortical homogenates (**G**). Two-way ANOVA analyses revealed a significant effect of SIRT3 location and an interaction between genotype and cellular fraction in human lymphoblasts [$F(1,18)=5.669$; $p=0.0281$] (**A**) and in striatal cells [$F(1,32)=7.933$; $p=0.0082$] (**B**). SIRT3 mRNA levels were analyzed by qPCR using specific primers for mitochondrial SIRT3 (**B**, **E**, **H**). SIRT3 activity was quantified in mitochondrial fractions by fluorimetry (**C, F**). Acetyl (Lys68) SOD2

levels were normalized for total SOD2 content in mitochondrial-enriched fractions from 12 month-old mice cortex (**I**). Data in graphs are the mean ± SEM of four-to-seven independent experiments. Statistical analysis: $^{*}p<0.05$ by two-way ANOVA followed by Bonferroni post-hoc test; $^{t}p<0.05$ by unpaired Student's t- test

5.3.2. SIRT3 overexpression decreases overall acetylation and apoptotic cell death

Based on data described in Figure 5.1, increased SIRT3 was hypothesized to act as a primary regulator of mitochondrial protein acetylation, controlling mitochondrial metabolism, redox status and possibly cell death, mechanisms that were previously shown to be compromised in HD ST*Hdh* striatal cells (Naia et al., 2016; Ribeiro et al., 2013, 2014; Ruan et al., 2004). Thus, despite increased SIRT3 activity in the HD models tested, we analyzed the influence of SIRT3 OE on mitochondrial function and cell death in mutant and wild-type ST*Hdh* striatal cells.

SIRT3 gene was inserted in a mammalian vector with C-terminal green fluorescent protein (GFP)-tag linked to a CMV promoter. We confirm SIRT3-GFP protein expression by western blotting with a visualized band at approximately 55 kDa (**Figure 5.2A**). Moreover, SIRT3-GFP cellular distribution was visualized by immunocytofluorescence. Interestingly, HD striatal cells showed an increased accumulation of SIRT3-GFP in mitochondria (pink arrows), in comparison to wild-type cells, in detriment to nuclear location (**Figure 5.2B**) (Carmo, 2015), similarly to what is observed in non-transfected cells. Increased SIRT3 activity after transfection was evidenced by a significant decrease in total Lys acetylation in both ST*Hdh*$^{Q7/Q7}$ and ST*Hdh*$^{Q111/Q111}$ cells (**Figure 5.2C**).

Results from cell death evaluation in ST*Hdh* were not always consistent. Initial data showed that ST*Hdh*$^{Q111/Q111}$ cells only exhibit increased neuronal death after toxic stimuli, e.g. 3-NP (Ruan et al., 2004). Concordantly, our group observed increased condensed nuclear DNA with intense Hoechst/PI fluorescence staining exclusively in ST*Hdh*$^{Q111/Q111}$ cells exposed to staurosporine (Rosenstock et al., 2011). However, more recently, we reported a significant increase in apoptotic cell death in the same mutant cells under basal conditions (Ribeiro et al., 2013). Here, we observed that apoptotic cell death account for less than 1% in these mutant ST*Hdh* striatal cells. Still, mutant cells exhibited a non-significant 1.7-fold increase in the percentage of apoptotic cells, compared to wild-type cells (**Figure 5.2D**). The discrepancy in the results may be due to the use of different cell clones or differential metabolic and/or functional status of these cells along passages, when considering the same clones; in the present work cell

passages above 17 were never used, as recommended by Coriell Cell Repositories, from where cells were obtained. In ST*Hdh*$^{Q7/Q7}$ coverslips transfected either with GFP or SIRT3-GFP no change in the percentage of apoptosis was observed. In ST*Hdh*$^{Q111/Q111}$ coverslips, cells that were successfully transfected with SIRT3-GFP presented no apoptotic death, however cells (from the same coverslips) that were not transfected, but were similarly exposed to the transfection reagent, exhibited increased cell death, in relation with SIRT3-transfected cells ($p<0.0001$) (**Figure 5.2E-G**). Exacerbation of cell death in SIRT3-non-OE mutant cells from the same coverslips as SIRT3-OE mutant cells may occur due to a possible toxic effect of transfection; data indicate that SIRT3-OE transfected cells are less prone to this effect.

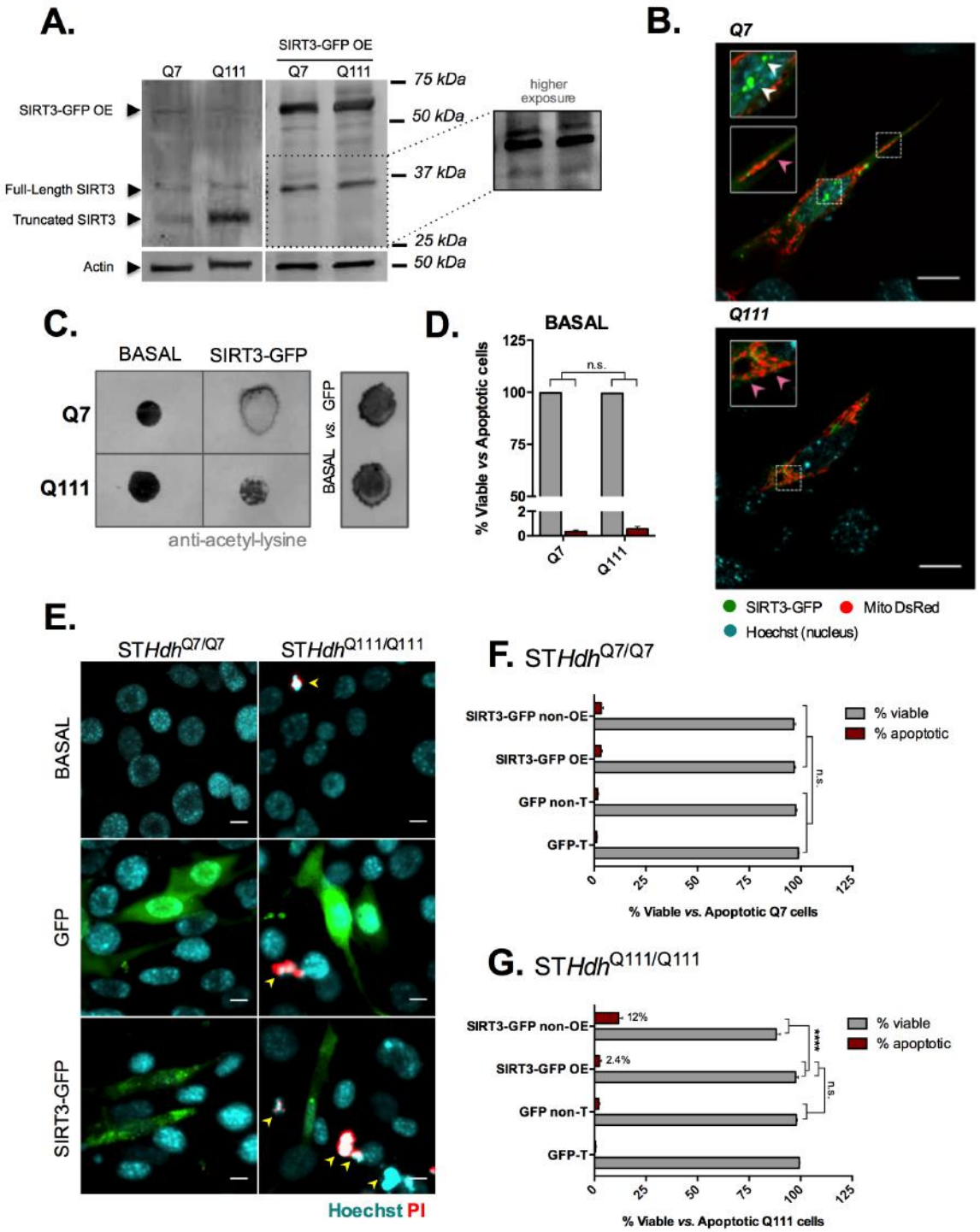

Figure 5.2 | SIRT3 overexpression modulates acetylation and protects mutant cells against apoptotic cell death. SIRT3 OE was observed by western blotting (**A**) and by immunofluorescence (**B**) in both ST*Hdh*$^{Q7/Q7}$ and ST*Hdh*$^{Q111/Q111}$ cells (or Q7, Q111, in short, respectively). White arrows show SIRT3-nucleus co-localization, whereas pink arrows evidence SIRT3-mitochondrial co-localization; scale bar = 10 μm (**B**). Total Lys acetylation was evaluated by dot blotting against acetyl-Lys antibody (**C**). Cell death quantification was performed both in GFP transfected (GFP-T) or non-transfected (GFP non-T) cells and in SIRT3 OE or SIRT3 non-OE cells from the same coverslip. Viable cells exhibit weak diffuse nuclear-associated fluorescence, whereas dying/dead cells (indicated by yellow arrows) exhibit intense punctate Hoechst/PI fluorescence (**E**). Scale bar = 300

μm. Graphical quantification of the Hoechst/PI images are represented in **D**, **F** and **G**. Two-way ANOVA analyses revealed a significant interaction between viability and transfection in ST*Hdh*$^{Q111/Q111}$ cells [F(4,50)=26.97; *p*=0.0001] (**G**). n.s., non-significant.

5.3.3. SIRT3 overexpression reverts the loss in mitochondrial membrane potential and mitochondrial-related transcription factors induced by mHTT

Preserved $\Delta\psi_m$ is essential to maintain ATP generation, mitochondrial Ca^{2+} handling and dynamics. $TMRM^+$ is a widely used membrane permeant cationic fluorescent probe that accumulates in mitochondria retaining a high mitochondrial transmembrane potential. Striatal cells were loaded with low nM $TMRM^+$ concentrations to avoid quenching of the fluorescence signal in the mitochondrial matrix; therefore approximately 75% of the total fluorescence observed should originate from the polarized organelle (Nicholls and Ward, 2000). Previously we showed by fluorometric analysis that ST*Hdh*$^{Q111/Q111}$ striatal cells exhibited decreased $\Delta\psi_m$ (Ribeiro et al., 2014). Here, we used single-cell spinning disk confocal microscopy to measure the fluorescence intensity of $TMRM^+$ in mitochondria before and after FCCP protonophore in the presence of oligomycin, which are recognized to cause a complete decay in $\Delta\psi_m$ releasing all $TMRM^+$ that had been accumulate in mitochondria (**Figure 5.3D**). Therefore, the higher decay in $TMRM^+$ fluorescence reflects its greater initial accumulation in mitochondria due to a high $\Delta\psi_m$. Mutant striatal cells showed approximately 25% lower $\Delta\psi_m$ than controls (p<0.0001) (**Figure 5.3A**). Importantly, GFP-transfected ST*Hdh* cells showed identical values of FCCP-induced $TMRM^+$ release from mitochondria than basal untransfected cells (data not shown). For all conditions studied, addition of oligomycin alone did not significantly reduce $TMRM^+$ mitochondrial fluorescence. Remarkably, SIRT3 OE significantly increased by about 1.2- and 1.3-fold the $\Delta\psi_m$ in ST*Hdh*$^{Q7/Q7}$ and ST*Hdh*$^{Q111/Q111}$ cells, respectively (p=0.0014) (**Figure 5.3B**, **C**). The increase in $TMRM^+$ release in mutant SIRT3 transfected cells, due to higher retention in polarized mitochondria (panel t=0 s; **Figure 5.3D**), was sufficient to reach the levels of wild-type GFP-transfected cells.

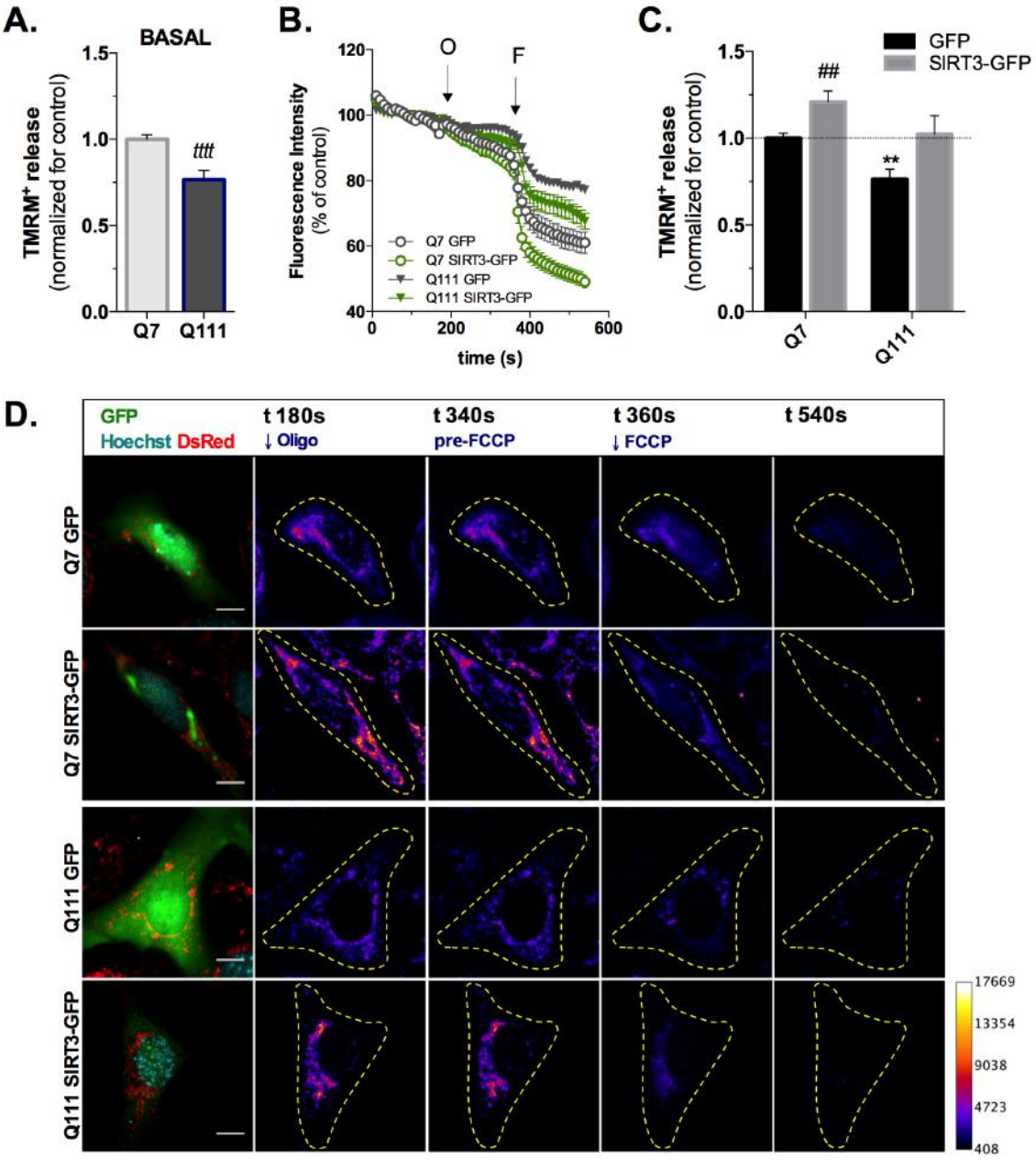

Figure 5.3 | SIRT3 enhanced FCCP-induced TMRM$^+$ release in ST*Hdh* striatal cells. Untransfected (**A**), GFP- or SIRT3-GFP transfected (**B-D**) cells were loaded with 10 nM TMRM$^+$ for 30 minutes (non-quenching conditions), washed and then analyzed by spinning disk confocal microscopy in the presence of TMRM$^+$. Fluorescence was monitored before and after exposure of cells to 2.5 μg/mL oligomycin (Oligo (O); at time-point of 180 s) and 2.5 μM FCCP (F; at time point of 360 s). Representative histogram and images of the experience are represented in **B** and **D**, respectively. Scale bar: 10 μm. The graph bars represent the mean ± SEM of 10 to 45 cells from at least four independent experiments, and were calculated based on the fluorescence intensity decay prior to FCCP stimuli (time point of 340 s) until the end of the experiment. Two-way ANOVA analyses revealed a significant effect of both genotype [$F(1,151)=8.528$; $p=0.0040$] and SIRT3 OE [$F(1,151)=10.53$; $p=0.0014$] in striatal cells. Statistics: $^{**}p<0.01$ Q7 GFP *vs* Q111 GFP, $^{\#\#}p<0.01$ Q7 GFP *vs* Q7 SIRT3 by two-way ANOVA followed by Bonferroni post-hoc test; $^{tttt}p<0.0001$ by unpaired Student's t- test.

Depolarized mitochondria are the substrate for selective mitochondrial degradation [reviewed in (Twig and Shirihai, 2011). Therefore, we further looked at mitochondrial mass and levels of mitochondrial biogenesis-related factors PGC-1α and TFAM. ST*Hdh*$^{Q111/Q111}$ cells were show to have lower mitochondrial mass, quantified as the percentage of the cell's area occupied by Mito-DsRed labeling, when compared to wild-type controls (p<0.01) (**Figure 5.4A**). Similarly, mutant cells exhibited approximately 30% and 40% lower PGC-1α (p<0.001) and mitochondrial TFAM levels (p<0.01), respectively, than wild-type cells (**Figure 5.4C, D**), supporting the previous results obtained in peripheral HD lymphoblasts (*described in Chapter IV*, **Figure 4.4A, B**). In contrast, mtDNA copies increased by 1.4-fold (although not significantly) in mutant cells (**Figure 5.4B**), which may correlate with increased fission over fusion described previously in this model (Carmo, 2015; Costa et al., 2010; Jin et al., 2013). SIRT3 OE in ST*Hdh*$^{Q7/Q7}$ resulted in increased PGC-1α levels (p<0.01). In ST*Hdh*$^{Q111/Q111}$ cells, SIRT3 OE slightly or completely reestablished PGC-1α and TFAM levels, respectively, to the levels of controls (**Figure 5.4C, E, F**). Despite SIRT3-evoked TFAM recovery, mitochondrial mass and mtDNA content were not restored (**Figure 5.4A, B**; data not shown).

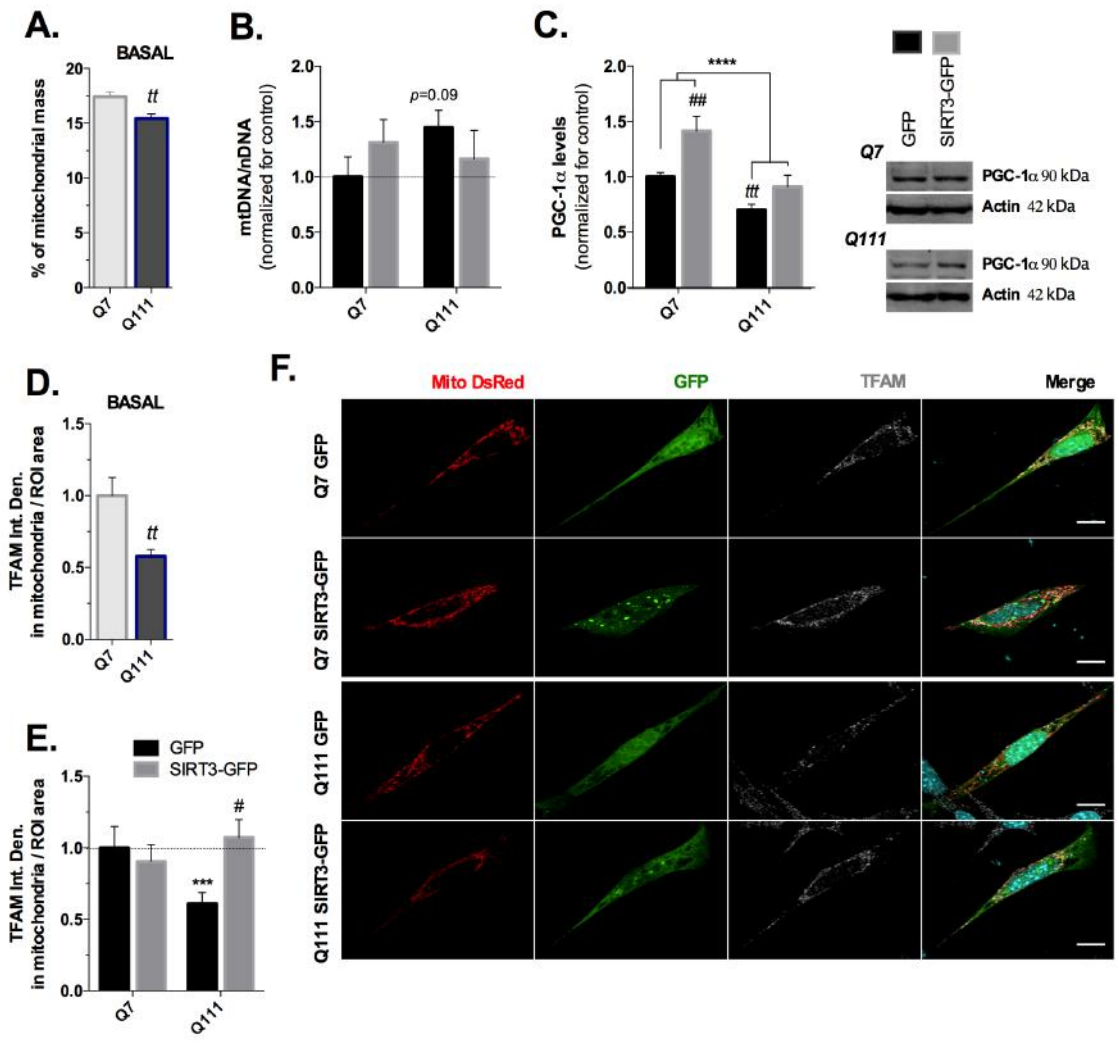

Figure 5.4 | Decreased PGC-1α and mitochondrial TFAM levels in ST*Hdh*$^{Q111/Q111}$ striatal cells are rescued after SIRT3 overexpression. Mitochondria were labeled using targeted DsRed and nuclei were stained with Hoechst. The percentage of cells area occupied by mitochondria was quantified in Image J, considering ~200 cells/condition (**A**). mDNA was quantified by qPCR using specific primers (**B**). Total PGC-1α levels were detected by western blotting and normalized for actin (**C**). Two-way ANOVA analyses revealed a significant effect of genotype [$F(1,28)=21.02$; $p<0.0001$] and SIRT3 OE [$F(1,28)=12.56$; $p=0.0014$] on PGC-1α levels. TFAM was immunostained using a specific antibody, in basal (**D**) or GFP and SIRT3-GFP transfected cells (**E**), considering 20-30 cells/condition from 3 independent experiments. A significant interaction was found between genotype and SIRT3 OE [$F(1,283)=4.593$; $p=0.0329$]. Confocal representative images of the graphical data are represented in **F**. Scale bar: 10 μm. Statistical significance: $^{tt}p<0.01$, $^{ttt}p<0.001$ by unpaired Student's t-test; $^{***}p<0.001$ *vs* Q7 GFP transfected cells, $^{\#}p<0.05$, $^{\#\#}p<0.01$ *vs* respective GFP transfected control by two-way ANOVA followed by Bonferroni post-hoc test.

5.4. DISCUSSION

SIRT3 regulates the global acetylation of mitochondrial proteins, and SIRT3-initiated metabolic adaptations may control mitochondrial function and oxidative stress-mediated cell death (Cheng et al., 2016; Lombard et al., 2007). Our findings provide evidence that SIRT3 mediates neuroprotective effects against mHtt-induced cell toxicity. We found that HD cells and cortical tissue from YAC128 transgenic mice show increased SIRT3 activity, most likely in response to high levels of oxidative damage (Hong et al., 2015; Ribeiro et al., 2013, 2014). Remarkably, increased expression of SIRT3 recovered $\Delta\psi_m$ and improved the protein levels of PGC-1α in ST*Hdh* cells, which regulates mitochondrial biogenesis and serves as transcription coactivator of TFAM, the guardian and transcription factor of mtDNA, which levels were also rescued in HD mutant striatal cells following SIRT3 OE. Moreover, stabilization of $\Delta\psi_m$ was associated with increased viability of SIRT3 OE ST*Hdh* clonal cells.

Several circumstances seem to regulate SIRT3 expression in CNS. Pharmacological interference with mitochondrial ETC using the complex III inhibitor antimycin A, which induces increased mitochondrial ROS levels, upregulates SIRT3 transcript expression in hippocampal neurons (Weir et al., 2012). Moreover, mitochondrial SIRT3 was reported to be increased in neurons where NAD^+ was depleted following NMDA stimuli (Kim et al., 2011b). In fact, striatal neuronal apoptosis is preferentially enhanced by NMDA receptor activation in transgenic HD neuronal models (Shehadeh et al., 2006; Zeron et al., 2002), and we previously showed that ST*Hdh*$^{Q111/Q111}$ cells exhibited increased cytosolic and mitochondrial ROS levels that were directly linked to apoptotic cell death activation (Ribeiro et al., 2013, 2014). Therefore, the observed increase in SIRT3 expression and activity in HD models can be assumed to act as a compensatory mechanism under stressed conditions evoked by expression of mutant huntingtin. Similar results were previously reported in other neurodegenerative models (Cieślik et al., 2015). Additionally, when overexpressed, SIRT3 exhibited a higher accumulation in mitochondria of ST*Hdh*$^{Q111/Q111}$ cells than wild-type counterparts. Under physiological conditions, SIRT3 not only localizes in the mitochondria, but also in the nucleus, where it can be transported to mitochondria upon DNA damage-mediated cellular stress (Scher et al., 2007), a commonly observed mechanism in HD models due to the excessive oxidant generation (Wang et al., 2013). Contrariwise, studies from Dr. Duan's laboratory reported no alterations in processed active SIRT3 isoform in ST*Hdh*$^{Q111/Q111}$ cells. Both isoforms were in fact significantly reduced in cells expressing mHtt following serum withdrawal for 24h, substantially affecting $\Delta\psi_m$ in both wild-type and mutant cells (Fu et al., 2012).

Although SIRT3 has been extensively studied in recent years, studies concerning its function on mitochondrial regulation in CNS are scarce. Recently, a well-designed study aimed to understand the role of SIRT3 in adaptive responses of neurons to metabolic and excitatory challenges. The authors found that neurons lacking SIRT3 exhibited increased vulnerability to excitotoxic, oxidative and metabolic stress induced by glutamate, H_2O_2 and 3-NP, respectively (Cheng et al., 2016). 3-NP, an irreversible mitochondrial complex II inhibitor, is classically used as a toxin-induced model for HD that produce striking similarities to the neuropathologic and neurochemical features of the disease on both rodents and primates (Beal et al., 1993). SIRT3 KO mice showed decreased survival after 7 days of 3-NP administration and rotarod performance was significantly impaired compared to wild-type mice. In addition, mitochondria isolated from SIRT3 KO mice cortex exhibited decreased levels of ATP, increased ROS and swelling associated with Ca^{2+} dehomeostasis (Cheng et al., 2016). Concordantly with these findings, we observed that SIRT3 OE reverted the susceptibility of mutant cells for transfection-induced toxicity, as well as ameliorated mitochondrial function by improving $\Delta\psi_m$. This electrochemical gradient across the membrane is sustained by correct transferring of electrons during OXPHOS. In clonal ST*Hdh*$^{Q111/Q111}$ cells mitochondrial respiration and ATP production are significantly reduced when either glutamate/malate or succinate, were used as substrates for complexes I and II, respectively (Milakovic and Johnson, 2005). Sustained expression of SIRT3 increases the expression of subunits of mitochondrial complexes such as cyt *c* oxidase subunit 2 (COX II) and 4 (COX IV), enhancing cellular respiration (Shi et al., 2005). In addition, two recent mass spectrometry assays identified several mitochondrial complexes subunits hyperacetylated in two or more Lys residues in SIRT3 KO mice, including complex I/NADH dehydrogenase 1α, 1β subcomplexes and flavoprotein 1, complex II/SDH flavoprotein and iron-sulfur subunits, and complex IV/cyt *c* oxidase subunits 4-7 (Hebert et al., 2013; Rardin et al., 2013). Although the present study was the first to evaluate the effect of SIRT3 OE in a genetic model of HD, a previous study screened a unique collection of naturally occurring resveratrol monomers and oligomers and semi-synthetic derivatives and found that trans-ε-viniferin preserved $\Delta\psi_m$ in a SIRT3-dependent manner in mHtt-expressing cells (Fu et al., 2012). ε-Viniferin increased SIRT3 and SOD2 deacetylated levels, scavenging ROS levels. Moreover, this resveratrol dimer also increased PGC-1α transcript in ST*Hdh*$^{Q111/Q111}$ cells (Fu et al., 2012). Previous evidence demonstrated that SIRT3 increased the content of mtDNA and the expression of mitochondrial biogenesis related transcription factors such as PGC-1α, NRF-1 and TFAM, in cortical neurons exposed to H_2O_2 (Dai et al., 2014). This may occur through

FOXO3a nuclear deacetylation by SIRT3 at K271/290 (Tseng et al., 2013). In fact, we observed that SIRT3 OE recovered PGC-1α and TFAM levels in mutant HD cells, corroborating the previous data that suggest that SIRT3 may have a relevant role in mitochondrial biogenesis in HD. Still, we failed to observe a rescue of mitochondrial mass and mtDNA content in ST*Hdh*$^{Q111/Q111}$ cells after SIRT3 OE. Notably, TFAM is not only important for mitochondrial replication, but it also plays a histone-like role in mitochondria, packaging, stabilizing and eventually protecting mtDNA pool (Kaufman et al., 2007; Ngo et al., 2014), a constant target of OXPHOS-generated ROS. Additionally, TFAM is deacetylated by SIRT3 at Lys107 (Rardin et al., 2013), whereas acetylation lowers its binding affinity to mtDNA (Hashemi Shabestari et al., 2016).

It is becoming increasingly clear that mitochondrial mass and mitochondrial morphology are mechanistically linked to mitochondrial function. Deregulation of PGC-1α-dependent biogenesis renders cells more susceptible to insults leading to mitochondrial fragmentation (Dabrowska et al., 2015). In turn, both PGC-1α and SIRT3 OE stimulate mitochondrial fusion events (Song et al., 2013). Conversely, depletion of $\Delta\psi_m$ is a triggering event for mitochondrial fission, recruiting Drp1 to constriction sites at the MOM (Bleazard et al., 1999). We have previously shown that more than half of the ST*Hdh*$^{Q111/Q111}$ cell population displayed mixed mitochondrial morphology. However, the remaining population was almost entirely composed of fragmented mitochondria, with a negligible percentage of tubular mitochondrial network, contrarily to wild-type cells (Carmo, 2015). Remarkably, SIRT3 OE restored mitochondrial morphology in HD striatal cells, leading to higher number of cells with tubular mitochondria. Decreased co-localization of Drp1 with mitochondria (Carmo, 2015) and the reestablishment of the $\Delta\psi_m$ observed in the present study may account for the elongation of mitochondrial network following SIRT3 OE. Moreover, SIRT3 is capable of deacetylating OPA1, a mitochondrial fusion protein, elevating its GTPase activity (Samant et al., 2014). Therefore, although no changes were observed in mitochondrial content, SIRT3 may mediate neuroprotection through regulation of mitochondrial dynamics, transcription and function in cells expressing mHtt.

CHAPTER VI

CONCLUSIONS AND PERSPECTIVES

HD is a complex genetic neurodegenerative disorder with many underlying dysfunctional pathways. KDACs are molecules with numerous cell targets that appear to have a relevant role in HD pathogenesis. In fact, the approaches used in the present study may seem paradoxical since strategies to promote both acetylation and deacetylation were used and, at some level, they all appeared to have a protective effect in HD-related pathology. Class I/IIa HDACi regulate gene expression mainly associated with changes in chromatin structure as a consequence of histone hyperacetylation, facilitating the access of transcriptional machinery to gene promoter; contrariwise, class III HDACs or SIRTs deacetylate proteins related with several pathways, from transcriptional factors to the subunits of mitochondrial ETC complexes, which can influence subsequent PTM. This complex network requires a thoroughly study about the molecular targets of each class or individual KDACs, so that we can fully understand their potential therapeutic effects.

Previously studies in our laboratory have shown that expression of FL mHtt was associated with deficits in mitochondrial-dependent Ca^{2+} handling that could be ameliorated following treatment with HDACi TSA and SB. Both inhibitors decreased the proportion of ST*Hdh* cells losing Ca^{2+} homeostasis after being challenged with either a Ca^{2+} ionophore or NMDA (Oliveira et al., 2006). Besides Ca^{2+} mishandling, we also showed that HD mitochondria exhibited diminished ATP production and increased oxidative stress, along with $\Delta\psi_m$ loss and activation of programmed cell death (Ferreira et al., 2010, 2011; Naia et al., 2015; Ribeiro et al., 2013, 2014). The decrease in energy production and metabolism were further linked to PDC dysfunction (Ferreira et al., 2011; Naia et al., 2016). In the first part of the work we explored deeper the regulation of this protein complex that links glycolysis to TCA cycle. We found that not only the most important catalytic subunit of the PDC, PDH E1α, was decreased, as the enzymes that regulate its phosphorylation/dephosphorylation, PDKs and PDPs, respectively, were also altered, causing a declined in PDC activity. Moreover, we showed that SB rescued PDC function by decreasing transcription of HIF-1α/PDK3 pathway, which led to improved mitochondrial respiratory capacity in striatal cells expressing mHtt (**Figure 6.1A**). PDK3 transcription repression also attenuated metabolic deficits in HD mice. In general, we unveiled a dysfunctional pathway that triggers metabolic deficits in HD, and can be ameliorated by HDACi.

We pursued the search for molecules that target transcription of mitochondrial-related genes. Several substrates were described to be activated or inhibited by SIRTs, which in turn are important for the functionality of vital cellular mechanisms, such as transcription regulation or energy production. In 2012, an outstanding research

coordinated by Dr. David Sinclair showed that RESV improves mitochondrial function and increases mitochondrial biogenesis in a SIRT1-dependent manner (Price et al., 2012). Interestingly, NAM, the amide form of vitamin B3 and a SIRT1 inhibitor, also had a positive effect on metabolism [e.g. (Liu et al., 2009)]. In fact, the role of Sir2/SIRT1 on HD neuroprotection has been controversial. It is puzzling how both activation and inhibition of a single enzyme (SIRT1) may lead to neuroprotection. SIRT1-dependent deacetylation can enhance the activity of specific protein targets and, at the same time, can repress local transcription, which is already severely affected in HD models. As an example, SIRT1 is capable of activating FOXO3a (Jiang et al., 2012), a pro-survival transcription factor, however it also deacetylates and inactivates the key chromatin-modifying complex p300/CBP (Bouras et al., 2005). Therefore, we proposed to better understand these mechanisms, in order to solidify the use of STACs as therapy for HD pathogenesis. We found that only RESV was able to improve mitochondrial biogenesis, while NAM treatment completely abolished mitochondrial-encoded gene transcription *in vivo*. *In vitr*o, NAM still showed protective effects, increasing NAD^+ levels and enhancing mitochondrial function, without interfering with mitochondrial biogenesis. Additionally, while some published studies in lower eukaryotes have previously shown that RESV is able to rescue mutant polyQ cytotoxicity, this was the first study showing that low doses of RESV completely recover motor coordination in a HD mouse model (**Figure 6.2B**).

Several studies, including the present work, have resorted to the use of pharmacological modulators that are not selective for a certain KDAC. Many of the effects of STACs (e.g. resveratrol) overlap with those triggered by SIRT1 overexpression; however these small molecules have been involved in several pathways. This multiple effect is not necessarily disadvantageous, provided that it only operates in deregulated pathways at pathological level, however it turns difficult to reconcile whether the observed effects are exclusively due to SIRT1 activation, despite the low dosage used. Moreover, small molecule inhibitors exhibit low potency and unattractive biopharmaceutical properties. In the same way, unselectively inhibition of HDACs elicits therapeutically responses, but can also show unexpected side effects. Therefore, widespread clinical use has still not been achieved. Considering the diversity of HDAC targets, temporal inhibition of individual HDACs may create more reliable results, as opposed to information gained from KO studies and thus, be more clinically useful. It is currently a challenge to develop strong and selective activators and inhibitors, as they would bring considerable benefits for the future therapeutic interventions in HD and other neurodegenerative diseases. Recent advances on the crystal structure of the catalytic core of HDACs and on specific binding modes of

inhibitory molecules have been made and offer valuable information for the design of novel targeting strategies (Maolanon et al., 2016). Synthetic SIRT1 activators are also a growing field [reviewed in (Hubbard and Sinclair, 2014). Nevertheless, modulators that target emerging KDACs, such as the case of mitochondrial SIRTs, remain largely unexplored.

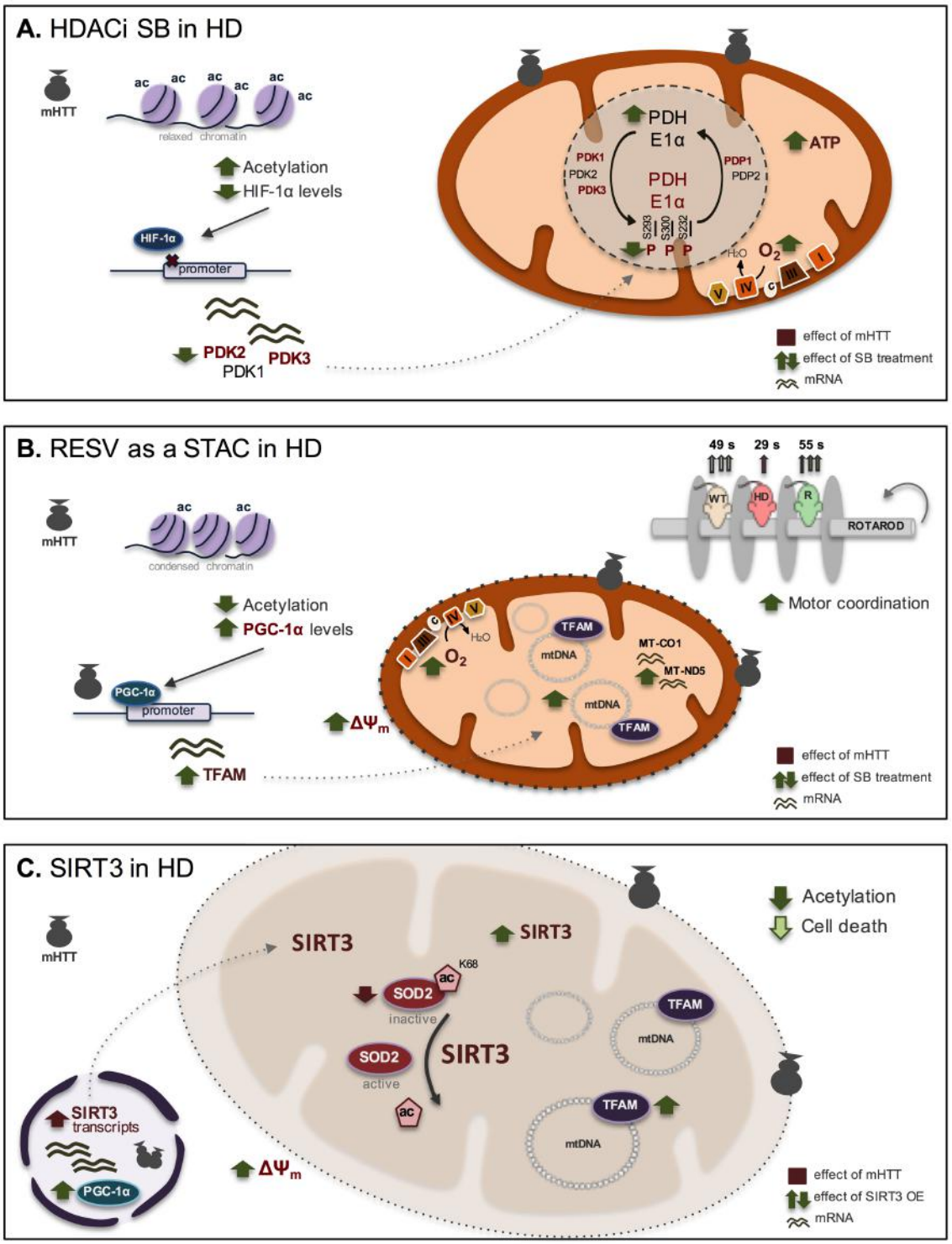

Figure 6.1 | Effects of KDACs modulation in HD pathogenesis. During the current work we showed that modulation of different lysine deacetylases isoforms are neuroprotective in models expressing FL-mHTT: **A**. SB is a HDAC class I and IIa inhibitor that was shown to significantly increase histone H3 acetylation. Increased nuclear acetylation was responsible for the decrease in HIF-1α levels, which when acetylated is degraded by proteasome and cannot longer serve as a transcription factor for glycolytic genes such as PDKs. Decreased PDK2 and PDK3 expression induced by SB treatment, prevented PDH phosphorylation, culminating in increased PDH activity, ATP production and respiration. **B**. RESV is a direct SIRT1 activator, therefore cellular supplementation of RESV decreased nuclear acetylation and increased protein levels of PGC-1α, a co-transcriptional factor that regulates the transcription of several mitochondrial proteins such as cyt *c* and mitochondrial transcriptional factor TFAM. Increased TFAM levels enhanced the expression of mtDNA-encoded genes that may help to restore general mitochondrial function, from $\Delta\psi_m$ to respiration. In HD mice, RESV supplementation for one month increased motor coordination to the levels of vehicle-treated wild-type mice. **C**. Increased oxidative stress in HD cells may favor SIRT3 transcription and activity, which in turn deacetylates and activates SOD2. SIRT3 overexpression (OE) decreased protein acetylation, influenced neuronal survival and enhanced mitochondrial-related transcription factors and $\Delta\psi_m$, a parameter of organelle functioning.

Despite the disadvantages, resveratrol and other potent synthetic STACs are currently in clinical trials mainly for type II diabetes, insulin resistance and metabolic syndrome, and are expected to provide critical information about the safety and efficacy of SIRT1 activation. Early positive data from such trials indicate that STACs can effectively treat metabolic diseases in patients (Tomé-Carneiro et al., 2013). Still, there is a need to further explore methods to optimize their bioavailability in humans. The first clinical trial using RESV in HD started last year and has as a main objective to evaluate the benefit of this compound on brain energy metabolism [ClinicalTrials.gov identifier: NCT02336633]. However, no results have been disclosed so far. Additionally, a phase II clinical trial (PHEND-HD) that enrolled 60 patients concluded that 15 g/day of PB is safe and well-tolerated in human HD [ClinicalTrials.gov identifier: NCT00212316; (Hogarth et al., 2007)]. In addition, early this year, another phase II/III clinical trial aimed to evaluate the efficacy of SB as a novel treatment for cognitive deficits in schizophrenia, however it did not pursue due to budget considerations [ClinicalTrials.gov identifier: NCT02654405].

Due to the issues associated with the use of STACs, we decided to further selectively target a mitochondrial sirtuin, by overexpressing SIRT3 in a HD cell model. SIRT3 is the new *saint grail* in aging processes, since it regulates mitochondrial ROS and cell death. Our first results point to a protective role of this mitochondrial SIRT on HD neuroprotection. As a whole, in our lab, we showed that SIRT3 OE reestablished mitochondrial biogenesis-related factors, transmembrane potential (**Figure 6.1C**) and

balance mitochondrial dynamics in HD striatal cells (Carmo, 2015) , essential features to maintain neuronal function and survival. Although the results obtained so far are satisfactory, signaling pathways regulated by SIRT3 in HD models need to be further addressed, as well as the effect of SIRT3 *in vivo*. Several hypotheses can be raised to explain our results. The classical explanation it that SIRT3 mainly acts as a ROS scavenging enzyme avoiding the opening of mPTP, which is sensitive to oxidizing agents, and consequent loss of $\Delta\psi_m$. SIRT3 was previously shown to deacetylate the regulatory component of the mPTP, CypD (on Lys166), increasing its affinity to cyclosporin A, a CypD inhibitor (Hafner et al., 2010). SIRT3 may also have a role on dynamics of mitochondria-associated membranes (MAMs), which are endoplasmic reticulum-mitochondria contact sites essential for fission and Ca^{2+} signaling. SIRT3 is known to deacetylate structural proteins at the MAMs, such as glucose-regulated protein 75 (Grp75) (Rardin et al., 2013); moreover Drp1, the fission inductor that we observed to be decreased in SIRT3 OE HD cells, can be recruited to the MAMs inducing mitochondrial fission. Additionally, in a quick search on Compendium of Protein Lysine Modification Database we found that both human and mouse Drp1 can the acetylated (Choudhary et al., 2009); therefore, protein interactions between SIRT3 and Drp1 are worth being studied. Despite the recent advances in this field, no SIRT3 selective pharmacological activators have been created or tested so far. ε-Viniferin showed neuroprotection that was dependent on SIRT3-induced LKB1 deacetylation (Fu et al., 2012), however either acetylation, cytosolic location and activity of this upstream AMPK kinase is also modulated by SIRT1 (Lan et al., 2008), which raises questions about the origin of the observed protective effects.

Taking into account all these therapeutic advances, we firmly believe that this study brings about new data that will help to build the KDACs puzzle in HD-related neurodegeneration.

CHAPTER VII

REFERENCES

Ahn, B.-H., Kim, H.-S., Song, S., Lee, I.H., Liu, J., Vassilopoulos, A., Deng, C.-X., and Finkel, T. (2008). A role for the mitochondrial deacetylase Sirt3 in regulating energy homeostasis. PNAS *105*, 14447–14452.

Albin, R., Reiner, A., Anderson, K.D., Dure, L.S., Handelin, B., Balfour, R., Whetsell, W.O., Penney, J.B., and Young, a B. (1992). Preferential loss of striato-external pallidal projection neurons in presymptomatic Huntington's disease. Ann. Neurol. *31*, 425–430.

Albin, R.L., Reiner, A., Anderson, K.D., Penney, J.B., and Young, A.B. (1990). Striatal and Nigral Neuron Subpopulations in Rgid Huntington ' s Disease : Implications for the Functional Anatomy of Chorea and Ihgidity-Ahnesia. Ann Neurol. *27*, 357–365.

Almeida, S., Sarmento-Ribeiro, A.B., Januário, C., Rego, A.C., and Oliveira, C.R. (2008). Evidence of apoptosis and mitochondrial abnormalities in peripheral blood cells of Huntington's disease patients. Biochem. Biophys. Res. Commun. *374*, 599–603.

Andreassen, O.A., Ferrante, R.J., Huang, H.M., Dedeoglu, A., Park, L., Ferrante, K.L., Kwon, J., Borchelt, D.R., Ross, C.A., Gibson, G.E., et al. (2001). Dichloroacetate exerts therapeutic effects in transgenic mouse models of Huntington's disease. Ann. Neurol. *50*, 112–117.

Andrew, S.E., Goldberg, Y.P., Kremer, B., Telenius, H., Theilmann, J., Adam, S., Starr, E., Squitieri, F., Lin, B., and Kalchman, M. a (1993). The relationship between trinucleotide (CAG) repeat length and clinical features of Huntington's disease. Nat. Genet. *4*, 398–403.

Antonini, A., Leenders, K.L., Spiegel, R., Meier, D., Vontobel, P., Weigell-Weber, M., Sanchez-Pernaute, R., De Yébenez, J.G., Boesiger, P., Weindl, A., et al. (1996). Striatal glucose metabolism and dopamine D2 receptor binding in asymptomatic gene carriers and patients with Huntington's disease. Brain *119*, 2085–2095.

Arenas, J., Campos, Y., Ribacoba, R., Martín, M. a, Rubio, J.C., Ablanedo, P., and Cabello, a (1998). Complex I defect in muscle from patients with Huntington's disease. Ann. Neurol. *43*, 397–400.

Arrasate, M., Mitra, S., Schweitzer, E.S., Segal, M.R., and Finkbeiner, S. (2004). Inclusion body formation reduces levels of mutant huntingtin and the risk of neuronal death. Nature *431*, 805–810.

Atwal, R.S., Xia, J., Pinchev, D., Taylor, J., Epand, R.M., and Truant, R. (2007). Huntingtin has a membrane association signal that can modulate huntingtin aggregation, nuclear entry and toxicity. Hum. Mol. Genet. *16*, 2600–2615.

Augood, S.J., Faull, R.L., Love, D.R., and Emson, P.C. (1996). Reduction in enkephalin and substance P messenger RNA in the striatum of early grade Huntington's disease: a detailed cellular in situ hybridization study. Neuroscience *72*, 1023–1036.

Avalos, J.L., Bever, K.M., and Wolberger, C. (2005). Mechanism of sirtuin inhibition by nicotinamide: altering the NAD(+) cosubstrate specificity of a Sir2 enzyme. Mol. Cell *17*, 855–868.

Barber, M.F., Michishita-Kioi, E., Xi, Y., Tasselli, L., Kioi, M., Moqtaderi, Z., Tennen, R.I., Paredes, S., Young, N.L., Chen, K., et al. (2012). SIRT7 links H3K18 deacetylation

to maintenance of oncogenic transformation. Nature *487*, 114–118.

Bardai, F.H., and D'Mello, S.R. (2011). Selective toxicity by HDAC3 in neurons: regulation by Akt and GSK3beta. J. Neurosci. *31*, 1746–1751.

Bardai, F.H., Price, V., Zaayman, M., Wang, L., and D'Mello, S.R. (2012). Histone deacetylase-1 (HDAC1) is a molecular switch between neuronal survival and death. J. Biol. Chem. *287*, 35444–35453.

Bardai, F.H., Verma, P., Smith, C., Rawat, V., Wang, L., and D'Mello, S.R. (2013). Disassociation of histone deacetylase-3 from normal huntingtin underlies mutant huntingtin neurotoxicity. J. Neurosci. *33*, 11833–11838.

Bates, G. (2003). Huntingtin aggregation and toxicity in Huntington's disease. Lancet (London, England) *361*, 1642–1644.

Bates, E.A., Victor, M., Jones, A.K., Shi, Y., and Hart, A.C. (2006). Differential contributions of Caenorhabditis elegans histone deacetylases to huntingtin polyglutamine toxicity. J. Neurosci. *26*, 2830–2838.

Bates, G.P., Dorsey, R., Gusella, J.F., Hayden, M.R., Kay, C., Leavitt, B.R., Nance, M., Ross, C. a., Scahill, R.I., Wetzel, R., et al. (2015). Huntington disease. Nat. Rev. Dis. Prim. 15005.

Baur, J.A., and Sinclair, D.A. (2006). Therapeutic potential of resveratrol: the in vivo evidence. Nat. Rev. Drug Discov. *5*, 493–506.

Baur, J.A., Pearson, K.J., Price, N.L., Jamieson, H.A., Lerin, C., Kalra, A., Prabhu, V. V, Allard, J.S., Lopez-Lluch, G., Lewis, K., et al. (2006). Resveratrol improves health and survival of mice on a high-calorie diet. Nature *444*, 337–342.

Beal, M.F., and Ferrante, R.J. (2004). Experimental therapeutics in transgenic mouse models of Huntington's disease. Nat. Rev. Neurosci. *5*, 373–384.

Beal, M.F., Brouillet, E., Jenkins, B.G., Ferrante, R.J., Kowall, N.W., Miller, J.M., Storey, E., Srivastava, R., Rosen, B.R., and Hyman, B.T. (1993). Neurochemical and histologic characterization of striatal excitotoxic lesions produced by the mitochondrial toxin 3-nitropropionic acid. J. Neurosci. *13*, 4181–4192.

Behal, R.H., Buxton, D.B., Robertson, J.G., and Olson, M.S. (1993). Regulation of the pyruvate dehydrogenase multienzyme complex. Annu. Rev. Nutr. *13*, 497–520.

Bell, E.L., and Guarente, L. (2011). The SirT3 Divining Rod Points to Oxidative Stress. Mol. Cell *42*, 561–568.

Benchoua, A., Trioulier, Y., Zala, D., Gaillard, M.C., Lefort, N., Dufour, N., Saudou, F., Elalouf, J.M., Hirsch, E., Hantraye, P., et al. (2006). Involvement of mitochondrial complex II defects in neuronal death produced by N-terminus fragment of mutated huntingtin. Mol Biol Cell *17*, 1652–1663.

Benn, C.L., Sun, T., Sadri-Vakili, G., McFarland, K.N., DiRocco, D.P., Yohrling, G.J., Clark, T.W., Bouzou, B., and Cha, J.-H.J. (2008). Huntingtin modulates transcription, occupies gene promoters in vivo, and binds directly to DNA in a polyglutamine-dependent manner. J. Neurosci. *28*, 10720–10733.

Berta, G.N., Salamone, P., Sprio, A.E., Di Scipio, F., Marinos, L.M., Sapino, S., Carlotti,

M.E., Cavalli, R., and Di Carlo, F. (2010). Chemoprevention of 7,12-dimethylbenz[a]anthracene (DMBA)-induced oral carcinogenesis in hamster cheek pouch by topical application of resveratrol complexed with 2-hydroxypropyl-beta-cyclodextrin. Oral Oncol. *46*, 42–48.

Bertrand, P. (2010). Inside HDAC with HDAC inhibitors. Eur. J. Med. Chem. *45*, 2095–2116.

Birsa, N., Norkett, R., Higgs, N., Lopez-Domenech, G., and Kittler, J.T. (2013). Mitochondrial trafficking in neurons and the role of the Miro family of GTPase proteins. Biochem. Soc. Trans. *41*, 1525–1531.

Bitterman, K.J., Anderson, R.M., Cohen, H.Y., Latorre-Esteves, M., and Sinclair, D.A. (2002). Inhibition of silencing and accelerated aging by nicotinamide, a putative negative regulator of yeast Sir2 and human SIRT1. J. Biol. Chem. *277*, 45099–45107.

Bleazard, W., McCaffery, J.M., King, E.J., Bale, S., Mozdy, A., Tieu, Q., Nunnari, J., and Shaw, J.M. (1999). The dynamin-related GTPase Dnm1 regulates mitochondrial fission in yeast. Nat. Cell Biol. *1*, 298–304.

Bobrowska, A., Paganetti, P., Matthias, P., and Bates, G.P. (2011). Hdac6 knock-out increases tubulin acetylation but does not modify disease progression in the R6/2 mouse model of Huntington's disease. PLoS One *6*, e20696.

Borovecki, F., Lovrecic, L., Zhou, J., Jeong, H., Then, F., Rosas, H.D., Hersch, S.M., Hogarth, P., Bouzou, B., Jensen, R. V, et al. (2005). Genome-wide expression profiling of human blood reveals biomarkers for Huntington's disease. Proc. Natl. Acad. Sci. U. S. A. *102*, 11023–11028.

Borra, M.T., Smith, B.C., and Denu, J.M. (2005). Mechanism of human SIRT1 activation by resveratrol. J. Biol. Chem. *280*, 17187–17195.

Bouras, T., Fu, M., Sauve, A.A., Wang, F., Quong, A.A., Perkins, N.D., Hay, R.T., Gu, W., and Pestell, R.G. (2005). SIRT1 deacetylation and repression of p300 involves lysine residues 1020/1024 within the cell cycle regulatory domain 1. J. Biol. Chem. *280*, 10264–10276.

Bowker-Kinley, M.M., Davis, W.I., Wu, P., Harris, R. A, and Popov, K.M. (1998). Evidence for existence of tissue-specific regulation of the mammalian pyruvate dehydrogenase complex. Biochem. J. *329 (Pt 1)*, 191–196.

Brandt, J., Strauss, M.E., Larus, J., Jensen, B., Folstein, S.E., and Folstein, M.F. (1984). Clinical correlates of dementia and disability in Huntington's disease. J Clin Neuropsychol *6*, 401–412.

Brett, A., Rosenstock, T., and Rego, A. (2014). Current Therapeutic Advances in Patients and Experimental Models of Huntington's Disease. Curr. Drug Targets *15*, 313–334.

Brouillet, E., Hantraye, P., Ferrante, R.J., Dolan, R., Leroy-Willig, a, Kowall, N.W., and Beal, M.F. (1995). Chronic mitochondrial energy impairment produces selective striatal degeneration and abnormal choreiform movements in primates. Proc. Natl. Acad. Sci. U. S. A. *92*, 7105–7109.

Brown, K., Xie, S., Qiu, X., Mohrin, M., Shin, J., Liu, Y., Zhang, D., Scadden, D.T., and Chen, D. (2013). SIRT3 reverses aging-associated degeneration. Cell Rep *3*, 319–327.

Brunelle, J.K., Bell, E.L., Quesada, N.M., Vercauteren, K., Tiranti, V., Zeviani, M., Scarpulla, R.C., and Chandel, N.S. (2005). Oxygen sensing requires mitochondrial ROS but not oxidative phosphorylation. Cell Metab. *1*, 409–414.

Brustovetsky, N., LaFrance, R., Purl, K.J., Brustovetsky, T., Keene, C.D., Low, W.C., and Dubinsky, J.M. (2005). Age-dependent changes in the calcium sensitivity of striatal mitochondria in mouse models of Huntington's disease. J. Neurochem. *93*, 1361–1370.

Burke, J.R., Enghild, J.J., Martin, M.E., Jou, Y.S., Myers, R.M., Roses, A.D., Vance, J.M., and Strittmatter, W.J. (1996). Huntingtin and DRPLA proteins selectively interact with the enzyme GAPDH. Nat. Med. *2*, 347–350.

Burnett, C., Valentini, S., Cabreiro, F., Goss, M., Somogyvári, M., Piper, M.D., Hoddinott, M., Sutphin, G.L., Leko, V., McElwee, J.J., et al. (2011). Absence of effects of Sir2 overexpression on lifespan in C. elegans and Drosophila. Nature *477*, 482–485.

Busch, A., Engemann, S., Lurz, R., Okazawa, H., Lehrach, H., and Wanker, E.E. (2003). Mutant huntingtin promotes the fibrillogenesis of wild-type huntingtin: a potential mechanism for loss of huntingtin function in Huntington's disease. J. Biol. Chem. *278*, 41452–41461.

Butterworth, J., Yates, C.M., and Reynolds, G.P. (1985). Distribution of phosphate-activated glutaminase, succinic dehydrogenase, pyruvate dehydrogenase and gamma-glutamyl transpeptidase in post-mortem brain from Huntington's disease and agonal cases. J. Neurol. Sci. *67*, 161–171.

Butterworth, N.J., Williams, L., Bullock, J.Y., Love, D.R., Faull, R.L., and Dragunow, M. (1998). Trinucleotide (CAG) repeat length is positively correlated with the degree of DNA fragmentation in Huntington's disease striatum. Neuroscience *87*, 49–53.

Cantó, C., Gerhart-Hines, Z., Feige, J.N., Lagouge, M., Noriega, L., Milne, J.C., Elliott, P.J., Puigserver, P., and Auwerx, J. (2009). AMPK regulates energy expenditure by modulating NAD+ metabolism and SIRT1 activity. Nature *458*, 1056–1060.

Carmo, C. (2015). Role of sirtuin 3 on mitochondrial dynamics in Huntington's disease striatal cells. Master Thesis in Molecular Genetics, presented to School of Health Sciences - University of Minho, Portugal. School of Health Sciences - University of Minho.

Caselli, R.J., Chen, K., Lee, W., Alexander, G.E., and Reiman, E.M. (2008). Correlating cerebral hypometabolism with future memory decline in subsequent converters to amnestic pre-mild cognitive impairment. Arch. Neurol. *65*, 1231–1236.

Cattaneo, E., Magrassi, L., Butti, G., Santi, L., Giavazzi, A., and Pezzotta, S. (1994). A short term analysis of the behaviour of conditionally immortalized neuronal progenitors and primary neuroepithelial cells implanted into the fetal rat brain. Brain Res. Dev. Brain Res. *83*, 197–208.

Cattaneo, E., Rigamonti, D., Goffredo, D., Zuccato, C., Squitieri, F., and Sipione, S. (2001). Loss of normal huntingtin function: new developments in Huntington's

disease research. Trends Neurosci. *24*, 182–188.

Caviston, J.P., and Holzbaur, E.L.F. (2009). Huntingtin as an essential integrator of intracellular vesicular trafficking. Trends Cell Biol. *19*, 147–155.

Cha, J.H., Kosinski, C.M., Kerner, J.A., Alsdorf, S.A., Mangiarini, L., Davies, S.W., Penney, J.B., Bates, G.P., and Young, A.B. (1998). Altered brain neurotransmitter receptors in transgenic mice expressing a portion of an abnormal human huntington disease gene. Proc. Natl. Acad. Sci. U. S. A. *95*, 6480–6485.

Chandel, N.S., Maltepe, E., Goldwasser, E., Mathieu, C.E., Simon, M.C., and Schumacker, P.T. (1998). Mitochondrial reactive oxygen species trigger hypoxia-induced transcription. Proc. Natl. Acad. Sci. U. S. A. *95*, 11715–11720.

Chang, H.-C., and Guarente, L. (2013). SIRT1 mediates central circadian control in the SCN by a mechanism that decays with aging. Cell *153*, 1448–1460.

Chaturvedi, R.K., and Beal, M.F. (2013). Mitochondrial diseases of the brain. Free Radic. Biol. Med. *63*, 1–29.

Chaturvedi, R.K., Adhihetty, P., Shukla, S., Hennessy, T., Calingasan, N., Yang, L., Starkov, A., Kiaei, M., Cannella, M., Sassone, J., et al. (2009). Impaired PGC-1alpha function in muscle in Huntington's disease. Hum. Mol. Genet. *18*, 3048–3065.

Chaturvedi, R.K., Calingasan, N.Y., Yang, L., Hennessey, T., Johri, A., and Beal, M.F. (2010). Impairment of PGC-1alpha expression, neuropathology and hepatic steatosis in a transgenic mouse model of Huntington's disease following chronic energy deprivation. Hum. Mol. Genet. *19*, 3190–3205.

Chen, L. (2011). Medicinal chemistry of sirtuin inhibitors. Curr. Med. Chem. *18*, 1936–1946.

Chen, H., and Chan, D.C. (2009). Mitochondrial dynamics-fusion, fission, movement, and mitophagy-in neurodegenerative diseases. Hum. Mol. Genet. *18*, 169–176.

Chen, Y., Zhang, J., Lin, Y., Lei, Q., Guan, K.-L., Zhao, S., and Xiong, Y. (2011). Tumour suppressor SIRT3 deacetylates and activates manganese superoxide dismutase to scavenge ROS. EMBO Rep. *12*, 534–541.

Chen, Y., Zhao, W., Yang, J.S., Cheng, Z., Luo, H., Lu, Z., Tan, M., Gu, W., and Zhao, Y. (2012). Quantitative acetylome analysis reveals the roles of SIRT1 in regulating diverse substrates and cellular pathways. Mol. Cell. Proteomics *11*, 1048–1062.

Cheng, A., Yang, Y., Zhou, Y., Maharana, C., Lu, D., Peng, W., Liu, Y., Wan, R., Marosi, K., Misiak, M., et al. (2016). Mitochondrial SIRT3 Mediates Adaptive Responses of Neurons to Exercise and Metabolic and Excitatory Challenges. Cell Metab. *23*, 128–142.

Chomyn, A., Lai, S.T., Shakeley, R., Bresolin, N., Scarlato, G., and Attardi, G. (1994). Platelet-mediated transformation of mtDNA-less human cells: analysis of phenotypic variability among clones from normal individuals--and complementation behavior of the tRNALys mutation causing myoclonic epilepsy and ragged red fibers. Am. J. Hum. Genet. *54*, 966–974.

Chong, Z.Z., Lin, S.H., Li, F., and Maiese, K. (2005). The sirtuin inhibitor nicotinamide

enhances neuronal cell survival during acute anoxic injury through AKT, BAD, PARP, and mitochondrial associated “anti-apoptotic” pathways. Curr Neurovasc Res *2*, 271–285.

Choo, Y.S., Johnson, G.V.W., MacDonald, M., Detloff, P.J., and Lesort, M. (2004). Mutant huntingtin directly increases susceptibility of mitochondria to the calcium-induced permeability transition and cytochrome c release. Hum. Mol. Genet. *13*, 1407–1420.

Choudhary, C., Kumar, C., Gnad, F., Nielsen, M.L., Rehman, M., Walther, T.C., Olsen, J. V., and Mann, M. (2009). Lysine Acetylation Targets Protein Complexes and Co-Regulates Major Cellular Functions. Science (80-.). *325*, 834–840.

Choudhary, C., Weinert, B.T., Nishida, Y., Verdin, E., and Mann, M. (2014). The growing landscape of lysine acetylation links metabolism and cell signalling. Nat. Rev. Mol. Cell Biol. *15*, 536–550.

Churchill, E.N., Murriel, C.L., Chen, C.-H., Mochly-Rosen, D., and Szweda, L.I. (2005). Reperfusion-induced translocation of deltaPKC to cardiac mitochondria prevents pyruvate dehydrogenase reactivation. Circ. Res. *97*, 78–85.

Ciammola, a, Sassone, J., Alberti, L., Meola, G., Mancinelli, E., Russo, M. a, Squitieri, F., and Silani, V. (2006). Increased apoptosis, Huntingtin inclusions and altered differentiation in muscle cell cultures from Huntington’s disease subjects. Cell Death Differ. *13*, 2068–2078.

Cicchetti, F., Lacroix, S., Cisbani, G., Vallières, N., Saint-Pierre, M., St-Amour, I., Tolouei, R., Skepper, J.N., Hauser, R.A., Mantovani, D., et al. (2014). Mutant huntingtin is present in neuronal grafts in Huntington disease patients. Ann. Neurol. *76*, 31–42.

Cieślik, M., Czapski, G.A., and Strosznajder, J.B. (2015). The Molecular Mechanism of Amyloid β42 Peptide Toxicity: The Role of Sphingosine Kinase-1 and Mitochondrial Sirtuins. PLoS One *10*, e0137193.

Claes, S., Van Zand, K., Legius, E., Dom, R., Malfroid, M., Baro, F., Godderis, J., and Cassiman, J.J. (1995). Correlations between triplet repeat expansion and clinical features in Huntington’s disease. Arch Neurol *52*, 749–753.

Cohen, A., Ross, L., Nachman, I., and Bar-Nun, S. (2012). Aggregation of PolyQ Proteins Is Increased upon Yeast Aging and Affected by Sir2 and Hsf1: Novel Quantitative Biochemical and Microscopic Assays. PLoS One *7*, 1–10.

Cong, S.-Y., Pepers, B.A., Evert, B.O., Rubinsztein, D.C., Roos, R.A.C., van Ommen, G.-J.B., and Dorsman, J.C. (2005). Mutant huntingtin represses CBP, but not p300, by binding and protein degradation. Mol. Cell. Neurosci. *30*, 12–23.

Cooper, A.J., Sheu, K.F., Burke, J.R., Onodera, O., Strittmatter, W.J., Roses, A.D., and Blass, J.P. (1998a). Inhibition of α-ketoglutarate-and pyruvate dehydrogenase complexes in E. coli by a glutathione S-transferase containing a pathological length poly-Q domain: A possible role of energy deficit in neurological diseases associated with poly-Q expansions? Age (Omaha). *21*, 25–30.

Cooper, J.K., Schilling, G., Peters, M.F., Herring, W.J., Sharp, A.H., Kaminsky, Z., Masone, J., Khan, F.A., Delanoy, M., Borchelt, D.R., et al. (1998b). Truncated N-

terminal fragments of huntingtin with expanded glutamine repeats form nuclear and cytoplasmic aggregates in cell culture. Hum. Mol. Genet. *7*, 783–790.

Costa, V., Giacomello, M., Hudec, R., Lopreiato, R., Ermak, G., Lim, D., Malorni, W., Davies, K.J.A., Carafoli, E., and Scorrano, L. (2010). Mitochondrial fission and cristae disruption increase the response of cell models of Huntington's disease to apoptotic stimuli. EMBO Mol. Med. *2*, 490–503.

Cui, L., Jeong, H., Borovecki, F., Parkhurst, C.N., Tanese, N., and Krainc, D. (2006). Transcriptional repression of PGC-1alpha by mutant huntingtin leads to mitochondrial dysfunction and neurodegeneration. Cell *127*, 59–69.

Cunha-Oliveira, T., Lusa, I., and Cristina, A. (2012). Consequences of Mitochondrial Dysfunction in Huntington's Disease and Protection via Phosphorylation Pathways. In Huntington's Disease - Core Concepts and Current Advances, (InTech), p.

Dabrowska, A., Venero, J.L., Iwasawa, R., Hankir, M.-K., Rahman, S., Boobis, A., and Hajji, N. (2015). PGC-1α controls mitochondrial biogenesis and dynamics in lead-induced neurotoxicity. Aging (Albany. NY). *7*, 629–647.

Dahl, H.H., Hunt, S.M., Hutchison, W.M., and Brown, G.K. (1987). The human pyruvate dehydrogenase complex. Isolation of cDNA clones for the E1 alpha subunit, sequence analysis, and characterization of the mRNA. J. Biol. Chem. *262*, 7398–7403.

Dai, S.-H., Chen, T., Wang, Y.-H., Zhu, J., Luo, P., Rao, W., Yang, Y.-F., Fei, Z., and Jiang, X.-F. (2014). Sirt3 protects cortical neurons against oxidative stress via regulating mitochondrial Ca2+ and mitochondrial biogenesis. Int. J. Mol. Sci. *15*, 14591–14609.

Daitoku, H., Sakamaki, J. ichi, and Fukamizu, A. (2011). Regulation of FoxO transcription factors by acetylation and protein-protein interactions. Biochim. Biophys. Acta - Mol. Cell Res. *1813*, 1954–1960.

Damiano, M., Galvan, L., Déglon, N., and Brouillet, E. (2010). Mitochondria in Huntington's disease. Biochim. Biophys. Acta - Mol. Basis Dis. *1802*, 52–61.

Davies, S.W., Turmaine, M., Cozens, B.A., DiFiglia, M., Sharp, A.H., Ross, C.A., Scherzinger, E., Wanker, E.E., Mangiarini, L., and Bates, G.P. (1997). Formation of neuronal intranuclear inclusions underlies the neurological dysfunction in mice transgenic for the HD mutation. Cell *90*, 537–548.

Deng, Y.P., Albin, R.L., Penney, J.B., Young, A.B., Anderson, K.D., and Reiner, A. (2004). Differential loss of striatal projection systems in Huntington's disease: A quantitative immunohistochemical study. J. Chem. Neuroanat. *27*, 143–164.

DiFiglia, M., Sapp, E., Chase, K., Schwarz, C., Meloni, A., Young, C., Martin, E., Vonsattel, J.P., Carraway, R., and Reeves, S.A. (1995). Huntingtin is a cytoplasmic protein associated with vesicles in human and rat brain neurons. Neuron *14*, 1075–1081.

DiFiglia, M., Sapp, E., Chase, K.O., Davies, S.W., Bates, G.P., Vonsattel, J.P., and Aronin, N. (1997). Aggregation of huntingtin in neuronal intranuclear inclusions and dystrophic neurites in brain. Science *277*, 1990–1993.

Dompierre, J.P., Godin, J.D., Charrin, B.C., Cordelières, F.P., King, S.J., Humbert, S., and Saudou, F. (2007). Histone deacetylase 6 inhibition compensates for the transport deficit in Huntington's disease by increasing tubulin acetylation. J. Neurosci. *27*, 3571–3583.

Donaldson, K.M., Li, W., Ching, K.A., Batalov, S., Tsai, C.-C., and Joazeiro, C.A.P. (2003). Ubiquitin-mediated sequestration of normal cellular proteins into polyglutamine aggregates. Proc. Natl. Acad. Sci. U. S. A. *100*, 8892–8897.

Donmez, G., and Outeiro, T.F. (2013). SIRT1 and SIRT2: Emerging targets in neurodegeneration. EMBO Mol. Med. *5*, 344–352.

Donmez, G., Wang, D., Cohen, D.E., and Guarente, L. (2010). SIRT1 suppresses beta-amyloid production by activating the alpha-secretase gene ADAM10. Cell *142*, 320–332.

Donmez, G., Arun, a., Chung, C.-Y., McLean, P.J., Lindquist, S., and Guarente, L. (2012). SIRT1 Protects against -Synuclein Aggregation by Activating Molecular Chaperones. J. Neurosci. *32*, 124–132.

Dragatsis, I., Levine, M.S., and Zeitlin, S. (2000). Inactivation of Hdh in the brain and testis results in progressive neurodegeneration and sterility in mice. Nat. Genet. *26*, 300–306.

Dröse, S., and Brandt, U. (2012). Molecular mechanisms of superoxide production by the mitochondrial respiratory chain. Adv. Exp. Med. Biol. *748*, 145–169.

Duarte, A.I., Santos, M.S., Oliveira, C.R., and Rego, A.C. (2005). Insulin neuroprotection against oxidative stress in cortical neurons - Involvement of uric acid and glutathione antioxidant defenses. Free Radic. Biol. Med. *39*, 876–889.

Duff, K., Paulsen, J.S., Beglinger, L.J., Langbehn, D.R., Wang, C., Stout, J.C., Ross, C.A., Aylward, E., Carlozzi, N.E., Queller, S., et al. (2010). "Frontal" behaviors before the diagnosis of Huntington's disease and their relationship to markers of disease progression: evidence of early lack of awareness. J Neuropsychiatry Clin Neurosci *22*, 196–207.

Dunah, A.W., Jeong, H., Griffin, A., Kim, Y.-M., Standaert, D.G., Hersch, S.M., Mouradian, M.M., Young, A.B., Tanese, N., and Krainc, D. (2002). Sp1 and TAFII130 transcriptional activity disrupted in early Huntington's disease. Science *296*, 2238–2243.

Duyao, M., Ambrose, C., Myers, R., Novelletto, A., Persichetti, F., Frontali, M., Folstein, S., Ross, C., Franz, M., and Abbott, M. (1993). Trinucleotide repeat length instability and age of onset in Huntington's disease. Nat. Genet. *4*, 387–392.

Duyao, M.P., Auerbach, A.B., Ryan, A., Persichetti, F., Barnes, G.T., McNeil, S.M., Ge, P., Vonsattel, J.P., Gusella, J.F., and Joyner, A.L. (1995). Inactivation of the mouse Huntington's disease gene homolog Hdh. Science *269*, 407–410.

Egorin, M.J., Yuan, Z.M., Sentz, D.L., Plaisance, K., and Eiseman, J.L. (1999). Plasma pharmacokinetics of butyrate after intravenous administration of sodium butyrate or oral administration of tributyrin or sodium butyrate to mice and rats. Cancer Chemother. Pharmacol. *43*, 445–453.

Ehrlich, M.E., Conti, L., Toselli, M., Taglietti, L., Fiorillo, E., Taglietti, V., Ivkovic, S., Guinea, B., Tranberg, A., Sipione, S., et al. (2001). ST14A Cells Have Properties of a Medium-Size Spiny Neuron. Exp. Neurol. *167*, 215–226.

Elias, S., Thion, M.S., Yu, H., Sousa, C.M., Lasgi, C., Morin, X., and Humbert, S. (2014). Huntingtin regulates mammary stem cell division and differentiation. Stem Cell Reports *2*, 491–506.

Evans, S.J.W., Douglas, I., Rawlins, M.D., Wexler, N.S., Tabrizi, S.J., and Smeeth, L. (2013). Prevalence of adult Huntington's disease in the UK based on diagnoses recorded in general practice records. J. Neurol. Neurosurg. Psychiatry *84*, 1156–1160.

Faber, P.W., Barnes, G.T., Srinidhi, J., Chen, J., Gusella, J.F., and MacDonald, M.E. (1998). Huntingtin interacts with a family of WW domain proteins. Hum. Mol. Genet. *7*, 1463–1474.

Fan, J., Shan, C., Kang, H.-B., Elf, S., Xie, J., Tucker, M., Gu, T.-L., Aguiar, M., Lonning, S., Chen, H., et al. (2014). Tyr phosphorylation of PDP1 toggles recruitment between ACAT1 and SIRT3 to regulate the pyruvate dehydrogenase complex. Mol. Cell *53*, 534–548.

Farrer, L. a, Cupples, L. a, Wiater, P., Conneally, P.M., Gusella, J.F., and Myers, R.H. (1993). The normal Huntington disease (HD) allele, or a closely linked gene, influences age at onset of HD. Am. J. Hum. Genet. *53*, 125–130.

Fath, D.M., Kong, X., Liang, D., Lin, Z., Chou, A., Jiang, Y., Fang, J., Caro, J., and Sang, N. (2006). Histone deacetylase inhibitors repress the transactivation potential of hypoxia-inducible factors independently of direct acetylation of HIF-alpha. J. Biol. Chem. *281*, 13612–13619.

Fernandes, H.B., Baimbridge, K.G., Church, J., Hayden, M.R., and Raymond, L. a (2007). Mitochondrial sensitivity and altered calcium handling underlie enhanced NMDA-induced apoptosis in YAC128 model of Huntington's disease. J. Neurosci. *27*, 13614–13623.

Ferrante, R.J., Kowall, N.W., Beal, M.F., Richardson, E.P., Bird, E.D., and Martin, J.B. (1985). Selective sparing of a class of striatal neurons in Huntington's disease. Science *230*, 561–563.

Ferrante, R.J., Kubilus, J.K., Lee, J., Ryu, H., Beesen, A., Zucker, B., Smith, K., Kowall, N.W., Ratan, R.R., Luthi-Carter, R., et al. (2003). Histone deacetylase inhibition by sodium butyrate chemotherapy ameliorates the neurodegenerative phenotype in Huntington's disease mice. J. Neurosci. *23*, 9418–9427.

Ferreira, I.L., Nascimento, M. V., Ribeiro, M., Almeida, S., Cardoso, S.M., Grazina, M., Pratas, J., Santos, M.J., Januário, C., Oliveira, C.R., et al. (2010). Mitochondrial-dependent apoptosis in Huntington's disease human cybrids. Exp. Neurol. *222*, 243–255.

Ferreira, I.L., Cunha-Oliveira, T., Nascimento, M. V., Ribeiro, M., Proença, M.T., Januário, C., Oliveira, C.R., and Rego, A.C. (2011). Bioenergetic dysfunction in Huntington's disease human cybrids. Exp. Neurol. *231*, 127–134.

Finley, L.W.S., Haas, W., Desquiret-Dumas, V., Wallace, D.C., Procaccio, V., Gygi, S.P.,

and Haigis, M.C. (2011). Succinate dehydrogenase is a direct target of sirtuin 3 deacetylase activity. PLoS One *6*.

Fischle, W., Dequiedt, F., Hendzel, M.J., Guenther, M.G., Lazar, M.A., Voelter, W., and Verdin, E. (2002). Enzymatic activity associated with class II HDACs is dependent on a multiprotein complex containing HDAC3 and SMRT/N-CoR. Mol. Cell *9*, 45–57.

Fisher, E.R., and Hayden, M.R. (2014). Multisource ascertainment of Huntington disease in Canada: prevalence and population at risk. Mov. Disord. *29*, 105–114.

Foroud, T., Gray, J., Ivashina, J., and Conneally, P.M. (1999). Differences in duration of Huntington's disease based on age at onset. J. Neurol. Neurosurg. Psychiatry *66*, 52–56.

Fouque, F., Brivet, M., Boutron, A., Vequaud, C., Marsac, C., Zabot, M.T., and Benelli, C. (2003). Differential effect of DCA treatment on the pyruvate dehydrogenase complex in patients with severe PDHC deficiency. Pediatr. Res. *53*, 793–799.

Frye, R. a (2000). Phylogenetic classification of prokaryotic and eukaryotic Sir2-like proteins. Biochem. Biophys. Res. Commun. *273*, 793–798.

Fu, J., Jin, J., Cichewicz, R.H., Hageman, S.A., Ellis, T.K., Xiang, L., Peng, Q., Jiang, M., Arbez, N., Hotaling, K., et al. (2012). trans-(-)-ε-Viniferin increases mitochondrial sirtuin 3 (SIRT3), activates AMP-activated protein kinase (AMPK), and protects cells in models of Huntington Disease. J. Biol. Chem. *287*, 24460–24472.

Fusco, F.R., Chen, Q., Lamoreaux, W.J., Figueredo-Cardenas, G., Jiao, Y., Coffman, J.A., Surmeier, D.J., Honig, M.G., Carlock, L.R., and Reiner, A. (1999). Cellular Localization of Huntingtin in Striatal and Cortical Neurons in Rats: Lack of Correlation with Neuronal Vulnerability in Huntington's Disease. J. Neurosci. *19*, 1189–1202.

Gafni, J., Papanikolaou, T., Degiacomo, F., Holcomb, J., Chen, S., Menalled, L., Kudwa, A., Fitzpatrick, J., Miller, S., Ramboz, S., et al. (2012). Caspase-6 activity in a BACHD mouse modulates steady-state levels of mutant huntingtin protein but is not necessary for production of a 586 amino acid proteolytic fragment. J. Neurosci. *32*, 7454–7465.

Galvan, L., André, V.M., Wang, E.A., Cepeda, C., and Levine, M.S. (2012). Functional Differences Between Direct and Indirect Striatal Output Pathways in Huntington's Disease. J. Huntingtons. Dis. *1*, 17–25.

Gauthier, L.R., Charrin, B.C., Borrell-Pagès, M., Dompierre, J.P., Rangone, H., Cordelières, F.P., De Mey, J., MacDonald, M.E., Lessmann, V., Humbert, S., et al. (2004). Huntingtin controls neurotrophic support and survival of neurons by enhancing BDNF vesicular transport along microtubules. Cell *118*, 127–138.

Gehm, B.D., McAndrews, J.M., Chien, P.Y., and Jameson, J.L. (1997). Resveratrol, a polyphenolic compound found in grapes and wine, is an agonist for the estrogen receptor. Proc. Natl. Acad. Sci. U. S. A. *94*, 14138–14143.

Genetic Modifiers of Huntington's Disease (GeM-HD) Consortium (2015). Identification of Genetic Factors that Modify Clinical Onset of Huntington's Disease. Cell *162*, 516–526.

Gerber, H.P., Seipel, K., Georgiev, O., Höfferer, M., Hug, M., Rusconi, S., and Schaffner, W. (1994). Transcriptional activation modulated by homopolymeric glutamine and proline stretches. Science *263*, 808–811.

Gerhart-Hines, Z., Rodgers, J.T., Bare, O., Lerin, C., Kim, S.-H., Mostoslavsky, R., Alt, F.W., Wu, Z., and Puigserver, P. (2007). Metabolic control of muscle mitochondrial function and fatty acid oxidation through SIRT1/PGC-1alpha. EMBO J. *26*, 1913–1923.

Ghosh, S., and Feany, M.B. (2004). Comparison of pathways controlling toxicity in the eye and brain in Drosophila models of human neurodegenerative diseases. Hum. Mol. Genet. *13*, 2011–2018.

Gil, J.M., and Rego, A.C. (2008). Mechanisms of neurodegeneration in Huntington's disease. Eur. J. Neurosci. *27*, 2803–2820.

Giralt, A., Puigdellívol, M., Carretón, O., Paoletti, P., Valero, J., Parra-Damas, A., Saura, C.A., Alberch, J., and Ginés, S. (2012). Long-term memory deficits in Huntington's disease are associated with reduced CBP histone acetylase activity. Hum. Mol. Genet. *21*, 1203–1216.

Gleyzer, N., Vercauteren, K., and Scarpulla, R.C. (2005). Control of mitochondrial transcription specificity factors (TFB1M and TFB2M) by nuclear respiratory factors (NRF-1 and NRF-2) and PGC-1 family coactivators. Mol. Cell. Biol. *25*, 1354–1366.

Goebel, H.H., Heipertz, R., Scholz, W., Iqbal, K., and Tellez-Nagel, I. (1978). Juvenile Huntington chorea: clinical, ultrastructural, and biochemical studies. Neurology *28*, 23–31.

Goffredo, D., Rigamonti, D., Tartari, M., De Micheli, A., Verderio, C., Matteoli, M., Zuccato, C., and Cattaneo, E. (2002). Calcium-dependent Cleavage of Endogenous Wild-type Huntingtin in Primary Cortical Neurons. J. Biol. Chem. *277*, 39594–39598.

Gräff, J., Kahn, M., Samiei, A., Gao, J., Ota, K.T., Rei, D., and Tsai, L.-H. (2013). A dietary regimen of caloric restriction or pharmacological activation of SIRT1 to delay the onset of neurodegeneration. J. Neurosci. *33*, 8951–8960.

Graham, R.K., Deng, Y., Slow, E.J., Haigh, B., Bissada, N., Lu, G., Pearson, J., Shehadeh, J., Bertram, L., Murphy, Z., et al. (2006). Cleavage at the caspase-6 site is required for neuronal dysfunction and degeneration due to mutant huntingtin. Cell *125*, 1179–1191.

Graham, R.K., Pouladi, M.A., Joshi, P., Lu, G., Deng, Y., Wu, N.-P., Figueroa, B.E., Metzler, M., André, V.M., Slow, E.J., et al. (2009). Differential susceptibility to excitotoxic stress in YAC128 mouse models of Huntington disease between initiation and progression of disease. J. Neurosci. *29*, 2193–2204.

Graham, R.K., Deng, Y., Carroll, J., Vaid, K., Cowan, C., Pouladi, M.A., Metzler, M., Bissada, N., Wang, L., Faull, R.L.M., et al. (2010). Cleavage at the 586 amino acid caspase-6 site in mutant huntingtin influences caspase-6 activation in vivo. J. Neurosci. *30*, 15019–15029.

Gray, M., Shirasaki, D.I., Cepeda, C., André, V.M., Wilburn, B., Lu, X.-H., Tao, J.,

Yamazaki, I., Li, S.-H., Sun, Y.E., et al. (2008). Full-length human mutant huntingtin with a stable polyglutamine repeat can elicit progressive and selective neuropathogenesis in BACHD mice. J. Neurosci. *28*, 6182–6195.

Grozinger, C.M., Chao, E.D., Blackwell, H.E., Moazed, D., and Schreiber, S.L. (2001). Identification of a Class of Small Molecule Inhibitors of the Sirtuin Family of NAD-dependent Deacetylases by Phenotypic Screening. J. Biol. Chem. *276*, 38837–38843.

Gu, M., Gash, M.T., Mann, V.M., Javoy-Agid, F., Cooper, J.M., and Schapira, A.H. V (1996). Mitochondrial defect in Huntington's disease caudate nucleus. Ann. Neurol. *39*, 385–389.

Guarente, L. (2011). Sirtuins, aging, and metabolism. Cold Spring Harb. Symp. Quant. Biol. *76*, 81–90.

Gudi, R., Bowker-Kinley, M.M., Kedishvili, N.Y., Zhao, Y., and Popov, K.M. (1995). Diversity of the pyruvate dehydrogenase kinase gene family in humans. J. Biol. Chem. *270*, 28989–28994.

Guedes-Dias, P., and Oliveira, J.M.A. (2013). Lysine deacetylases and mitochondrial dynamics in neurodegeneration. Biochim. Biophys. Acta - Mol. Basis Dis. *1832*, 1345–1359.

Guedes-Dias, P., de Proença, J., Soares, T.R., Leitão-Rocha, A., Pinho, B.R., Duchen, M.R., and Oliveira, J.M.A. (2015). HDAC6 inhibition induces mitochondrial fusion, autophagic flux and reduces diffuse mutant huntingtin in striatal neurons. Biochim. Biophys. Acta *1852*, 2484–2493.

Guidetti, P., Charles, V., Chen, E.Y., Reddy, P.H., Kordower, J.H., Whetsell, W.O., Schwarcz, R., and Tagle, D.A. (2001). Early degenerative changes in transgenic mice expressing mutant huntingtin involve dendritic abnormalities but no impairment of mitochondrial energy production. Exp. Neurol. *169*, 340–350.

Gusella, J.F., Wexler, N.S., Conneally, P.M., Naylor, S.L., Anderson, M. a, Tanzi, R.E., Watkins, P.C., Ottina, K., Wallace, M.R., and Sakaguchi, a Y. (1983). A polymorphic DNA marker genetically linked to Huntington's disease. Nature *306*, 234–238.

Hafner, A. V., Dai, J., Gomes, A.P., Xiao, C.-Y., Palmeira, C.M., Rosenzweig, A., and Sinclair, D.A. (2010). Regulation of the mPTP by SIRT3-mediated deacetylation of CypD at lysine 166 suppresses age-related cardiac hypertrophy. Aging (Albany. NY). *2*, 914–923.

Hallows, W.C., Albaugh, B.N., and Denu, J.M. (2008). Where in the cell is SIRT3?--functional localization of an NAD+-dependent protein deacetylase. Biochem. J. *411*, e11-3.

Hamilton, J., Pellman, J.J., Brustovetsky, T., Harris, R.A., and Brustovetsky, N. (2015). Oxidative metabolism in YAC128 mouse model of Huntington ' s disease. 1–47.

Hamilton, J., Pellman, J.J., Brustovetsky, T., Harris, R.A., and Brustovetsky, N. (2016). Oxidative metabolism and Ca2+ handling in isolated brain mitochondria and striatal neurons from R6/2 mice, a model of Huntington's disease. Hum. Mol. Genet. 1–51.

Hamilton, J.M., Wolfson, T., Peavy, G.M., Jacobson, M.W., and Corey-Bloom, J. (2004). Rate and correlates of weight change in Huntington's disease. J. Neurol. Neurosurg. Psychiatry *75*, 209–212.

Hankes, L. V, Coenen, H.H., Rota, E., Langen, K.J., Herzog, H., Wutz, W., Stoecklin, G., and Feinendegen, L.E. (1991). Effect of Huntington's and Alzheimer's diseases on the transport of nicotinic acid or nicotinamide across the human blood-brain barrier. Adv.Exp.Med.Biol. *294*, 675–678.

Harris, R.A., Huang, B., and Wu, P. (2001). Control of pyruvate dehydrogenase kinase gene expression. Adv. Enzyme Regul. *41*, 269–288.

Harris, R.A., Bowker-Kinley, M.M., Huang, B., and Wu, P. (2002). Regulation of the activity of the pyruvate dehydrogenase complex. In Advances in Enzyme Regulation, pp. 249–259.

Hashemi Shabestari, M., King, A., Roos, H., Suzuki, C., and Wuite, G. (2016). The Role of Phosphorylation and Acetylation of TFAM in DNA Binding Regulation using Single-Molecule Manipulation and Fluorescence Microscopy. In Biophysical Journal, p. 547a.

Hathorn, T., Snyder-Keller, A., and Messer, A. (2011). Nicotinamide improves motor deficits and upregulates PGC-1α and BDNF gene expression in a mouse model of Huntington's disease. Neurobiol. Dis. *41*, 43–50.

HD collaborative, and research group (1993). A novel gene containing a trinucleotide repeat that is expanded and unstable on Huntington's disease chromosomes. The Huntington's Disease Collaborative Research Group. Cell *72*, 971–983.

Hebert, A.S., Dittenhafer-Reed, K.E., Yu, W., Bailey, D.J., Selen, E.S., Boersma, M.D., Carson, J.J., Tonelli, M., Balloon, A.J., Higbee, A.J., et al. (2013). Calorie restriction and SirT3 trigger global reprogramming of the mitochondrial protein acetylome. Mol. Cell *49*, 186–199.

Heng, M.Y., Tallaksen-Greene, S.J., Detloff, P.J., and Albin, R.L. (2007). Longitudinal Evaluation of the Hdh(CAG)150 Knock-In Murine Model of Huntington's Disease. J. Neurosci. *27*, 8989–8998.

Heng, M.Y., Detloff, P.J., and Albin, R.L. (2008). Rodent genetic models of Huntington disease. Neurobiol. Dis. *32*, 1–9.

Henriksen, P., Wagner, S. a., Weinert, B.T., Sharma, S., Bacinskaja, G., Rehman, M., Juffer, a. H., Walther, T.C., Lisby, M., and Choudhary, C. (2012). Proteome-wide analysis of lysine acetylation suggests its broad regulatory scope in Saccharomyces cerevisiae. Mol. Cell. Proteomics 1510–1522.

Hermel, E., Gafni, J., Propp, S.S., Leavitt, B.R., Wellington, C.L., Young, J.E., Hackam, A.S., Logvinova, A. V, Peel, A.L., Chen, S.F., et al. (2004). Specific caspase interactions and amplification are involved in selective neuronal vulnerability in Huntington's disease. Cell Death Differ. *11*, 424–438.

Herranz, D., Muñoz-Martin, M., Cañamero, M., Mulero, F., Martinez-Pastor, B., Fernandez-Capetillo, O., and Serrano, M. (2010). Sirt1 improves healthy ageing and protects from metabolic syndrome-associated cancer. Nat. Commun. *1*, 3.

Hilditch-Maguire, P., Trettel, F., Passani, L.A., Auerbach, A., Persichetti, F., and MacDonald, M.E. (2000). Huntingtin: an iron-regulated protein essential for normal nuclear and perinuclear organelles. Hum. Mol. Genet. *9*, 2789–2797.

Hitosugi, T., Fan, J., Chung, T.-W., Lythgoe, K., Wang, X., Xie, J., Ge, Q., Gu, T.-L., Polakiewicz, R.D., Roesel, J.L., et al. (2011). Tyrosine phosphorylation of mitochondrial pyruvate dehydrogenase kinase 1 is important for cancer metabolism. Mol. Cell *44*, 864–877.

Ho, D.J., Calingasan, N.Y., Wille, E., Dumont, M., and Beal, M.F. (2010). Resveratrol protects against peripheral deficits in a mouse model of Huntington's disease. Exp. Neurol. *225*, 74–84.

Ho, L.W., Brown, R., Maxwell, M., Wyttenbach, A., and Rubinsztein, D.C. (2001). Wild type Huntingtin reduces the cellular toxicity of mutant Huntingtin in mammalian cell models of Huntington's disease. J. Med. Genet. *38*, 450–452.

Hockly, E., Richon, V.M., Woodman, B., Smith, D.L., Zhou, X., Rosa, E., Sathasivam, K., Ghazi-Noori, S., Mahal, A., Lowden, P.A.S., et al. (2003). Suberoylanilide hydroxamic acid, a histone deacetylase inhibitor, ameliorates motor deficits in a mouse model of Huntington's disease. Proc. Natl. Acad. Sci. U. S. A. *100*, 2041–2046.

Hodgson, J.G., Smith, D.J., McCutcheon, K., Koide, H.B., Nishiyama, K., Dinulos, M.B., Stevens, M.E., Bissada, N., Nasir, J., Kanazawa, I., et al. (1996). Human huntingtin derived from YAC transgenes compensates for loss of murine huntingtin by rescue of the embryonic lethal phenotype. Hum. Mol. Genet. *5*, 1875–1885.

Hodgson, J.G., Agopyan, N., Gutekunst, C.A., Leavitt, B.R., LePiane, F., Singaraja, R., Smith, D.J., Bissada, N., McCutcheon, K., Nasir, J., et al. (1999). A YAC mouse model for Huntington's disease with full-length mutant huntingtin, cytoplasmic toxicity, and selective striatal neurodegeneration. Neuron *23*, 181–192.

Hoffmann, E., Wald, J., Lavu, S., Roberts, J., Beaumont, C., Haddad, J., Elliott, P., Westphal, C., and Jacobson, E. (2013). Pharmacokinetics and tolerability of SRT2104, a first-in-class small molecule activator of SIRT1, after single and repeated oral administration in man. Br. J. Clin. Pharmacol. *75*, 186–196.

Hogarth, P., Lovrecic, L., and Krainc, D. (2007). Sodium phenylbutyrate in Huntington's disease: A dose-finding study. Mov. Disord. *22*, 1962–1964.

Hong, C., Seo, H., Kwak, M., Jeon, J., Jang, J., Jeong, E.M., Myeong, J., Hwang, Y.J., Ha, K., Kang, M.J., et al. (2015). Increased TRPC5 glutathionylation contributes to striatal neuron loss in Huntington's disease. Brain *138*, 3030–3047.

Howitz, K., Bitterman, J., and Cohen, H. (2003). Small molecule activators of sirtuins extend Saccharomyces cerevisiae lifespan. Nature *425*, 191–196.

del Hoyo, P., García-Redondo, A., de Bustos, F., Molina, J.A., Sayed, Y., Alonso-Navarro, H., Caballero, L., Arenas, J., and Jiménez-Jiménez, F.J. (2006). Oxidative stress in skin fibroblasts cultures of patients with Huntington's disease. Neurochem. Res. *31*, 1103–1109.

Hu, Y., Benedict, M.A., Ding, L., and Núñez, G. (1999). Role of cytochrome c and dATP/ATP hydrolysis in Apaf-1-mediated caspase-9 activation and apoptosis.

EMBO J. *18*, 3586–3595.

Huang, B., Gudi, R., Wu, P., Harris, R.A., Hamilton, J., and Popov, K.M. (1998). Isoenzymes of pyruvate dehydrogenase phosphatase. DNA-derived amino acid sequences, expression, and regulation. J. Biol. Chem. *273*, 17680–17688.

Hubbard, B.P., and Sinclair, D.A. (2014). Small molecule SIRT1 activators for the treatment of aging and age-related diseases. Trends Pharmacol. Sci. *35*, 146–154.

Hubbard, B.P., Gomes, A.P., Dai, H., Li, J., Case, A.W., Considine, T., Riera, T. V, Lee, J.E., E, S.Y., Lamming, D.W., et al. (2013). Evidence for a common mechanism of SIRT1 regulation by allosteric activators. Science *339*, 1216–1219.

Humbert, S., Bryson, E.A., Cordelières, F.P., Connors, N.C., Datta, S.R., Finkbeiner, S., Greenberg, M.E., and Saudou, F. (2002). The IGF-1/Akt pathway is neuroprotective in Huntington's disease and involves Huntingtin phosphorylation by Akt. Dev. Cell *2*, 831–837.

Iourgenko, V., Zhang, W., Mickanin, C., Daly, I., Jiang, C., Hexham, J.M., Orth, A.P., Miraglia, L., Meltzer, J., Garza, D., et al. (2003). Identification of a family of cAMP response element-binding protein coactivators by genome-scale functional analysis in mammalian cells. Proc. Natl. Acad. Sci. U. S. A. *100*, 12147–12152.

Ismailoglu, I., Chen, Q., Popowski, M., Yang, L., Gross, S.S., and Brivanlou, A.H. (2014). Huntingtin protein is essential for mitochondrial metabolism, bioenergetics and structure in murine embryonic stem cells. Dev. Biol. *391*, 230–240.

Iwahara, T., Bonasio, R., Narendra, V., and Reinberg, D. (2012). SIRT3 functions in the nucleus in the control of stress-related gene expression. Mol. Cell. Biol. *32*, 5022–5034.

Jackson, M.D., Schmidt, M.T., Oppenheimer, N.J., and Denu, J.M. (2003). Mechanism of Nicotinamide Inhibition and Transglycosidation by Sir2 Histone/Protein Deacetylases. J. Biol. Chem. *278*, 50985–50998.

Jacobsen, J.C., Gregory, G.C., Woda, J.M., Thompson, M.N., Coser, K.R., Murthy, V., Kohane, I.S., Gusella, J.F., Seong, I.S., MacDonald, M.E., et al. (2011). HD CAG-correlated gene expression changes support a simple dominant gain of function. Hum. Mol. Genet. *20*, 2846–2860.

Jenkins, B.G., Koroshetz, W.J., Beal, M.F., and Rosen, B.R. (1993). Evidence for impairment of energy metabolism in vivo in Huntington's disease using localized 1H NMR spectroscopy. Neurology *43*, 2689–2695.

Jenkins, B.G., Rosas, H.D., Chen, Y.-C.I., Makabe, T., Myers, R., MacDonald, M., Rosen, B.R., Beal, M.F., and Koroshetz, W.J. (1998). 1H NMR spectroscopy studies of Huntington's disease: Correlations with CAG repeat numbers. Neurology *50*, 1357–1365.

Jeong, H., Cohen, D.E., Cui, L., Supinski, a, Savas, J.N., Mazzulli, J.R., Yates 3rd, J.R., Bordone, L., Guarente, L., and Krainc, D. (2012a). Sirt1 mediates neuroprotection from mutant huntingtin by activation of the TORC1 and CREB transcriptional pathway. Nat Med *18*, 159–165.

Jeong, J.W., Bae, M.K., Ahn, M.Y., Kim, S.H., Sohn, T.K., Bae, M.H., Yoo, M.A., Song,

E.J., Lee, K.J., and Kim, K.W. (2002). Regulation and destabilization of HIF-1α by ARD1-mediated acetylation. Cell *111*, 709–720.

Jeong, J.Y., Jeoung, N.H., Park, K.-G., and Lee, I.-K. (2012b). Transcriptional regulation of pyruvate dehydrogenase kinase. Diabetes Metab. J. *36*, 328–335.

Jia, H., Pallos, J., Jacques, V., Lau, A., Tang, B., Cooper, A., Syed, A., Purcell, J., Chen, Y., Sharma, S., et al. (2012). Histone deacetylase (HDAC) inhibitors targeting HDAC3 and HDAC1 ameliorate polyglutamine-elicited phenotypes in model systems of Huntington's disease. Neurobiol. Dis. *46*, 351–361.

Jia, H., Morris, C.D., Williams, R.M., Loring, J.F., and Thomas, E. a. (2015). HDAC inhibition imparts beneficial transgenerational effects in Huntington's disease mice via altered DNA and histone methylation. Proc. Natl. Acad. Sci. *112*, E56–E64.

Jiang, M., Wang, J., Fu, J., Du, L., Jeong, H., West, T., Xiang, L., Peng, Q., Hou, Z., Cai, H., et al. (2012). Neuroprotective role of Sirt1 in mammalian models of Huntington's disease through activation of multiple Sirt1 targets. Nat. Med. *18*, 153–158.

Jiang, M., Zheng, J., Peng, Q., Hou, Z., Zhang, J., Mori, S., Ellis, J.L., Vlasuk, G.P., Fries, H., Suri, V., et al. (2014). Sirtuin 1 activator SRT2104 protects Huntington's disease mice. Ann. Clin. Transl. Neurol. *1*, 1047–1052.

Jin, L., Galonek, H., Israelian, K., Choy, W., Morrison, M., Xia, Y., Wang, X., Xu, Y., Yang, Y., Smith, J.J., et al. (2009). Biochemical characterization, localization, and tissue distribution of the longer form of mouse SIRT3. Protein Sci. *18*, 514–525.

Jin, Y.N., Yu, Y. V., Gundemir, S., Jo, C., Cui, M., Tieu, K., and Johnson, G.V.W. (2013). Impaired Mitochondrial Dynamics and Nrf2 Signaling Contribute to Compromised Responses to Oxidative Stress in Striatal Cells Expressing Full-Length Mutant Huntingtin. PLoS One *8*.

Jing, E., O'Neill, B.T., Rardin, M.J., Kleinridders, A., Ilkeyeva, O.R., Ussar, S., Bain, J.R., Lee, K.Y., Verdin, E.M., Newgard, C.B., et al. (2013). Sirt3 regulates metabolic flexibility of skeletal muscle through reversible enzymatic deacetylation. Diabetes *62*, 3404–3417.

Johri, A., and Beal, M.F. (2012). Antioxidants in Huntington's disease. Biochim. Biophys. Acta *1822*, 664–674.

Ju, T.-C., Chen, H.-M., Chen, Y.-C., Chang, C.-P., Chang, C., and Chern, Y. (2014). AMPK-α1 functions downstream of oxidative stress to mediate neuronal atrophy in Huntington's disease. Biochim. Biophys. Acta *1842*, 1668–1680.

Kaelin, W.G. (2005). ROS: Really involved in Oxygen Sensing. Cell Metab. *1*, 357–358.

Kaltenbach, L.S., Romero, E., Becklin, R.R., Chettier, R., Bell, R., Phansalkar, A., Strand, A., Torcassi, C., Savage, J., Hurlburt, A., et al. (2007). Huntingtin interacting proteins are genetic modifiers of neurodegeneration. PLoS Genet. *3*, 689–708.

Kang, K.W., Lee, S.J., and Kim, S.G. (2005). Molecular Mechanism of Nrf2 Activation by Oxidative Stress. Antioxid. Redox Signal. *7*, 1664–1673.

Karpova, T., Danchuk, S., Kolobova, E., and Popov, K.M. (2003). Characterization of the

isozymes of pyruvate dehydrogenase phosphatase: Implications for the regulation of pyruvate dehydrogenase activity. Biochim. Biophys. Acta - Proteins Proteomics *1652*, 126–135.

Kato, M., Chuang, J.L., Tso, S.-C., Wynn, R.M., and Chuang, D.T. (2005). Crystal structure of pyruvate dehydrogenase kinase 3 bound to lipoyl domain 2 of human pyruvate dehydrogenase complex. EMBO J. *24*, 1763–1774.

Kaufman, B.A., Durisic, N., Mativetsky, J.M., Costantino, S., Hancock, M.A., Grutter, P., and Shoubridge, E.A. (2007). The mitochondrial transcription factor TFAM coordinates the assembly of multiple DNA molecules into nucleoid-like structures. Mol. Biol. Cell *18*, 3225–3236.

Kawaguchi, Y., Wilson, C.J., and Emson, P.C. (1990). Projection subtypes of rat neostriatal matrix cells revealed by intracellular injection of biocytin. J. Neurosci. *10*, 3421–3438.

Kay, C., Collins, J.A., Miedzybrodzka, Z., Madore, S.J., Gordon, E.S., Gerry, N., Davidson, M., Slama, R.A., and Hayden, M.R. (2016). Huntington disease reduced penetrance alleles occur at high frequency in the general population. Neurology.

Kegel, K.B., Kim, M., Sapp, E., McIntyre, C., Castaño, J.G., Aronin, N., and DiFiglia, M. (2000). Huntingtin expression stimulates endosomal-lysosomal activity, endosome tubulation, and autophagy. J. Neurosci. *20*, 7268–7278.

Kieburtz, K., MacDonald, M., Shih, C., Feigin, A., Steinberg, K., Bordwell, K., Zimmerman, C., Srinidhi, J., Sotack, J., and Gusella, J. (1994). Trinucleotide repeat length and progression of illness in Huntington's disease. J. Med. Genet. *31*, 872–874.

Kiilerich, K., Adser, H., Jakobsen, A.H., Pedersen, P. a, Hardie, D.G., Wojtaszewski, J.F.P., and Pilegaard, H. (2010). PGC-1alpha increases PDH content but does not change acute PDH regulation in mouse skeletal muscle. Am. J. Physiol. Regul. Integr. Comp. Physiol. *299*, R1350–R1359.

Kim, G.W., and Chan, P.H. (2002). Involvement of superoxide in excitotoxicity and DNA fragmentation in striatal vulnerability in mice after treatment with the mitochondrial toxin, 3-nitropropionic acid. J. Cereb. Blood Flow Metab. *22*, 798–809.

Kim, D., Nguyen, M.D., Dobbin, M.M., Fischer, A., Sananbenesi, F., Rodgers, J.T., Delalle, I., Baur, J.A., Sui, G., Armour, S.M., et al. (2007a). SIRT1 deacetylase protects against neurodegeneration in models for Alzheimer's disease and amyotrophic lateral sclerosis. EMBO J. *26*, 3169–3179.

Kim, J., Moody, J.P., Edgerly, C.K., Bordiuk, O.L., Cormier, K., Smith, K., Flint Beal, M., and Ferrante, R.J. (2010). Mitochondrial loss, dysfunction and altered dynamics in Huntington's disease. Hum. Mol. Genet. *19*, 3919–3935.

Kim, J.W., Tchernyshyov, I., Semenza, G.L., and Dang, C. V. (2006). HIF-1-mediated expression of pyruvate dehydrogenase kinase: A metabolic switch required for cellular adaptation to hypoxia. Cell Metab. *3*, 177–185.

Kim, S.-H., Jeong, J.-W., Park, J.A., Lee, J.-W., Seo, J.H., Jung, B.-K., Bae, M.-K., and Kim, K.-W. (2007b). Regulation of the HIF-1 alpha stability by histone deacetylases. Oncol. Rep. *17*, 647–651.

Kim, S.H., Thomas, C.A., André, V.M., Cummings, D.M., Cepeda, C., Levine, M.S., and Ehrlich, M.E. (2011a). Forebrain striatal-specific expression of mutant huntingtin protein in vivo induces cell-autonomous age-dependent alterations in sensitivity to excitotoxicity and mitochondrial function. ASN Neuro *3*, e00060.

Kim, S.H., Lu, H.F., and Alano, C.C. (2011b). Neuronal sirt3 protects against excitotoxic injury in mouse cortical neuron culture. PLoS One *6*.

Kim, Y.J., Yi, Y., Sapp, E., Wang, Y., Cuiffo, B., Kegel, K.B., Qin, Z.-H., Aronin, N., and DiFiglia, M. (2001). Caspase 3-cleaved N-terminal fragments of wild-type and mutant huntingtin are present in normal and Huntington's disease brains, associate with membranes, and undergo calpain-dependent proteolysis. Proc. Natl. Acad. Sci. *98*, 12784–12789.

Kincaid, B., and Bossy-Wetzel, E. (2013). Forever young: SIRT3 a shield against mitochondrial meltdown, aging, and neurodegeneration. Front. Aging Neurosci. *5*, 1–13.

Klaidman, L., Morales, M., Kem, S., Yang, J., Chang, M.L., and Adams, J.D. (2003). Nicotinamide offers multiple protective mechanisms in stroke as a precursor for NAD+, as a PARP inhibitor and by partial restoration of mitochondrial function. Pharmacology *69*, 150–157.

Klivenyi, P., Starkov, A.A., Calingasan, N.Y., Gardian, G., Browne, S.E., Yang, L., Bubber, P., Gibson, G.E., Patel, M.S., and Beal, M.F. (2004). Mice deficient in dihydrolipoamide dehydrogenase show increased vulnerability to MPTP, malonate and 3-nitropropionic acid neurotoxicity. J Neurochem *88*, 1352–1360.

Knoepfler, P.S., and Eisenman, R.N. (1999). Sin meets NuRD and other tails of repression. Cell *99*, 447–450.

Kodsi, M.H., and Swerdlow, N.R. (1997). Mitochondrial toxin 3-nitropropionic acid produces startle reflex abnormalities and striatal damage in rats that model some features of Huntington's disease. Neurosci. Lett. *231*, 103–107.

Kolobova, E., Tuganova, A, Boulatnikov, I., and Popov, K.M. (2001). Regulation of pyruvate dehydrogenase activity through phosphorylation at multiple sites. Biochem. J. *358*, 69–77.

Kong, X., Lin, Z., Liang, D., Fath, D., Sang, N., and Caro, J. (2006). Histone deacetylase inhibitors induce VHL and ubiquitin-independent proteasomal degradation of hypoxia-inducible factor 1alpha. Mol. Cell. Biol. *26*, 2019–2028.

Kong, X., Wang, R., Xue, Y., Liu, X., Zhang, H., Chen, Y., Fang, F., and Chang, Y. (2010). Sirtuin 3, a new target of PGC-1alpha, plays an important role in the suppression of ROS and mitochondrial biogenesis. PLoS One *5*, e11707.

Konsoula, Z., and Barile, F.A. (2012). Epigenetic histone acetylation and deacetylation mechanisms in experimental models of neurodegenerative disorders. J. Pharmacol. Toxicol. Methods *66*, 215–220.

Koroshetz, W.J., Jenkins, B.G., Rosen, B.R., and Beal, M.F. (1997). Energy metabolism defects in Huntington's disease and effects of coenzyme Q10. Ann Neurol *41*, 160–165.

Korotchkina, L.G., and Patel, M.S. (1995). Mutagenesis studies of the phosphorylation sites of recombinant human pyruvate dehydrogenase. Site-specific regulation. J. Biol. Chem. *270*, 14297–14304.

Korotchkina, L.G., and Patel, M.S. (2001). Site specificity of four pyruvate dehydrogenase kinase isoenzymes toward the three phosphorylation sites of human pyruvate dehydrogenase. J. Biol. Chem. *276*, 37223–37229.

Kuemmerle, S., Gutekunst, C.A., Klein, A.M., Li, X.J., Li, S.H., Beal, M.F., Hersch, S.M., and Ferrante, R.J. (1999). Huntington aggregates may not predict neuronal death in Huntington's disease. Ann. Neurol. *46*, 842–849.

Kuhl, D.E., Phelps, M.E., Markham, C.H., Metter, E.J., Riege, W.H., and Winter, J. (1982). Cerebral metabolism and atrophy in Huntington's disease determined by 18FDG and computed tomographic scan. Ann. Neurol. *12*, 425–434.

Kuwert, T., Lange, H.W., Langen, K.J., Herzog, H., Aulich, A., and Feinendegen, L.E. (1989). Cerebral glucose consumption measured by PET in patients with and without psychiatric symptoms of Huntington's disease. Psychiatry Res. *29*, 361–362.

Labbadia, J., and Morimoto, R.I. (2013). Huntington's disease: underlying molecular mechanisms and emerging concepts. Trends Biochem. Sci. *38*, 378–385.

Lagouge, M., Argmann, C., Gerhart-Hines, Z., Meziane, H., Lerin, C., Daussin, F., Messadeq, N., Milne, J., Lambert, P., Elliott, P., et al. (2006). Resveratrol improves mitochondrial function and protects against metabolic disease by activating SIRT1 and PGC-1alpha. Cell *127*, 1109–1122.

Lan, F., Cacicedo, J.M., Ruderman, N., and Ido, Y. (2008). SIRT1 modulation of the acetylation status, cytosolic localization, and activity of LKB1. Possible role in AMP-activated protein kinase activation. J. Biol. Chem. *283*, 27628–27635.

Langbehn, D.R., Brinkman, R.R., Falush, D., Paulsen, J.S., and Hayden, M.R. (2004). A new model for prediction of the age of onset and penetrance for Huntington's disease based on CAG length. Clin. Genet. *65*, 267–277.

Lardenoije, R., Iatrou, A., Kenis, G., Kompotis, K., Steinbusch, H.W.M., Mastroeni, D., Coleman, P., Lemere, C.A., Hof, P.R., van den Hove, D.L.A., et al. (2015). The epigenetics of aging and neurodegeneration. Prog. Neurobiol. *131*, 21–64.

Laurent, G., German, N.J., Saha, A.K., de Boer, V.C.J., Davies, M., Koves, T.R., Dephoure, N., Fischer, F., Boanca, G., Vaitheesvaran, B., et al. (2013). SIRT4 coordinates the balance between lipid synthesis and catabolism by repressing malonyl CoA decarboxylase. Mol. Cell *50*, 686–698.

Lee, J., Gillis, T., Mysore, J.S., Ramos, E.M., Myers, R.H., Hayden, M.R., Morrison, P.J., Nance, M., Ross, C.A., Margolis, R.L., et al. (2012). Common SNP-Based Haplotype Analysis of the 4p16 . 3 Huntington Disease Gene Region. Am. J. Hum. Genet. *90*, 434–444.

Legros, F., Lombès, A., Frachon, P., and Rojo, M. (2002). Mitochondrial fusion in human cells is efficient, requires the inner membrane potential, and is mediated by mitofusins. Mol. Biol. Cell *13*, 4343–4354.

Leitman, J., Ulrich Hartl, F., and Lederkremer, G.Z. (2013). Soluble forms of polyQ-expanded huntingtin rather than large aggregates cause endoplasmic reticulum stress. Nat. Commun. *4*, 2753.

Li, H., Wyman, T., Yu, Z.X., Li, S.H., and Li, X.J. (2003). Abnormal association of mutant huntingtin with synaptic vesicles inhibits glutamate release. Hum. Mol. Genet. *12*, 2021–2030.

Li, S.H., Schilling, G., Young, W.S., Li, X.J., Margolis, R.L., Stine, O.C., Wagster, M. V, Abbott, M.H., Franz, M.L., and Ranen, N.G. (1993). Huntington's disease gene (IT15) is widely expressed in human and rat tissues. Neuron *11*, 985–993.

Li, S.H., Cheng, A.L., Li, H., and Li, X.J. (1999). Cellular defects and altered gene expression in PC12 cells stably expressing mutant huntingtin. J. Neurosci. *19*, 5159–5172.

Li, Y., Yokota, T., Gama, V., Yoshida, T., Gomez, J. a, Ishikawa, K., Sasaguri, H., Cohen, H.Y., Sinclair, D. a, Mizusawa, H., et al. (2007). Bax-inhibiting peptide protects cells from polyglutamine toxicity caused by Ku70 acetylation. Cell Death Differ. *14*, 2058–2067.

Lim, D., Fedrizzi, L., Tartari, M., Zuccato, C., Cattaneo, E., Brini, M., and Carafoli, E. (2008). Calcium homeostasis and mitochondrial dysfunction in striatal neurons of Huntington disease. J. Biol. Chem. *283*, 5780–5789.

Lin, C.H., Tallaksen-Greene, S., Chien, W.M., Cearley, J.A., Jackson, W.S., Crouse, A.B., Ren, S., Li, X.J., Albin, R.L., and Detloff, P.J. (2001). Neurological abnormalities in a knock-in mouse model of Huntington's disease. Hum. Mol. Genet. *10*, 137–144.

Lin, J., Wu, P.-H., Tarr, P.T., Lindenberg, K.S., St-Pierre, J., Zhang, C.-Y., Mootha, V.K., Jäger, S., Vianna, C.R., Reznick, R.M., et al. (2004). Defects in adaptive energy metabolism with CNS-linked hyperactivity in PGC-1alpha null mice. Cell *119*, 121–135.

Lin, S.-J., Kaeberlein, M., Andalis, A.A., Sturtz, L.A., Defossez, P.-A., Culotta, V.C., Fink, G.R., and Guarente, L. (2002). Calorie restriction extends Saccharomyces cerevisiae lifespan by increasing respiration. Nature *418*, 344–348.

Linn, T.C., Pettit, F.H., and Reed, L.J. (1969). Alpha-keto acid dehydrogenase complexes. X. Regulation of the activity of the pyruvate dehydrogenase complex from beef kidney mitochondria by phosphorylation and dephosphorylation. Proc. Natl. Acad. Sci. U. S. A. *62*, 234–241.

Van Lint, C., Emiliani, S., and Verdin, E. (1996). The expression of a small fraction of cellular genes is changed in response to histone hyperacetylation. Gene Expr. *5*, 245–253.

Liot, G., Bossy, B., Lubitz, S., Kushnareva, Y., Sejbuk, N., and Bossy-Wetzel, E. (2009). Complex II inhibition by 3-NP causes mitochondrial fragmentation and neuronal cell death via an NMDA- and ROS-dependent pathway. Cell Death Differ. *16*, 899–909.

Liszt, G., Ford, E., Kurtev, M., and Guarente, L. (2005). Mouse Sir2 homolog SIRT6 is a nuclear ADP-ribosyltransferase. J. Biol. Chem. *280*, 21313–21320.

Liu, D., Gharavi, R., Pitta, M., Gleichmann, M., and Mattson, M.P. (2009). Nicotinamide prevents NAD+ depletion and protects neurons against excitotoxicity and cerebral Ischemia: NAD+ consumption by sirt1 may endanger energetically compromised neurons. NeuroMolecular Med. *11*, 28–42.

Lodi, R., Schapira, A.H. V, Manners, D., Styles, P., Wood, N.W., Taylor, D.J., and Warner, T.T. (2000). Abnormal in vivo skeletal muscle energy metabolism in Huntington's disease and dentatorubropallidoluysian atrophy. Ann. Neurol. *48*, 72–76.

Lombard, D.B., Alt, F.W., Cheng, H.-L.H.-L., Bunkenborg, J., Streeper, R.S., Mostoslavsky, R., Kim, J., Yancopoulos, G., Valenzuela, D., Murphy, A., et al. (2007). Mammalian Sir2 homolog SIRT3 regulates global mitochondrial lysine acetylation. Mol. Cell. Biol. *27*, 8807–8814.

Lopes, C., Ribeiro, M., Duarte, A.I., Humbert, S., Saudou, F., Pereira de Almeida, L., Hayden, M., and Rego, A.C. (2014). IGF-1 Intranasal Administration Rescues Huntington's Disease Phenotypes in YAC128 Mice. Mol. Neurobiol. *49*, 1126–1142.

Lopes, C., Aubert, S., Bourgois-Rocha, F., Barnat, M., Rego, A.C., Déglon, N., Perrier, A.L., and Humbert, S. (2016). Dominant-Negative Effects of Adult-Onset Huntingtin Mutations Alter the Division of Human Embryonic Stem Cells-Derived Neural Cells. PLoS One *11*, e0148680.

Lopes Costa, A., Le bachelier, C., Mathieu, L., Rotig, A., Boneh, A., De lonlay, P., Tarnopolsky, M.A., Thorburn, D.R., Bastin, J., and Djouadi, F. (2014). Beneficial effects of resveratrol on respiratory chain defects in patients' fibroblasts involve estrogen receptor and estrogen-related receptor alpha signaling. Hum. Mol. Genet. *23*, 2106–2119.

Lu, C.W., Lin, S.C., Chen, K.F., Lai, Y.Y., and Tsai, S.J. (2008). Induction of pyruvate dehydrogenase kinase-3 by hypoxia-inducible factor-1 promotes metabolic switch and drug resistance. J. Biol. Chem. *283*, 28106–28114.

Luo, J., Nikolaev, A.Y., Imai, S., Chen, D., Su, F., Shiloh, A., Guarente, L., and Gu, W. (2001). Negative control of p53 by Sir2alpha promotes cell survival under stress. Cell *107*, 137–148.

Luthi-Carter, R., Strand, A., Peters, N.L., Solano, S.M., Hollingsworth, Z.R., Menon, A.S., Frey, A.S., Spektor, B.S., Penney, E.B., Schilling, G., et al. (2000). Decreased expression of striatal signaling genes in a mouse model of Huntington's disease. Hum. Mol. Genet. *9*, 1259–1271.

Luthi-Carter, R., Hanson, S. a, Strand, A.D., Bergstrom, D. a, Chun, W., Peters, N.L., Woods, A.M., Chan, E.Y., Kooperberg, C., Krainc, D., et al. (2002). Dysregulation of gene expression in the R6/2 model of polyglutamine disease: parallel changes in muscle and brain. Hum. Mol. Genet. *11*, 1911–1926.

Luthi-Carter, R., Taylor, D.M., Pallos, J., Lambert, E., Amore, A., Parker, A., Moffitt, H., Smith, D.L., Runne, H., Gokce, O., et al. (2010). SIRT2 inhibition achieves neuroprotection by decreasing sterol biosynthesis. Proc. Natl. Acad. Sci. U. S. A. *107*, 7927–7932.

MacDonald, M.E., Barnes, G., Srinidhi, J., Duyao, M.P., Ambrose, C.M., Myers, R.H., Gray, J., Conneally, P.M., Young, A., and Penney, J. (1993). Gametic but not somatic instability of CAG repeat length in Huntington's disease. J. Med. Genet. *30*, 982–986.

Madabushi, A., Hwang, B.-J., Jin, J., and Lu, A.-L. (2013). Histone deacetylase SIRT1 modulates and deacetylates DNA base excision repair enzyme thymine DNA glycosylase. Biochem. J. *456*, 89–98.

Mangiarini, L., Sathasivam, K., Seller, M., Cozens, B., Harper, A., Hetherington, C., Lawton, M., Trottier, Y., Lehrach, H., Davies, S.W., et al. (1996). Exon 1 of the HD gene with an expanded CAG repeat is sufficient to cause a progressive neurological phenotype in transgenic mice. Cell *87*, 493–506.

Mantamadiotis, T., Lemberger, T., Bleckmann, S.C., Kern, H., Kretz, O., Martin Villalba, A., Tronche, F., Kellendonk, C., Gau, D., Kapfhammer, J., et al. (2002). Disruption of CREB function in brain leads to neurodegeneration. Nat. Genet. *31*, 47–54.

Maolanon, A.R., Madsen, A.S., and Olsen, C.A. (2016). Innovative Strategies for Selective Inhibition of Histone Deacetylases. Cell Chem. Biol. *23*, 759–768.

Marks, P.A., and Breslow, R. (2007). Dimethyl sulfoxide to vorinostat: development of this histone deacetylase inhibitor as an anticancer drug. Nat. Biotechnol. *25*, 84–90.

Martin, W.R.W., Wieler, M., and Hanstock, C.C. (2007). Is brain lactate increased in Huntington's disease? J. Neurol. Sci. *263*, 70–74.

Masri, S., Patel, V.R., Eckel-Mahan, K.L., Peleg, S., Forne, I., Ladurner, A.G., Baldi, P., Imhof, A., and Sassone-Corsi, P. (2013). Circadian acetylome reveals regulation of mitochondrial metabolic pathways. Proc. Natl. Acad. Sci. *110*, 3339–3344.

Mathias, R.A., Greco, T.M., Oberstein, A., Budayeva, H.G., Chakrabarti, R., Rowland, E.A., Kang, Y., Shenk, T., and Cristea, I.M. (2014). Sirtuin 4 is a lipoamidase regulating pyruvate dehydrogenase complex activity. Cell *159*, 1615–1625.

Mattevi, A., Obmolova, G., Schulze, E., Kalk, K.H., Westphal, A.H., de Kok, A., and Hol, W.G. (1992). Atomic structure of the cubic core of the pyruvate dehydrogenase multienzyme complex. Science *255*, 1544–1550.

Mazziotta, J.C., Phelps, M.E., Pahl, J.J., Huang, S.C., Baxter, L.R., Riege, W.H., Hoffman, J.M., Kuhl, D.E., Lanto, A.B., Wapenski, J.A., et al. (1987). Reduced cerebral glucose metabolism in asymptomatic subjects at risk for Huntington's disease. N Engl J Med *316*, 357–362.

McFarland, K.N., Das, S., Sun, T.T., Leyfer, D., Xia, E., Sangrey, G.R., Kuhn, A., Luthi-Carter, R., Clark, T.W., Sadri-Vakili, G., et al. (2012). Genome-wide histone acetylation is altered in a transgenic mouse model of Huntington's disease. PLoS One *7*.

Menalled, L.B., Sison, J.D., Wu, Y., Olivieri, M., Li, X.-J., Li, H., Zeitlin, S., and Chesselet, M.-F. (2002). Early motor dysfunction and striosomal distribution of huntingtin microaggregates in Huntington's disease knock-in mice. J. Neurosci. *22*, 8266–8276.

Menalled, L.B., Sison, J.D., Dragatsis, I., Zeitlin, S., and Chesselet, M.-F. (2003). Time course of early motor and neuropathological anomalies in a knock-in mouse model of Huntington's disease with 140 CAG repeats. J. Comp. Neurol. *465*, 11–26.

Mercken, E.M., Mitchell, S.J., Martin-Montalvo, A., Minor, R.K., Almeida, M., Gomes, A.P., Scheibye-Knudsen, M., Palacios, H.H., Licata, J.J., Zhang, Y., et al. (2014). SRT2104 extends survival of male mice on a standard diet and preserves bone and muscle mass. Aging Cell *13*, 787–796.

Mielcarek, M., Benn, C.L., Franklin, S.A., Smith, D.L., Woodman, B., Marks, P.A., and Bates, G.P. (2011). SAHA decreases HDAC 2 and 4 levels in vivo and improves molecular phenotypes in the R6/2 mouse model of Huntington's disease. PLoS One *6*, e27746.

Mielcarek, M., Landles, C., Weiss, A., Bradaia, A., Seredenina, T., Inuabasi, L., Osborne, G.F., Wadel, K., Touller, C., Butler, R., et al. (2013). HDAC4 reduction: a novel therapeutic strategy to target cytoplasmic huntingtin and ameliorate neurodegeneration. PLoS Biol. *11*, e1001717.

Milakovic, T., and Johnson, G.V.W. (2005). Mitochondrial respiration and ATP production are significantly impaired in striatal cells expressing mutant huntingtin. J. Biol. Chem. *280*, 30773–30782.

Milakovic, T., Quintanilla, R.A., and Johnson, G.V.W. (2006). Mutant Huntingtin expression induces mitochondrial calcium handling defects in clonal striatal cells: Functional consequences. J. Biol. Chem. *281*, 34785–34795.

Milne, J.C., Lambert, P.D., Schenk, S., Carney, D.P., Smith, J.J., Gagne, D.J., Jin, L., Boss, O., Perni, R.B., Vu, C.B., et al. (2007). Small molecule activators of SIRT1 as therapeutics for the treatment of type 2 diabetes. Nature *450*, 712–716.

Mitsui, K., Nakayama, H., Akagi, T., Nekooki, M., Ohtawa, K., Takio, K., Hashikawa, T., and Nukina, N. (2002). Purification of polyglutamine aggregates and identification of elongation factor-1alpha and heat shock protein 84 as aggregate-interacting proteins. J. Neurosci. *22*, 9267–9277.

Mo, C., Hannan, A.J., and Renoir, T. (2015). Environmental factors as modulators of neurodegeneration: Insights from gene-environment interactions in Huntington's disease. Neurosci. Biobehav. Rev. *52*, 178–192.

Mochel, F., and Haller, R.G. (2011). Energy deficit in Huntington disease: Why it matters. J. Clin. Invest. *121*, 493–499.

Mochel, F., N'Guyen, T.M., Deelchand, D., Rinaldi, D., Valabregue, R., Wary, C., Carlier, P.G., Durr, A., and Henry, P.G. (2012a). Abnormal response to cortical activation in early stages of Huntington disease. Mov. Disord. *27*, 907–910.

Mochel, F., Durant, B., Meng, X., O'Callaghan, J., Yu, H., Brouillet, E., Wheeler, V.C., Humbert, S., Schiffmann, R., and Durr, A. (2012b). Early alterations of brain cellular energy homeostasis in huntington disease models. J. Biol. Chem. *287*, 1361–1370.

Moffitt, H., McPhail, G.D., Woodman, B., Hobbs, C., and Bates, G.P. (2009). Formation of Polyglutamine Inclusions in a Wide Range of Non-CNS Tissues in the HdhQ150 Knock-In Mouse Model of Huntington's Disease. PLoS One *4*, e8025.

Monoi, H., Futaki, S., Kugimiya, S., Minakata, H., and Yoshihara, K. (2000). Poly-L-glutamine forms cation channels: relevance to the pathogenesis of the polyglutamine diseases. Biophys. J. *78*, 2892–2899.

Moreno, C.L., Ehrlich, M.E., and Mobbs, C. V (2016). Protection by dietary restriction in the YAC128 mouse model of Huntington's disease: Relation to genes regulating histone acetylation and HTT. Neurobiol. Dis. *85*, 25–34.

Morrison, P.J. (2012). Prevalence estimates of Huntington disease in Caucasian populations are gross underestimates. Mov. Disord. *27*, 1707–1708.

Morten, K.J., Caky, M., and Matthews, P.M. (1998). Stabilization of the pyruvate dehydrogenase E1alpha subunit by dichloroacetate. Neurology *51*, 1331–1335.

Morton, A.J., Lagan, M.A., Skepper, J.N., and Dunnett, S.B. (2000). Progressive formation of inclusions in the striatum and hippocampus of mice transgenic for the human Huntington's disease mutation. J. Neurocytol. *29*, 679–702.

Moumné, L., Campbell, K., Howland, D., Ouyang, Y., and Bates, G.P. (2012). Genetic knock-down of HDAC3 does not modify disease-related phenotypes in a mouse model of Huntington's disease. PLoS One *7*, e31080.

Movafagh, S., Crook, S., and Vo, K. (2015). Regulation of hypoxia-inducible Factor-1a by reactive oxygen species: New developments in an old debate. J. Cell. Biochem. *116*, 696–703.

Myers, R.H. (2004). Huntington's disease genetics. NeuroRx *1*, 255–262.

Naga, K.K., Sullivan, P.G., and Geddes, J.W. (2007). High cyclophilin D content of synaptic mitochondria results in increased vulnerability to permeability transition. J. Neurosci. *27*, 7469–7475.

Naia, L., and Rego, A.C. (2015). Sirtuins: double players in Huntington's disease. Biochim. Biophys. Acta - Mol. Basis Dis. *1852*, 2183–2194.

Naia, L., Ribeiro, M.J., and Rego, A.C. (2011). Mitochondrial and metabolic-based protective strategies in Huntington's disease: The case of creatine and coenzyme Q. Rev. Neurosci. *23*, 13–28.

Naia, L., Ferreira, I.L., Cunha-Oliveira, T., Duarte, A.I., Ribeiro, M., Rosenstock, T.R., Laço, M.N., Ribeiro, M.J., Oliveira, C.R., Saudou, F., et al. (2015). Activation of IGF-1 and Insulin Signaling Pathways Ameliorate Mitochondrial Function and Energy Metabolism in Huntington's Disease Human Lymphoblasts. Mol. Neurobiol. *51*, 331–348.

Naia, L., Ribeiro, M., Rodrigues, J., Duarte, A.I., Lopes, C., Rosenstock, T.R., Hayden, M.R., and Rego, A.C. (2016). Insulin and IGF-1 regularize energy metabolites in neural cells expressing full-length mutant huntingtin. Neuropeptides 1–9.

Nakagawa, T., Lomb, D.J., Haigis, M.C., and Guarente, L. (2009). SIRT5 Deacetylates Carbamoyl Phosphate Synthetase 1 and Regulates the Urea Cycle. Cell *137*, 560–570.

Nakahata, Y., Kaluzova, M., Grimaldi, B., Sahar, S., Hirayama, J., Chen, D., Guarente, L.P., and Sassone-Corsi, P. (2008). The NAD+-Dependent Deacetylase SIRT1 Modulates CLOCK-Mediated Chromatin Remodeling and Circadian Control. Cell

134, 329–340.

Napoli, E., Wong, S., Hung, C., Ross-Inta, C., Bomdica, P., and Giulivi, C. (2013). Defective mitochondrial disulfide relay system, altered mitochondrial morphology and function in Huntington's disease. Hum. Mol. Genet. *22*, 989–1004.

Nath, S., Munsie, L.N., and Truant, R. (2015). A huntingtin-mediated fast stress response halting endosomal trafficking is defective in Huntington's disease. Hum. Mol. Genet. *24*, 450–462.

Nemoto, S., Fergusson, M.M., and Finkel, T. (2005). SIRT1 functionally interacts with the metabolic regulator and transcriptional coactivator PGC-1{alpha}. J. Biol. Chem. *280*, 16456–16460.

Ngo, H.B., Lovely, G.A., Phillips, R., and Chan, D.C. (2014). Distinct structural features of TFAM drive mitochondrial DNA packaging versus transcriptional activation. Nat. Commun. *5*, 3077.

Nicholls, D.G., and Ward, M.W. (2000). Mitochondrial membrane potential and neuronal glutamate excitotoxicity: mortality and millivolts. Trends Neurosci. *23*, 166–174.

Nishino, T.G., Miyazaki, M., Hoshino, H., Miwa, Y., Horinouchi, S., and Yoshida, M. (2008). 14-3-3 regulates the nuclear import of class IIa histone deacetylases. Biochem. Biophys. Res. Commun. *377*, 852–856.

Nogueiras, R., Habegger, K.M., Chaudhary, N., Finan, B., Banks, A.S., Dietrich, M.O., Horvath, T.L., Sinclair, D.A., Pfluger, P.T., and Tschop, M.H. (2012). Sirtuin 1 and sirtuin 3: physiological modulators of metabolism. Physiol Rev *92*, 1479–1514.

Noriega, L.G., Feige, J.N., Canto, C., Yamamoto, H., Yu, J., Herman, M. a, Mataki, C., Kahn, B.B., and Auwerx, J. (2011). CREB and ChREBP oppositely regulate SIRT1 expression in response to energy availability. EMBO Rep. *12*, 1069–1076.

Nucifora, F.C., Sasaki, M., Peters, M.F., Huang, H., Cooper, J.K., Yamada, M., Takahashi, H., Tsuji, S., Troncoso, J., Dawson, V.L., et al. (2001). Interference by huntingtin and atrophin-1 with cbp-mediated transcription leading to cellular toxicity. Science *291*, 2423–2428.

Okazawa, H. (2003). Polyglutamine diseases: A transcription disorder? Cell. Mol. Life Sci. *60*, 1427–1439.

Oliveira, J.M.A., Chen, S., Almeida, S., Riley, R., Gonçalves, J., Oliveira, C.R., Hayden, M.R., Nicholls, D.G., Ellerby, L.M., and Rego, A.C. (2006). Mitochondrial-dependent Ca2+ handling in Huntington's disease striatal cells: effect of histone deacetylase inhibitors. J. Neurosci. *26*, 11174–11186.

Oliveira, J.M.A., Jekabsons, M.B., Chen, S., Lin, A., Rego, A.C., Gonçalves, J., Ellerby, L.M., and Nicholls, D.G. (2007). Mitochondrial dysfunction in Huntington's disease: The bioenergetics of isolated and in situ mitochondria from transgenic mice. J. Neurochem. *101*, 241–249.

Onyango, P., Celic, I., McCaffery, J.M., Boeke, J.D., and Feinberg, A.P. (2002). SIRT3, a human SIR2 homologue, is an NAD- dependent deacetylase localized to mitochondria. Proc. Natl. Acad. Sci. *99*, 13653–13658.

Orr, A.L., Li, S., Wang, C.-E., Li, H., Wang, J., Rong, J., Xu, X., Mastroberardino, P.G.,

Greenamyre, J.T., and Li, X.-J. (2008). N-terminal mutant huntingtin associates with mitochondria and impairs mitochondrial trafficking. J. Neurosci. *28*, 2783–2792.

Pacholec, M., Bleasdale, J.E., Chrunyk, B., Cunningham, D., Flynn, D., Garofalo, R.S., Griffith, D., Griffor, M., Loulakis, P., Pabst, B., et al. (2010). SRT1720, SRT2183, SRT1460, and resveratrol are not direct activators of SIRT1. J. Biol. Chem. *285*, 8340–8351.

Palidwor, G.A., Shcherbinin, S., Huska, M.R., Rasko, T., Stelzl, U., Arumughan, A., Foulle, R., Porras, P., Sanchez-Pulido, L., Wanker, E.E., et al. (2009). Detection of alpha-rod protein repeats using a neural network and application to huntingtin. PLoS Comput. Biol. *5*.

Pallos, J., Bodai, L., Lukacsovich, T., Purcell, J.M., Steffan, J.S., Thompson, L.M., and Marsh, J.L. (2008). Inhibition of specific HDACs and sirtuins suppresses pathogenesis in a Drosophila model of Huntington's disease. Hum. Mol. Genet. *17*, 3767–3775.

Palo, J., Somer, H., Ikonen, E., Karila, L., and Peltonen, L. (1987). Low prevalence of Huntington's disease in Finland. Lancet (London, England) *2*, 805–806.

Panov, A. V, Gutekunst, C.A., Leavitt, B.R., Hayden, M.R., Burke, J.R., Strittmatter, W.J., and Greenamyre, J.T. (2002). Early mitochondrial calcium defects in Huntington's disease are a direct effect of polyglutamines. Nat Neurosci *5*, 731–736.

Panov, A. V, Burke, J.R., Strittmatter, W.J., and Greenamyre, J.T. (2003). In vitro effects of polyglutamine tracts on Ca2+-dependent depolarization of rat and human mitochondria: relevance to Huntington's disease. Arch. Biochem. Biophys. *410*, 1–6.

Di Paola, M., and Lorusso, M. (2006). Interaction of free fatty acids with mitochondria: Coupling, uncoupling and permeability transition. Biochim. Biophys. Acta - Bioenerg. *1757*, 1330–1337.

Papandreou, I., Cairns, R.A., Fontana, L., Lim, A.L., and Denko, N.C. (2006). HIF-1 mediates adaptation to hypoxia by actively downregulating mitochondrial oxygen consumption. Cell Metab. *3*, 187–197.

Park, J., Chen, Y., Tishkoff, D.X., Peng, C., Tan, M., Dai, L., Xie, Z., Zhang, Y., Zwaans, B.M.M., Skinner, M.E., et al. (2013). SIRT5-mediated lysine desuccinylation impacts diverse metabolic pathways. Mol. Cell *50*, 919–930.

Parker, J.A., Arango, M., Abderrahmane, S., Lambert, E., Tourette, C., Catoire, H., and Néri, C. (2005). Resveratrol rescues mutant polyglutamine cytotoxicity in nematode and mammalian neurons. Nat. Genet. *37*, 349–350.

Parker, W.D., Boyson, S.J., Luder, A.S., and Parks, J.K. (1990). Evidence for a defect in NADH: ubiquinone oxidoreductase (complex I) in Huntington's disease. Neurology *40*, 1231–1234.

Patel, M.S., and Korotchkina, L.G. (2001). Regulation of mammalian pyruvate dehydrogenase complex by phosphorylation: complexity of multiple phosphorylation sites and kinases. Exp. Mol. Med. *33*, 191–197.

Patel, M.S., and Korotchkina, L.G. (2006). Regulation of the pyruvate dehydrogenase complex. Biochem. Soc. Trans. *34*, 217–222.

Patel, M.S., and Roche, T.E. (1990). Molecular biology and biochemistry of pyruvate dehydrogenase complexes. FASEB J. *4*, 3224–3233.

Patel, M.S., Nemeria, N.S., Furey, W., and Jordan, F. (2014). The pyruvate dehydrogenase complexes: structure-based function and regulation. J. Biol. Chem. *289*, 16615–16623.

Paulsen, J.S., Nehl, C., Hoth, K.F., Kanz, J.E., Benjamin, M., Conybeare, R., McDowell, B., and Turner, B. (2005). Depression and stages of Huntington's disease. J. Neuropsychiatry Clin. Neurosci. *17*, 496–502.

Pearson, C.E. (2003). Slipping while sleeping? Trinucleotide repeat expansions in germ cells. Trends Mol. Med. *9*, 490–495.

Pearson, K.J., Baur, J.A., Lewis, K.N., Peshkin, L., Price, N.L., Labinskyy, N., Swindell, W.R., Kamara, D., Minor, R.K., Perez, E., et al. (2008). Resveratrol Delays Age-Related Deterioration and Mimics Transcriptional Aspects of Dietary Restriction without Extending Life Span. Cell Metab. *8*, 157–168.

Pecho-Vrieseling, E., Rieker, C., Fuchs, S., Bleckmann, D., Esposito, M.S., Botta, P., Goldstein, C., Bernhard, M., Galimberti, I., Müller, M., et al. (2014). Transneuronal propagation of mutant huntingtin contributes to non-cell autonomous pathology in neurons. Nat. Neurosci. *17*, 1064–1072.

Peled, T., Shoham, H., Aschengrau, D., Yackoubov, D., Frei, G., Rosenheimer G, N., Lerrer, B., Cohen, H.Y., Nagler, A., Fibach, E., et al. (2012). Nicotinamide, a SIRT1 inhibitor, inhibits differentiation and facilitates expansion of hematopoietic progenitor cells with enhanced bone marrow homing and engraftment. Exp. Hematol. *40*.

Pellman, J.J., Hamilton, J., Brustovetsky, T., and Brustovetsky, N. (2015). Ca 2+ handling in isolated brain mitochondria and cultured neurons derived from the YAC128 mouse model of Huntington's disease. J. Neurochem. *134*, 652–667.

Pérez-Severiano, F., Santamaría, A., Pedraza-Chaverri, J., Medina-Campos, O.N., Ríos, C., and Segovia, J. (2004). Increased formation of reactive oxygen species, but no changes in glutathione peroxidase activity, in striata of mice transgenic for the Huntington's disease mutation. Neurochem. Res. *29*, 729–733.

Perluigi, M., Poon, H.F., Maragos, W., Pierce, W.M., Klein, J.B., Calabrese, V., Cini, C., De Marco, C., and Butterfield, D.A. (2005). Proteomic analysis of protein expression and oxidative modification in r6/2 transgenic mice: a model of Huntington disease. Mol. Cell. Proteomics *4*, 1849–1861.

Portera-Cailliau, C., Hedreen, J.C., Price, D.L., and Koliatsos, V.E. (1995). Evidence for apoptotic cell death in Huntington disease and excitotoxic animal models. J. Neurosci. *15*, 3775–3787.

Powers, W.J., Videen, T.O., Markham, J., McGee-Minnich, L., Antenor-Dorsey, J. V, Hershey, T., and Perlmutter, J.S. (2007). Selective defect of in vivo glycolysis in early Huntington's disease striatum. Proc. Natl. Acad. Sci. *104*, 2945–2949.

Prasad, N., Topping, R.S., Zhou, D., and Decker, S.J. (2000). Oxidative stress and vanadate induce tyrosine phosphorylation of phosphoinositide-dependent kinase 1 (PDK1). Biochemistry *39*, 6929–6935.

Price, N.L., Gomes, A.P., Ling, A.J.Y., Duarte, F. V., Martin-Montalvo, A., North, B.J., Agarwal, B., Ye, L., Ramadori, G., Teodoro, J.S., et al. (2012). SIRT1 is required for AMPK activation and the beneficial effects of resveratrol on mitochondrial function. Cell Metab. *15*, 675–690.

Prigione, A., Rohwer, N., Hoffmann, S., Mlody, B., Drews, K., Bukowiecki, R., Blümlein, K., Wanker, E.E., Ralser, M., Cramer, T., et al. (2014). HIF1α modulates cell fate reprogramming through early glycolytic shift and upregulation of PDK1-3 and PKM2. Stem Cells *32*, 364–376.

Probst, A. V, Dunleavy, E., and Almouzni, G. (2009). Epigenetic inheritance during the cell cycle. Nat. Rev. Mol. Cell Biol. *10*, 192–206.

Project, T.U.S. –Venezuel. C.R., and Wexler, N.S. (2004). Venezuelan kindreds reveal that genetic and environmental factors modulate Huntington's disease age of onset. Proc. Natl. Acad. Sci. United States Am. *101*, 3498–3503.

Pruitt, K., Zinn, R.L., Ohm, J.E., McGarvey, K.M., Kang, S.H.L., Watkins, D.N., Herman, J.G., and Baylin, S.B. (2006). Inhibition of SIRT1 reactivates silenced cancer genes without loss of promoter DNA hypermethylation. PLoS Genet. *2*, 0344–0352.

Punnett, R.C. (1908). Mendelian inheritance in man. Proc. R. Soc. Med. 135–168.

Puranam, K.L., Wu, G., Strittmatter, W.J., and Burke, J.R. (2006). Polyglutamine expansion inhibits respiration by increasing reactive oxygen species in isolated mitochondria. Biochem. Biophys. Res. Commun. *341*, 607–613.

Qiu, X., Brown, K., Hirschey, M.D., Verdin, E., and Chen, D. (2010). Calorie restriction reduces oxidative stress by SIRT3-mediated SOD2 activation. Cell Metab. *12*, 662–667.

Quarrell, O.W.J., Nance, M.A., Nopoulos, P., Paulsen, J.S., Smith, J.A., and Squitieri, F. (2013). Managing juvenile Huntington's disease. Neurodegener. Dis. Manag. *3*, 267–276.

Quintanilla, R. a, Jin, Y.N., von Bernhardi, R., and Johnson, G.V.W. (2013). Mitochondrial permeability transition pore induces mitochondria injury in Huntington disease. Mol. Neurodegener. *8*, 45.

Quinti, L., Chopra, V., Rotili, D., Valente, S., Amore, A., Franci, G., Meade, S., Valenza, M., Altucci, L., Maxwell, M.M., et al. (2010). Evaluation of histone deacetylases as drug targets in Huntington's disease models. Study of HDACs in brain tissues from R6/2 and CAG140 knock-in HD mouse models and human patients and in a neuronal HD cell model. PLoS Curr. *2*.

Van Raamsdonk, J.M. (2005). Cognitive Dysfunction Precedes Neuropathology and Motor Abnormalities in the YAC128 Mouse Model of Huntington's Disease. J. Neurosci. *25*, 4169–4180.

Van Raamsdonk, J.M., Pearson, J., Slow, E.J., Hossain, S.M., Leavitt, B.R., and

Hayden, M.R. (2005a). Cognitive dysfunction precedes neuropathology and motor abnormalities in the YAC128 mouse model of Huntington's disease. J. Neurosci. *25*, 4169–4180.

Van Raamsdonk, J.M., Murphy, Z., Slow, E.J., Leavitt, B.R., and Hayden, M.R. (2005b). Selective degeneration and nuclear localization of mutant huntingtin in the YAC128 mouse model of Huntington disease. Hum. Mol. Genet. *14*, 3823–3835.

Van Raamsdonk, J.M., Gibson, W.T., Pearson, J., Murphy, Z., Lu, G., Leavitt, B.R., and Hayden, M.R. (2006). Body weight is modulated by levels of full-length huntingtin. Hum. Mol. Genet. *15*, 1513–1523.

Van Raamsdonk, J.M., Metzler, M., Slow, E., Pearson, J., Schwab, C., Carroll, J., Graham, R.K., Leavitt, B.R., and Hayden, M.R. (2007a). Phenotypic abnormalities in the YAC128 mouse model of Huntington disease are penetrant on multiple genetic backgrounds and modulated by strain. Neurobiol. Dis. *26*, 189–200.

Van Raamsdonk, J.M., Warby, S.C., and Hayden, M.R. (2007b). Selective degeneration in YAC mouse models of Huntington disease. Brain Res. Bull. *72*, 124–131.

Ragot, A., Pietropaolo, S., Vincent, J., Delage, P., Zhang, H., Allinquant, B., Leinekugel, X., Fischer, A., and Cho, Y.H. (2015). Genetic deletion of the Histone Deacetylase 6 exacerbates selected behavioral deficits in the R6/1 mouse model for Huntington's disease. Brain Behav. *5*, e00361.

Rahman, M., Nirala, N.K., Singh, A., Zhu, L.J., Taguchi, K., Bamba, T., Fukusaki, E., Shaw, L.M., Lambright, D.G., Acharya, J.K., et al. (2014). Drosophila Sirt2/mammalian SIRT3 deacetylates ATP synthase β and regulates complex V activity. J. Cell Biol. *206*, 289–305.

Ramadori, G., Fujikawa, T., Anderson, J., Berglund, E.D., Frazao, R., Michán, S., Vianna, C.R., Sinclair, D.A., Elias, C.F., and Coppari, R. (2011). SIRT1 deacetylase in SF1 neurons protects against metabolic imbalance. Cell Metab. *14*, 301–312.

Ranen, N.G., Stine, O.C., Abbott, M.H., Sherr, M., Codori, A.M., Franz, M.L., Chao, N.I., Chung, A.S., Pleasant, N., and Callahan, C. (1995). Anticipation and instability of IT-15 (CAG)n repeats in parent-offspring pairs with Huntington disease. Am. J. Hum. Genet. *57*, 593–602.

Rardin, M.J., Wiley, S.E., Naviaux, R.K., Murphy, A.N., and Dixon, J.E. (2009). Monitoring phosphorylation of the pyruvate dehydrogenase complex. Anal. Biochem. *389*, 157–164.

Rardin, M.J., Newman, J.C., Held, J.M., Cusack, M.P., Sorensen, D.J., Li, B., Schilling, B., Mooney, S.D., Kahn, C.R., Verdin, E., et al. (2013). Label-free quantitative proteomics of the lysine acetylome in mitochondria identifies substrates of SIRT3 in metabolic pathways. Proc. Natl. Acad. Sci. *110*, 6601–6606.

Ratovitski, T., Chighladze, E., Arbez, N., Boronina, T., Herbrich, S., Cole, R.N., and Ross, C.A. (2012). Huntingtin protein interactions altered by polyglutamine expansion as determined by quantitative proteomic analysis. Cell Cycle *11*, 2006–2021.

Rawlins, M.D., Wexler, N.S., Wexler, A.R., Tabrizi, S.J., Douglas, I., Evans, S.J.W., and

Smeeth, L. (2016). The prevalence of huntington's disease. Neuroepidemiology *46*, 144–153.

Reddy, P.H., Williams, M., Charles, V., Garrett, L., Pike-Buchanan, L., Whetsell, W.O., Miller, G., and Tagle, D.A. (1998). Behavioural abnormalities and selective neuronal loss in HD transgenic mice expressing mutated full-length HD cDNA. Nat. Genet. *20*, 198–202.

Reddy, P.H., Williams, M., and Tagle, D.A. (1999a). Recent advances in understanding the pathogenesis of Huntington's disease. Trends Neurosci. *22*, 248–255.

Reddy, P.H., Charles, V., Williams, M., Miller, G., Whetsell, W.O., and Tagle, D.A. (1999b). Transgenic mice expressing mutated full-length HD cDNA: a paradigm for locomotor changes and selective neuronal loss in Huntington's disease. Philos. Trans. R. Soc. Lond. B. Biol. Sci. *354*, 1035–1045.

Rego, A.C., Vesce, S., and Nicholls, D.G. (2001). The mechanism of mitochondrial membrane potential retention following release of cytochrome c in apoptotic GT1-7 neural cells. Cell Death Differ. *8*, 995–1003.

Reiner, A., Dragatsis, I., and Dietrich, P. (2011). Genetics and neuropathology of Huntington's disease. Int. Rev. Neurobiol. *98*, 325–372.

Ribeiro, M., Rosenstock, T.R., Cunha-Oliveira, T., Ferreira, I.L., Oliveira, C.R., and Rego, A.C. (2012). Glutathione redox cycle dysregulation in Huntington's disease knock-in striatal cells. Free Radic. Biol. Med. *53*, 1857–1867.

Ribeiro, M., Silva, A.C., Rodrigues, J., Naia, L., and Rego, A.C. (2013). Oxidizing effects of exogenous stressors in Huntington's disease knock-in striatal cells-protective effect oflcystamine and creatine. Toxicol. Sci. *136*, 487–499.

Ribeiro, M., Rosenstock, T.R., Oliveira, A.M., Oliveira, C.R., and Rego, A.C. (2014). Insulin and IGF-1 improve mitochondrial function in a PI-3K/Akt-dependent manner and reduce mitochondrial generation of reactive oxygen species in Huntington's disease knock-in striatal cells. Free Radic. Biol. Med. *74*, 129–144.

Rigamonti, D., Bauer, J.H., De-Fraja, C., Conti, L., Sipione, S., Sciorati, C., Clementi, E., Hackam, A., Hayden, M.R., Li, Y., et al. (2000). Wild-type huntingtin protects from apoptosis upstream of caspase-3. J. Neurosci. *20*, 3705–3713.

Rigamonti, D., Sipione, S., Goffredo, D., Zuccato, C., Fossale, E., and Cattaneo, E. (2001). Huntingtin's Neuroprotective Activity Occurs via Inhibition of Procaspase-9 Processing. J. Biol. Chem. *276*, 14545–14548.

Rogina, B., and Helfand, S.L. (2004). Sir2 mediates longevity in the fly through a pathway related to calorie restriction. Proc. Natl. Acad. Sci. U. S. A. *101*, 15998–16003.

Rosenblatt, A., Kumar, B. V., Mo, A., Welsh, C.S., Margolis, R.L., and Ross, C.A. (2012). Age, CAG repeat length, and clinical progression in Huntington's disease. Mov. Disord. *27*, 272–276.

Rosenstock, T.R., Duarte, A.I., and Rego, A.C. (2010). Mitochondrial-associated metabolic changes and neurodegeneration in Huntington's disease - from clinical features to the bench. Curr.Drug Targets. *11*, 1218–1236.

Rosenstock, T.R., De Brito, O.M., Lombardi, V., Louros, S., Ribeiro, M., Almeida, S., Ferreira, I.L., Oliveira, C.R., and Rego, A.C. (2011). FK506 ameliorates cell death features in Huntington's disease striatal cell models. Neurochem. Int. *59*, 600–609.

Rosenstock, T.R., Brett, A.C., and Rego, A.C. (2012). Neuronal pathways affected in Huntington's disease. In Multidisciplinary Viewpoint on Neurodegenerative Diseases, M.S.B.P.L.. B.D. Di Carlo, ed. (Kerala, India: Transword Research Network), pp. 1–16.

Ross, C.A., Pantelyat, A., Kogan, J., and Brandt, J. (2014a). Determinants of functional disability in Huntington's disease: role of cognitive and motor dysfunction. Mov. Disord. *29*, 1351–1358.

Ross, C. a, Aylward, E.H., Wild, E.J., Langbehn, D.R., Long, J.D., Warner, J.H., Scahill, R.I., Leavitt, B.R., Stout, J.C., Paulsen, J.S., et al. (2014b). Huntington disease: natural history, biomarkers and prospects for therapeutics. Nat. Rev. Neurol. *10*, 204–216.

Rothgiesser, K.M., Erener, S., Waibel, S., Lüscher, B., and Hottiger, M.O. (2010). SIRT2 regulates NF-κB dependent gene expression through deacetylation of p65 Lys310. J. Cell Sci. *123*, 4251–4258.

Ruan, Q., Lesort, M., MacDonald, M.E., and Johnson, G.V.W. (2004). Striatal cells from mutant huntingtin knock-in mice are selectively vulnerable to mitochondrial complex II inhibitor-induced cell death through a non-apoptotic pathway. Hum. Mol. Genet. *13*, 669–681.

Rué, L., López-Soop, G., Gelpi, E., Martínez-Vicente, M., Alberch, J., and Pérez-Navarro, E. (2013). Brain region- and age-dependent dysregulation of p62 and NBR1 in a mouse model of Huntington's disease. Neurobiol. Dis. *52*, 219–228.

Rui, Y.-N., Xu, Z., Patel, B., Chen, Z., Chen, D., Tito, A., David, G., Sun, Y., Stimming, E.F., Bellen, H.J., et al. (2015). Huntingtin functions as a scaffold for selective macroautophagy. Nat. Cell Biol. *17*, 262–275.

Sadoul, K., Boyault, C., Pabion, M., and Khochbin, S. (2008). Regulation of protein turnover by acetyltransferases and deacetylases. Biochimie *90*, 306–312.

Saft, C., Zange, J., Andrich, J., Müller, K., Lindenberg, K., Landwehrmeyer, B., Vorgerd, M., Kraus, P.H., Przuntek, H., and Schöls, L. (2005). Mitochondrial impairment in patients and asymptomatic mutation carriers of Huntington's disease. Mov. Disord. *20*, 674–679.

Salceda, S., and Caro, J. (1997). Hypoxia-inducible factor 1α (HIF-1α) protein is rapidly degraded by the ubiquitin-proteasome system under normoxic conditions. Its stabilization by hypoxia depends on redox-induced changes. J. Biol. Chem. *272*, 22642–22647.

Samant, S.A., Zhang, H.J., Hong, Z., Pillai, V.B., Sundaresan, N.R., Wolfgeher, D., Archer, S.L., Chan, D.C., and Gupta, M.P. (2014). SIRT3 deacetylates and activates OPA1 to regulate mitochondrial dynamics during stress. Mol. Cell. Biol. *34*, 807–819.

Samikkannu, T., Chen, C.-H., Yih, L.-H., Wang, A.S.S., Lin, S.-Y., Chen, T.-C., and Jan, K.-Y. (2003). Reactive oxygen species are involved in arsenic trioxide inhibition of

pyruvate dehydrogenase activity. Chem. Res. Toxicol. *16*, 409–414.

Santamaría, A., Pérez-Severiano, F., Rodríguez-Martínez, E., Maldonado, P.D., Pedraza-Chaverri, J., Ríos, C., and Segovia, J. (2001). Comparative analysis of superoxide dismutase activity between acute pharmacological models and a transgenic mouse model of Huntington's disease. Neurochem. Res. *26*, 419–424.

Sapp, E., Ge, P., Aizawa, H., Bird, E., Penney, J., Young, A.B., Vonsattel, J.P., and Difiglia, M. (1995). Evidence for a preferential loss of enkephalin immunoreactivity in the external globus pallidus in low grade Huntington's disease using high resolution image analysis. Neuroscience *64*, 397–404.

Sassone, J., Colciago, C., Cislaghi, G., Silani, V., and Ciammola, A. (2009). Huntington's disease: The current state of research with peripheral tissues. Exp. Neurol. *219*, 385–397.

Satoh, A., Brace, C.S., Rensing, N., Cliften, P., Wozniak, D.F., Herzog, E.D., Yamada, K.A., and Imai, S.I. (2013). Sirt1 extends life span and delays aging in mice through the regulation of Nk2 Homeobox 1 in the DMH and LH. Cell Metab. *18*, 416–430.

Saudou, F., and Humbert, S. (2016). The Biology of Huntingtin. Neuron *89*, 910–926.

Sauve, A. a (2008). NAD+ and vitamin B3: from metabolism to therapies. J. Pharmacol. Exp. Ther. *324*, 883–893.

Sawa, a, Wiegand, G.W., Cooper, J., Margolis, R.L., Sharp, a H., Lawler, J.F., Greenamyre, J.T., Snyder, S.H., and Ross, C. A (1999). Increased apoptosis of Huntington disease lymphoblasts associated with repeat length-dependent mitochondrial depolarization. Nat. Med. *5*, 1194–1198.

Scarpulla, R.C. (2011). Metabolic control of mitochondrial biogenesis through the PGC-1 family regulatory network. Biochim. Biophys. Acta *1813*, 1269–1278.

Schatz, G. (1995). Mitochondria: beyond oxidative phosphorylation. BBA - Mol. Basis Dis. *1271*, 123–126.

Scher, M.B., Vaquero, A., and Reinberg, D. (2007). SirT3 is a nuclear NAD+-dependent histone deacetylase that translocates to the mitochondria upon cellular stress. Genes Dev. *21*, 920–928.

Schilling, G., Becher, M.W., Sharp, A.H., Jinnah, H.A., Duan, K., Kotzuk, J.A., Slunt, H.H., Ratovitski, T., Cooper, J.K., Jenkins, N.A., et al. (1999). Intranuclear inclusions and neuritic aggregates in transgenic mice expressing a mutant N-terminal fragment of huntingtin. Hum. Mol. Genet. *8*, 397–407.

Schmeisser, K., Mansfeld, J., Kuhlow, D., Weimer, S., Priebe, S., Heiland, I., Birringer, M., Groth, M., Segref, A., Kanfi, Y., et al. (2013). Role of sirtuins in lifespan regulation is linked to methylation of nicotinamide. Nat. Chem. Biol. *9*, 693–700.

Scholz, C., Weinert, B.T., Wagner, S.A., Beli, P., Miyake, Y., Qi, J., Jensen, L.J., Streicher, W., McCarthy, A.R., Westwood, N.J., et al. (2015). Acetylation site specificities of lysine deacetylase inhibitors in human cells. Nat Biotech *33*, 415–423.

Schwer, B., Eckersdorff, M., Li, Y., Silva, J.C., Fermin, D., Kurtev, M. V., Giallourakis, C.,

Comb, M.J., Alt, F.W., and Lombard, D.B. (2009). Calorie restriction alters mitochondrial protein acetylation. Aging Cell *8*, 604–606.

Seigneurin-Berny, D., Verdel, A., Curtet, S., Lemercier, C., Garin, J., Rousseaux, S., and Khochbin, S. (2001). Identification of components of the murine histone deacetylase 6 complex: link between acetylation and ubiquitination signaling pathways. Mol. Cell. Biol. *21*, 8035–8044.

Semaka, A., Collins, J.A., and Hayden, M.R. (2010). Unstable familial transmissions of huntington disease alleles with 27-35 CAG repeats (intermediate alleles). Am. J. Med. Genet. Part B Neuropsychiatr. Genet. *153*, 314–320.

Seong, I.S., Ivanova, E., Lee, J.M., Choo, Y.S., Fossale, E., Anderson, M.A., Gusella, J.F., Laramie, J.M., Myers, R.H., Lesort, M., et al. (2005). HD CAG repeat implicates a dominant property of huntingtin in mitochondrial energy metabolism. Hum. Mol. Genet. *14*, 2871–2880.

Shahbazian, M.D., and Grunstein, M. (2007). Functions of site-specific histone acetylation and deacetylation. Annu. Rev. Biochem. *76*, 75–100.

Shan, C., Kang, H.-B., Elf, S., Xie, J., Gu, T.-L., Aguiar, M., Lonning, S., Hitosugi, T., Chung, T.-W., Arellano, M., et al. (2014). Tyr-94 phosphorylation inhibits pyruvate dehydrogenase phosphatase 1 and promotes tumor growth. J. Biol. Chem. *289*, 21413–21422.

Shehadeh, J., Fernandes, H.B., Zeron Mullins, M.M., Graham, R.K., Leavitt, B.R., Hayden, M.R., and Raymond, L.A. (2006). Striatal neuronal apoptosis is preferentially enhanced by NMDA receptor activation in YAC transgenic mouse model of Huntington disease. Neurobiol. Dis. *21*, 392–403.

Shi, T., Wang, F., Stieren, E., and Tong, Q. (2005). SIRT3, a mitochondrial sirtuin deacetylase, regulates mitochondrial function and thermogenesis in brown adipocytes. J. Biol. Chem. *280*, 13560–13567.

Shimohata, T., Nakajima, T., Yamada, M., Uchida, C., Onodera, O., Naruse, S., Kimura, T., Koide, R., Nozaki, K., Sano, Y., et al. (2000). Expanded polyglutamine stretches interact with TAFII130, interfering with CREB-dependent transcription. Nat. Genet. *26*, 29–36.

Shin, B.H., Lim, Y., Oh, H.J., Park, S.M., Lee, S.K., Ahnn, J., Kim, D.H., Song, W.K., Kwak, T.H., and Park, W.J. (2013). Pharmacological Activation of Sirt1 Ameliorates Polyglutamine-Induced Toxicity through the Regulation of Autophagy. PLoS One *8*.

Shirendeb, U., Reddy, A.P., Manczak, M., Calkins, M.J., Mao, P., Tagle, D.A., and Reddy, P.H. (2011). Abnormal mitochondrial dynamics, mitochondrial loss and mutant huntingtin oligomers in Huntington's disease: Implications for selective neuronal damage. Hum. Mol. Genet. *20*, 1438–1455.

Shulga, N., Wilson-Smith, R., and Pastorino, J.G. (2010). Sirtuin-3 deacetylation of cyclophilin D induces dissociation of hexokinase II from the mitochondria. J. Cell Sci. *123*, 894–902.

Silva, A.C., Almeida, S., Laço, M., Duarte, A.I., Domingues, J., Oliveira, C.R., Januário, C., and Rego, A.C. (2013). Mitochondrial respiratory chain complex activity and

bioenergetic alterations in human platelets derived from pre-symptomatic and symptomatic huntington's disease carriers. Mitochondrion *13*, 801–809.

Simões-Pires, C., Zwick, V., Nurisso, A., Schenker, E., Carrupt, P.-A., and Cuendet, M. (2013). HDAC6 as a target for neurodegenerative diseases: what makes it different from the other HDACs? Mol. Neurodegener. *8*, 7.

Slow, E.J., van Raamsdonk, J., Rogers, D., Coleman, S.H., Graham, R.K., Deng, Y., Oh, R., Bissada, N., Hossain, S.M., Yang, Y.Z., et al. (2003). Selective striatal neuronal loss in a YAC128 mouse model of Huntington disease. Hum. Mol. Genet. *12*, 1555–1567.

Smirnova, E., Shurland, D.L., Ryazantsev, S.N., and van der Bliek, A.M. (1998). A human dynamin-related protein controls the distribution of mitochondria. J. Cell Biol. *143*, 351–358.

Smith, J.J., Kenney, R.D., Gagne, D.J., Frushour, B.P., Ladd, W., Galonek, H.L., Israelian, K., Song, J., Razvadauskaite, G., Lynch, A. V, et al. (2009). Small molecule activators of SIRT1 replicate signaling pathways triggered by calorie restriction in vivo. BMC Syst. Biol. *3*, 31.

Smith, M.R., Syed, A., Lukacsovich, T., Purcell, J., Barbaro, B.A., Worthge, S.A., Wei, S.R., Pollio, G., Magnoni, L., Scali, C., et al. (2014). A potent and selective sirtuin 1 inhibitor alleviates pathology in multiple animal and cell models of huntington's disease. Hum. Mol. Genet. *23*, 2995–3007.

Sol, E.M., Wagner, S.A., Weinert, B.T., Kumar, A., Kim, H.S., Deng, C.X., Choudhary, C., and Imhof, A. (2012). Proteomic Investigations of Lysine Acetylation Identify Diverse Substrates of Mitochondrial Deacetylase Sirt3. PLoS One *7*, 1–9.

Sommer, M., Poliak, N., Upadhyay, S., Ratovitski, E., Nelkin, B.D., Donehower, L.A., and Sidransky, D. (2006). DeltaNp63alpha overexpression induces downregulation of Sirt1 and an accelerated aging phenotype in the mouse. Cell Cycle *5*, 2005–2011.

Song, W., Chen, J., Petrilli, A., Liot, G., Klinglmayr, E., Zhou, Y., Poquiz, P., Tjong, J., Pouladi, M.A., Hayden, M.R., et al. (2011). Mutant huntingtin binds the mitochondrial fission GTPase dynamin-related protein-1 and increases its enzymatic activity. Nat. Med. *17*, 377–382.

Song, W., Song, Y., Kincaid, B., Bossy, B., and Bossy-Wetzel, E. (2013). Mutant SOD1G93A triggers mitochondrial fragmentation in spinal cord motor neurons: neuroprotection by SIRT3 and PGC-1α. Neurobiol. Dis. *51*, 72–81.

Song, Z., Ghochani, M., McCaffery, J.M., Frey, T.G., and Chan, D.C. (2009). Mitofusins and OPA1 mediate sequential steps in mitochondrial membrane fusion. Mol. Biol. Cell *20*, 3525–3532.

Sorbi, S., Bird, E.D., and Blass, J.P. (1983). Decreased pyruvate dehydrogenase complex activity in Huntington and Alzheimer brain. Ann. Neurol. *13*, 72–78.

Sørensen, S.A., and Fenger, K. (1992). Causes of death in patients with Huntington's disease and in unaffected first degree relatives. J. Med. Genet. *29*, 911–914.

Sorolla, M.A., Reverter-Branchat, G., Tamarit, J., Ferrer, I., Ros, J., and Cabiscol, E. (2008). Proteomic and oxidative stress analysis in human brain samples of

Huntington disease. Free Radic. Biol. Med. *45*, 667–678.

Sorolla, M.A., Rodríguez-Colman, M.J., Tamarit, J., Ortega, Z., Lucas, J.J., Ferrer, I., Ros, J., and Cabiscol, E. (2010). Protein oxidation in Huntington disease affects energy production and vitamin B6 metabolism. Free Radic. Biol. Med. *49*, 612–621.

Squitieri, F., Almqvist, E.W., Cannella, M., Cislaghi, G., and Hayden, M.R. (2003). Predictive testing for persons at risk for homozygosity for CAG expansion in the Huntington disease gene. Clin. Genet. *64*, 524–525.

Squitieri, F., Cannella, M., Sgarbi, G., Maglione, V., Falleni, A., Lenzi, P., Baracca, A., Cislaghi, G., Saft, C., Ragona, G., et al. (2006). Severe ultrastructural mitochondrial changes in lymphoblasts homozygous for Huntington disease mutation. Mech. Ageing Dev. *127*, 217–220.

Squitieri, F., Griguoli, A., Capelli, G., Porcellini, A., and D'Alessio, B. (2016). Epidemiology of Huntington disease: First post-HTT gene analysis of prevalence in Italy. Clin. Genet. *89*, 367–370.

St-Pierre, J., Drori, S., Uldry, M., Silvaggi, J.M., Rhee, J., Jäger, S., Handschin, C., Zheng, K., Lin, J., Yang, W., et al. (2006). Suppression of reactive oxygen species and neurodegeneration by the PGC-1 transcriptional coactivators. Cell *127*, 397–408.

Stack, E.C., Kubilus, J.K., Smith, K., Cormier, K., Del Signore, S.J., Guelin, E., Ryu, H., Hersch, S.M., and Ferrante, R.J. (2005). Chronology of behavioral symptoms and neuropathological sequela in R6/2 Huntington's disease transgenic mice. J. Comp. Neurol. *490*, 354–370.

Steffan, J.S., Kazantsev, A., Spasic-Boskovic, O., Greenwald, M., Zhu, Y.Z., Gohler, H., Wanker, E.E., Bates, G.P., Housman, D.E., and Thompson, L.M. (2000). The Huntington's disease protein interacts with p53 and CREB-binding protein and represses transcription. Proc Natl Acad Sci U S A *97*, 6763–6768.

Steffan, J.S., Bodai, L., Pallos, J., Poelman, M., McCampbell, a, Apostol, B.L., Kazantsev, a, Schmidt, E., Zhu, Y.Z., Greenwald, M., et al. (2001). Histone deacetylase inhibitors arrest polyglutamine-dependent neurodegeneration in Drosophila. Nature *413*, 739–743.

Stojanovski, D., Koutsopoulos, O.S., Okamoto, K., and Ryan, M.T. (2004). Levels of human Fis1 at the mitochondrial outer membrane regulate mitochondrial morphology. J. Cell Sci. *117*, 1201–1210.

Strand, A.D., Baquet, Z.C., Aragaki, A.K., Holmans, P., Yang, L., Cleren, C., Beal, M.F., Jones, L., Kooperberg, C., Olson, J.M., et al. (2007). Expression profiling of Huntington's disease models suggests that brain-derived neurotrophic factor depletion plays a major role in striatal degeneration. J. Neurosci. *27*, 11758–11768.

Strong, T. V, Tagle, D. a, Valdes, J.M., Elmer, L.W., Boehm, K., Swaroop, M., Kaatz, K.W., Collins, F.S., and Albin, R.L. (1993). Widespread expression of the human and rat Huntington's disease gene in brain and nonneural tissues. Nat. Genet. *5*, 259–265.

Struhl, K. (1998). Histone acetylation and transcriptional regulatory mechanisms. Genes Dev. *12*, 599–606.

Sugars, K.L., and Rubinsztein, D.C. (2003). Transcriptional abnormalities in Huntington disease. Trends Genet. *19*, 233–238.

Sugden, M.C., and Holness, M.J. (2006). Mechanisms underlying regulation of the expression and activities of the mammalian pyruvate dehydrogenase kinases. Arch. Physiol. Biochem. *112*, 139–149.

Sun, B., Fan, W., Balciunas, A., Cooper, J.K., Bitan, G., Steavenson, S., Denis, P.E., Young, Y., Adler, B., Daugherty, L., et al. (2002). Polyglutamine repeat length-dependent proteolysis of huntingtin. Neurobiol. Dis. *11*, 111–122.

Sundaresan, N.R., Samant, S. a, Pillai, V.B., Rajamohan, S.B., and Gupta, M.P. (2008). SIRT3 is a stress-responsive deacetylase in cardiomyocytes that protects cells from stress-mediated cell death by deacetylation of Ku70. Mol. Cell. Biol. *28*, 6384–6401.

Suopanki, J., Götz, C., Lutsch, G., Schiller, J., Harjes, P., Herrmann, A., and Wanker, E.E. (2006). Interaction of huntingtin fragments with brain membranes - Clues to early dysfunction in Huntington's disease. J. Neurochem. *96*, 870–884.

Süssmuth, S.D., Haider, S., Landwehrmeyer, G.B., Farmer, R., Frost, C., Tripepi, G., Andersen, C.A., Di Bacco, M., Lamanna, C., Diodato, E., et al. (2015). An exploratory double-blind, randomized clinical trial with selisistat, a SirT1 inhibitor, in patients with Huntington's disease. Br. J. Clin. Pharmacol. *79*, 465–476.

Swerdlow, R.H., Parks, J.K., Cassarino, D.S., Shilling, A.T., Bennett, J.P., Harrison, M.B., and Parker, W.D. (1999). Characterization of Cybrid Cell Lines Containing mtDNA from Huntington's Disease Patients. Biochem. Biophys. Res. Commun. *261*, 701–704.

Tabatabaie, T., Potts, J.D., and Floyd, R. a (1996). Reactive oxygen species-mediated inactivation of pyruvate dehydrogenase. Arch. Biochem. Biophys. *336*, 290–296.

Tabrizi, S.J., Cleeter, M.W.J., Xuereb, J., Taanman, J.W., Cooper, J.M., and Schapira, A.H. V (1999). Biochemical abnormalities and excitotoxicity in Huntington's disease brain. Ann. Neurol. *45*, 25–32.

Tabrizi, S.J., Scahill, R.I., Durr, A., Roos, R.A.C., Leavitt, B.R., Jones, R., Landwehrmeyer, G.B., Fox, N.C., Johnson, H., Hicks, S.L., et al. (2011). Biological and clinical changes in premanifest and early stage Huntington's disease in the TRACK-HD study: The 12-month longitudinal analysis. Lancet Neurol. *10*, 31–42.

Taherzadeh-Fard, E., Saft, C., Akkad, D. a, Wieczorek, S., Haghikia, A., Chan, A., Epplen, J.T., and Arning, L. (2011). PGC-1alpha downstream transcription factors NRF-1 and TFAM are genetic modifiers of Huntington disease. Mol. Neurodegener. *6*, 32.

Tanner, K.G., Landry, J., Sternglanz, R., and Denu, J.M. (2000). Silent information regulator 2 family of NAD- dependent histone/protein deacetylases generates a unique product, 1-O-acetyl-ADP-ribose. Proc. Natl. Acad. Sci. U. S. A. *97*, 14178–14182.

Tanno, M., Sakamoto, J., Miura, T., Shimamoto, K., and Horio, Y. (2007). Nucleocytoplasmic shuttling of the NAD+-dependent histone deacetylase SIRT1. J. Biol. Chem. *282*, 6823–6832.

The HD iPSC Consortium (2012). Induced pluripotent stem cells from patients with huntington's disease show cag-repeat-expansion-associated phenotypes. Cell Stem Cell *11*, 264–278.

Thomas, E.A., Coppola, G., Desplats, P.A., Tang, B., Soragni, E., Burnett, R., Gao, F., Fitzgerald, K.M., Borok, J.F., Herman, D., et al. (2008). The HDAC inhibitor 4b ameliorates the disease phenotype and transcriptional abnormalities in Huntington's disease transgenic mice. Proc. Natl. Acad. Sci. U. S. A. *105*, 15564–15569.

Tissenbaum, H. a, and Guarente, L. (2001). Increased dosage of a sir-2 gene extends lifespan in Caenorhabditis elegans. Nature *410*, 227–230.

Tiwari, G., Tiwari, R., and Rai, A.K. (2010). Cyclodextrins in delivery systems: Applications. J. Pharm. Bioallied Sci. *2*, 72–79.

Tomé-Carneiro, J., Larrosa, M., González-Sarrías, A., Tomás-Barberán, F.A., García-Conesa, M.T., and Espín, J.C. (2013). Resveratrol and clinical trials: the crossroad from in vitro studies to human evidence. Curr. Pharm. Des. *19*, 6064–6093.

Trettel, F., Rigamonti, D., Hilditch-Maguire, P., Wheeler, V.C., Sharp, A.H., Persichetti, F., Cattaneo, E., and MacDonald, M.E. (2000). Dominant phenotypes produced by the HD mutation in STHdh(Q111) striatal cells. Hum. Mol. Genet. *9*, 2799–2809.

Trushina, E., Dyer, R.B., Badger, J.D., Ure, D., Eide, L., Tran, D.D., Vrieze, B.T., Legendre-Guillemin, V., McPherson, P.S., Mandavilli, B.S., et al. (2004). Mutant huntingtin impairs axonal trafficking in mammalian neurons in vivo and in vitro. Mol. Cell. Biol. *24*, 8195–8209.

Tsang, T.M., Woodman, B., McLoughlin, G.A., Griffin, J.L., Tabrizi, S.J., Bates, G.P., and Holmes, E. (2006). Metabolic characterization of the R6/2 transgenic mouse model of Huntington's disease by high-resolution MAS 1H NMR spectroscopy. J. Proteome Res. *5*, 483–492.

Tseng, A.H.H., Shieh, S.S., and Wang, D.L. (2013). SIRT3 deacetylates FOXO3 to protect mitochondria against oxidative damage. Free Radic. Biol. Med. *63*, 222–234.

Tsunemi, T., Ashe, T.D., Morrison, B.E., Soriano, K.R., Au, J., Roque, R.A.V., Lazarowski, E.R., Damian, V.A., Masliah, E., and La Spada, A.R. (2012). PGC-1α rescues Huntington's disease proteotoxicity by preventing oxidative stress and promoting TFEB function. Sci. Transl. Med. *4*, 142ra97.

Tulino, R., Benjamin, A.C., Jolinon, N., Smith, D.L., Chini, E.N., Carnemolla, A., and Bates, G.P. (2016). SIRT1 Activity Is Linked to Its Brain Region-Specific Phosphorylation and Is Impaired in Huntington's Disease Mice. PLoS One *11*, e0145425.

Túnez, I., Sánchez-López, F., Agüera, E., Fernández-Bolaños, R., Sánchez, F.M., and Tasset-Cuevas, I. (2011). Important role of oxidative stress biomarkers in Huntington's disease. J. Med. Chem. *54*, 5602–5606.

Turner, C., Cooper, J.M., and Schapira, A.H. V (2007). Clinical correlates of mitochondrial function in Huntington's disease muscle. Mov. Disord. *22*, 1715–1721.

Twig, G., and Shirihai, O.S. (2011). The interplay between mitochondrial dynamics and mitophagy. Antioxid. Redox Signal. *14*, 1939–1951.

Uldry, M., Yang, W., St-Pierre, J., Lin, J., Seale, P., and Spiegelman, B.M. (2006). Complementary action of the PGC-1 coactivators in mitochondrial biogenesis and brown fat differentiation. Cell Metab. *3*, 333–341.

Um, J., Park, S., Kang, H., Yang, S., Foretz, M., Mcburney, M.W., Kim, M.K., Viollet, B., and Chung, J.H. (2010). AMP-Activated Protein Kinase – Deficient Mice Are Resistant to the Metabolic Effects of Resveratrol. Diabetes *59*, 554–563.

Vale, T.C., and Cardoso, F. (2015). Chorea: A Journey through History. Tremor Other Hyperkinet. Mov. (N. Y). *5*, 1–6.

Valenza, M., Carroll, J.B., Leoni, V., Bertram, L.N., Björkhem, I., Singaraja, R.R., Di Donato, S., Lutjohann, D., Hayden, M.R., and Cattaneo, E. (2007). Cholesterol biosynthesis pathway is disturbed in YAC128 mice and is modulated by huntingtin mutation. Hum. Mol. Genet. *16*, 2187–2198.

Vang, O., Ahmad, N., Baile, C.A., Baur, J.A., Brown, K., Csiszar, A., Das, D.K., Delmas, D., Gottfried, C., Lin, H.Y., et al. (2011). What is new for an old molecule? systematic review and recommendations on the use of resveratrol. PLoS One *6*.

Vaquero, A., Scher, M., Lee, D., Erdjument-Bromage, H., Tempst, P., and Reinberg, D. (2004). Human SirT1 interacts with histone H1 and promotes formation of facultative heterochromatin. Mol. Cell *16*, 93–105.

Velier, J., Kim, M., Schwarz, C., Kim, T.W., Sapp, E., Chase, K., Aronin, N., and DiFiglia, M. (1998). Wild-type and mutant huntingtins function in vesicle trafficking in the secretory and endocytic pathways. Exp. Neurol. *152*, 34–40.

Venegas, V., and Halberg, M.C. (2012). Measurement of mitochondrial DNA copy number. Methods Mol. Biol. *837*, 327–335.

Verdin, E. (2014). The many faces of sirtuins: Coupling of NAD metabolism, sirtuins and lifespan. Nat. Med. *20*, 25–27.

Vingtdeux, V., Giliberto, L., Zhao, H., Chandakkar, P., Wu, Q., Simon, J.E., Janle, E.M., Lobo, J., Ferruzzi, M.G., Davies, P., et al. (2010). AMP-activated protein kinase signaling activation by resveratrol modulates amyloid-beta peptide metabolism. J. Biol. Chem. *285*, 9100–9113.

Vis, J.C., Schipper, E., de Boer-van Huizen, R.T., Verbeek, M.M., de Waal, R.M.W., Wesseling, P., ten Donkelaar, H.J., and Kremer, B. (2005). Expression pattern of apoptosis-related markers in Huntington's disease. Acta Neuropathol. *109*, 321–328.

Vlessis, A.A., Muller, P., Bartos, D., and Trunkey, D. (1991). Mechanism of peroxide-induced cellular injury in cultured adult cardiac myocytes. FASEB J. *5*, 2600–2605.

Vonsattel, J.P., and DiFiglia, M. (1998). Huntington disease. J. Neuropathol. Exp. Neurol. *57*, 369–384.

Vonsattel, J.P., Myers, R.H., Stevens, T.J., Ferrante, R.J., Bird, E.D., and Richardson Jr., E.P. (1985). Neuropathological classification of Huntington's disease. J Neuropathol Exp Neurol *44*, 559–577.

Vonsattel, J.P.G., Keller, C., and Del Pilar Amaya, M. (2008). Neuropathology of Huntington's disease. Handb. Clin. Neurol. *89*, 599–618.

Vonsattel, J.P.G., Keller, C., and Cortes Ramirez, E.P. (2011). Huntington's disease - neuropathology.

Waelter, S., Boeddrich, A., Lurz, R., Scherzinger, E., Lueder, G., Lehrach, H., and Wanker, E.E. (2001). Accumulation of mutant huntingtin fragments in aggresome-like inclusion bodies as a result of insufficient protein degradation. Mol. Biol. Cell *12*, 1393–1407.

Waltregny, D., Glénisson, W., Tran, S.L., North, B.J., Verdin, E., Colige, A., and Castronovo, V. (2005). Histone deacetylase HDAC8 associates with smooth muscle alpha-actin and is essential for smooth muscle cell contractility. FASEB J. *19*, 966–968.

Wang, H., Lim, P.J., Karbowski, M., and Monteiro, M.J. (2009). Effects of overexpression of Huntingtin proteins on mitochondrial integrity. Hum. Mol. Genet. *18*, 737–752.

Wang, J.-Q., Chen, Q., Wang, X., Wang, Q.-C., Wang, Y., Cheng, H.-P., Guo, C., Sun, Q., Chen, Q., and Tang, T.-S. (2013). Dysregulation of mitochondrial calcium signaling and superoxide flashes cause mitochondrial genomic DNA damage in Huntington disease. J. Biol. Chem. *288*, 3070–3084.

Weeks, R.A., Piccini, P., Harding, A.E., and Brooks, D.J. (1996). Striatal D1 and D2 dopamine receptor loss in asymptomatic mutation carriers of Huntington's disease. Ann. Neurol. *40*, 49–54.

Weir, H.J.M., Murray, T.K., Kehoe, P.G., Love, S., Verdin, E.M., O'Neill, M.J., Lane, J.D., and Balthasar, N. (2012). CNS SIRT3 expression is altered by reactive oxygen species and in Alzheimer's disease. PLoS One *7*, e48225.

Wellington, C.L., Ellerby, L.M., Gutekunst, C.-A., Rogers, D., Warby, S., Graham, R.K., Loubser, O., van Raamsdonk, J., Singaraja, R., Yang, Y.-Z., et al. (2002). Caspase cleavage of mutant huntingtin precedes neurodegeneration in Huntington's disease. J. Neurosci. *22*, 7862–7872.

Weydt, P., Pineda, V. V, Torrence, A.E., Libby, R.T., Satterfield, T.F., Lazarowski, E.R., Gilbert, M.L., Morton, G.J., Bammler, T.K., Strand, A.D., et al. (2006). Thermoregulatory and metabolic defects in Huntington's disease transgenic mice implicate PGC-1alpha in Huntington's disease neurodegeneration. Cell Metab. *4*, 349–362.

Wheeler, V.C., White, J.K., Gutekunst, C.A., Vrbanac, V., Weaver, M., Li, X.J., Li, S.H., Yi, H., Vonsattel, J.P., Gusella, J.F., et al. (2000). Long glutamine tracts cause nuclear localization of a novel form of huntingtin in medium spiny striatal neurons in HdhQ92 and HdhQ111 knock-in mice. Hum. Mol. Genet. *9*, 503–513.

Wheeler, V.C., Gutekunst, C.-A., Vrbanac, V., Lebel, L.-A., Schilling, G., Hersch, S., Friedlander, R.M., Gusella, J.F., Vonsattel, J.-P., Borchelt, D.R., et al. (2002). Early phenotypes that presage late-onset neurodegenerative disease allow testing

of modifiers in Hdh CAG knock-in mice. Hum. Mol. Genet. *11*, 633–640.

White, J.K., Auerbach, W., Duyao, M.P., Vonsattel, J.-P., Gusella, J.F., Joyner, A.L., and MacDonald, M.E. (1997). Huntingtin is required for neurogenesis and is not impaired by the Huntington's disease CAG expansion. Nat. Genet. *17*, 404–410.

Whitehouse, S., Cooper, R.H., and Randle, P.J. (1974). Mechanism of activation of pyruvate dehydrogenase by dichloroacetate and other halogenated carboxylic acids. Biochem. J. *141*, 761–774.

Wong, Y.C., and Holzbaur, E.L.F. (2014). The regulation of autophagosome dynamics by huntingtin and HAP1 is disrupted by expression of mutant huntingtin, leading to defective cargo degradation. J. Neurosci. *34*, 1293–1305.

Wyttenbach, a, Swartz, J., Kita, H., Thykjaer, T., Carmichael, J., Bradley, J., Brown, R., Maxwell, M., Schapira, a, Orntoft, T.F., et al. (2001). Polyglutamine expansions cause decreased CRE-mediated transcription and early gene expression changes prior to cell death in an inducible cell model of Huntington's disease. Hum. Mol. Genet. *10*, 1829–1845.

Xie, Y., Hayden, M.R., and Xu, B. (2010). BDNF overexpression in the forebrain rescues Huntington's disease phenotypes in YAC128 mice. J. Neurosci. *30*, 14708–14718.

Yang, D., Gong, X., Yakhnin, A., and Roche, T.E. (1998). Requirements for the adaptor protein role of dihydrolipoyl acetyltransferase in the up-regulated function of the pyruvate dehydrogenase kinase and pyruvate dehydrogenase phosphatase. J. Biol. Chem. *273*, 14130–14137.

Yang, S.J., Choi, J.M., Kim, L., Park, S.E., Rhee, E.J., Lee, W.Y., Oh, K.W., Park, S.W., and Park, C.Y. (2014). Nicotinamide improves glucose metabolism and affects the hepatic NAD-sirtuin pathway in a rodent model of obesity and type 2 diabetes. J. Nutr. Biochem. *25*, 66–72.

Yang, W., Dunlap, J.R., Andrews, R.B., and Wetzel, R. (2002). Aggregated polyglutamine peptides delivered to nuclei are toxic to mammalian cells. Hum. Mol. Genet. *11*, 2905–2917.

Yano, H., Baranov, S. V, Baranova, O. V, Kim, J., Pan, Y., Yablonska, S., Carlisle, D.L., Ferrante, R.J., Kim, A.H., and Friedlander, R.M. (2014). Inhibition of mitochondrial protein import by mutant huntingtin. Nat Neurosci *17*, 822–831.

Yeh, H.H., Young, D., Gelovani, J.G., Robinson, A., Davidson, Y., Herholz, K., and Mann, D.M.A. (2013). Histone deacetylase class II and acetylated core histone immunohistochemistry in human brains with Huntington's disease. Brain Res. *1504*, 16–24.

Yeung, F., Hoberg, J.E., Ramsey, C.S., Keller, M.D., Jones, D.R., Frye, R.A., and Mayo, M.W. (2004). Modulation of NF-kB-dependent transcription and cell survival by the SIRT1 deacetylase. EMBO J. *23*, 2369–2380.

Yoshida, M., Kijima, M., Akita, M., and Beppu, T. (1990). Potent and specific inhibition of mammalian histone deacetylase both in vivo and in vitro by trichostatin A. J. Biol. Chem. *265*, 17174–17179.

Young, A.B., Shoulson, I., Penney, J.B., Starosta-Rubinstein, S., Gomez, F., Travers, H.,

Ramos-Arroyo, M.A., Snodgrass, S.R., Bonilla, E., and Moreno, H. (1986). Huntington's disease in Venezuela: neurologic features and functional decline. Neurology *36*, 244–249.

Zeron, M.M., Hansson, O., Chen, N., Wellington, C.L., Leavitt, B.R., Brundin, P., Hayden, M.R., and Raymond, L.A. (2002). Increased sensitivity to N-methyl-D-aspartate receptor-mediated excitotoxicity in a mouse model of Huntington's disease. Neuron *33*, 849–860.

Zhai, W., Jeong, H., Cui, L., Krainc, D., and Tjian, R. (2005). In vitro analysis of huntingtin-mediated transcriptional repression reveals multiple transcription factor targets. Cell *123*, 1241–1253.

Zhang, B., Cui, S., Bai, X., Zhuo, L., Sun, X., Hong, Q., Fu, B., Wang, J., Chen, X., and Cai, G. (2013). Sirt3 overexpression antagonizes high glucose accelerated cellular senescence in human diploid fibroblasts via the sirt3-foxo1 signaling pathway. Age (Omaha). *35*, 2237–2253.

Zhang, S.F., Hennessey, T., Yang, L., Starkova, N.N., Beal, M.F., and Starkov, A.A. (2011). Impaired brain creatine kinase activity in Huntington's disease. Neurodegener. Dis. *8*, 194–201.

Zhang, Y., Ona, V.O., Li, M., Drozda, M., Dubois-Dauphin, M., Przedborski, S., Ferrante, R.J., and Friedlander, R.M. (2003). Sequential activation of individual caspases, and of alterations in Bcl-2 proapoptotic signals in a mouse model of Huntington's disease. J. Neurochem. *87*, 1184–1192.

Zhao, S., Xu, W., Jiang, W., Yu, W., Lin, Y., Zhang, T., Yao, J., Zhou, L., Zeng, Y., Li, H., et al. (2010). Regulation of cellular metabolism by protein lysine acetylation. Science *327*, 1000–1004.

Zhong, L., D'Urso, A., Toiber, D., Sebastian, C., Henry, R.E., Vadysirisack, D.D., Guimaraes, A., Marinelli, B., Wikstrom, J.D., Nir, T., et al. (2010). The histone deacetylase Sirt6 regulates glucose homeostasis via Hif1alpha. Cell *140*, 280–293.

Zhou, Q., Lam, P.Y., Han, D., and Cadenas, E. (2009). Activation of c-Jun-N-terminal kinase and decline of mitochondrial pyruvate dehydrogenase activity during brain aging. FEBS Lett. *583*, 1132–1140.

Zuccato, C., Ciammola, A., Rigamonti, D., Leavitt, B.R., Goffredo, D., Conti, L., MacDonald, M.E., Friedlander, R.M., Silani, V., Hayden, M.R., et al. (2001). Loss of huntingtin-mediated BDNF gene transcription in Huntington's disease. Science *293*, 493–498.

Zuccato, C., Tartari, M., Crotti, A., Goffredo, D., Valenza, M., Conti, L., Cataudella, T., Leavitt, B.R., Hayden, M.R., Timmusk, T., et al. (2003). Huntingtin interacts with REST/NRSF to modulate the transcription of NRSE-controlled neuronal genes. Nat. Genet. *35*, 76–83.

Zuccato, C., Valenza, M., and Cattaneo, E. (2010). Molecular Mechanisms and Potential Therapeutical Targets in Huntington's Disease. Physiol. Rev. *90*, 905–981.

ANNEX

ELSEVIER LICENSE
TERMS AND CONDITIONS

Sep 13, 2016

This Agreement between Luana Naia ("You") and Elsevier ("Elsevier") consists of your license details and the terms and conditions provided by Elsevier and Copyright Clearance Center.

License Number	3947170761686
License date	Sep 13, 2016
Licensed Content Publisher	Elsevier
Licensed Content Publication	Elsevier Books
Licensed Content Title	Handbook of Clinical Neurology
Licensed Content Author	Jean Paul G. Vonsattel,Christian Keller,Etty Paola Cortes Ramirez
Licensed Content Date	2011
Licensed Content Pages	18
Start Page	83
End Page	100
Type of Use	reuse in a thesis/dissertation
Portion	figures/tables/illustrations
Number of figures/tables/illustrations	1
Format	both print and electronic
Are you the author of this Elsevier chapter?	No
Will you be translating?	No
Order reference number	
Original figure numbers	figure 4.1
Title of your thesis/dissertation	Role of lysine deacetylases in transcription regulation and mitochondrial function in Huntington's disease
Expected completion date	Sep 2016
Estimated size (number of pages)	190
Elsevier VAT number	GB 494 6272 12
Requestor Location	Luana Naia Estrada da Beira, nº 166, 2ºC Coimbra, 3030-173 Portugal Attn: Luana Naia